

Copyright is owned by the Author of the thesis. Permission is given for a copy to be downloaded by an individual for the purpose of research and private study only. The thesis may not be reproduced elsewhere without the permission of the Author.

# The Synthesis and Chemistry of Quinolino[7,8-*h*]quinoline Derivatives

A thesis presented in partial fulfilment of requirements for the degree of

Doctor of Philosophy

in

Chemistry

at

Massey University, Manawatu, New Zealand

by

**REBECCA J. SEVERINSEN**



**MASSEY UNIVERSITY**  
**TE KUNENGA KI PŪREHUROA**  

---

**UNIVERSITY OF NEW ZEALAND**

2021



## Abstract

Proton sponges are a class of neutral organic superbases. Quinolino[7,8-*h*]quinoline (QQ) is one such molecule. Structurally it has two closely positioned nitrogen atoms which cause a destabilising lone electron overlap which manifests as a helical torsional twist that can be relieved by monoprotonation or complexation. These compounds are highly basic and are chelators that can accommodate a variety of ion sizes. Exploration of the structural properties of QQ provides an avenue for non-symmetric compound synthesis. Research interest arose in developing original synthetic pathways and exploring the chemistry of this QQ moiety, and its potential uses. This work primarily focussed on the development of methods towards new derivatives containing the QQ core structure, of which several were developed. Exploration of their properties as bases was begun in the context of both experimental measurements and theoretical calculations, allowing some to be classified as superbases. Computational analysis also gave insight into structural changes taking place during the protonation process. Potential uses of QQ derivatives as chelators for metals were examined. An X-ray crystal structure of a beryllium containing 4,9-dihydroxyquinolino[7,8-*h*]quinoline was achieved, the 7<sup>th</sup> reported ion to be chelated by a QQ compound.





# Contributions

All the work in this thesis was completed by Rebecca Severinsen.

## Except:

- In collaboration with The University of Marburg, Germany, Dr Magnus Buchner and his research group, including Nils Spang, characterised the complex including the beryllium-containing crystal structure discussed in Chapter 6, and that of 9-methoxyquinolino[7,8-*h*]quinoline-4(1*H*)-one in Chapter 2.
- In collaboration with the University of Tartu, Estonia, Prof. Ivo Leito and his research group obtained the experimental  $pK_{aH}$  data discussed in Chapter 4.
- In collaboration with the Ruđer Bošković Institute, Croatia, Dr. Robert Vianello and his research group obtained the computational basicity data also discussed in Chapter 4.
- Computational calculations of Chapter 5 were performed by fellow group member Tyson Dais.

## Publications

Two papers were published during the course of this project, including:

- Rowlands, G. J.; Severinsen, R. J.; Buchanan, J. K.; Shaffer, K. J.; Jameson, H. T.; Thennakoon, N.; Leito, I.; Lőkóv, M.; Kütt, A.; Vianello, R.; Despotović, I.; Radić, N.; Plieger, P. G., Synthesis and Basicity Studies of Quinolino[7,8-*h*]quinoline Derivatives. *J. Org. Chem.* **2020**, *85* (17), 11297-11308.
- Severinsen, R. J.; Rowlands, G. J.; Plieger, P. G., Coordination Cages in Catalysis. *J. Inclusion Phenom. Macrocyclic Chem.* **2020**, *96* (1-2), 29-42.

And contributions were made to:

- Buchner, M. R.; Mueller, M.; Raymond, O.; Severinsen, R. J.; Nixon, D. J.; Henderson, W.; Brothers, P. J.; Rowlands, G. J.; Plieger, P. G., Synthesis of a Boronic Acid Anhydride Based Ligand and Its Application in Beryllium Coordination. *Eur. J. Inorg. Chem.* **2019**, *2019* (34), 3863-3868.



# Acknowledgements

Firstly, I would like to express my gratitude for my supervisors Prof. Paul Plieger and Assoc. Prof. Gareth Rowlands for the guidance, support, and patience they have provided that have enabled this goal to be reached.

I would also like to thank the current, former, and honorary members of the Plieger Group for a great working environment and all the fun, support and help over the years: Jenna Buchanan, Michael Brown, Tyson Dais, Marryllyn Donaldson, Hossein Etemadi, Leonie Etheridge, Liam McGarry, Brodie Matheson, David Nixon, Suraj Patel, and Sidney Woodhouse.

Thank you also to all the other Massey staff of the towers who have been instrumental in this process. This includes Dave Lun, Pat Edwards and Graham Freeman for assistance with unfamiliar techniques, equipment training and instrument use, and the Administration team for all that they do.

Last, but certainly not least, my overwhelming gratitude to the family and friends who have been there for me during these years, you know who you are. Your love and support have kept me going and allowed me to make it this far.

Thank you.



# Contents

Abstract .....	i
Contributions .....	iii
Acknowledgements .....	v
List of Figures .....	x
List of Tables .....	xvii
Abbreviations.....	xviii
Chapter 1 - Introduction .....	1
1.1 - Proton Sponges .....	1
1.2 - Coordination potential of diamines and proton sponges .....	3
1.3 - A New Type of Proton Sponge – quinolino[7,8- <i>h</i> ]quinoline .....	8
1.3.1 - Synthesis of Quinolino[7,8- <i>h</i> ]quinoline .....	10
1.3.2 - Naming and numbering of quinolino[7,8- <i>h</i> ]quinoline derivatives.....	14
1.3.3 - Derivatisation of quinolino[7,8- <i>h</i> ]quinoline.....	15
1.3.4 - Other organic compounds with the QQ substructure .....	21
1.3.5 - QQ Coordination.....	23
1.3.6 - Computational/Theoretical Studies .....	27
1.3.7 - Patents – Organic Electronic Devices.....	28
1.4 - Beryllium Coordination .....	28
1.5 - Coordination cages .....	29
1.6 - Summary.....	30
1.7 - Proposed Aims .....	30
Chapter 2 - Synthesis of New Derivatives.....	31
2.1 - Overview .....	31
2.2 - Symmetrical QQ derivatives.....	33
2.2.1 - Challenges.....	33
2.2.2 - Suzuki-Miyaura Coupling .....	36
2.2.3 - Other symmetrical substitution.....	43
2.2.4 - Synthesis of 9-(dimethylamino)quinolino[7,8- <i>h</i> ]quinoline-4(1 <i>H</i> )-one (Q12) .....	45
2.2.5 - Symmetrical QQ derivatives - Summary.....	46
2.3 - Non-symmetrical QQ derivatives .....	46

2.3.1 - Synthesis of 9-(2-propyn-1-yloxy)-quinolino[7,8- <i>h</i> ]quinolin-4(1 <i>H</i> )-one (Q10)	47
2.3.2 - Synthesis of 4-chloro-9-(2-propyn-1-yloxy)-quinolino[7,8- <i>h</i> ]quinoline (Q13)	48
2.3.3 - Synthesis of 9-(2-propyn-1-yloxy)-1,4,9,12-tetrahydro-4,9-dioxo-2,11-dimethylester-quinolo[7,8- <i>h</i> ]quinoline-2,11-dicarboxylic acid (Q15)	49
2.3.4 - Synthesis of 4-bromo-9-(pyridin-4-yl)-quinolino[7,8- <i>h</i> ]quinoline (Q14)	51
2.3.5 - Non-symmetrical QQ derivatives - Summary	53
2.4 - 9-methoxyquinolino[7,8- <i>h</i> ]quinoline-4(1 <i>H</i> )-one	53
2.5 - Selected Incomplete/unsuccessful QQ Transformations	54
2.5.1 - Synthesis of 4,9-di(4-benzoic acid ethyl ester)quinolino[7,8- <i>h</i> ]quinoline (Q8)	54
2.5.2 - Sonogashira Coupling	55
2.5.3 - Transhalogenation	57
2.5.4 - QQ boronic ester – Change of coupling partners	58
2.5.5 - 6,7-dinitroquinolino[7,8- <i>h</i> ]quinoline-4,9(1 <i>H</i> ,12 <i>H</i> )-dione	59
2.5.6 - 4-bromo-9-chloro-quinolino[7,8- <i>h</i> ]quinoline	59
2.6 - Non-QQ Synthesis	61
2.6.1 - Synthesis and characterisation of a boronic acid anhydride-based ligand	61
2.6.2 - Synthesis of 2-hydroxy-5-(3-pyridyl)-benzaldehyde oxime (L1)	62
2.7 - Conclusion	64
Chapter 3 - Experimental Synthesis Methods	65
3.1 - General QQ experimental and characterisation notes	65
3.2 - Experimental methods	69
3.2.1 - Synthesis of tetramethyl-2,2'-(naphthalene-1,8-diylbis(azanediyl) difumarate (N)	69
3.2.2 - Synthesis of 4,9-dioxo-1,4,9,12-tetrahydroquinolino[7,8- <i>h</i> ]quinoline-2,11-dicarboxylate (Q1)	70
3.2.3 - Synthesis of quinolino[7,8- <i>h</i> ]quinoline-4,9-(1 <i>H</i> ,12 <i>H</i> )-dione (Q2)	71
3.2.4 - Synthesis of 4,9-dichloroquinolino[7,8- <i>h</i> ]quinoline (Q3)	72
3.2.5 - Synthesis of 4,9-dibromoquinolino[7,8- <i>h</i> ]quinoline (Q4)	73
3.2.6 - Synthesis of 4,9-di(pyridin-4-yl)quinolino[7,8- <i>h</i> ]quinoline (Q5)	74
3.2.7 - Synthesis of 4,9-di(pyridin-3-yl)quinolino[7,8- <i>h</i> ]quinoline (Q5)	75
3.2.8 - Synthesis of <i>N</i> <sup>4</sup> , <i>N</i> <sup>4</sup> , <i>N</i> <sup>9</sup> , <i>N</i> <sup>9</sup> -tetraethylquinolino[7,8- <i>h</i> ]quinoline-4,9-diamine	76
3.2.9 - Synthesis of 4-bromo-9-oxo-9,12-dihydroquinolino[7,8- <i>h</i> ]quinoline (Q9)	77

3.2.10 - Synthesis of 9-(2-propyn-1-yloxy)-quinolino[7,8- <i>h</i> ]quinolin-4(1 <i>H</i> )-one (Q10).....	78
3.2.11 - Synthesis of 9-(dimethylamino)quinolino[7,8- <i>h</i> ]quinoline-4(1 <i>H</i> )-one (Q12) .....	79
3.2.12 - Synthesis of 4-chloro-9-(2-propyn-1-yloxy)-quinolino[7,8- <i>h</i> ]quinoline (Q14).....	80
3.2.13 - Synthesis of 4-bromo-9-(pyridin-4-yl)quinolino[7,8- <i>h</i> ]quinoline (Q14).....	81
3.2.14 - Synthesis of 9-(2-propyn-1-yloxy)-1,4,9,12-tetrahydro-4,9-dioxo-2,11-dimethylester-quinolo[7,8- <i>h</i> ]quinoline-2,11-dicarboxylic acid (Q15) .....	82
3.2.15 - Synthesis of 4,9-dichloro-6,7-dinitroquinolino[7,8- <i>h</i> ]quinoline (Q18).....	83
3.2.16 - Synthesis of 3-pyridine boronic acid pinacol ester .....	83
3.3 - Other Experimental.....	84
3.3.1 - Synthesis of a boronic acid anhydride-based ligand.....	84
3.3.2 - Synthesis of 2-hydroxy-5-(3-pyridyl)-benzaldehyde oxime (L1).....	85
Chapter 4 - Quinolino[7,8- <i>h</i> ]quinoline p <i>K</i> <sub>aH</sub> Research .....	86
4.1 - Introduction .....	86
4.2 - Results and Discussion .....	88
4.2.1 - Theoretical QQ Derivatives .....	94
4.3 - Comparison to existing Proton Sponges .....	97
4.4 - Conclusion.....	99
Chapter 5 - Structural insights using Computational Chemistry.....	100
5.1 - Methods.....	101
5.2 - Results and Discussion .....	103
5.2.1 - Gas Phase Basicity .....	107
5.3 - Conclusion.....	110
Chapter 6 - Coordination .....	111
6.1 - Quino[7,8- <i>h</i> ]quinoline Coordination - General.....	111
6.1.1 - Results.....	113
6.2 - Beryllium Coordination .....	116
6.3 - Conclusion.....	122
Chapter 7 - Future Work.....	123
Chapter 8 - Conclusion.....	126
References .....	128
Appendices .....	137



Appendix A – X-ray summary data for 4,9-di(pyridin-4-yl)quinolino[7,8- <i>h</i> ]quinoline (Q4) .....	137
Appendix B – X-ray summary data for 9-methoxyquinolino[7,8- <i>h</i> ]quinoline-4(1H)-one .....	139
Appendix C - Selected Experimental NMR Characterisation .....	141
Appendix D - QQ Computational .....	175
Appendix E – Crystal data and refinement for [BeBr(MeCN)(QQ(OH) <sub>2</sub> )]Br .....	177
Appendix F - QQ Derivative names and codes.....	179

## List of Figures

<b>Figure 1-1:</b>	1,8-Bis(dimethylamino)naphthalene (DMAN) - The original Proton Sponge™ ... 1
<b>Figure 1-2:</b>	X-ray structures of DMAN in neutral (left) and protonated (right) forms. Images generated in Olex2 <sup>8</sup> from CCDC files DMANAP01 <sup>9</sup> and CEJGUU <sup>10</sup> with 50% ellipsoids. Counter-ion (CF <sub>3</sub> O <sub>3</sub> S <sup>-</sup> ) omitted from DMANH <sup>+</sup> (right) for clarity. .... 2
<b>Figure 1-3:</b>	Structures of triguanidinophosphazene (B) <i>N</i> <sup>4</sup> , <i>N</i> <sup>4</sup> , <i>N</i> <sup>5</sup> , <i>N</i> <sup>5</sup> -tetramethyl-1,8-dioxide-arsenino[2,3- <i>b</i> ]arsenin-4,5-diamine (C)..... 2
<b>Figure 1-4:</b>	<i>pK</i> <sub>a</sub> values in acetonitrile for the conjugate acids of DMAN (A), TMGN (D) and HMPN (E). <sup>16-18</sup> ..... 3
<b>Figure 1-5:</b>	Example of a light-responsive coordination complex (F) involving bidentate diamine binding sites. Adapted with permission from Mobian et al. <sup>20</sup> Copyright 2004 Wiley-VCH. .... 4
<b>Figure 1-6:</b>	Example of a multistep catalysis (right) by a hexahedral coordination cage (G) featuring a ligand (H) with bidentate diamine binding sites. <sup>36</sup> ..... 5
<b>Figure 1-7:</b>	Coordination of a Pd(II) ion by DMAN (I), completed with a 1,3-diphenylpropane-1,3-dionato-O, <i>O</i> '- ligand. Hydrogen and counter-ion (HFAC <sup>-</sup> ) omitted for clarity. Image generated in Olex2 <sup>8</sup> from CCDC file OBEJIP <sup>38</sup> with 50% ellipsoids. .... 6
<b>Figure 1-8:</b>	Complexes of TMPN with Ga(III) (J) and Al(III) (K) in front (top) and side-plane (lower) views. Hydrogen omitted for clarity. Images generated in Olex2 <sup>8</sup> from CCDC files BIXQEG and BIXQAC with 50% ellipsoids. <sup>40</sup> ..... 7
<b>Figure 1-9:</b>	Structures of DMAN (A), 1,10-phen (L) and quinolino[7,8- <i>h</i> ]quinoline (QQ). .... 8
<b>Figure 1-10:</b>	4,9-dichloroquinolino[7,8- <i>h</i> ]quinoline (Q3) structures in neutral (left) and protonated (right) forms. Images generated in Olex2 <sup>8</sup> from CCDC files PANFOB and PANFUH with 50% ellipsoids. <sup>41</sup> Counter-ion (BF <sub>4</sub> <sup>-</sup> ) omitted from (right) for clarity. .... 9
<b>Figure 1-11:</b>	All tautomers of quinolino[7,8- <i>h</i> ]quinoline-4,9-(1 <i>H</i> ,12 <i>H</i> )-dione (Q2). .... 9
<b>Figure 1-12:</b>	Skraup reaction (top) and mechanism (partial) to form quinoline. <sup>48</sup> ..... 10
<b>Figure 1-13:</b>	Attempted formation of QQ by Skraup condensation by Sauvage and coworkers that resulted in formation of 2-mdp (N). <sup>52</sup> ..... 11
<b>Figure 1-14:</b>	Proposed mechanism of formation of 2-mdp (N) from 1,8-diacetaminonaphthalene (M). .... 12
<b>Figure 1-15:</b>	Initial quinolino[7,8- <i>h</i> ]quinoline synthesis by Zirnstein and Staab, 1987. <sup>11,54</sup> Reaction conditions and yields: (i) DMAD, MeOH, RT, 71%; (ii) Ph <sub>2</sub> O, 240 °C, 64%; (iii) (a) KOH, 100 °C; (b) HCl, H <sub>2</sub> O, 93%; (iv) 370 °C, 10 <sup>-5</sup> torr 76%; (v) POCl <sub>3</sub> , 130 °C, 81%; (vi) Pd/C, HOAc, NaOAc, 39%. .... 13
<b>Figure 1-16:</b>	Total QQ structures (with assigned CAS numbers) published 1987-2019. Data points indicate years in which one or more QQ-derivative-containing publications were released. Data includes complexes and salts, and those present only in patent literature. Some of these publications are discussed in the following sections. .... 14
<b>Figure 1-17:</b>	Nomenclature of quinolino[7,8- <i>h</i> ]quinoline (left) and numbering scheme for atoms/substituents (right). .... 15
<b>Figure 1-18:</b>	Quinolino[7,8- <i>h</i> ]quinoline substituent numbering. .... 15
<b>Figure 1-19:</b>	Selected examples of published 4,9-substituted QQ derivatives. <sup>11, 15</sup> ..... 17
<b>Figure 1-20:</b>	Crystal structures of dimethyl 4,9-dichloroquinolino[7,8- <i>h</i> ]quinoline-2,11-dicarboxylate (Q16) and <i>N</i> -[2-(methylthio)benzo[ <i>h</i> ]quinolin-10-yl]acetamide

	(U). Counter-ion ( $\text{BF}_4^-$ ) not shown for clarity (left). Images generated in Olex2 <sup>8</sup> using CCDC files FEJXID and FEJXEZ with 50% ellipsoids. <sup>15</sup> .....	18
<b>Figure 1-21:</b>	Attempted synthesis of QQ from 1,8-diaminonaphthalene (O) and 3-bis(methylthio)acrolein by Skraup condensation, resulting in the formation of <i>N</i> -[2-(methylthio)benzo[ <i>h</i> ]quinolin-10-yl]acetamide (U) instead of the desired disubstituted product (V). .....	19
<b>Figure 1-22:</b>	Nitration of 4,9-dichloroquinolino[7,8- <i>h</i> ]quinoline (Q3). <sup>54</sup> .....	19
<b>Figure 1-23:</b>	X-ray structure of 4-chloro-9-oxo-9,12-dihydro-6,7-dinitroquino[7,8- <i>h</i> ]quinoline (Q21). <sup>11</sup> Generated in Olex2 <sup>8</sup> with 50% ellipsoids. ....	20
<b>Figure 1-24:</b>	Resonance structures of QQ showing the partial positive character of positions 5 and 8. ....	21
<b>Figure 1-25:</b>	Examples of other organic compounds with the QQ substructure, with a polycyclic 'croissant-like' compound (W) and acequinolino[7,8- <i>h</i> ]quinoline (AceQQ). ....	22
<b>Figure 1-26:</b>	Proposed mechanism for the formation of aceQQ. ....	23
<b>Figure 1-27:</b>	Pt and Re complexes of 4,9-dichloroquinolino[7,8- <i>h</i> ]quinoline (Q3). Hydrogen omitted for clarity. Images generated in Olex2 <sup>8</sup> using CCDC files ACEQAA and ACEPUT with 50% ellipsoids. <sup>56</sup> .....	24
<b>Figure 1-28:</b>	Boron-chelates of 4,9-dichloroQQ (left) and QQ (right). Hydrogen and counter-ions ( $\text{BF}_4^-$ ) omitted for clarity. Images generated in Olex2 <sup>8</sup> using CCDC files PANGES and PANGAO with 50% ellipsoids. <sup>41</sup> .....	25
<b>Figure 1-29:</b>	QQ spatial changes associated with (left) coordination to large metal ions (M) such as Pt and Re and (right) protonation or coordination to smaller ions (Y) such as $\text{BF}_2$ . <sup>15</sup> .....	26
<b>Figure 1-30:</b>	Cu(II) complexes of 4,9-dichloroquinolino[7,8- <i>h</i> ]quinoline (Q3, left) and quinolino[7,8- <i>h</i> ]quinoline (QQ, right). Hydrogen and counter-ions removed for clarity. Images generated in Olex2 <sup>8</sup> using CCDC files NIBSOI and NIBSIC with 50% ellipsoids. <sup>58</sup> .....	26
<b>Figure 1-31:</b>	Crystal structure of $(\text{Be}(\text{PhC}(\text{O})\text{O})_2)_{12}$ obtained by Müller and Buchner as an example of an existing beryllium complex. <sup>82</sup> Image generated in Olex2 <sup>8</sup> from the CCDC file YEZQAY. ....	28
<b>Figure 1-32:</b>	Molecular mechanics representation of a potential QQ cage structure. ....	29
<b>Figure 2-1:</b>	Summarised QQ reaction scheme. ....	32
<b>Figure 2-2:</b>	<sup>1</sup> H NMR of Q2 in <i>d</i> -trifluoroacetic acid (TFA- <i>d</i> ) showing four aromatic proton signals, indicative of a symmetrical QQ structure ((a), with trifluoroacetate anion). ....	33
<b>Figure 2-3:</b>	Synthesis of Q9 from Q4. ....	34
<b>Figure 2-4:</b>	Proposed mechanism for partial hydroxyl substitution and tautomerisation from 4,9-dibromoQQ. ....	36
<b>Figure 2-5:</b>	Generalised Suzuki-Miyaura coupling mechanism showing the oxo-Pd pathway. Boronate pathway transmetalation proceeds by the reaction of '2' directly with the boronate species without formation of '3'. ....	37
<b>Figure 2-6:</b>	Possible Suzuki-Miyaura coupling pathways for the formation of mono- and di-substituted QQ derivatives. X = Cl or Br. ....	38
<b>Figure 2-7:</b>	Synthesis of Q5 from Q4. ....	39
<b>Figure 2-8:</b>	Images of the X-ray structure of 4,9-dipyridylquino[7,8- <i>h</i> ]quinoline (Q5), generated in Olex2 with 50% ellipsoids. <sup>8</sup> .....	41
<b>Figure 2-9:</b>	Successful synthesis of Q6 from Q4. ....	41

<b>Figure 2-10:</b>	Attempted synthesis of Q6 from Q3.....	42
<b>Figure 2-11:</b>	Synthesis of Q7 from Q4.....	44
<b>Figure 2-12:</b>	Synthesis of Q12 from Q4.....	45
<b>Figure 2-13:</b>	Synthesis of Q10 from Q2.....	47
<b>Figure 2-14:</b>	Synthesis of Q13 from Q10.....	48
<b>Figure 2-15:</b>	Synthesis of Q15 from Q1.....	50
<b>Figure 2-16:</b>	Synthesis of Q14 from Q11.....	51
<b>Figure 2-17:</b>	<sup>1</sup> H NMR spectra of Q14 taken after <1hr (top) ~30hrs (lower) in DMSO- <i>d</i> <sub>6</sub> . Note the appearance of many new peaks (e.g. 17.2 and 15.6 ppm, highlighted by ‘*’ symbols), some of which correspond to degradation to Q11. ....	52
<b>Figure 2-18:</b>	Schematic (left) and crystal (right) structures of 9-methoxyquinolino[7,8- <i>h</i> ]quinoline-4(1 <i>H</i> )-one showing two different viewpoints. Image generated in Olex2 with 50% ellipsoids. <sup>8</sup> .....	53
<b>Figure 2-19:</b>	Crystal structure packing of 9-methoxyquinolino[7,8- <i>h</i> ]quinoline-4(1 <i>H</i> )-one. Images generated in Olex2 with 50% ellipsoids. <sup>8</sup> .....	54
<b>Figure 2-20:</b>	Synthesis of Q8 from Q4.....	55
<b>Figure 2-21:</b>	High-resolution mass spectrum of Q8 synthesis. ....	55
<b>Figure 2-22:</b>	Triple-cavity Pd <sub>4</sub> L <sub>4</sub> cage constructed by Crowley and coworkers, where R=O(CH <sub>2</sub> ) <sub>2</sub> O(CH <sub>2</sub> ) <sub>2</sub> OCH <sub>3</sub> Image adapted from Ref. [101]. For further permissions related to this image, contact the ACS. <a href="https://pubs.acs.org/doi/10.1021/jacs.6b11982">https://pubs.acs.org/doi/10.1021/jacs.6b11982</a> . Copyright American Chemical Society (2017). <sup>101</sup> .....	56
<b>Figure 2-23:</b>	Synthesis of 4,9-di(X-ethynylpyridyl)quinolino[7,8- <i>h</i> ]quinoline and 4-(X-ethynylpyridyl)-9-oxo-9,12-dihydroquinolino[7,8- <i>h</i> ]quinoline from Q4, where X = 3 or 4.....	56
<b>Figure 2-24:</b>	Low-res mass spectrum of a Sonogashira coupling attempt showing three different products.....	57
<b>Figure 2-25:</b>	Attempted transhalogenation of Q3 to 4,9-diiodoquinolino[7,8- <i>h</i> ]quinoline...	58
<b>Figure 2-26:</b>	Attempted formation of 4,9-bis(4,4,5,5-tetramethyl-1,3,2-dioxaborolan-2-yl)-quinolino[7,8- <i>h</i> ]quinoline.....	58
<b>Figure 2-27:</b>	Synthesis of 6,7-dinitroquinolino[7,8- <i>h</i> ]quinoline-4,9(1 <i>H</i> ,12 <i>H</i> )-dione.....	59
<b>Figure 2-28:</b>	Synthesis of 4-bromo-9-chloro-quinolino[7,8- <i>h</i> ]quinoline.....	59
<b>Figure 2-29:</b>	Mass spectrum of attempted formation of 4-bromo-9-chloro-quinolino[7,8- <i>h</i> ]quinoline (left) and proposed mechanism (right). ....	60
<b>Figure 2-30:</b>	Synthesis of C3 from C1.....	61
<b>Figure 2-31:</b>	Synthesis of 2-hydroxy-5-(3-pyridyl)-benzaldehyde oxime (L1) from 4-bromophenol.....	62
<b>Figure 2-32:</b>	Pt <sub>4</sub> L <sub>4</sub> metallomacrocyclic synthesised by MacLachlan and coworkers. <sup>114</sup> .....	63
<b>Figure 3-1:</b>	<sup>1</sup> H NMR spectra comparison of Q7 showing the aromatic region. Upper spectrum is ~ 3-4x more concentrated (exact concentrations were not recorded). ....	66
<b>Figure 3-2:</b>	<sup>1</sup> H NMR signals corresponding to HA (left) and HB (right). Both proton signals should present as doublets, however this is not observed here. ....	67
<b>Figure 4-1:</b>	Structure of the Proton Sponge™ DMAN (left) and quinolino[7,8- <i>h</i> ]quinoline (right). ....	86
<b>Figure 4-2:</b>	Example of framework buttressing effects on organic bases (left) and hybridised N donor atoms in DBU (right). ....	87

<b>Figure 4-3:</b>	Relative strength of selected electron withdrawing and donating substituents. .... 88
<b>Figure 4-4:</b>	Key to R <sup>1</sup> -R <sup>3</sup> QQ substituent position codes..... 89
<b>Figure 4-5:</b>	Calculated pK <sub>aH</sub> values compared to degree of torsional twists of synthesised QQ derivatives..... 91
<b>Figure 4-6:</b>	Variation of QQ basicity correlated with substituent electronic effects..... 94
<b>Figure 4-7:</b>	Effects of substituent position on resulting pK <sub>aH</sub> ..... 96
<b>Figure 4-8:</b>	Structural comparison of quinolino[7,8- <i>h</i> ]quinoline (left), TMGN (middle) and HMPN (right) ..... 97
<b>Figure 5-1:</b>	Structures explored in this chapter using Gaussian09 (G09) ..... 100
<b>Figure 5-2:</b>	Optimised gas-phase neutral geometries of A: 4,9-di(3-pyridyl)quinolino[7,8- <i>h</i> ]quinoline (Q6); B: 4,9-di(4-pyridyl)quinolino[7,8- <i>h</i> ]quinoline (Q5); C: 4-chloro-9-(2-propyn-1-yloxy)-quinolino[7,8- <i>h</i> ]quinoline (Q13); D: 4,9-diaminoquinolino[7,8- <i>h</i> ]quinoline; E: N <sup>4</sup> ,N <sup>4</sup> ,N <sup>9</sup> ,N <sup>9</sup> -tetramethylquinolino[7,8- <i>h</i> ]quinoline-4,9-diamine (left) and protonated geometries (right)..... 103
<b>Figure 5-3:</b>	Comparison between angle of torsional twist in QQ derivative neutral structures and magnitude of N...N distance change upon protonation ..... 105
<b>Figure 5-4:</b>	Change in bond lengths in QQ core of derivatives A-E upon protonation. Bonds associated with the 'protonated' quinoline side (N1) to the left and the 'non-protonated' to the right. .... 106
<b>Figure 5-5:</b>	QQ core structure with bonds that significantly change upon protonation. Orange bonds increase length, blue decrease, and grey/black show little change. .... 107
<b>Figure 5-6:</b>	Optimised structure images of protonated E with calculated plane (left) showing slight bowing. NMe <sub>2</sub> side groups omitted from the left image for clarity of the plane..... 107
<b>Figure 5-7:</b>	Calculated basicity (Gas Phase Basicity (GPB, circle) or Proton Affinity (PA, square)) compared with degree of torsional twist in the neutral structures. 109
<b>Figure 6-1:</b>	QQ spatial changes associated with (a) coordination to large metal ions such as Pt and Re and (b) protonation or coordination to smaller ions such as BF <sub>2</sub> . (C): X-ray structure of a Cu-QQ complex, produced in Olex2 with 50% ellipsoids from CCDC file NIBSIC. <sup>8</sup> Anions and hydrogen removed for clarity. (a)/(b) reproduced from Shaffer et al., 2012. <sup>41</sup> ..... 112
<b>Figure 6-2:</b>	Mass spectra of attempted complex formation. A: Attempted Q5-B(III) complexation showing only the Q5 ligand. B: Attempted Q4-Cu(II) complexation, showing decomposition of Q4 to the mono-halide Q9..... 114
<b>Figure 6-3:</b>	Mass spectrum of complexation attempt between Pt(II) and Q6. .... 115
<b>Figure 6-4:</b>	QQ-BF <sub>2</sub> complex with 50% ellipsoids. <sup>41</sup> Image generated in Olex2 from CCDC deposition number PANGAO. <sup>8</sup> ..... 116
<b>Figure 6-5:</b>	[BeBr(MeCN)(QQ(OH) <sub>2</sub> )]Br crystal structure (Be-QQ(OH) <sub>2</sub> ) in two different views with 50% ellipsoids. Images generated in Olex2. <sup>8</sup> ..... 119
<b>Figure 6-6:</b>	Be-QQ(OH) <sub>2</sub> crystal structure showing a layer of packing (50% ellipsoids). Image generated in Olex2. <sup>8</sup> ..... 120
<b>Figure 7-1:</b>	Structure of computationally calculated QQ derivatives with high pK <sub>aH</sub> values given in chapter 4..... 123
<b>Figure 7-2:</b>	Attempted synthesis of 4,9-di(dimethylamine)quinolino[7,8- <i>h</i> ]quinoline ..... 123
<b>Figure 7-3:</b>	Examples of possible transformations of Q10 and Q13 (R <sup>1</sup> = OH (tautomer) or Cl respectively). R <sup>2</sup> /R <sup>3</sup> = alkyl group. .... 124

<b>Figure 7-4:</b>	A: Acequinolinoquinoline (aceQQ), also called dipyrido[3,2-e:2',3'-h]acenaphthene. <sup>59</sup> B: AceQQ with possible functionalisation positions from synthesis by QQ methods.....	125
<b>Figure C-1:</b>	<sup>1</sup> H NMR spectrum of 4,9-di(pyridin-4-yl)quinolino[7,8- <i>h</i> ]quinoline (Q5).....	141
<b>Figure C-2:</b>	<sup>13</sup> C NMR spectrum of 4,9-di(pyridin-4-yl)quinolino[7,8- <i>h</i> ]quinoline (Q5).....	142
<b>Figure C-3:</b>	COSY (top) and HMQC (lower) spectra of 4,9-di(pyridin-4-yl)quinolino[7,8- <i>h</i> ]quinoline (Q5).....	143
<b>Figure C-4:</b>	<sup>1</sup> H NMR spectrum of 4,9-di(pyridin-3-yl)quinolino[7,8- <i>h</i> ]quinoline (Q6).....	144
<b>Figure C-5:</b>	<sup>13</sup> C NMR spectrum of 4,9-di(pyridin-3-yl)quinolino[7,8- <i>h</i> ]quinoline (Q6).....	145
<b>Figure C-6:</b>	HMQC (top) and COSY (lower) spectra of 4,9-di(pyridin-3-yl)quinolino[7,8- <i>h</i> ]quinoline (Q6).....	146
<b>Figure C-7:</b>	<sup>1</sup> H NMR spectrum of <i>N</i> <sup>4</sup> , <i>N</i> <sup>4</sup> , <i>N</i> <sup>9</sup> , <i>N</i> <sup>9</sup> -tetraethylquinolino[7,8- <i>h</i> ]quinoline-4,9-diamine (Q7).....	147
<b>Figure C-8:</b>	<sup>13</sup> C NMR spectrum of <i>N</i> <sup>4</sup> , <i>N</i> <sup>4</sup> , <i>N</i> <sup>9</sup> , <i>N</i> <sup>9</sup> -tetraethylquinolino[7,8- <i>h</i> ]quinoline-4,9-diamine (Q7).....	148
<b>Figure C-9:</b>	HMQC (top) and COSY (lower) spectra of <i>N</i> <sup>4</sup> , <i>N</i> <sup>4</sup> , <i>N</i> <sup>9</sup> , <i>N</i> <sup>9</sup> -tetraethylquinolino[7,8- <i>h</i> ]quinoline-4,9-diamine (Q7).....	149
<b>Figure C-10:</b>	<sup>1</sup> H NMR spectrum of 4-bromo-9-oxo-9,12-dihydroquinolino[7,8- <i>h</i> ]quinoline (Q9).....	150
<b>Figure C-11:</b>	<sup>13</sup> C NMR spectrum of 4-bromo-9-oxo-9,12-dihydroquinolino[7,8- <i>h</i> ]quinoline (Q9).....	151
<b>Figure C-12:</b>	HMQC (top) and COSY (lower) spectra of 4-bromo-9-oxo-9,12-dihydroquinolino[7,8- <i>h</i> ]quinoline (Q9). .....	152
<b>Figure C-13:</b>	<sup>1</sup> H NMR spectrum of 9-(2-propyn-1-yloxy)-quinolino[7,8- <i>h</i> ]quinolin-4(1 <i>H</i> )-one (Q10).....	153
<b>Figure C-14:</b>	<sup>13</sup> C NMR spectrum of 9-(2-propyn-1-yloxy)-quinolino[7,8- <i>h</i> ]quinolin-4(1 <i>H</i> )-one (Q10).....	154
<b>Figure C-15:</b>	HMQC (top) and COSY (lower) spectra of 9-(2-propyn-1-yloxy)-quinolino[7,8- <i>h</i> ]quinolin-4(1 <i>H</i> )-one (Q10).....	155
<b>Figure C-16:</b>	<sup>1</sup> H NMR spectrum of 9-(dimethylamino)quinolino[7,8- <i>h</i> ]quinoline-4(1 <i>H</i> )-one (Q12).....	156
<b>Figure C-17:</b>	<sup>13</sup> C NMR spectrum of 9-(dimethylamino)quinolino[7,8- <i>h</i> ]quinoline-4(1 <i>H</i> )-one (Q12).....	157
<b>Figure C-18:</b>	Overlay of <sup>13</sup> C and DEPT-135 NMR spectra of 9-(dimethylamino)quinolino[7,8- <i>h</i> ]quinoline-4(1 <i>H</i> )-one (Q12).....	158
<b>Figure C-19:</b>	<sup>1</sup> H NMR spectrum of 4-chloro-9-(2-propyn-1-yloxy)-quinolino[7,8- <i>h</i> ]quinoline (Q13).....	159
<b>Figure C-20:</b>	<sup>13</sup> C NMR spectrum of 4-chloro-9-(2-propyn-1-yloxy)-quinolino[7,8- <i>h</i> ]quinoline (Q13).....	160
<b>Figure C-21:</b>	HMQC (top) and COSY (lower) spectra of 4-chloro-9-(2-propyn-1-yloxy)-quinolino[7,8- <i>h</i> ]quinolin-4(1 <i>H</i> )-one (Q13).....	161
<b>Figure C-22:</b>	<sup>1</sup> H NMR of 4-bromo-9-(pyridin-4-yl)quinolino[7,8- <i>h</i> ]quinoline (Q14).....	162
<b>Figure C-23:</b>	<sup>13</sup> C NMR of 4-bromo-9-(pyridin-4-yl)quinolino[7,8- <i>h</i> ]quinoline (Q14).....	163
<b>Figure C-24:</b>	HSQC (top) and COSY (lower) spectra of 4-bromo-9-(pyridin-4-yl)quinolino[7,8- <i>h</i> ]quinoline (Q14).....	164
<b>Figure C-25:</b>	HMBC (top) spectrum of 4-bromo-9-(pyridin-4-yl)quinolino[7,8- <i>h</i> ]quinoline (Q14).....	165

<b>Figure C-26:</b>	<sup>1</sup> H NMR spectrum of 9-(2-propyn-1-yloxy)-1,4,9,12-tetrahydro-4,9-dioxo-2,11-dimethylester-quino[7,8- <i>h</i> ]quinoline-2,11-dicarboxylic acid (Q15).....	166
<b>Figure C-27:</b>	<sup>13</sup> C NMR spectrum of 9-(2-propyn-1-yloxy)-1,4,9,12-tetrahydro-4,9-dioxo-2,11-dimethylester-quino[7,8- <i>h</i> ]quinoline-2,11-dicarboxylic acid (Q15).....	167
<b>Figure C-28:</b>	HMQC (top) and COSY (lower) spectra of 9-(2-propyn-1-yloxy)-1,4,9,12-tetrahydro-4,9-dioxo-2,11-dimethylester-quino[7,8- <i>h</i> ]quinoline-2,11-dicarboxylic acid (Q15) .....	168
<b>Figure C-29:</b>	<sup>1</sup> H NMR spectrum of a boronic anhydride-based ligand (compound 3) .....	169
<b>Figure C-30:</b>	<sup>11</sup> B NMR spectrum of a boronic anhydride-based ligand (compound 3) in CDCl <sub>3</sub> . External BF <sub>3</sub> .Et <sub>2</sub> O standard used. ....	170
<b>Figure C-31:</b>	IR spectrum (ATR) of a boronic anhydride-based ligand (compound 3) .....	171
<b>Figure C-32:</b>	<sup>1</sup> H NMR spectrum of 2-hydroxy-5-(3-pyridyl)-benzaldehyde oxime (L1).....	172
<b>Figure C-33:</b>	<sup>13</sup> C spectrum of 2-hydroxy-5-(3-pyridyl)-benzaldehyde oxime (L1) .....	173
<b>Figure C-34:</b>	HMQC (top) and COSY (lower) spectra of 2-hydroxy-5-(3-pyridyl)-benzaldehyde oxime (L1).....	174

## List of Tables

<b>Table 1-1:</b>	Calculated N···N distances (neutral structures) and $pK_a$ (conjugate acids) of QQ (left) and coordination compound 623559-12-6 (right). Data published in Bucher et al. <sup>76</sup> ..... 27
<b>Table 4-1:</b>	Experimentally determined $pK_{aH}$ , calculated proton affinities (PA), gas-phase basicities (GB) calculated $pK_{aH}$ and helical torsional twists of quinolino[7,8- <i>h</i> ]quinoline derivatives (in their neutral states). ..... 90
<b>Table 4-2:</b>	Comparison of QQ basicity and sum of electron withdrawing effects using the quantity $\Delta V_c$ . *Experimental $pK_{aH}$ values are listed for all except compound Q18, which is computationally derived. .... 93
<b>Table 4-3:</b>	Calculated data for theoretical QQ derivatives. .... 95
<b>Table 5-1:</b>	Selected structural properties of calculated QQ structures. Angles and distances calculated using Olex2. .... 104
<b>Table 5-2:</b>	Calculated gas phase basicities (GPB) and proton affinities (PA) of calculated QQ derivatives, where QQ represents quinolino[7,8- <i>h</i> ]quinoline. The substituents are attached at the 4 and 9 positions. Sorted in order of descending GPB. .... 109
<b>Table 6-1:</b>	Summary of all complexes published to date involving quinolino[7,8- <i>h</i> ]quinoline derivatives (excluding those only published in patents). <sup>79, 133-134</sup> ..... 112
<b>Table 6-2:</b>	Selected QQ derivative complexation attempts. .... 113
<b>Table 6-3:</b>	QQ derivatives sent to Germany for Beryllium coordination ..... 118
<b>Table 6-4:</b>	Angles and distances associated with halogen bonding in Be-QQ(OH) <sub>2</sub> and complex naming key (right) ..... 120
<b>Table 6-5:</b>	Selected Distances (in Å) of QQ Complexes. Blue represents distances shorter than (or equal to) the corresponding distance in neutral QQCl <sub>2</sub> (4,9-dichloroquinolino[7,8- <i>h</i> ]quinoline, Q3) while orange represents greater length. The 'NCCCN plane' represents the plane formed by the 5 atoms of the central Q derivative binding pocket. .... 121
<b>Table A-1:</b>	Crystal data and structure refinement for 4,9-di(pyridin-4-yl)quinolino[7,8- <i>h</i> ]quinoline. .... 137
<b>Table A-2:</b>	Bond Lengths for 4,9-di(pyridin-4-yl)quinolino[7,8- <i>h</i> ]quinoline. .... 138
<b>Table A-3:</b>	Bond Angles for 4,9-di(pyridin-4-yl)quinolino[7,8- <i>h</i> ]quinoline ..... 138
<b>Table B-1:</b>	Crystal data and structure refinement for 9-methoxyquinolino[7,8- <i>h</i> ]quinoline-4(1 <i>H</i> )-one. .... 139
<b>Table B-2:</b>	Bond Lengths for 9-methoxyquinolino[7,8- <i>h</i> ]quinoline-4(1 <i>H</i> )-one. .... 140
<b>Table B-3:</b>	Bond Angles for 9-methoxyquinolino[7,8- <i>h</i> ]quinoline-4(1 <i>H</i> )-one. .... 140
<b>Table D-1:</b>	Bond lengths and changes of neutral and protonated structures of Chapter 5. Lengths and length changes given in Å. .... 175
<b>Table D-2:</b>	Free energies and enthalpies of computational structures (Chapter 5) used for gas phase basicity and proton affinity calculations. .... 176
<b>Table E-1:</b>	Crystal data and structure refinement for [BeBr(MeCN)(QQ(OH) <sub>2</sub> )]Br. .... 177
<b>Table E-2:</b>	Selected bond lengths of the Be-QQ(OH) <sub>2</sub> crystal structure ..... 178
<b>Table E-3:</b>	Selected angles of Be-QQ(OH) <sub>2</sub> structure ..... 178



# Abbreviations

$^{13}\text{C}$ NMR	Carbon Nuclear Magnetic Resonance
$^1\text{H}$ NMR	Proton Nuclear Magnetic Resonance
B3LYP	3-parameter hybrid Becke exchange/Lee-Yang-Parr
CCDC	Cambridge Crystallographic Data Centre
COSY	Correlation Spectroscopy
DCE	Dichloroethane
DCM	Dichloromethane
DEPT	Distortionless Enhancement by Polarisation Transfer
DMAD	Dimethyl acetylenedicarboxylate
DMAN	1,8-Bis(dimethylamino)naphthalene
DMF	Dimethylformamide
DMSO- $d_6$	Deuterated dimethylsulfoxide
ESI	Electrospray Ionisation
G09	Gaussian 09 version: ES64L-G09RevD.01
HFAC	1,1,1,5,5,5-Hexafluoropentane-2,4-dionate
HMPN	1,8-Bis(hexamethyltriaminophosphazanyl)naphthalene
HMQC	Heteronuclear Multiple Quantum Coherence
HR	High resolution
IHB	Intramolecular Hydrogen Bond
IR	Infrared
LR	Low resolution
Me	Methyl Group
MESP	Molecular Electrostatic Potential
MS	Mass spectrometry
NOESY	Nuclear Overhauser Effect Spectroscopy
QQ	Quinolino[7,8- <i>h</i> ]quinoline
RT	Room Temperature
TFA- <i>d</i>	Deuterated trifluoroacetic acid
TMGN	1,8-Bis(tetramethylguanidino)naphthalene
TMPN	Dimethyl-((naphthalene-1,8-diylidene(nitrilo))bistrimethylphosphorane))
XPhos	2-dicyclohexylphosphino-2',4',6'-triisopropylbiphenyl

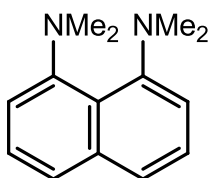




# Chapter 1 - Introduction

## 1.1 - Proton Sponges

In 1968 Alder et al. published a paper on 1,8-bis(dimethylamino)naphthalene (DMAN), which promoted a new field of basic-compound studies.<sup>1-3</sup> This compound was designated the first Proton Sponge™,<sup>4</sup> a neutral organic superbases with a  $pK_a$  (of the conjugate acid) of  $\sim 12.2$  in water and 18.63 in acetonitrile.<sup>5-6</sup>



**A**

**Figure 1-1: 1,8-Bis(dimethylamino)naphthalene (DMAN) - The original Proton Sponge™**

The relatively simple structure of DMAN is shown in figure 1-1, where the structural aspects that impart its superbasic properties may not be immediately apparent. The lone pairs of electrons on the two nitrogen atoms are in close proximity, which results in electrostatic repulsion and a significant strain on the neutral molecule. Protonation effectively reduces this strain and flattens the helical-twisted neutral structure ( $19.9^\circ$  torsion) into a planar conformation (fig. 1-2). This is accompanied by a reduction in  $N\cdots N$  distance from  $2.804 \text{ \AA}$  to  $2.574 \text{ \AA}$ . The hydrogen bond is strongly shielded by the methyl groups, so although DMAN has a high thermodynamic basicity, both its kinetic basicity and N-nucleophilicity are low – the latter an advantage for avoiding reaction interference by base coordination, such as in transition metal catalysed reactions or those with components sensitive to Lewis bases.<sup>1,7</sup>

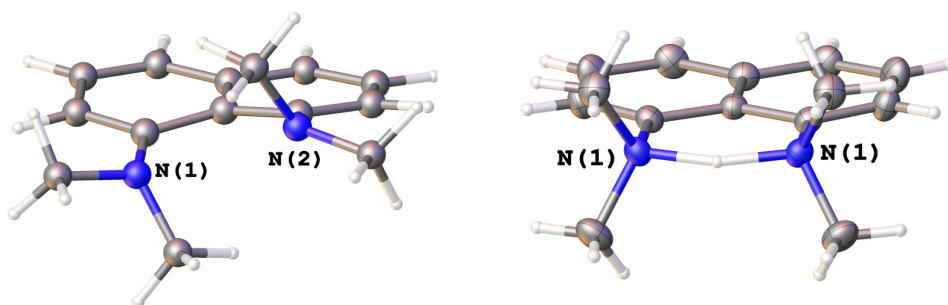


Figure 1-2: X-ray structures of DMAN in neutral (left) and protonated (right) forms. Images generated in Olex2<sup>8</sup> from CCDC files DMANAP01<sup>9</sup> and CEJGUU<sup>10</sup> with 50% ellipsoids. Counterion (CF<sub>3</sub>O<sub>3</sub>S<sup>-</sup>) omitted from DMANH<sup>+</sup> (right) for clarity.

The discovery of this structural phenomenon led to the development of new neutral organic superbases - the definition used here is of ‘a base with a  $pK_a$  of the conjugate acid greater than that of the proton sponge DMAN<sup>3, 11</sup> - with varied chemical moieties. For example some, like triguanidinophosphazene (fig. 1-3B) and *N*<sup>4</sup>,*N*<sup>4</sup>,*N*<sup>5</sup>,*N*<sup>5</sup>-tetramethyl-1,8-dioxide-arsenino[2,3-*b*]arsenin-4,5-diamine (fig. 1-3C), feature phosphazene and aromatic pnictogen oxide groups respectively.<sup>11-14</sup>

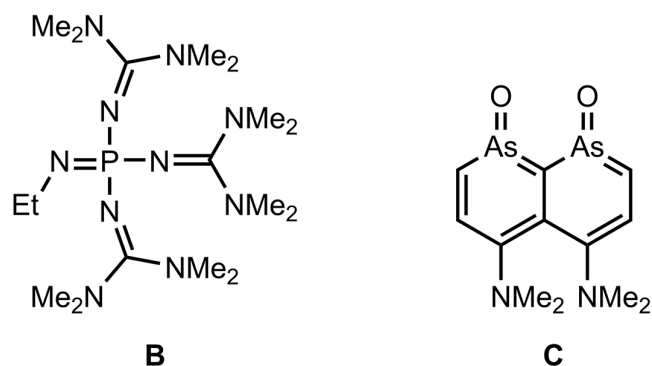
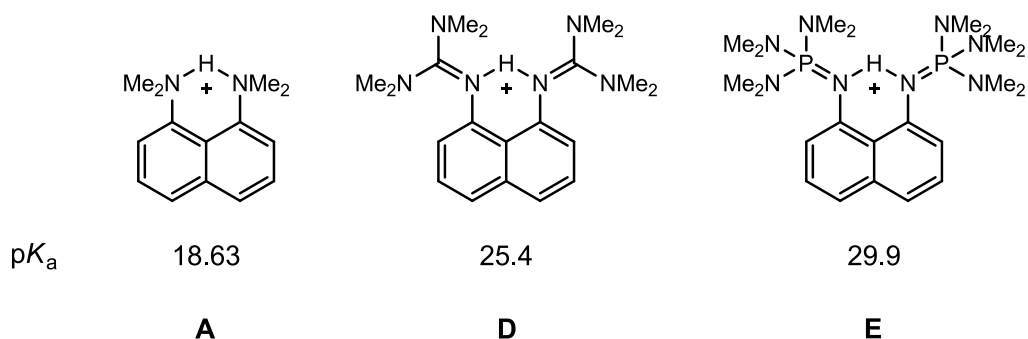


Figure 1-3: Structures of triguanidinophosphazene (B) *N*<sup>4</sup>,*N*<sup>4</sup>,*N*<sup>5</sup>,*N*<sup>5</sup>-tetramethyl-1,8-dioxide-arsenino[2,3-*b*]arsenin-4,5-diamine (C).

This new subset of organic superbases are, like the parent DMAN, known as proton sponges. The exact parameters defining the category of ‘proton sponges’ varies,<sup>1, 15</sup> however molecules are commonly classed as such with a superbasic  $pK_a$  (as above) combined with the feature enhanced basicities resulting from the formation of intramolecular hydrogen bonds upon protonation, often with the “destabilising overlap of the lone pair of electrons on adjacent nitrogen atoms within the molecule”<sup>15, 16</sup> The  $pK_a$  values of the conjugate acids of two newer proton sponges, TMGN<sup>17</sup> and HMPN<sup>18</sup>, are shown in figure 1-4. As in DMAN (fig. 1-4A), these are also derivatives of 1,8-

diaminonaphthalene, however the structural alterations resulted in significantly increased basicities: In TMGN (fig. 1-4D), this is contributed to by the inherent basicity of the guanidinium moieties, and high strength of the resulting intramolecular hydrogen bond (IHB). The conjugate acid of HMPN also has a strong IHB, and this combines with the reduction of the significant steric strain of the bulky groups of the neutral molecule to give a  $pK_a$  of 29.9 (fig. 1-4E).



**Figure 1-4:**  $pK_a$  values in acetonitrile for the conjugate acids of DMAN (A), TMGN (D) and HMPN (E).<sup>16-18</sup>

See chapter 4 for more information on TMGN and HMGN.

## 1.2 - Coordination potential of diamines and proton sponges

Proton sponges containing nitrogen proton acceptors that form intramolecular N-H $\cdots$ N hydrogen bonds are typically stronger bases than the O-H $\cdots$ O equivalents, so diamines are a common feature.<sup>16</sup>

Throughout literature, diamines of various forms are one of the most common bidentate metal-binding moieties in a range of chemical fields, from 2,2'-bipyridine in luminescent compounds to the salen ligands widespread in catalysis. They are also present in large coordination structures that show structural and/or functional changes in response to a series of stimuli, such as light (fig. 1-5), mechanical or pH.<sup>19</sup>

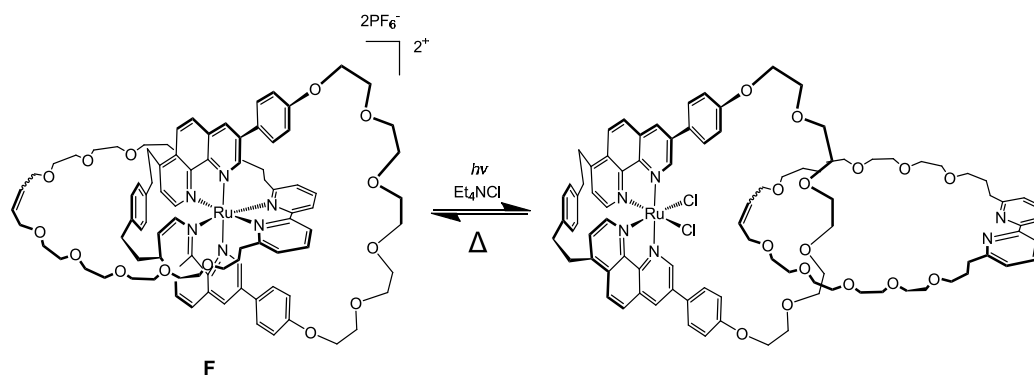


**Figure 1-5: Example of a light-responsive coordination complex (F) involving bidentate diamine binding sites. Adapted with permission from Mobian et al.<sup>20</sup> Copyright 2004 Wiley-VCH.**

Coordination cages are a type of large, multinuclear coordination structure in which bidentate, diamine ligands are a common feature. They consist of organic linkers connected by metallic components to form discrete structures with well-defined cavities. This is a growing field and several excellent reviews have been published showcasing recent developments.<sup>21-33</sup> Methods of construction are being developed to widen the functionality of coordination cages, with applications of these including: research into uses of cages from elucidation of reaction mechanisms,<sup>34</sup> potential drug delivery systems,<sup>35</sup> to a more recent focus on catalysis (fig. 1-6).<sup>36-37</sup> The unique microenvironments within cages provide a wealth of opportunities<sup>37</sup> – these include effects of increased local concentrations by enclosing reaction components within the cage ‘walls’ of a cage and manipulation of components into orientations that may otherwise be unfavourable in solution, and thus induce the formation of uncommon synthetic conformations. Research into the addition of stimuli-responsive properties is ongoing, and has the potential to significantly enhance cage function.<sup>19</sup>

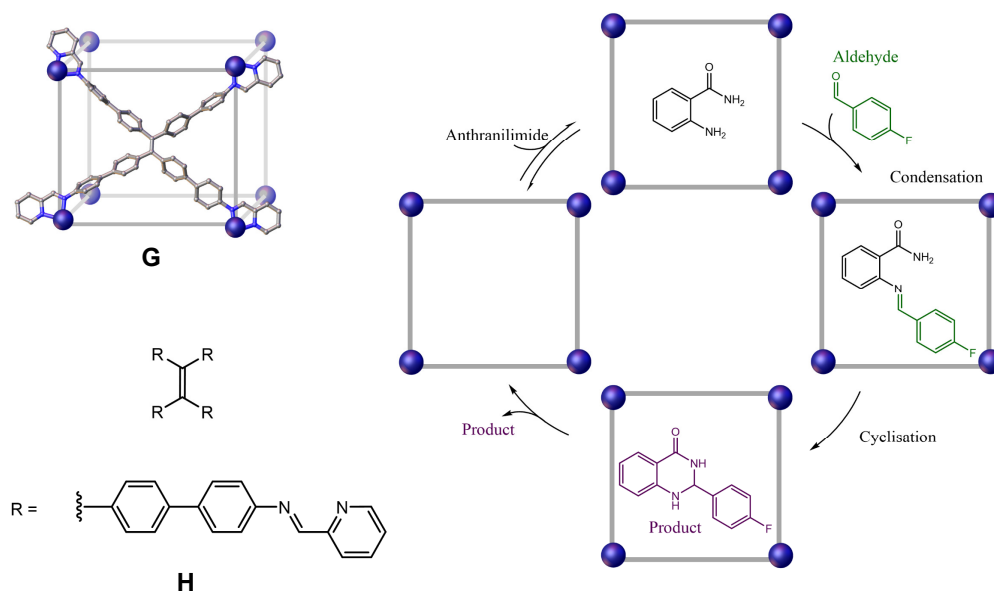


**Figure 1-6: Example of a multistep catalysis (right) by a hexahedral coordination cage (G) featuring a ligand (H) with bidentate diamine binding sites.<sup>36</sup>**

Given the significant structural changes observed during protonation in proton sponge materials, there is interest in finding proton sponge organic superbases that could also act as ligands, as these could be used to create stimuli-responsive metal complexes.<sup>11</sup>

Although numerous proton sponges contain bidentate diamine moieties similar to those used in coordination structures, the ability of many of them to chelate metal ions is as yet in the early stages of exploration, and has been hampered by obstacles. Sixteen years passed after the synthesis of DMAN before a transition metal complex involving the molecule (with Pd(II)) was published - to date it is the only one reported (fig. 1-7).<sup>38</sup> In part, the lack of complexes is caused by the very aspects of DMAN that contribute to the high  $pK_a$ . The N-methyl groups that provide hydrophobic shielding to the hydrogen bond that forms also sterically hinder the coordination process, significantly reducing this diamine's coordination potential.

In contrast to the reduced N...N separation and planar conformation of DMAN observed on protonation (fig. 1-2), the Pd(II)-coordinated DMAN showed significant increases in both the torsional twist ( $34.7^\circ$  vs.  $19.9^\circ$ ) and N...N distance ( $2.94 \text{ \AA}$  vs.  $2.80 \text{ \AA}$ ) while the



metal ion is located 0.862 Å above the NCCCN plane (fig. 1-7). The complex has low thermodynamic stability, and the metal ion can be displaced by water.

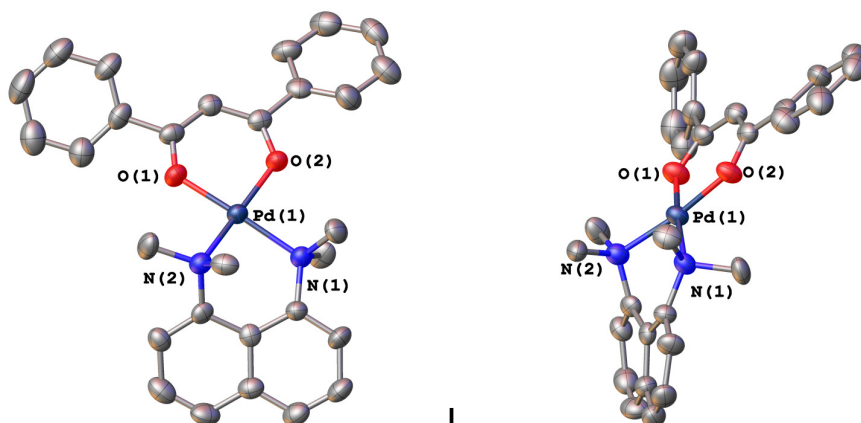


**Figure 1-7: Coordination of a Pd(II) ion by DMAN (I), completed with a 1,3-diphenylpropane-1,3-dionato-O,O<sup>-</sup> ligand. Hydrogen and counter-ion (HFAC<sup>-</sup>) omitted for clarity. Image generated in Olex2<sup>8</sup> from CCDC file OBEJIP<sup>38</sup> with 50% ellipsoids.**

Publications featuring a metal ion coordinated to the proton binding site of ‘proton sponges’ are relatively few.<sup>39-40</sup> Several of these chelating sponges are derivatives of DMAN with the foundation 1,8-diaminonaphthalene core, such as TMPN (conjugate acid  $pK_a$  29.3 in MeCN), which has formed the Ga(III) and Al(III) TMPN metal complexes in figure 1-8. These show the coordinated ions to be sitting similarly out of plane ((1.207 Å and 1.11 Å) above the NCCCN plane respectively) but showing significantly more planar ligand structures than the Pd(II) DMAN complex (fig. 1-7) with only slight torsional twists (1.47° and 2.64°, fig. 1-8).<sup>40</sup>

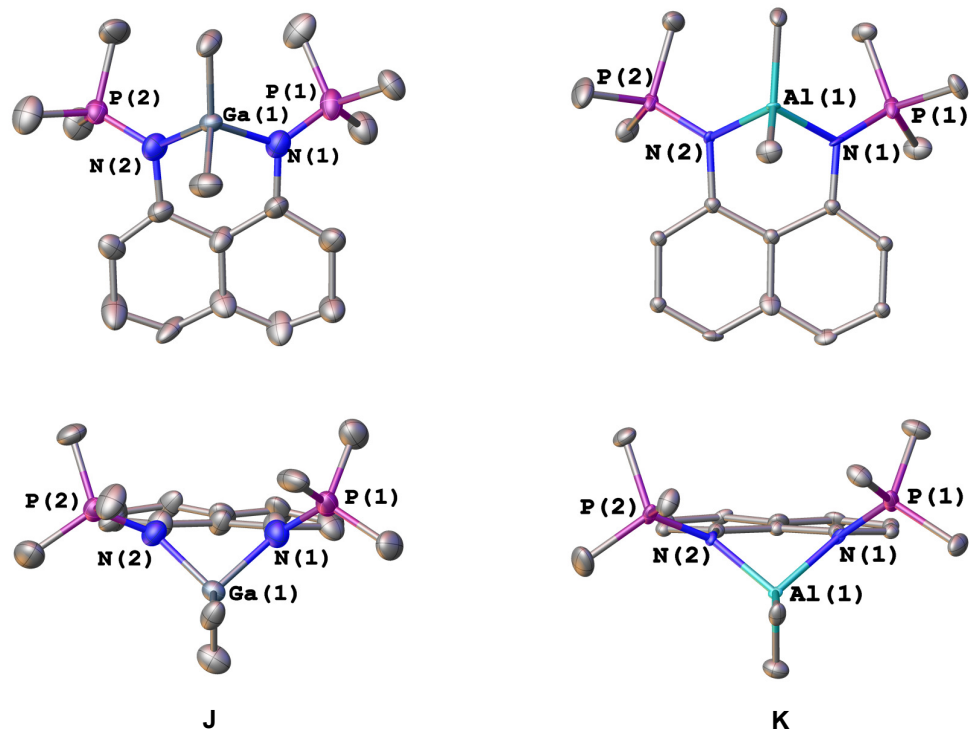


**Figure 1-8: Complexes of TMPN with Ga(III) (J) and Al(III) (K) in front (top) and side-plane (lower) views. Hydrogen omitted for clarity. Images generated in Olex2<sup>8</sup> from CCDC files BIXQEG and BIXQAC with 50% ellipsoids.<sup>40</sup>**

Towards the opposite end of the scale of coordination publication numbers to DMAN and other proton sponges is the aromatic bidentate diamine 1,10-phenanthroline (phen) (fig. 1-9L). Derivatives of this are ubiquitous in coordination chemistry: A SciFinder structural search featuring the phen substructure with a centrally-bound metal ion produces more than 83000 results.<sup>41</sup> However, unsubstituted phen only has a  $pK_a$  of 4.27, falling far short of the basicity required for the classification of a 'proton sponge'.

This gap between proton-sponges and coordinating ligands could be bridged with other promising aromatic diamines: such as derivatives of the proton sponge quinolino[7,8-*h*]quinoline (<20 SciFinder metal complex hits, fig. 1-9QQ).<sup>41</sup>

### 1.3 - A New Type of Proton Sponge – quinolino[7,8-*h*]quinoline

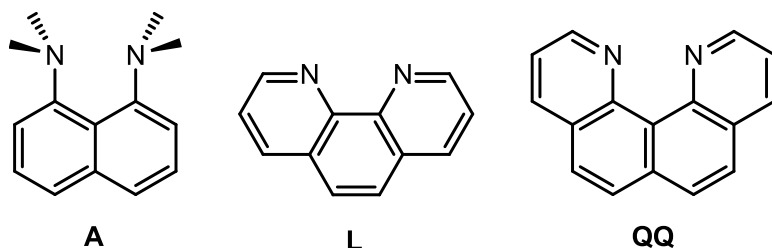
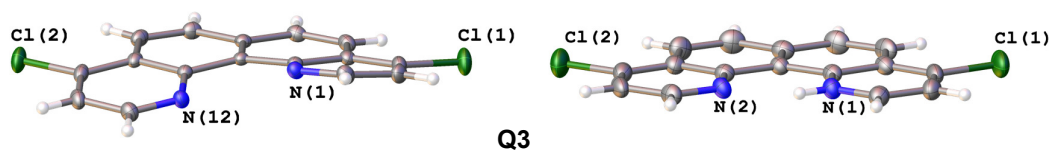


Figure 1-9: Structures of DMAN (A), 1,10-phen (L) and quinolino[7,8-*h*]quinoline (QQ).

This new structure was the first example of a proton sponge that lacks the type of steric alkyl shielding observed in the original DMAN proton sponge (1,8-bis(dimethylamino)naphthalene) and many the same that have been developed on that naphthalene structure. As the shielding contributed to reduced proton exchange rates, the usefulness and potential of QQ, a kinetically active organic superbases, in chemical reaction applications is increased.<sup>42</sup> The ring structure of QQ allows for a wide range of functionalisation, and thus potential applications, such as: development of synthons for supramolecular chemistry,<sup>37</sup> with inclusion of multiple binding sites; small ion chelation;<sup>43</sup> or novel compound synthesis.

As described in 1.1, the molecule DMAN has a N...N separation of 2.804 Å;<sup>44</sup> whereas the two nitrogen atoms of QQ are forced into an even closer proximity at 2.7271(18) Å<sup>45</sup> by the rigid ortho-fused ring structure. This causes a destabilising overlap of electron lone pairs; which manifests as a significant helical distortion that disrupts the planarity, and thus aromaticity. The binding of a single proton in the central cavity reduces the repulsion and removes the strain, flattening the rings into a planar formation and thus some of the QQ derivatives are considered superbasic, placing them in the category of proton sponges.<sup>41</sup> Computational analysis gives the helical distortion of derivative 4,9-dichloroquinolino[7,8-*h*]quinoline (**Q3**) to be 21.1°, which is closely matched to the observed single crystal X-ray experimental data of 20.02(9)° for crystals grown under anhydrous conditions (fig. 1-10). Once singly-protonated, planarity in the crystal structure is observed (fig. 1-10).<sup>41</sup>



**Figure 1-10:** 4,9-dichloroquinolino[7,8-*h*]quinoline (**Q3**) structures in neutral (left) and protonated (right) forms. Images generated in Olex2<sup>8</sup> from CCDC files PANFOB and PANFUH with 50% ellipsoids.<sup>41</sup> Counter-ion ( $\text{BF}_4^-$ ) omitted from (right) for clarity.

The structure of unsubstituted, non-protonated quino[7,8-*h*]quinoline was initially reported to exist as planar,<sup>45</sup> but further data analysis of the X-ray crystal data suggested a hydrogen-bonded bridging water molecule acted in a similar role to a proton, reducing the strain and flattening the compound.<sup>11</sup>

The drive to stabilise the  $\text{N}\cdots\text{N}$  interaction also gives rise to stabilised keto-enol tautomerism in QQ derivatives containing oxo groups in 4 and/or 9 positions. Although the initial QQ synthesis reported the diketo structure of **Q2** as seen in figure 1-11, IR spectroscopic evidence supports the keto-enol tautomer (fig. 1-11) as the major form.<sup>41</sup> This is supported by calculations that have also shown this tautomer being more stable than both the 4,9-dihydroxy and diketo tautomers (fig. 1-11) by 17.6 and 12.0 kcal mol<sup>-1</sup> respectively (B3LYP/6-31+G(d,p)).<sup>11</sup>

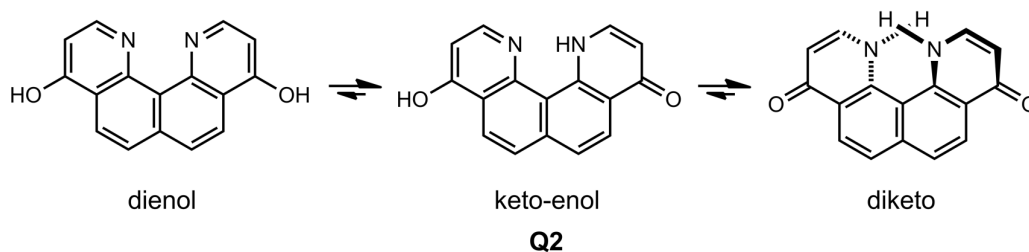


**Figure 1-11:** All tautomers of quinolino[7,8-*h*]quinoline-4,9-(1*H*,12*H*)-dione (**Q2**).

The analogous keto-enol tautomers are also present in equilibrium for **Q1** (fig. 1-15), however this compound is depicted as the diketone tautomer for consistency with literature.<sup>42, 46</sup>

Further effects of the keto-enol tautomerism of QQ derivatives are discussed in chapter 2.

### 1.3.1 - Synthesis of Quinolino[7,8-*h*]quinoline

The first structurally confirmed synthesis of the proton sponge quinolino[7,8-*h*]quinoline (QQ) was published in 1987 by Zirnstein and Staab.<sup>42</sup> Following the synthesis of DMAN, this research group was one of several that explored the base potential of other aromatic backbones with reduced N...N distances (such as 4,5-bis(dimethylamino)phenanthrene) that could be capable of forming intermolecular N-H...N bonds with an optimised geometry (linear).<sup>3, 47</sup>

Prior to the Staab synthesis, however, two other QQ syntheses were reported, both by attempts at double Skraup condensation, the well-established methodology used for the synthesis of quinolines. The Skraup reaction involves several steps, shown in figure 1-12. These include glycerol dehydration to give acrolein, which then undergoes nucleophilic addition to the aniline derivative (fig. 1-12(i)). This precedes protonation, electrophilic attack of the aromatic ring by the aldehyde, cyclisation (fig. 1-12(ii - iv)), and aromatisation (fig. 1-12(v)).<sup>48</sup>

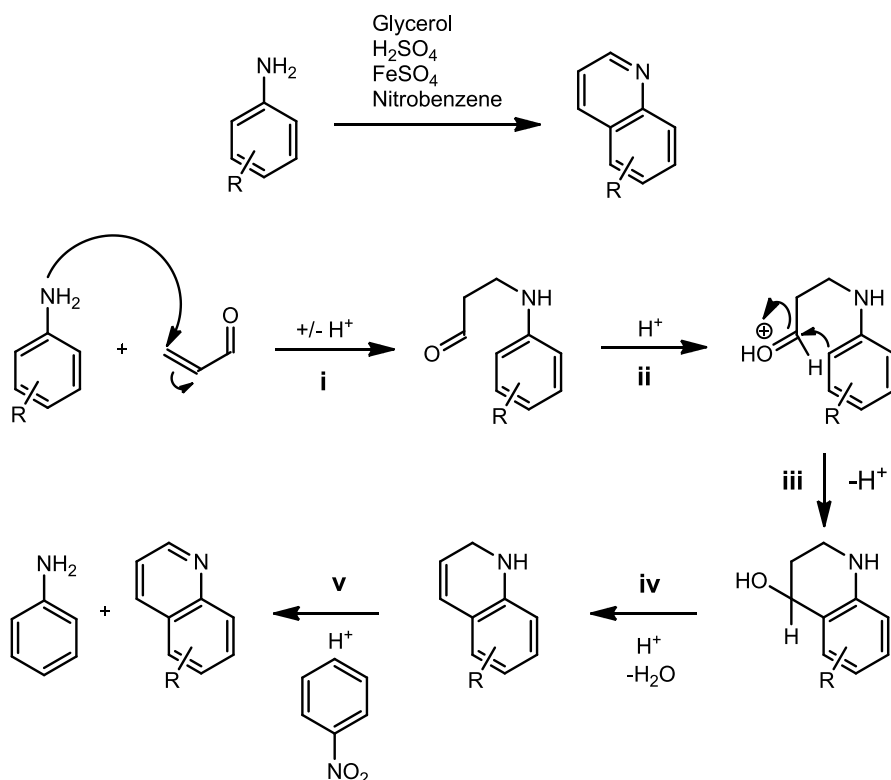
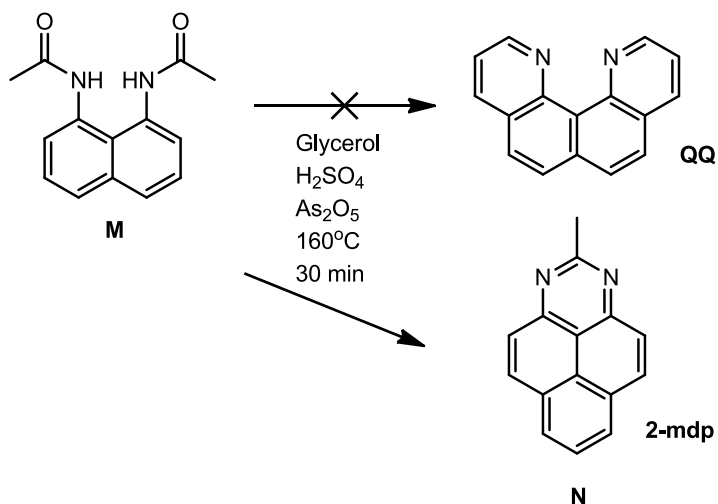


Figure 1-12: Skraup reaction (top) and mechanism (partial) to form quinoline.<sup>48</sup>

The first, reported in 1950<sup>49</sup>, utilised 1,8-diaminonaphthalene, however this was later noted by the authors to be an incorrect product identification.<sup>50</sup> Dufour et al. (1967) also tried to replicate the 1950 procedure, and, when that was unsuccessful, reported the synthesis of quinolino[7,8-*h*]quinoline from 1,8-diacetaminonaphthalene: however elemental analysis, a melting point and the formation of a picrate salt was the only characterisation provided.<sup>51</sup>

Attempts were made to use the 1967 research methods for QQ synthesis by Sauvage and coworkers in 1985, however successful replication was not achieved. Researchers found that instead of the desired double Skraup condensation, addition across the two diamide nitrogen atoms occurred, along with the C-C bond formation to produce 2-methyl-diazapyrene (2-mdp), with confirmation of identity by mass and <sup>1</sup>H NMR spectroscopies (fig. 1-13N).<sup>52</sup>



**Figure 1-13: Attempted formation of QQ by Skraup condensation by Sauvage and coworkers that resulted in formation of 2-mdp (N).<sup>52</sup>**

The reaction to form 2-mdp from 1,8-diacetaminonaphthalene (fig. 1-13) involves the formation of a 6-membered perimidine ring, then a Bally-Scholl type reaction.<sup>52</sup> This begins with the conjugate addition of acrolein (formed by glycerol dehydration in the first step of the Skraup condensation), then cyclisation, water loss and aromatisation (fig. 1-14).<sup>53</sup>

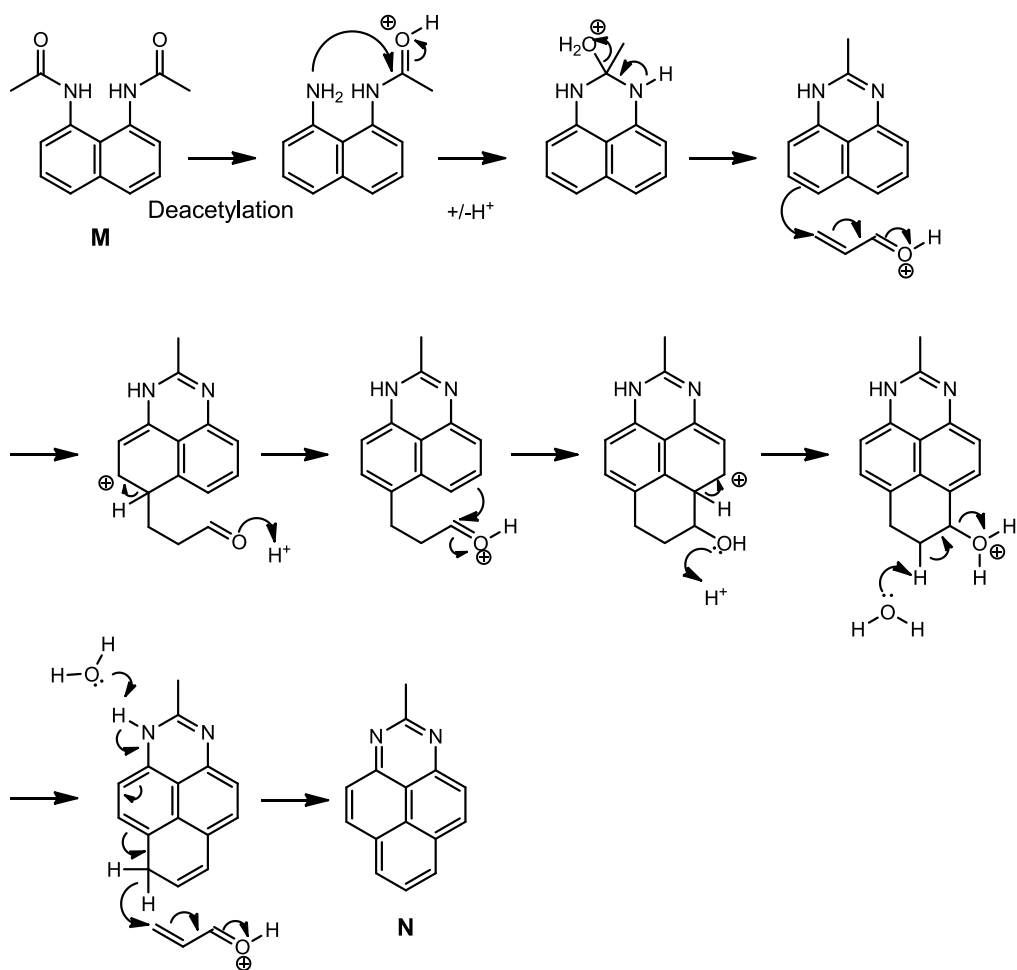
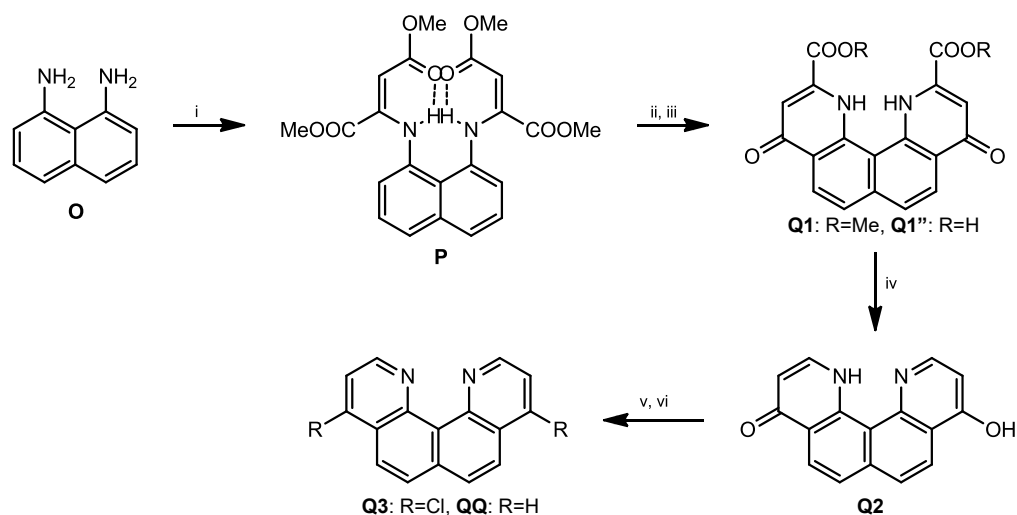


Figure 1-14: Proposed mechanism of formation of 2-mdp (N) from 1,8-diacetaminonaphthalene (M).

### 1.3.1.1 - Staab (1987) and Plieger (2012) QQ syntheses



**Figure 1-15: Initial quinolino[7,8-*h*]quinoline synthesis by Zirnstein and Staab, 1987.<sup>11,54</sup>**  
Reaction conditions and yields: (i) DMAD, MeOH, RT, 71%; (ii) Ph<sub>2</sub>O, 240 °C, 64%; (iii) (a) KOH, 100 °C; (b) HCl, H<sub>2</sub>O, 93%; (iv) 370 °C, 10<sup>-5</sup> torr 76%; (v) POCl<sub>3</sub>, 130 °C, 81%; (vi) Pd/C, HOAc, NaOAc, 39%.

The confirmed synthesis by Zirnstein and Staab, as presented in figure 1-15, took seven steps, starting from 1,8-diaminonaphthalene (O) and dimethyl acetylenedicarboxylate (DMAD) (fig. 1-15).

The product (P) of the first reaction (fig. 1-15(i)) was thermally cyclised and subject to an alkaline hydrolysis (Q1'') before undergoing a high temperature low pressure decarboxylation to produce 9-hydroxyquino[7,8-*h*]quinolin-4(1*H*)-one (Q2). Subsequently, Q2 was subject to halogenation with concomitant aromatisation of the second ring to produce the dihalide Q3, which was converted into pure unsubstituted quinolino[7,8-*h*]quinoline (QQ) by catalytic hydrogenation. The first two steps modified methodology developed by Honda et al. (1983)<sup>46</sup>

Subsequent research by other groups was slow. Zewge et al.<sup>55</sup> synthesised quinolino[7,8-*h*]quinoline-4,9-(1*H*,12*H*)-dione (fig. 1-15, Q2) as part of a wider study looking at quinolone heterocycle synthesis in 2007, but that, and a study by Wüstefeld et al.<sup>56</sup> on metal complexes, were the only new non-theoretical papers involving QQ published for 25 years after the initial Staab synthesis.<sup>42</sup>



A breakthrough in quinolino[7,8-*h*]quinoline research was made by the Plieger group, with a change in the synthetic procedure published in 2012 that improved research accessibility to the derivatives.<sup>41</sup> Amongst modifications that improved several steps in the pathway, the bottleneck two-step low pressure/high temperature de-esterification was altered to a milder synthetic route, based on the work of Strauss and Trainor.<sup>57</sup> The introduction of hydrothermal methods with a pressurised reaction vessel removed a synthetic step, resulting in a reliable ‘one-pot’ reaction (fig. 1-15, **Q1**→**Q2**) with comparable yields and reduced time cost. Smaller amounts of **Q2** could also be obtained in microwave reactor reaction, however the scale was much more limited (0.1 g of **Q1** vs. 0.8 g).<sup>41</sup>

Following this publication, both the frequency of publications involving QQ, and the number of overall QQ structures published has increased (fig. 1-16).

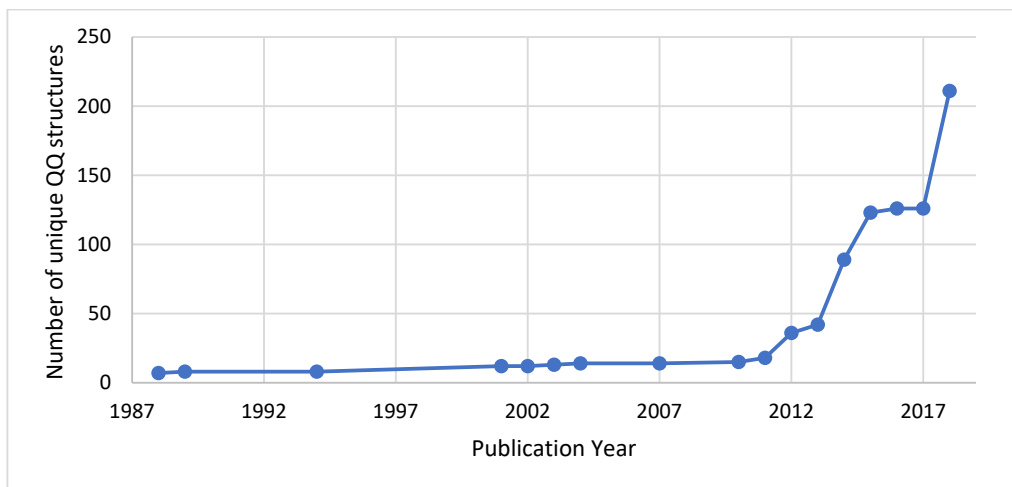


**Figure 1-16: Total QQ structures (with assigned CAS numbers) published 1987-2019. Data points indicate years in which one or more QQ-derivative-containing publications were released. Data includes complexes and salts, and those present only in patent literature. Some of these publications are discussed in the following sections.**

### 1.3.2 - Naming and numbering of quinolino[7,8-*h*]quinoline derivatives

IUPAC regulations prior to 2013 described the prefix quino- as an acceptable short form of quinoline for the ortho-fused substituent heterocycle,<sup>15, 41-42, 45-46, 52, 56, 58-59</sup> and this is

commonly used in past publications involving QQ. Updated regulations state this prefix to be no longer accepted nomenclature:<sup>60</sup> Quinolino- will be used hereafter. Quinolino[7,8-*h*]quinoline naming and numbering is shown in Figure 1-17.

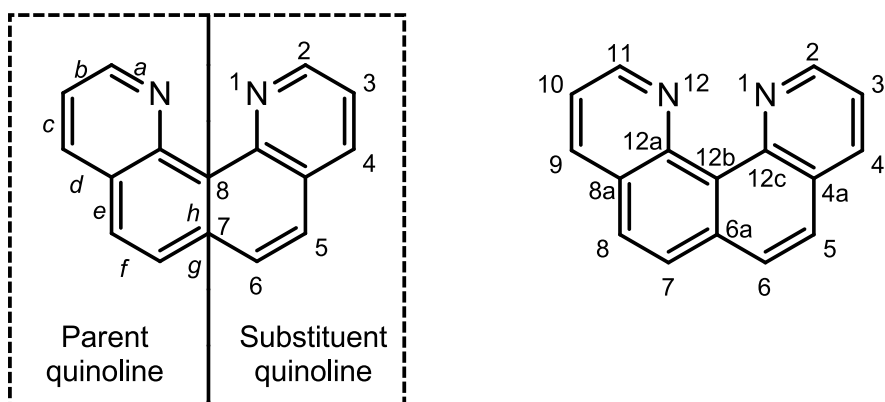


**Figure 1-17: Nomenclature of quinolino[7,8-*h*]quinoline (left) and numbering scheme for atoms/substituents (right).**

Described by Rowlands et al., the naming system is based on the fused quinoline substituent and parent ring structures, with the fusion locant described as 7,8-*h*: they are joined across the *h*-face between atoms 7 and 8. For the correct numbering of this type of fused-ring system, the compound is positioned to give the greatest number of rings first laterally, then turned so the maximum number of rings are above and to the right of this row. Numbering is assigned clockwise from the top right ring, other than the bridgehead atoms which are labelled with letters and the number of the preceding numbered atom as shown, beginning at the most counter clockwise atom (nitrogen atom).<sup>11, 61-63</sup>

### 1.3.3 - Derivatisation of quinolino[7,8-*h*]quinoline

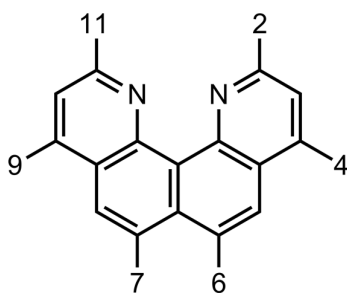


**Figure 1-18: Quinolino[7,8-*h*]quinoline substituent numbering.**

A substructure search of the SciFinder database revealed a total of 33 structures with the QQ core published (outside of patents) across 14 publications from 1987-2019. These 33 are based on ~ 14 organic derivatives in a variety of complex and salt forms. Structures containing the QQ substructure but with additional fused rings (2 or more bridging atoms) are discussed in 1.3.4.

A further ~178 QQ structures can be found in the patent literature. These are not detailed in this section. Additionally, derivatives first published in Rowlands et al. are generally excluded from this chapter as the majority were produced in the course of this project.<sup>11</sup>

Quinolino[7,8-*h*]quinoline shows similarities to its components, the aromatic heterocycle quinoline, with reflected regioselectivity and substitution patterns, making the wealth of quinoline chemistry a useful resource in the development of quinolino[7,8-*h*]quinoline pathways. However, there are important differences that affect the synthetic chemistry involved - including the basicity of QQ. Without the structural factors (discussed earlier) that give QQ the properties of a proton sponge, quinoline is a weak base, with a  $pK_a$  (conjugate acid) of only 4.9, affecting comparative interactions with protic or base-sensitive reaction components.<sup>64</sup> This structure also makes quinoline a better nucleophile, as the nitrogen atom of quinoline is less sterically hindered than those in QQ. Additionally, the solubility of QQ derivatives are often more limited than those of quinoline, of which the core structure is soluble in many organic solvents as well as alcohols and, to a slight extent, water.<sup>65</sup>

#### **1.3.3.1 - 4,9-Derivatisation**

Research has shown the 4- and 9- positions of the QQ ring are the easiest places for functionalisation and the formation of new derivatives. The first quinolino[7,8-*h*]quinoline derivative synthesised was by Staab et al. in 1987<sup>42</sup> - 4,9-dichloroquinolino[7,8-*h*]quinoline (**Q3**), which was formed during the penultimate reaction of the QQ synthetic pathway.

Along with other halogen equivalents, in particular 4,9-dibromoQQ, this is an effective and versatile starting point for many other reactions, including Suzuki–Miyaura coupling, simple substitutions, amine formation etc.<sup>11</sup>

The Plieger Group, with the altered core synthetic route, synthesised several different derivatives in this manner, ranging from tertiary amines to methoxides such as 4,9-dimethoxyquinolino[7,8-*h*]quinoline (**Q20**).<sup>15</sup> A number of different 4,9-QQ derivatives have also been synthesised (under CN patent) by Qiu, Tang, Li, Fan, Duan, Ren and Xueyan who focussed on tertiary amines with large bulky aromatic groups and utilised the methodology of the Plieger Group.<sup>15, 66</sup>

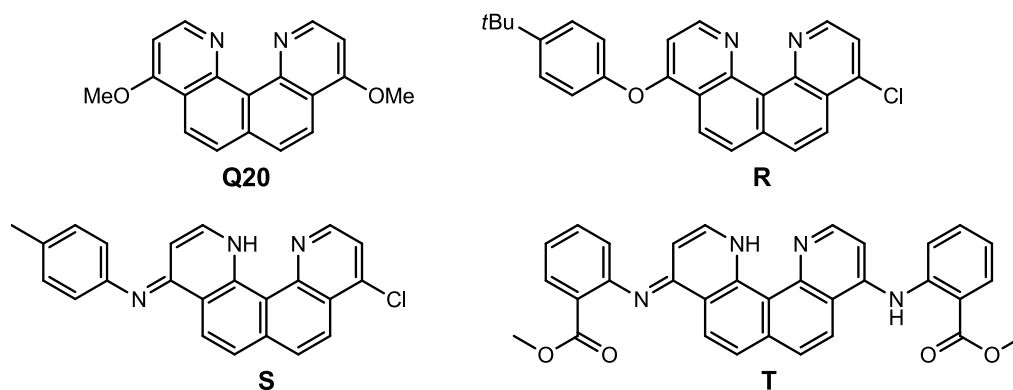


**Figure 1-19: Selected examples of published 4,9-substituted QQ derivatives.**<sup>11, 15</sup>

During some of the attempted 4,9-halogen substitution reactions, side products were observed in which one of the halogen atoms was unexpectedly substituted with an oxo group.<sup>15</sup> Researchers hypothesised this was due to the proton sponge properties (strong basicities) of the compounds giving rise to stabilised keto-enol tautomerism following hydroxyl group substitution.

Consequently, this stability means kinetically less favourable 4,9-substitution reactions often result in non-symmetric compound formation, with one halogen group reacting as desired while the other is converted back to an oxo- group, allowing the tautomer of the type figure 1-11 (keto-enol) to form. This behaviour creates an opportunity; an exciting new avenue of research for the synthesis of non-symmetric derivatives is opened up,

with the second position able to be substituted by a different group - something that is typically difficult to achieve with symmetrical starting materials.

The opportunities and complications arising from this phenomenon of keto-enol tautomerism, and from the high basicity of QQ derivatives, are discussed further in the synthesis section (chapter 2).

### 1.3.3.2 - 2,11-Derivatisation

Functionalisation of the 2 and 11 positions of quinolino[7,8-*h*]quinoline can be achieved by forgoing the de-esterification step (fig. 1-15, **Q1**→**Q2**) to leave the methyl esters attached, while the remaining ring positions can theoretically still be accessed by the aforementioned methods. A crystal structure was obtained of such a compound (fig. 1-20, 2,11 = COOMe, 4,9 = Cl),<sup>15</sup> however subsequent alteration of either the ester or chloride groups is as yet unsuccessful.<sup>54</sup>

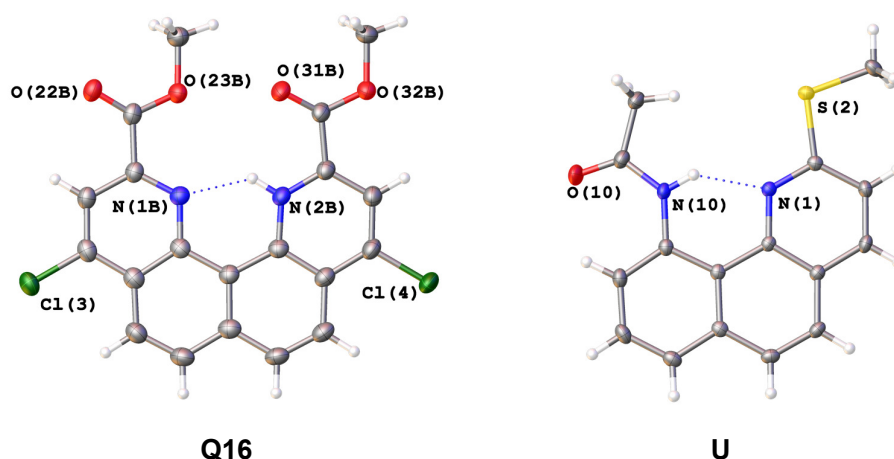


**Figure 1-20:** Crystal structures of dimethyl 4,9-dichloroquinolino[7,8-*h*]quinoline-2,11-dicarboxylate (**Q16**) and *N*-[2-(methylthio)benzo[*h*]quinolin-10-yl]acetamide (**U**). Counter-ion ( $\text{BF}_4^-$ ) not shown for clarity (left). Images generated in Olex2<sup>8</sup> using CCDC files FEJXID and FEJXEZ with 50% ellipsoids.<sup>15</sup>

In 2004 Panda et al. reported a new pathway to 2-(methylthio)quinolines by a double Skraup cyclisation,<sup>67</sup> which could have provided an alternate functionalisation option, however the chemistry was unable to be repeated despite several attempts – it was suspected that the reaction does not proceed further than single cyclisation and acetylation to produce *N*-[2-(methylthio)benzo[*h*]quinolin-10-yl]acetamide (fig. 1-21U),

made favourable by the formation of the intramolecular hydrogen bond bridged between the central nitrogen atoms of this product. This compound was obtained in small amounts and was confirmed by X-ray crystallography (fig. 1-20U).<sup>11, 15</sup> As the purification methods described by the authors are incompatible with those typically successful for QQ, and as no analytical data was presented, the initial reported QQ synthesis may have been incorrect.<sup>54</sup>

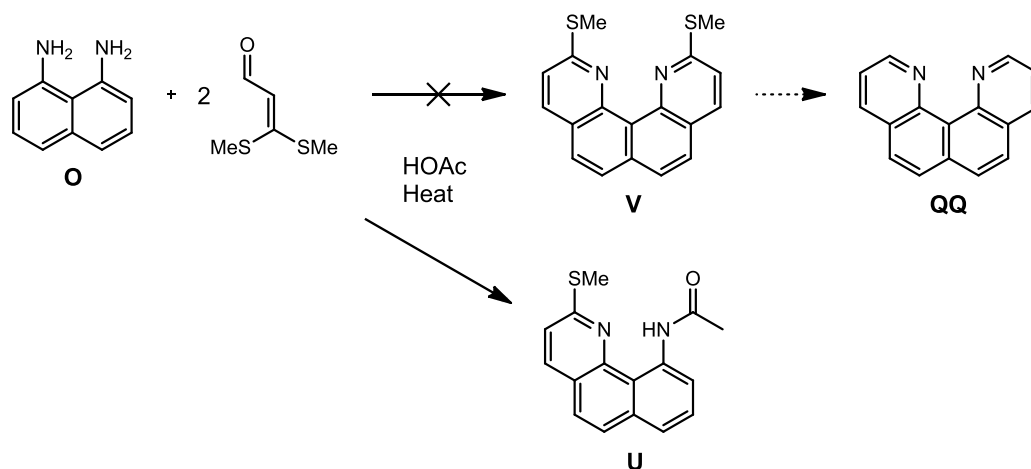


**Figure 1-21:** Attempted synthesis of QQ from 1,8-diaminonaphthalene (O) and 3-bis(methylthio)acrolein by Skraup condensation, resulting in the formation of *N*-[2-(methylthio)benzo[*h*]quinolin-10-yl]acetamide (U) instead of the desired disubstituted product (V).

### 1.3.3.3 - 6,7-derivatisation

The 6,7 positions on the QQ ring can be functionalised by a standard HNO<sub>3</sub>/H<sub>2</sub>SO<sub>4</sub> nitration of 4,9-dichloroquinolino[7,8-*h*]quinoline (fig. 1-22, Q3), which occurs with good regioselectivity<sup>54</sup> – a substitution pattern that matches that of the nitration of 4-hydroxyquinoline.<sup>68</sup>

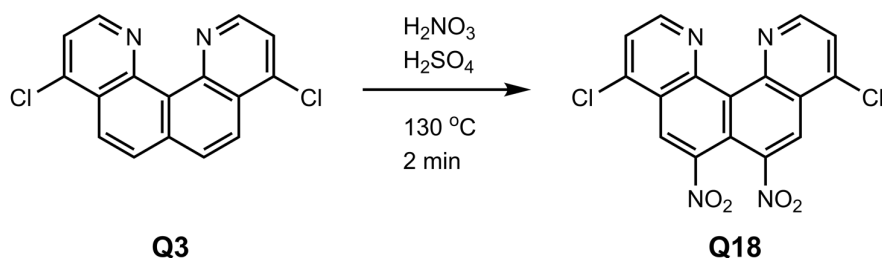


**Figure 1-22:** Nitration of 4,9-dichloroquinolino[7,8-*h*]quinoline (Q3).<sup>54</sup>

However, although NMR and mass spectroscopic evidence very strongly supported the formation of 4,9-dichloro-6,7-dinitroquino[7,8-*h*]quinoline (fig. 1-22, **Q18**), X-ray crystallographic data collected on crystals grown in CH<sub>3</sub>CN revealed that over some time period this compound had partially hydrolysed to 4-chloro-9-oxo-9,12-dihydro-6,7-dinitroquino[7,8-*h*]quinoline (fig. 1-23), made favourable by the keto-enol tautomerism (discussed in chapter 2).<sup>11</sup>

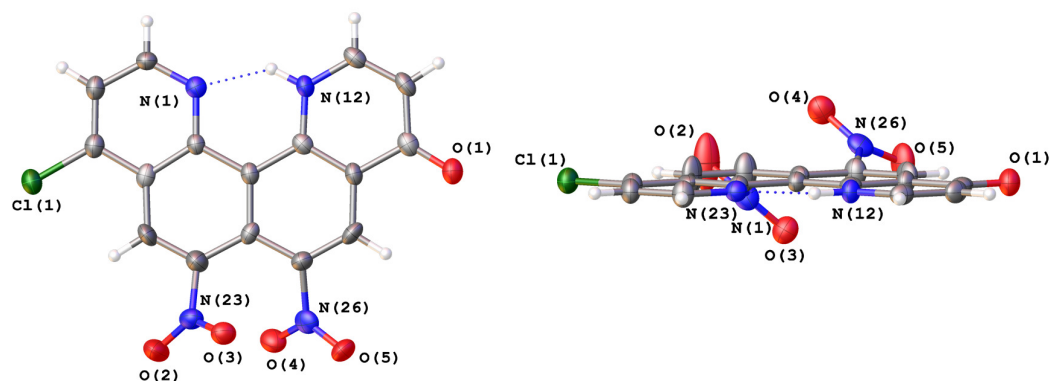
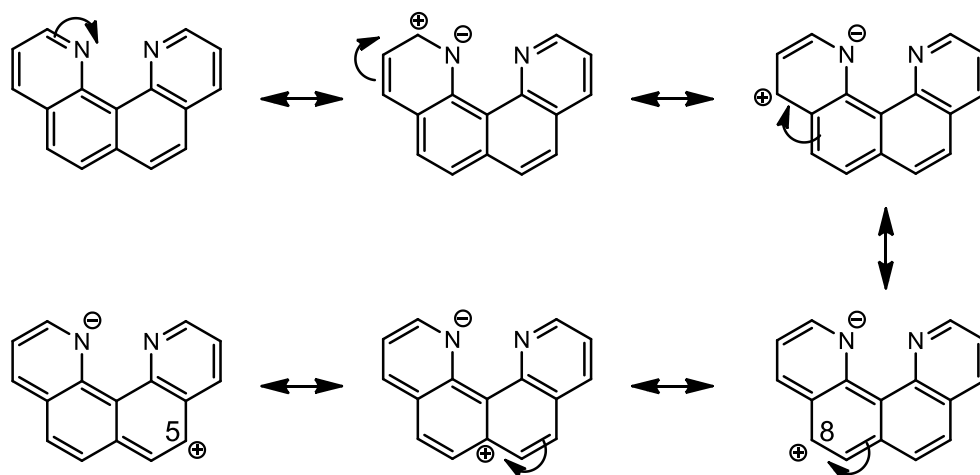


Figure 1-23: X-ray structure of 4-chloro-9-oxo-9,12-dihydro-6,7-dinitroquino[7,8-*h*]quinoline (**Q21**).<sup>11</sup> Generated in Olex2<sup>8</sup> with 50% ellipsoids.

#### 1.3.3.4 - 5,8-derivatisation

To date, no QQ structures containing modifications at the 5 and 8 positions have been published (excluding fused ring systems).<sup>41</sup> As with quinoline, nucleophilic substitution occurs more readily on the electron poor pyridine ring, and electrophilic aromatic substitution on the benzene ring. However, resonance structures can be drawn that give the 5 and 8 positions partial positive character, thus reducing the favourability of electrophilic attack (fig. 1-24).



**Figure 1-24: Resonance structures of QQ showing the partial positive character of positions 5 and 8.**

This is reflected in published quinoline structures – SciFinder substructure searches of quinoline derivatives with single non-hydrogen ring substitutions gives the lowest number of results for the 5 position (followed by the 3<6<4<2 positions).<sup>69</sup>

### 1.3.4 - Other organic compounds with the QQ substructure

Selected publications outside of patent literature feature compounds with a QQ substructure, but not classed as QQ derivatives for the purposes of this project, which show one or more of the core ring positions fused to another ring. These include large extended polycyclic aromatic hydrocarbons, where the substructure is a small part of a larger system with covalent carbon links between the nitrogen positions and across ring carbons,<sup>70</sup> or aza-fullerenes.<sup>71</sup> A DFT study published Peran et al. examined the superbasic properties of smaller polycyclic ‘croissant-like’ compounds like the example shown in figure 1-25 (W), which have the QQ core but contain rings across the 2,3 and 10,11 carbon atoms of QQ. The synthesis of these compounds was not reported.<sup>72</sup>



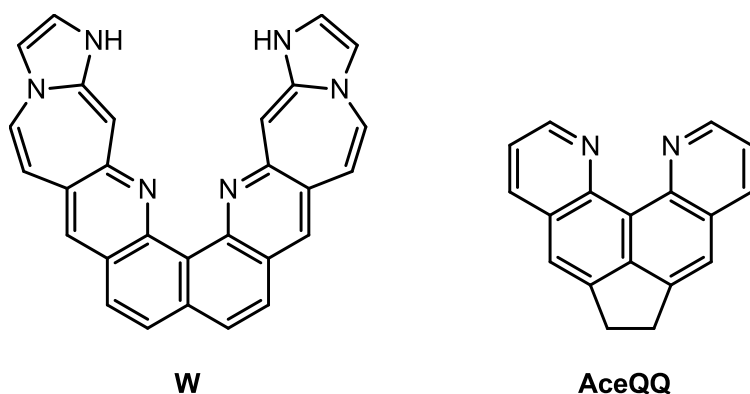


**Figure 1-25: Examples of other organic compounds with the QQ substructure, with a polycyclic 'croissant-like' compound (W) and acequinolino[7,8-*h*]quinoline (AceQQ).**

Of the other QQ substructure-containing compounds in literature, the one with the most similar structure to QQ, is acequinolinoquinoline (fig. 1-25), a strong base with a conjugate acid  $pK_a$  of 7.9 in DMSO, greater than DMAN at 7.5 (in DMSO). The synthesis of this compound was first reported in 1968 by Dufour et al. by a Skraup synthesis,<sup>73</sup> but the compound captured little research interest until the recent modified procedure published by Pozharskii et al. (2019).<sup>59</sup> Researchers used a Skraup reaction with glycerol, sodium *m*-nitrobenzenesulfonate,  $FeSO_4 \cdot 7H_2O$  and  $H_2SO_4$  to form aceQQ in 58% yield (purified by column chromatography). A mechanism for this procedure is given in figure 1-26.

The ethyl ring carbon linker significantly increases the rigidity of the heterocycle, which increases fluorescence over the more flexible QQ, however may reduce metal ion coordination potential. While the more direct synthesis of aceQQ is more efficient than QQ's, the pathway means avenues for ring functionalisation are reduced, with no derivatives yet reported outside of patent literature.<sup>59</sup>

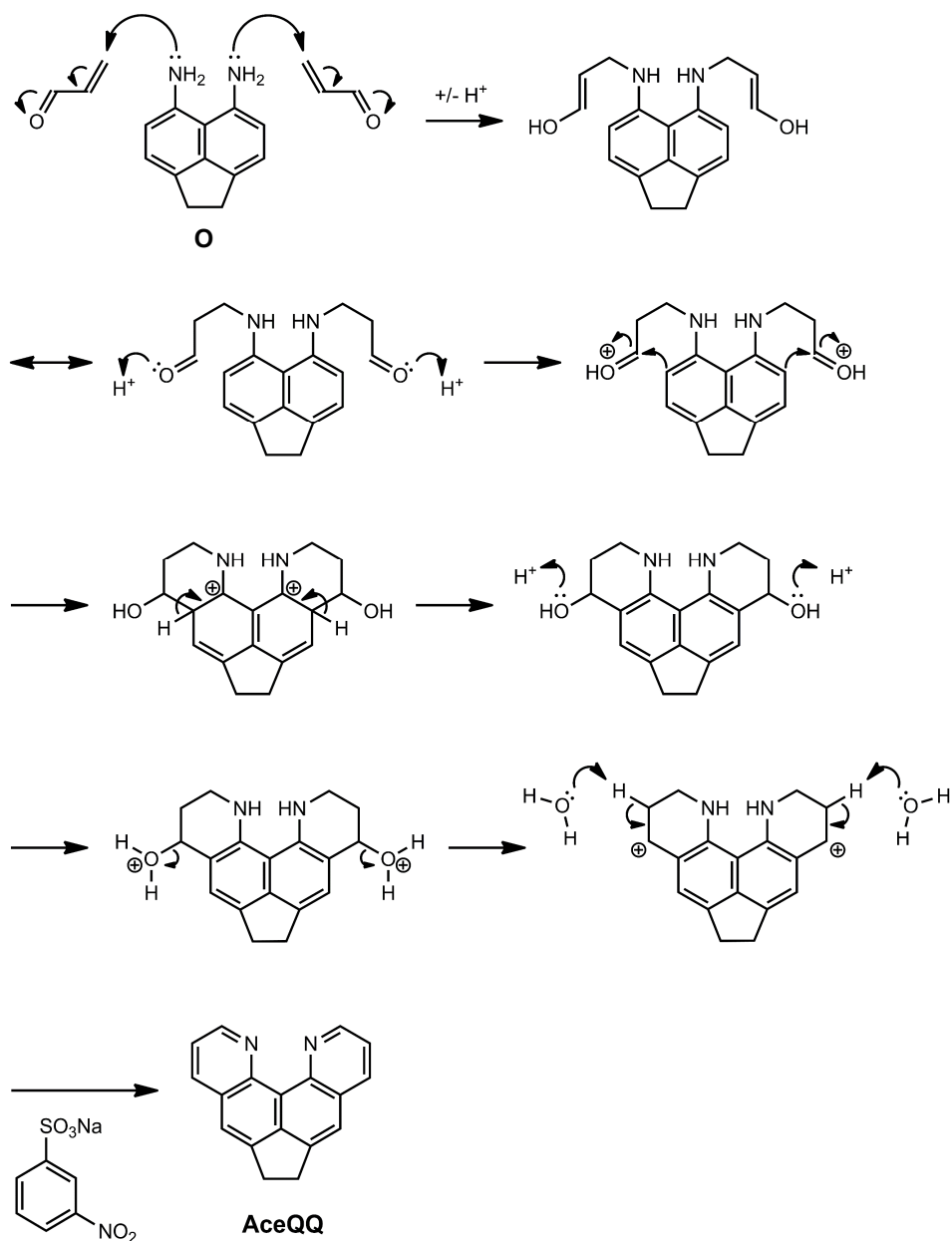


**Figure 1-26: Proposed mechanism for the formation of aceQQ.**

### 1.3.5 - QQ Coordination

The early synthetic difficulties of the original de-esterification (fig. 1-15) are likely one of the reasons for the enormous gap between publications involving phen and of QQ, and why 14 years passed between the initial synthesis of QQ by Staab et al.<sup>42</sup> and the publication of the first QQ coordination complex – which was also reported to be the first successful attempt to make stable coordination complexes with any proton

sponge.<sup>56</sup> The Wüstefeld group published transition metal complexes of 4,9-dichloroquinolino[7,8-*h*]quinoline (**Q3**) in 2001.<sup>56</sup> They synthesised and obtained crystal structures of platinum and rhenium QQ complexes (fig. 1-27) with interesting structural insights.

The short N...N distance (2.7683(16) Å)<sup>41</sup> of 4,9-dichloroquinolino[7,8-*h*]quinoline (**Q3**) creates a significantly different coordination environment to the much more spacious phen. Unlike phen, complexation of the large metal ions Pt(II) and Rh(II) required significant bowing of the core ring structure (0.742 Å and 0.498 Å respectively), and the ions were forced out of the plane at distances of 1.43 and 1.42 Å.<sup>56</sup>

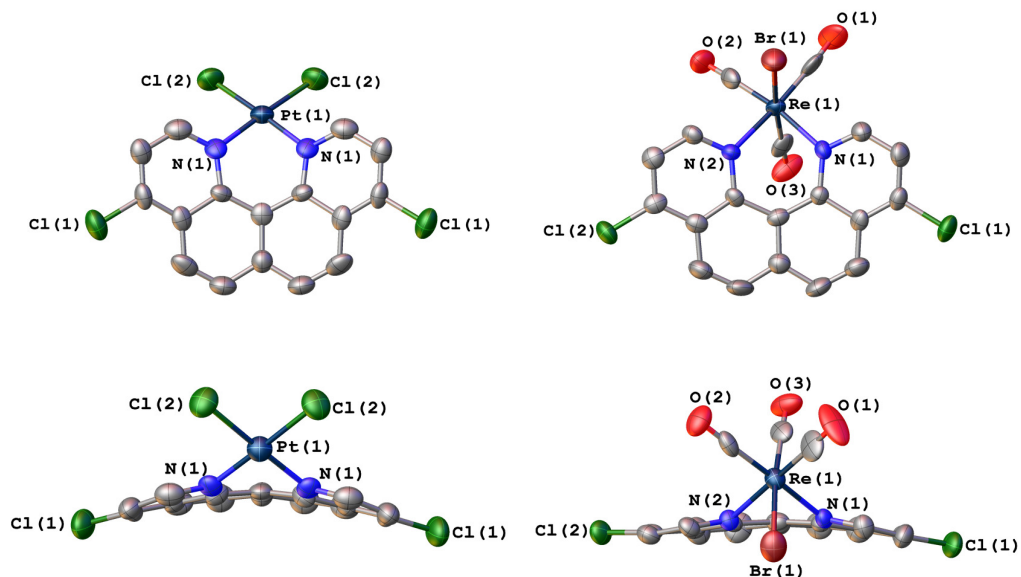
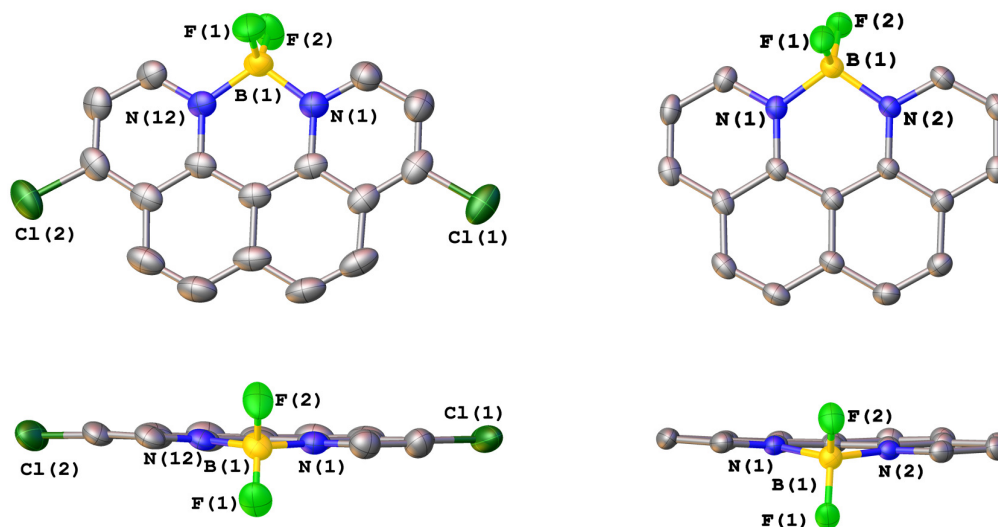


**Figure 1-27: Pt and Re complexes of 4,9-dichloroquinolino[7,8-*h*]quinoline (**Q3**). Hydrogen omitted for clarity. Images generated in Olex2<sup>8</sup> using CCDC files ACEQAA and ACEPUT with 50% ellipsoids.<sup>56</sup>**

The aforementioned lack of hydrophobic methyl shielding on the nitrogen atoms typically increases the thermodynamic stability of complexes formed.<sup>74</sup> The type of structure achieved by the Wüstefeld group conferred high thermal stability on the complexes, with platinum-QQ (fig. 1-27) able to be heated to 380 °C for several days without decomposition. Additionally, the out of plane position makes the metal centres more reactive and accessible, opening up the potential for interactions and reactions that may otherwise be blocked by the coordinated ligand, such as catalysis.

The metal ion positioning for the Wüstefeld QQ complexes is further out of the NCCCN plane than observed for the Ga(III) and Al(III) TMPN complexes described on page 6 (fig. 1-8), and for a similar TMPN(PtCl<sub>2</sub>) complex (1.29 Å) crystallised by Wild et al.,<sup>75</sup> however the high temperature stabilities of these complexes have not been evaluated.

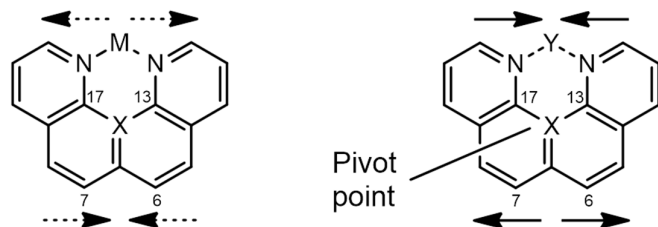
Shaffer et al. synthesised and obtained X-ray crystallographic structures of boron difluoride chelates of both quinolino[7,8-*h*]quinoline (QQ) and the substituted 4,9-dichloroquinolino[7,8-*h*]quinoline (Q3).<sup>41</sup> The successful formation of these structures, with the small coordinated ion, along with the complexes of Wüstefeld et al.,<sup>56</sup> makes the versatility of QQ ligands in accommodating ions of different sizes apparent. Unlike the Pt and Re QQ complexes, the relatively small boron atom fits well to the size of the chelation site, sitting only slightly above the mean plane and showing only minor ring bowing (fig. 1-28).



**Figure 1-28: Boron-chelates of 4,9-dichloroQQ (left) and QQ (right). Hydrogen and counterions (BF<sub>4</sub><sup>-</sup>) omitted for clarity. Images generated in Olex2<sup>8</sup> using CCDC files PANGES and PANGAO with 50% ellipsoids.<sup>41</sup>**

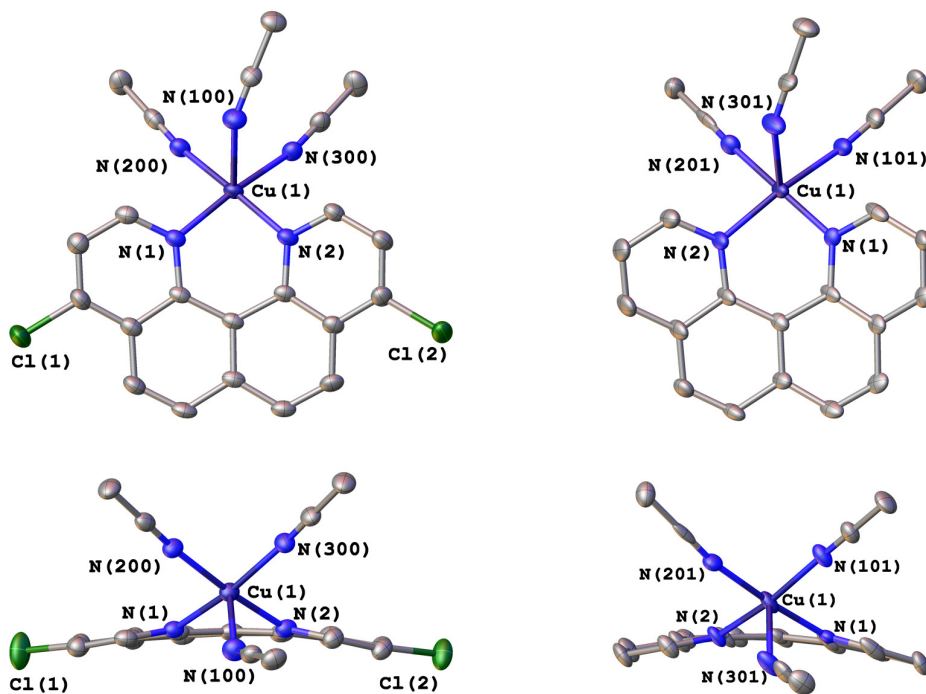
A variety of bond length and spatial changes accompanied the coordination, including reduced distances between the N...N (reflecting both the accommodation of the small ion and the reduction in lone pair strain) and C13-C17 (flattening of torsional twist) atom pairs, and slight increases in C6-C7 distances (fig. 1-29(right)). Similar changes can be observed with protonation instead of small-ion complexation, while coordination to larger metal ions (fig. 1-27) induce increased N...N and decreased C6-C7 distances in a

pincer-like action with a central pivot (fig. 1-29(left)).<sup>41</sup> See chapter 5 for more detailed discussion of QQ bond length changes occurring upon protonation.



**Figure 1-29: QQ spatial changes associated with (left) coordination to large metal ions (M) such as Pt and Re and (right) protonation or coordination to smaller ions (Y) such as  $\text{BF}_2$ .**<sup>15</sup>

Copper(II) complexes of 4,9-dichloroquinolino[7,8-*h*]quinoline (Q3) and pure unsubstituted QQ are closer in structure to the Pt and Re complexes, showing some bowing of the central aromatic ring structure and the Cu(II) ions residing above the plane (fig. 1-30).<sup>58</sup>

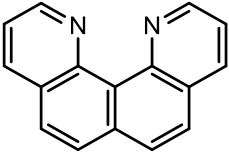
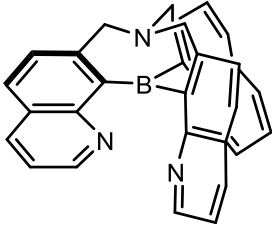


**Figure 1-30: Cu(II) complexes of 4,9-dichloroquinolino[7,8-*h*]quinoline (Q3, left) and quinolino[7,8-*h*]quinoline (QQ, right). Hydrogen and counter-ions removed for clarity. Images generated in Olex2<sup>8</sup> using CCDC files NIBSOI and NIBSIC with 50% ellipsoids.**<sup>58</sup>

### 1.3.6 - Computational/Theoretical Studies

A number of computational/theoretical studies that include quinolino[7,8-*h*]quinolines have been published. Bucher published one of the first in 2003.<sup>76</sup> This calculated proton affinities,  $pK_a$  values and some geometric parameters for a series of bases containing two (e.g. DMAN and QQ), three, and four nitrogen lone pairs to examine how that affects the basicity and other parameters. While QQ had a shorter N...N distance, the three to four nitrogen bridged bases had far greater basicities (example shown in table 1-1).

**Table 1-1: Calculated N...N distances (neutral structures) and  $pK_a$  (conjugate acids) of QQ (left) and coordination compound 623559-12-6 (right). Data published in Bucher et al.<sup>76</sup>**

		
<b>N...N distance (pm)</b>	274	343
<b><math>pK_{AH}</math></b>	19.2	26.0

Some of the proton affinity values calculated in this paper were included in a later study (2010) by Bachrach and Wilbanks.<sup>77</sup> They investigated a different type of superbase which had 'arms' containing atoms with electron lone pairs that could bend inwards, rather than those that were held in close proximity by a more rigid structure. The DFT calculated affinities of several of these were higher than that of QQ and the original DMAN proton sponge, indicating other types of compounds may form more effective superbase scaffolds than these early proton sponges.<sup>77</sup>

In the following year, Horbatenko and Vyboishchikov published a study on intramolecular N-H...N hydrogen bonds in eight proton sponges, including QQ, through a variety of functionals and computational methods – this research indicated that the centrally bound proton in protonated QQ was largely delocalised.<sup>78</sup>

### 1.3.7 - Patents – Organic Electronic Devices

More than one patent has also been published with molecules containing the QQ core that look at their use in electronic devices, including one in 2010 by Shibata et al. investigating organic white luminescent devices,<sup>79</sup> and another in 2011 by Stoessel et al. which focussed more on coordination compounds for electronic devices.<sup>80</sup> Other patents involving QQ have included the topics of battery electrolytes.<sup>81</sup> As these patents have not yet translated into other publications, further details of compounds involved will not be discussed.

### 1.4 - Beryllium Coordination

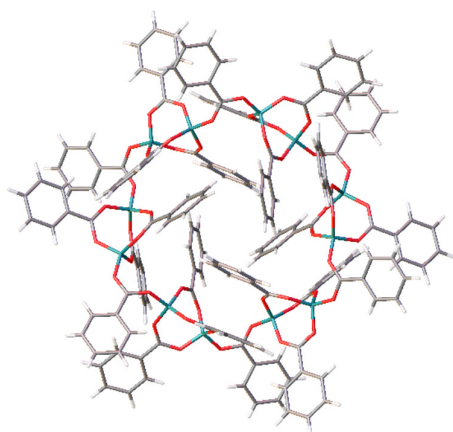


**Figure 1-31: Crystal structure of  $(\text{Be}(\text{PhC}(\text{O})\text{O})_2)_{12}$  obtained by Müller and Buchner as an example of an existing beryllium complex.<sup>82</sup> Image generated in Olex2<sup>8</sup> from the CCDC file YEZQAY.**

With the proven proton sponge and chelation abilities of QQ, it was theorised that QQ derivatives could be effective and selective chelators of beryllium metal ions ( $\text{Be}(\text{II})$ ). The small QQ chelation site should allow for coordination of  $\text{Be}(\text{II})$ , the smallest and hardest metal ion, without much distortion - similar to  $\text{B}(\text{III})$  (fig. 1-28).

Research into the interactions, chemistry, and coordination of beryllium compounds (fig. 1-31) is an ongoing and developing field. Beryllium is an exceptionally useful metal with a wide range of applications based on its unique properties. This metal element has

a relatively low density ( $1.8 \text{ g/cm}^3$ ) and high boiling point ( $2970 \text{ }^\circ\text{C}$ ).<sup>83</sup> It can be used to improve the electrical and thermal conductivity of copper and nickel in the form of an alloy, can impart high elasticity and be incorporated into windows for X-ray tubes as beryllium is transparent to X-rays.

Beryllium has long been considered the most toxic non-radioactive element,<sup>84</sup> and is both a carcinogen and the cause of the potentially-fatal chronic beryllium disease (CBD).<sup>85-86</sup> It should be noted, however, that the acute toxicity of  $\text{Be}^{2+}$  ions ( $\text{LD}_{50}$ ) is lower than that of other known toxic ions such as  $\text{Cd}^{2+}$  and  $\text{Ba}^{2+}$ .<sup>87</sup> There is also approximately 35 mg of beryllium present in the human body, although it has no known biological role.<sup>88</sup>

Theoretical modelling has provided significant insight into the prediction of structures and properties of beryllium metal-ligand complexes, allowing for ligand design towards the most effective chelators.<sup>85</sup>

## 1.5 - Coordination cages

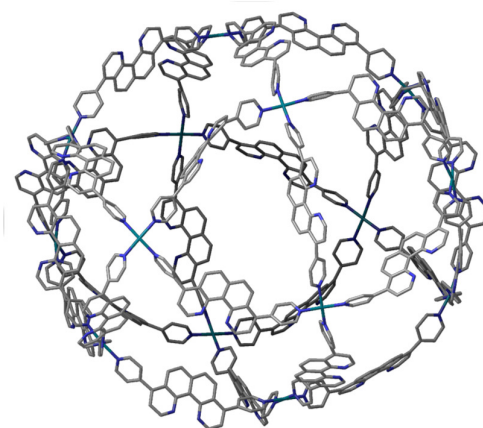


**Figure 1-32: Molecular mechanics representation of a potential QQ cage structure.**

Quinolino[7,8-*h*]quinoline derivatives have potential as building blocks for multinuclear organometallic structures (e.g. fig. 1-32). The compounds have: scope in the size of metals that could be bound; a range of existing substituents, and the angles of some



side groups that are responsive to changes in protonation and/or metal binding states. These factors could be the basis of stimuli-responsive coordination cages.<sup>37</sup>

## 1.6 - Summary

Quinolino[7,8-*h*]quinoline is a unique heterocyclic compound with tunable proton sponge properties. However, research involving derivatives of this structure has been limited - by difficult core syntheses and synthetic obstacles that are partially consequences of some of the properties that make it a research interest, including strong basicities and non-symmetric compound formation. With proven metal-coordination, and the ability to functionalise the heterocycle, some of these obstacles can be turned into opportunities, and the development of QQ synthesis and chemistry is a research avenue with high potential.

## 1.7 - Proposed Aims

The main objectives of this thesis are as follows:

- Synthesise a range of new derivatives based on the quinolino[7,8-*h*]quinoline core structure, and develop knowledge of their synthetic behaviour and general chemistry.
- Gain insight into the structural changes involved in the protonation and/or coordination of these derivatives.
- Analyse the superbasic properties and trends of QQ derivatives in collaboration with international research groups.
- Explore the use of QQ derivatives in forming coordination complexes with small Be(II) ions, based on their proton sponge properties, also involving international collaboration.
- Coordination of QQ derivatives with metal ions of different sizes, including in the formation of supramolecular structures.

## Chapter 2 - Synthesis of New Derivatives

This section will focus mainly on the synthesis of symmetrical and non-symmetrical compounds based on the quinolino[7,8-*h*]quinoline (QQ) core structure. QQ derivatives have high  $pK_a$  values and flexible coordination properties and have received little attention, making them desirable targets to explore further. Refer to Chapter 1 (introduction) for further information.

The formation of QQ derivatives involved difficult syntheses, working with small quantities and low yields. Additional challenges, as described throughout this chapter, included problematic QQ purification. Side reactions commonly resulted in compounds with similar physical properties to the desired products, such as similar solubilities and polarities (similar  $R_f$  values in column chromatography conditions). It was found that fractional recrystallisation in solvents such as DCE often gave the purest products.

### 2.1 - Overview

The reaction scheme in figure 2-1 presents a summary of the pathways developed and optimised to produce a variety of quinolino[7,8-*h*]quinoline based compounds. Some early-stage reactions have been employed in a similar manner to those previously published, while others, particularly the later steps, have been designed for purpose or heavily modified and combined from multiple sources.

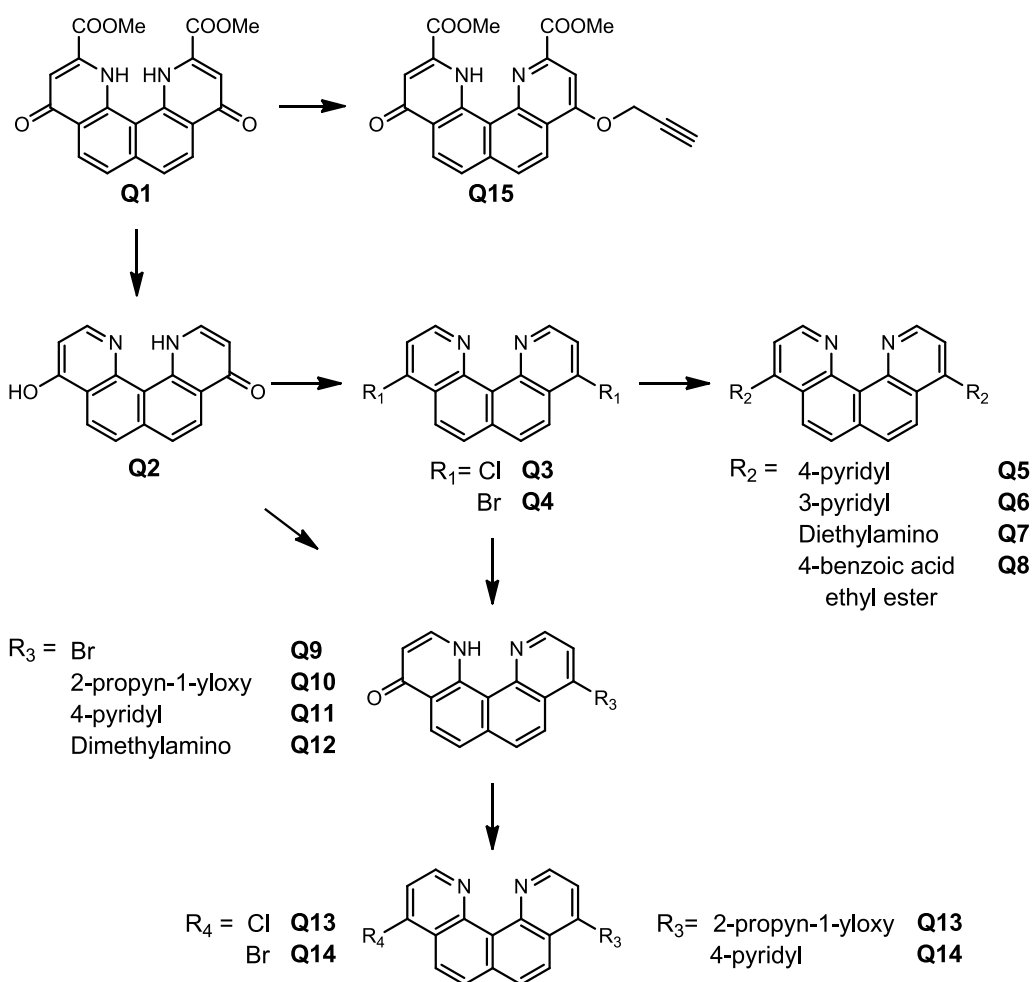


**Figure 2-1: Summarised QQ reaction scheme.**

As discussed in chapter 1, the keto-enol tautomer of quinolino[7,8-*h*]quinoline-4,9-(1*H*,12*H*)-dione (**Q2**) presented in figure 2-1 is the most stable form for this compound<sup>11</sup> - although the NMR spectra shows a symmetric compound, it is collected in strong acid (TFA-*d*) (fig. 2-2). Halogen substitution of **Q2** gives the dihalide products 4,9-dichloroquinolino[7,8-*h*]quinoline (**Q3**) and 4,9-dibromoquinolino[7,8-*h*]quinoline (**Q4**) that provide the main entry points to the new 4,9- functionalisations.

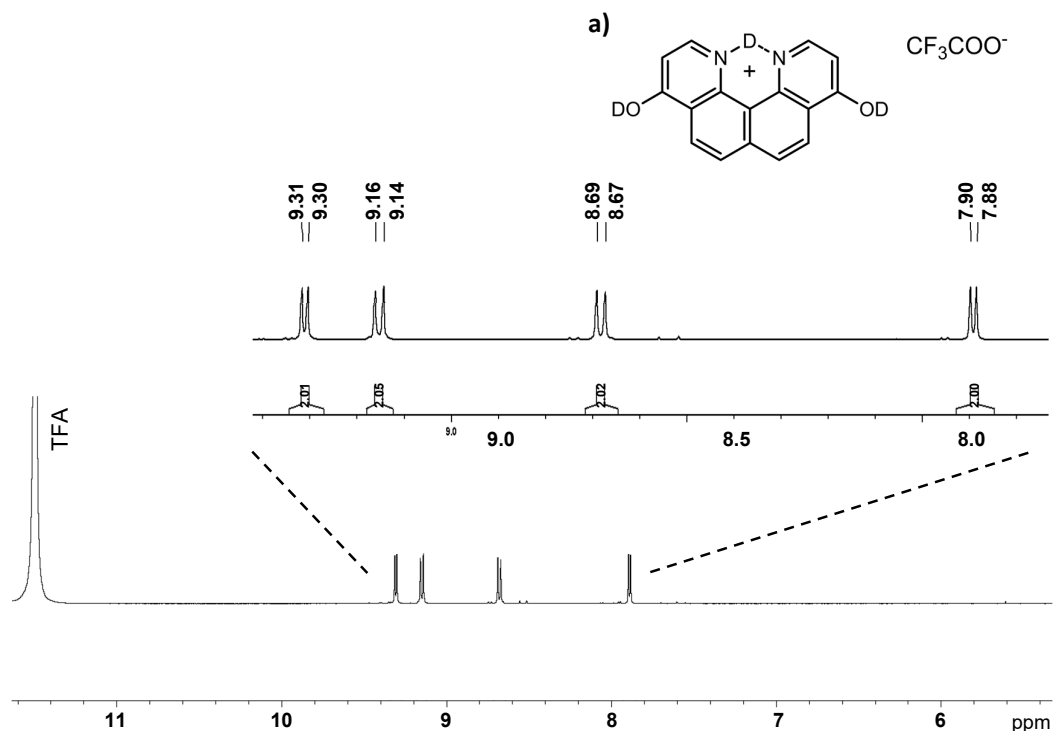


**Figure 2-2:**  $^1\text{H}$  NMR of Q2 in *d*-trifluoroacetic acid (TFA-*d*) showing four aromatic proton signals, indicative of a symmetrical QQ structure ((a), with trifluoroacetate anion).

Although some QQ derivatives with functional groups at positions other than 4 and 9 have been made previously (see chapter 1), these proved difficult to modify and were not the focus for this project. NMR spectra corresponding to the syntheses described in this chapter can be found in appendix C.

## 2.2 - Symmetrical QQ derivatives

### 2.2.1 - Challenges

A common obstacle ubiquitous in QQ synthesis, particularly of symmetrical di-substituted compounds at the 4 and 9 positions, is competition between the desired transformation and other reactions that act to cleave halide substituents in these positions; the most common of which is hydrolysis, causing reversion back to the relatively inactive oxo groups. This process is energetically favourable as it allows for keto-enol tautomerism and subsequent protonation of one central nitrogen atom – this

is driven by the relief of nitrogen lone pair → lone pair destabilisation energy/torsional strain. See Chapter 1 (intro) for further information.

This phenomenon led to competing, alternative pathway issues throughout the project and was found to be mediated/accelerated by the presence of water (see 2.2.1.1 for more detail). Reactions designed to produce doubly R-substituted QQs regularly resulted in mixtures of the desired product and some singly R-substituted products, at various ratios. In the majority of results, these single 'R' side products featured one of the 4 or 9 positioned halide 'active sites' having been substituted with the desired R group, while the other underwent hydrolysis, with the oxo tautomeric group in the place of the secondary halide which prevented the subsequent R substitution from taking place. In some syntheses, the problem could sometimes be mitigated by using reactants in relative excess, freshly distilling solvents/reactants just prior to use, and/or by running the reaction in a dry argon atmosphere. In select situations, where the substitution reaction was less favourable, halide cleavage/hydrolysis occurred under reaction conditions without substitution, resulting in mono-halide QQ species – this was later supported experimentally by the synthesis of **Q9**.

#### 2.2.1.1 - Synthesis of 9-bromoquinolino[7,8-*h*]quinoline-4(1H)-one (**Q9**)

With mounting evidence arising from the synthesis of QQ derivatives supporting the notion that the presence of water accelerates halide hydrolysis, experiments were performed involving 4,9-dibromoquinolino[7,8-*h*]quinoline (**Q4**) and water in the absence of other reagents.

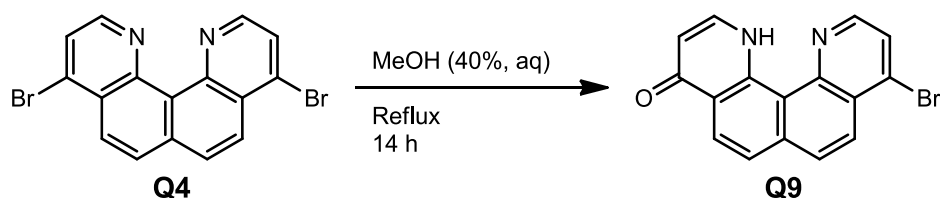


Figure 2-3: Synthesis of **Q9** from **Q4**.

Heating **Q4** to reflux overnight in a solution of 40% MeOH (included for solubility) in H<sub>2</sub>O resulted in partial hydrolysis, with close to 100% conversion to 9-bromoquinolino[7,8-

*h*]quinoline-4(1*H*)-one (**Q9**), confirming the role of water in this common QQ phenomenon.

NMR analysis showed the expected loss of symmetry, with the number of aromatic signals corresponding to core QQ hydrogen atoms doubling from four to eight each with appropriate 1H integrations, concurrent with the appearance of the central nitrogen proton signal (fig. C-10). Matching J-coupling values and 2D correlation NMR spectroscopy (<sup>1</sup>H COSY and <sup>1</sup>H/<sup>13</sup>C HMBC, fig. C-12) allowed for the identification of spin coupled protons and aided in <sup>13</sup>C assignments, and a <sup>1</sup>H/<sup>13</sup>C HMBC assisted in <sup>13</sup>C assignments (fig. C-12). Some ambiguity remains on the assignment of spin-coupled pairs of proton signals therefore the final assignments are tentative. Identification was further supported by high-resolution mass spectrometry, with a close match between the observed parent ion peak at 326.9975 m/z, a close match to the calculated [M+H]<sup>+</sup> value calculated for **Q9** (326.9951).

The proposed hydroxyl-substitution-tautomerisation mechanism of this reaction is shown in figure 2-4. Calculations supported this, showing that of the keto and enol forms of **Q9**, the enol was less stable by 16.4 kcal mol<sup>-1</sup>. The hydrolysis only occurs once as there is no further reduction of strain to be gained by the addition of a second oxygen.<sup>11</sup>

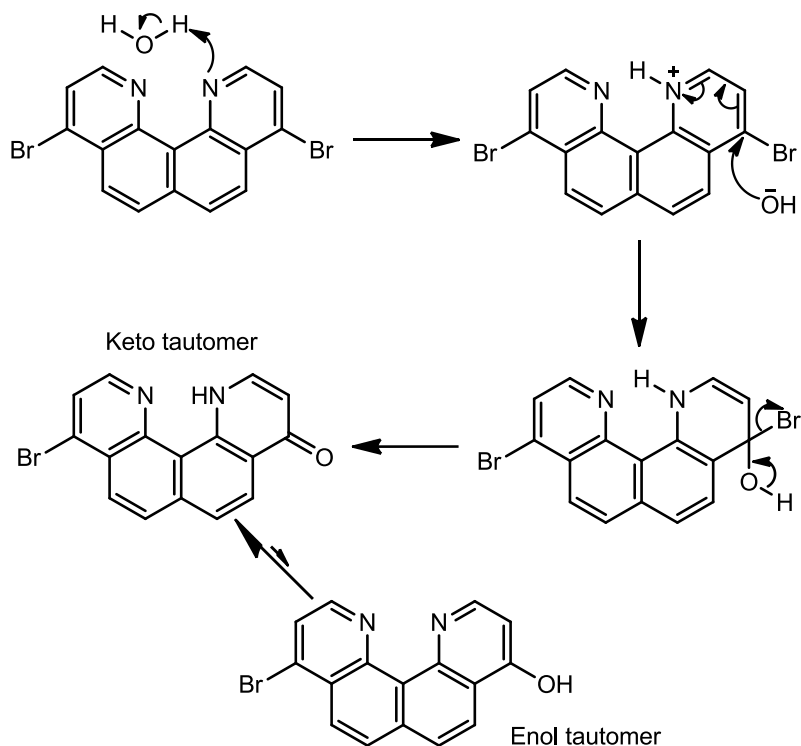


**Figure 2-4: Proposed mechanism for partial hydroxyl substitution and tautomerisation from 4,9-dibromoQQ.**

With a **Q9** yield of ~60% (that may be improvable upon further optimisation), this reaction presents a fresh entrance point for asymmetric synthesis and the creation of new QQ derivatives, such as a mixed pyridin-4-yl- and pyridin-3-yl- substituted compound.

### 2.2.2 - Suzuki-Miyaura Coupling

The Suzuki-Miyaura coupling reaction has become a cornerstone of organic chemistry for the formation of new carbon-carbon bonds since its development in 1979.<sup>89-90</sup> It is a palladium(0) catalysed reaction between an organic halide compound (usually aryl or vinyl) and an organoboronic acid derivative that results in the formation of a carbon-carbon bond, with the foundation reaction typically requiring the two coupling partner reactants described, a Pd(0) catalyst (or Pd(II) pre-catalyst), a base (e.g. K<sub>2</sub>CO<sub>3</sub>) and solvent.<sup>89</sup> This method can be applied to a wide variety of reactants and be mediated by altering catalysts, co-catalysts and solvents, making it an ideal candidate for use in

quinolino[7,8-*h*]quinoline chemistry. A generalised Suzuki-Miyaura coupling mechanism is shown in figure 2-5.<sup>91</sup>

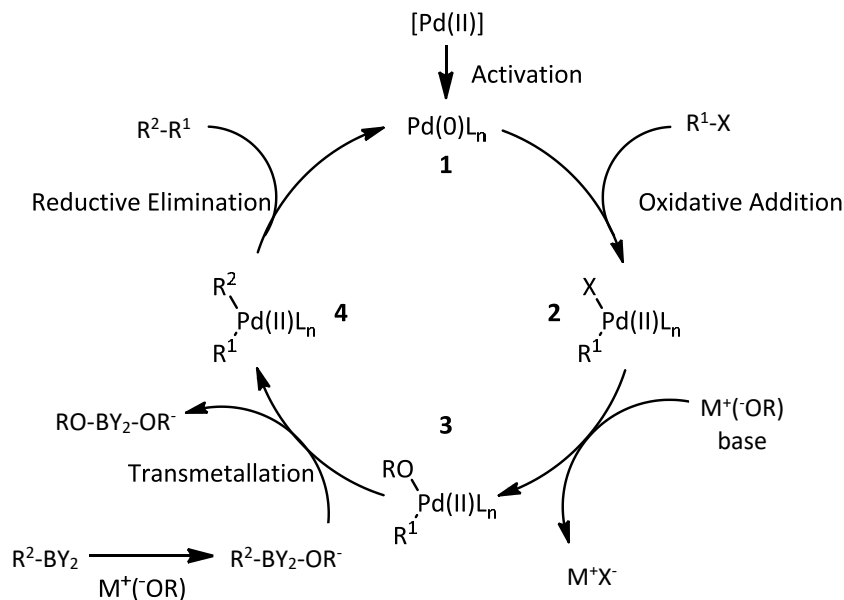


**Figure 2-5: Generalised Suzuki-Miyaura coupling mechanism showing the oxo-Pd pathway. Boronate pathway transmetalation proceeds by the reaction of '2' directly with the boronate species without formation of '3'.**

Water is a common addition in Suzuki-Miyaura cross-coupling reactions, and initial hypotheses suggested its inclusion in QQ chemistry would be beneficial – for facilitation of the formation of an oxo-Pd (fig. 2-5,3) or boronate species, base-solubility, or acceleration of boronic ester hydrolysis.<sup>11, 92</sup> However, it was discovered that the inclusion of water severely hinders the formation of doubly-substituted QQ derivatives. As described in 2.2.1, an aqueous-based solvent system accelerates the hydrolysis of one halide from the starting material over the formation of a disubstituted compound – because of this, a switch to dry solvents (usually DMF on the basis of solubility) was made when di-substitution was the goal. With side products of similar properties, purification was problematic, and yields could not be optimised.



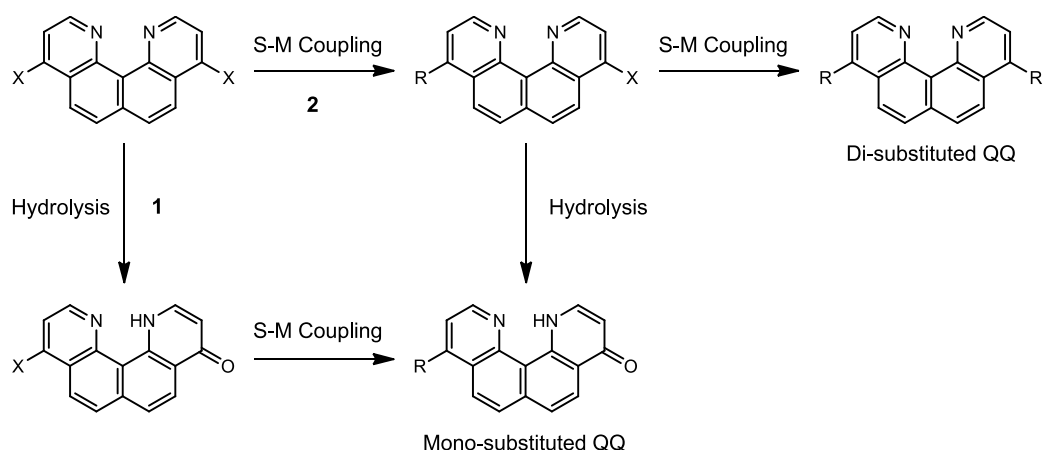


**Figure 2-6: Possible Suzuki-Miyaura coupling pathways for the formation of mono- and di-substituted QQ derivatives. X = Cl or Br.**

Because of the stabilisation effect of halide hydrolysis (2.2.1.1), the pathway to form the monosubstituted QQ derivatives/side products is hypothesised to primarily proceed by pathway 1 shown in figure 2-6.

Symmetrical di-substituted QQ compounds formed by Suzuki-Miyaura coupling reactions include 4,9-di(pyridin-4-yl)quinolino[7,8-*h*]quinoline (**Q5**), 4,9-di(pyridin-3-yl)quinolino[7,8-*h*]quinoline (**Q6**) and 4,9-di(4-benzoic acid ethyl ester)quinolino[7,8-*h*]quinoline (**Q8**). Pyridyl substituents were focussed on, instead of more simple phenyl structures, for their coordination potential – they are a common motif in ligands used to build coordination cages.<sup>38</sup>

Although the exact nature of the reactive species of a boronic acid pinacol ester coupling partner during transmetalation is unclear,<sup>92</sup> it was found that the use of this increased the yield over the corresponding boronic acid moiety. This was most likely due to the relative increase in stability of the boronic ester, that reduces the possibility of decomposition or reactions by other pathways such as homocoupling. Although the boronic ester derivative was readily commercially available, conversion from the boronic acid was straightforward, involving a simple overnight reaction with pinacol.<sup>93</sup>

### 2.2.2.1 - Synthesis of 4,9-di(pyridin-4-yl)quinolino[7,8-h]quinoline (Q5)

This was the first di-substituted quinolino[7,8-h]quinoline synthesised in the project through Suzuki-Miyaura coupling.

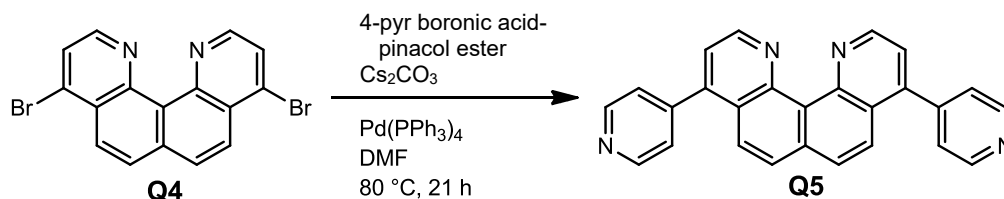


Figure 2-7: Synthesis of Q5 from Q4.

Successful conditions discovered to produce **Q5** in isolatable quantities included the use of 4-pyridyl boronic acid pinacol ester, caesium carbonate, a palladium(II) catalyst and dry DMF as the reaction solvent.

Initially, multiple variations of the Suzuki-Miyaura coupling conditions (involving a 4-pyridyl boronic coupling partner) produced the monopyrindyl compound (**Q11**) as the major product, which had been previously synthesised by the Plieger Group.<sup>11</sup> These attempts included changing 4-pyridine boronic acid for the analogous pinacol ester – a choice based on the successful use of the 4-pyridine boronic acid pinacol ester in ‘one pot’ reactions during which multiple Suzuki-Miyaura couplings took place.<sup>94</sup> The use of 60:40 dioxane or dimethoxyethane : water solvent mixtures were also trialled to speed up transmetalation and/or to assist in base solubility. <sup>1</sup>H NMR analysis showed these resulting product mixtures contained negligible amounts of what is now known to be **Q5**. Exchanging K<sub>2</sub>CO<sub>3</sub> for Cs<sub>2</sub>CO<sub>3</sub> (a stronger base to speed up transmetalation and reduce the probability of central nitrogen protonation and bromide hydrolysis (fig. 2-4))<sup>95</sup> resulted in cleaner <sup>1</sup>H NMR spectra but was insufficient to prevent monopyrindyl formation (**Q11**) as the major product. A ratio of 4:1 boronic acid pinacol ester to **Q4** was used to speed up the reaction and to ensure completion if any of the ester reacted by alternative pathways.

It was during the course of these attempts to form **Q5** that the water sensitivity of 4,9-(halide) QQ derivatives was discovered. The breakthrough in the **Q5** synthesis was

achieved by water-free conditions, with dry DMF as the reaction solvent. This altered the balance of Suzuki-Miyaura coupling versus competing halide hydrolysis sufficiently to allow the disubstituted **Q5** to become the major product. Similar yields to the overnight Suzuki-Miyaura reaction could be obtained in a microwave synthesiser in 2 hours.

With low solubility in many organic solvents, purification was problematic, and attempts at column chromatography commonly resulted in streaking. Recrystallisation in hot DCE gave the pure material with an optimised yield of 26%. The melting point of **Q5** was determined to be above 300 °C. NMR analysis of the product showed two additional sets of aromatic <sup>1</sup>H peaks (4H each) when compared with the starting material, consistent with symmetrical 4,9-(pyridin-4-yl) substitution, along with the expected 12 x <sup>13</sup>C signals, which were assigned with the aid of <sup>1</sup>H COSY and <sup>1</sup>H/<sup>13</sup>C HMBC spectra (fig. C-1). The high-resolution mass spectrometry peak found at a m/z of 385.1447 supported the identification, with a close match to the calculated 385.1448 for [M+H]<sup>+</sup>.

Small plate-like crystals of 4,9-di(pyridin-4-yl)quinolino[7,8-*h*]quinoline were obtained by slow evaporation of **Q5** in a 1:1:1 solvent mixture of DCM, MeOH and CHCl<sub>3</sub>. The structure was solved in the space group Pbnb, and the asymmetric unit contains one half of the molecule with the remainder generated by the C2 rotation axis passing through the centre of the molecule.<sup>96</sup> X-ray crystallographic analysis (fig. 2-8) suggests the compound has increased strain compared to **Q3**, with the observed helical twist significantly >4° larger at 24.19(12)° (possibly due to the electron donating nature of the pyridyl substituents compared to the electron withdrawing chlorides of **Q3**) and a smaller N...N distance of 2.744(6) Å. X-ray summary data and selected bond lengths can be found in appendix A.

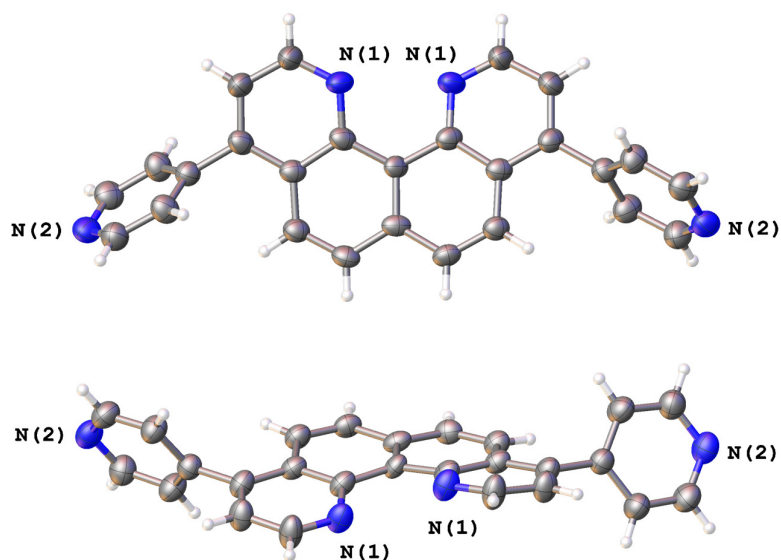


Figure 2-8: Images of the X-ray structure of 4,9-dipyridylquino[7,8-*h*]quinoline (**Q5**), generated in Olex2 with 50% ellipsoids.<sup>8</sup>

#### 2.2.2.2 - Synthesis of 4,9-di(pyridin-3-yl)quinolino[7,8-*h*]quinoline (**Q6**)

After trials of varying conditions, successful synthesis of **Q6** was eventually achieved from **Q4** using an overnight Suzuki-Miyaura coupling reaction with Pd<sub>2</sub>(dba)<sub>3</sub>, phosphine (t-Bu)<sub>3</sub>PHBF<sub>4</sub>, Cs<sub>2</sub>CO<sub>3</sub> and 3-pyridine boronic acid pinacol ester, heated in degassed DMF.

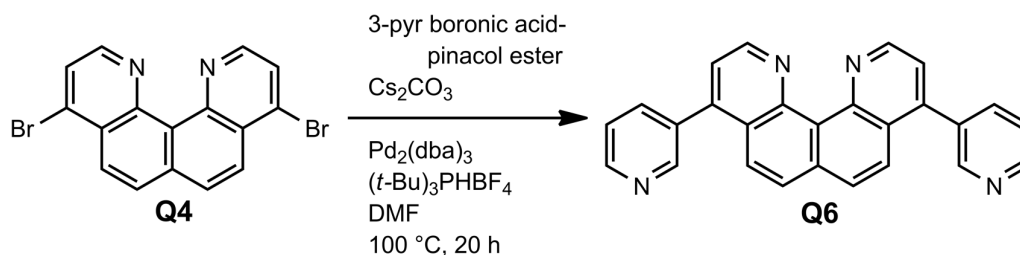
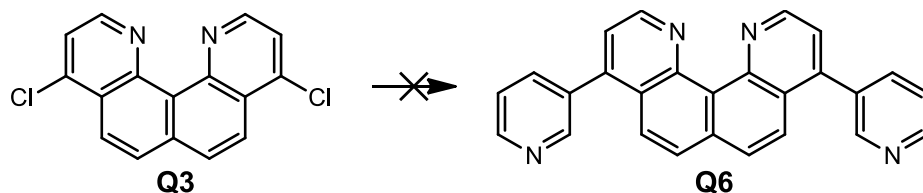


Figure 2-9: Successful synthesis of **Q6** from **Q4**.

Although aryl chlorides have lower reactivity for Suzuki-Miyaura coupling than aryl bromides,<sup>97</sup> multiple attempts were made to use 4,9-dichloroquinolino[7,8-*h*]quinoline (**Q3**) instead of the dibromide (**Q4**). The synthesis of **Q3** used cheaper reagents and is operationally easier to perform (less air sensitive, POCl<sub>3</sub> is a liquid at room temperature, and can be easily purified by distillation). A survey of the literature seemed to indicate pyridin-3-ylboronic acids are more reactive than their 4-isomers, so it appeared a viable option.

These attempts involved the use of different combinations of catalysts, co-catalysts and bases including Xphos, Pd<sub>2</sub>(dba)<sub>3</sub>, Pd(PPh<sub>3</sub>)<sub>4</sub>, Pd(OAc)<sub>2</sub>, Cs<sub>2</sub>CO<sub>3</sub> and K<sub>2</sub>CO<sub>3</sub>.



**Figure 2-10: Attempted synthesis of Q6 from Q3.**

As with the synthesis of **Q5**, dry solvents were used to reduce unwanted hydroxyl substitution during the reaction. All coupling attempts that utilised 4,9-dichloroQQ as the starting halide resulted in mixtures of different products that contained either no or small traces of the desired disubstituted compound. This method was therefore abandoned in favour of using the more reactive 4,9-dibromoQQ as the QQ source.

Like the pyridin-4-yl isomer **Q5**, the reaction product only had limited solubility in halogenated organics like DCM and CHCl<sub>3</sub> which allowed for workup, characterisation, and purification.

Conversion to the di-substituted 3-pyridyl compound was high but incomplete, however the desired product could be isolated by recrystallisation of the crude mixture in boiling dichloroethane (DCE) to give ~30% yield (pure). Although low, with some material degraded, or lost during recrystallisation, this is a significant improvement over the initial attempts. One of the side products was tentatively identified as 9-(pyridin-3-yl)quinolono[7,8-h]quinoline-4(1*H*)-one – the pattern of peaks observed in the crude <sup>1</sup>H NMR showed similar aromatic shifts to the mono-(pyridin-4-yl)-substituted **Q11**, with the high number of peaks suggestive of a non-symmetric compound - however this product was not isolated. Comparison of the NMR spectra of the purified product and **Q4** (starting material) showed the shifts expected of **Q6** - with the additional four sets of aromatic proton signals (2H each) that correspond to symmetrical di-(pyridin-3-yl) substitution, the expected 14 x <sup>13</sup>C peaks, and the complement of 2D spectra (fig. C-6). Identification was supported by high-resolution mass spectrometry, where the observed

m/z peak found at 385.1482 corresponded to the calculated value of 385.1448 for singly-protonated **Q6**.

Crystals (of **Q6**) of sufficient quality for single-crystal X-ray analysis were not obtained. Factors contributing to this included: poor solubility in many solvents which reduced the range of crystal growth media possibilities and limited solutions to very dilute concentrations; synthetic difficulties, limited quantity of material available for crystal growth attempts and the tendency of these materials to precipitate rather than crystallise.

### **2.2.3 - Other symmetrical substitution**

As the yields of Suzuki-Miyaura coupling reactions to form symmetrical disubstituted QQs were continually low, making further exploration of their chemistry difficult, other methods of core functionalisation were explored. These included Sonogashira coupled products which aimed at producing extended ligands for cage systems – see section 2.5 for further information.

Other methods were trialled to expand the range of QQ compounds and further explore their properties as strong bases – these aimed to produce derivatives with heteroatoms at the 4- and 9- positions instead of C-C coupling. The most successful of these was, surprisingly, the simplest to perform – the direct non-catalysed substitution of diethylamine to form *N*<sup>4</sup>,*N*<sup>4</sup>,*N*<sup>9</sup>,*N*<sup>9</sup>-tetraethylquinolino[7,8-*h*]quinoline-4,9-diamine (**Q7**).

#### **2.2.3.1 - Synthesis of *N*<sup>4</sup>,*N*<sup>4</sup>,*N*<sup>9</sup>,*N*<sup>9</sup>-tetraethylquinolino[7,8-*h*]quinoline-4,9-diamine (**Q7**)**

To better understand the effects of different electron withdrawing and donating substituents upon the p*K*<sub>aH</sub> of the central nitrogen pocket, the amine based derivative **Q7** was designed, synthesised, and the reaction optimised.

This simple-to-perform method involved heating 4,9-dibromo[7,8-*h*]quinoline (**Q4**) to reflux in neat diethylamine over 2-3 days. This achieved a good conversion rate and high crude yield (~90 %). While **Q7** was also the major product when the synthesis was attempted with chloride **Q3** as a starting material, both yields and conversion rates were significantly poorer.

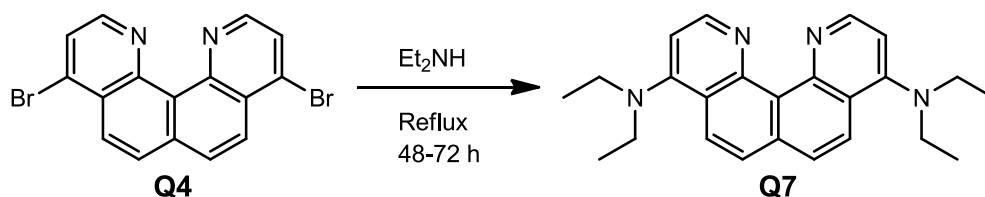


**Figure 2-11: Synthesis of Q7 from Q4.**

Interestingly, the presence of these diethylamino substituents significantly increased the solubility of the compound in a wide range of different solvents, including EtOH, to a degree not previously observed with other quinolino[7,8-*h*]quinoline derivatives. This expands the range of the derivative's potential applications.

Purification attempts of **Q7** varied – streaking difficulties arose in standard column chromatography with different media (including acidic silica gel and basic/neutral alumina) likely due in part to the multiple basic nitrogen atoms present. The extreme hygroscopicity of **Q7**, along with its high solubility, made removing final solvent traces difficult which precluded recrystallisation as a purification method. Additionally, the use of decolourising charcoal (often used to remove traces of small, coloured compounds in a mixture) appeared to absorb both the desired compound and impurities equally. Methods such as sublimation and ion-exchange chromatography were not trialled.

Eventually, pure samples were achieved by rigorous control of the starting material purity, including the use of freshly distilled diethylamine to reduce amine impurities and water content.

In addition to shifts observed in the core aromatic  $^1\text{H}$  NMR signals of the **Q7** product (to the starting **Q4**), additional aliphatic region peaks were observed, with integrations of

12H and 8H consistent with the symmetrical substitution of diethylamine groups (fig. C-7). Matching J-coupling values and  $^1\text{H}$  COSY cross-peaks between spin-coupled proton pairs (such as 5/6-H and 7/8-H) aided proton assignments, as did the  $^1\text{H}/^{13}\text{C}$  HMQC and DEPT-135 spectra for the  $^{13}\text{C}$  spectrum. A strong contrast between the starting material and product  $^{13}\text{C}$  spectra was also provided by the appearance of the aliphatic  $\text{CH}_3$  and  $\text{CH}_2$  signals. High-resolution mass spectrometry showed an  $m/z$  peak of 373.2385, consistent with that calculated for the **Q7** formula (373.2387).

Attempts at forming crystals suitable for X-ray crystallography have been unsuccessful to date – both the singly-protonated and deprotonated forms of 4,9-di(diethylamine)QQ result in either oily compounds or powders.

#### 2.2.4 - Synthesis of 9-(dimethylamino)quinolino[7,8-*h*]quinoline-4(1*H*)-one (**Q12**)

Following the successful synthesis of the **Q7** diamine, a logical step was to attempt the synthesis of  $N^4, N^4, N^9, N^9$ -tetramethylquinolino[7,8-*h*]quinoline-4,9-diamine (**Q12**) under similar conditions - starting from the **Q4** halide with a 40% aqueous dimethylamine solution (dimethylamine is a gas above  $\sim 8^\circ\text{C}$ ).

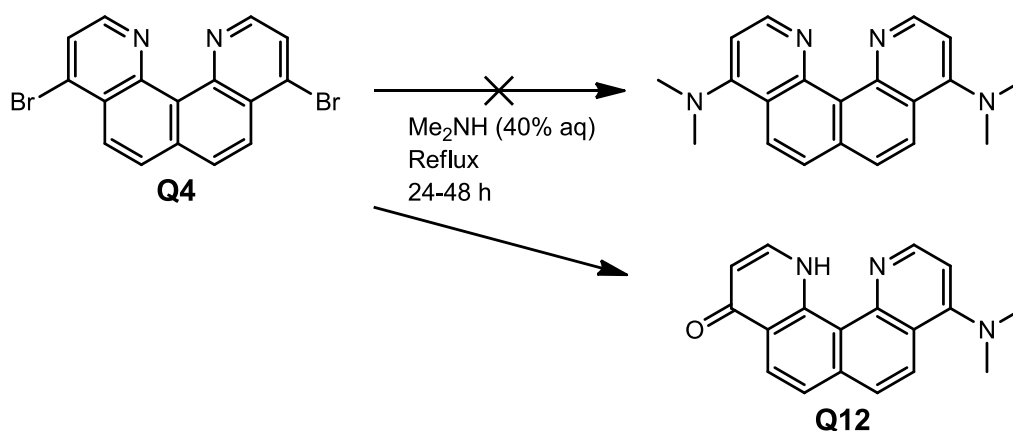


Figure 2-12: Synthesis of **Q12** from **Q4**.

Single substitution of a dimethylamine substituent occurred readily, however with the high water content, the competing reaction of halide hydrolysis also took place,



resulting relatively clean conversion to 9-(dimethylamino)quinolino[7,8-*h*]quinoline-4(1*H*)-one (**Q12**).

Identification was supported by NMR analysis of the product – the eight sets of <sup>1</sup>H aromatic <sup>1</sup>H signals were consistent with a non-symmetrical QQ derivative. Additionally, the single substitution of a dimethylamine group was supported by the appearance of new aliphatic 6H <sup>1</sup>H and <sup>13</sup>C signals and (consistent with the two new CH<sub>3</sub> groups) (fig. C-16 and C-17). The high-resolution mass spectrographic m/z peak found at 290.1278 also closely matched the expected [M+H]<sup>+</sup> value for C<sub>18</sub>H<sub>16</sub>N<sub>3</sub>O of 290.1288.

### 2.2.5 - Symmetrical QQ derivatives - Summary

A number of symmetrical QQ derivatives were synthesised and characterised, through the use of C-C coupling and direct substitution techniques. Challenges arose in the process, including limited solubilities, competing reactions and purification. Some of these led to unsuccessful synthesis (see 2.5), others were overcome, adding to the library of existing QQ compounds and their known chemistry, while others led to the synthesis of non-symmetrical derivatives (**Q9** and **Q12**).

## 2.3 - Non-symmetrical QQ derivatives

The keto-enol tautomerism and proclivity of quinolino[7,8-*h*]quinoline derivatives to revert back to a 4-substituted oxo-species (fig. 2-4) is a major challenge in the synthesis of symmetrical QQ derivatives, but it also affords an opportunity - These properties provide an unusual avenue to explore the formation of new non-symmetric derivatives from symmetric starting materials, or the process could be repeated to form symmetrical QQ species.

In the project, the non-symmetrical QQ derivatives containing the 4-oxo group were observed to generally have good stability in terms of neither reacting further nor losing the single 9-positioned substituent.

### 2.3.1 - Synthesis of 9-(2-propyn-1-yloxy)-quinolino[7,8-*h*]quinolin-4(1*H*)-one (Q10)

**Q10** was the result of reacting **Q2** with propargyl bromide under basic conditions.

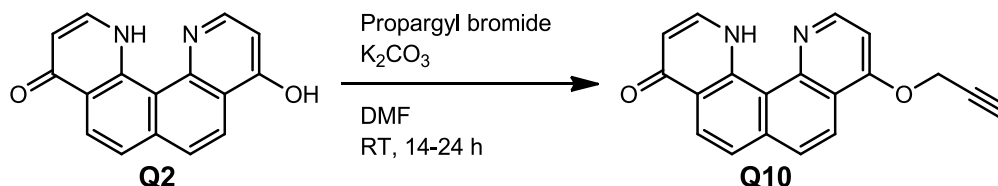


**Figure 2-13: Synthesis of Q10 from Q2.**

With the difficulties arising from halide hydrolysis in the synthesis QQ derivatives, attempts were made to further explore the reactivity of quinolino[7,8-*h*]quinolin-4,9-(1*H*,12*H*)-dione (**Q2**) – to date, the only successful reactions involving this compound as a starting material were with  $POCl_3$  and  $POBr_3$  to produce **Q3** and **Q4**, respectively. **Q2** has extremely low solubility in most organic solvents, which limits its scope – this is illustrated by the need to run NMR spectra of **Q2** in TFA-*d* to reach sufficient concentrations for quality data (fig. 2-2). **Q2** was found to be partially soluble in dimethylformamide (DMF), which presented an opportunity to expand its reaction pathways beyond halide substitution reactions (run in neat reactants at elevated temperatures). The chemistry published by Zhang et al. (in DMF) was attempted, which involved the reaction of propargyl bromide with the enol-tautomer of a quinoline derivative.<sup>98</sup>

The product **Q10** was more soluble than the starting material, so a simple workup involving cooling the reaction mixture and filtering through both cotton wool and filter paper to remove any remaining **Q2** dione was sufficient purification in most runs to give a yield of ~70%. The reaction mixtures could also be purified to a limited extent by silica gel chromatography with a solvent mixture of 9:1:0.5 DCM : MeOH :  $Et_3N$ , however this often resulted in partial loss of product.

Product identification was supported by the non-symmetric QQ pattern of aromatic  $^1H$  NMR peaks, and the appearance of 2H and 1H  $^1H$ -peaks consistent with the  $CH_2$  and

terminal CH protons of the propynyloxy substituent, as well as the corresponding alkyl and alkynyl  $^{13}\text{C}$  signals, with 2D spectra ( $^1\text{H}$  COSY and  $^1\text{H}/^{13}\text{C}$  HMBC) allowing for aromatic proton and carbon assignments (fig. C-13 - C-14). The observed high-resolution mass spectrographic  $m/z$  peak of 301.0970 was consistent with the calculated  $[\text{M} + \text{H}]^+$  value of 301.0972 for  $\text{C}_{19}\text{H}_{13}\text{N}_2\text{O}$ .

The increased stability of the keto tautomer over the enol (fig. 1-11, chapter 1) meant that double substitution attempts were unsuccessful. These attempts involved the addition of excess propargyl bromide and/or heat, and/or extension of reaction times (from overnight to several days). Also re-reacting the isolated product with a fresh batch of propargyl bromide was trialled, but double substitution could not be achieved.

### 2.3.2 - Synthesis of 4-chloro-9-(2-propyn-1-yloxy)-quinolino[7,8-*h*]quinoline (Q13)

Expanding from the synthesis of propynyloxy derivative **Q10**, was the reaction with phosphoryl chloride to produce **Q13**.

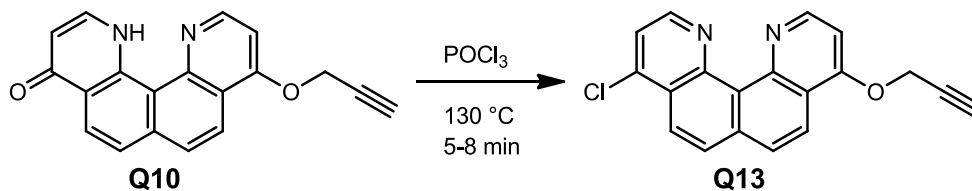


Figure 2-14: Synthesis of **Q13** from **Q10**.

Given the consistent success of transforming **Q2** to the heteroarylchloride-derivative **Q3**, a logical step was to attempt the conversion of the 4-oxo site of **Q10** to the halide. This was successfully performed under similar conditions, forming a new non-symmetric QQ compound.

The simple workup involved suspending the resulting reaction mixture in  $\text{CHCl}_3$  and washing with water and  $\text{KOH}$  to give **Q13** in a  $\sim 40\%$  yield. If the phosphorous oxychloride used in the reaction was new or recently distilled, further purification beyond this

workup was not required. Appropriate column chromatography conditions were therefore not fully explored.

As the phosphorous oxychloride stocks used were acidic ( $\text{POCl}_3$  reacts with  $\text{H}_2\text{O}$  and degrades to form  $\text{HCl}$  and  $\text{H}_3\text{PO}_4$ ), the success of this reaction clearly indicates the stability of the 2-propyn-1-yloxy substituent towards acidic conditions under elevated temperatures.

As expected, similar peak patterns were observed in the NMR spectra of **Q13** and the starting material **Q10**, including the retention of the propynyloxy substituent peaks, with small chemical shift changes consistent with the substitution of the strongly electron-withdrawing chloride at position 4.  $^1\text{H}$  COSY and  $^1\text{H}/^{13}\text{C}$  HMBC spectra aided in completing peak assignment (fig. C-21). Mass spectrometry supported the identification, with the  $m/z$   $[\text{M} + \text{H}]^+$  peak found at 319.23 close to that calculated for  $\text{C}_{19}\text{H}_{11}\text{ClN}_2\text{O}$  (319.06) and showing the expected 3:1 pattern characteristic of a chlorine containing derivative.

Attempts were made to continue this non-symmetric pathway by reacting **Q13** with diethylamine to substitute the chloride group for the amine. Unfortunately,  $^1\text{H}$  NMR spectra showed substitution occurred at both positions to give **Q7** instead (2.2.3.1), indicating a possible base-sensitivity of the propynyloxy substituent (when attached to QQ). Further transformation of **Q13** has not yet been achieved. However, while the stability of propargyl ether moieties in literature varies with their substituents,<sup>99</sup> propargyl ether moieties have been used as stable protecting groups of alcohols,<sup>100</sup> so it is theorised that reactions involving a non-nucleophilic base may have potential.

### **2.3.3 - Synthesis of 9-(2-propyn-1-yloxy)-1,4,9,12-tetrahydro-4,9-dioxo-2,11-dimethylester-quinolo[7,8-*h*]quinoline-2,11-dicarboxylic acid (Q15)**

The synthesis of **Q15** was achieved using similar conditions to **Q10**.

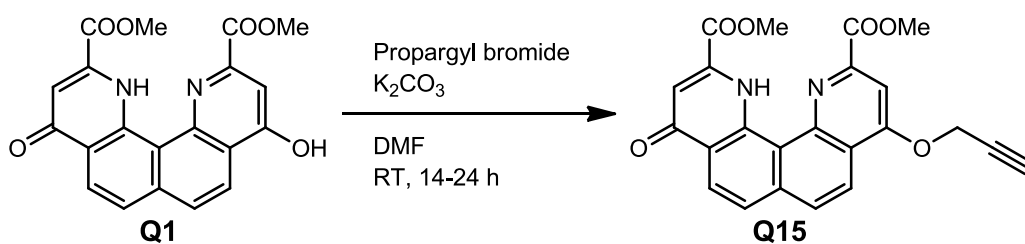


**Figure 2-15: Synthesis of Q15 from Q1.**

The starting material 1,4,9,12-tetrahydro-4,9-dioxo-2,11-dimethylester-quinol[7,8-*h*]quinoline-2,11-dicarboxylic acid (**Q1**) has a slightly higher organic solubility range than the decarboxylation product **Q2**, however it is still generally low. The hydrolysis followed by decarboxylation process to convert **Q1** to **Q2** was an obstacle in early quinolino[7,8-*h*]quinoline research, and although this was solved with the use of a pressurised reaction vessel,<sup>15</sup> there is interest in expanding the QQ reactivity from this derivative, which has steric shielding of the central binding cavity by the ester groups. Previous research involving **Q1** converted it to dimethyl-4,9-dichloroquinolino[7,8-*h*]quinoline-2,11-dicarboxylate (**Q16**), which was the first confirmed quinolino[7,8-*h*]quinoline derivative with 2,11 substitution.<sup>15</sup> Subsequent functionalisation of either the 4,9 or 2,11 groups of this dihalide compound proved difficult to modify, however.<sup>54</sup>

Reacting **Q1** with propargyl bromide in DMF with  $K_2CO_3$  produced **Q15**. Conversion was incomplete; however the off-white product could be easily separated from the less soluble tan/grey starting material and other side products with a workup procedure that included removal of the DMF solvent from the filtered reaction mixture, suspension of the crude product in  $CHCl_3$ , and alternate brine and  $H_2O$  washes of the organic layer. Once dried, this gave **Q15** at sufficient purity in a low ~11% yield. To the best of current knowledge, this is the first non-symmetric 2,11-substituted QQ derivative (excluding those published only in patents).

NMR analysis (fig. C-26 - C-28) of the purified product was consistent with the non-symmetric single substitution, showing the retention of the methyl ester groups with individual 3H signals from the  $CH_3$  groups in a non-equal chemical environment, and the appearances of similar  $CH_2$  and terminal alkyne CH signals to **Q10**. Matching J-coupling

values between spin coupled protons, and the information provided by 2D spectra, allowed for assignment of the remaining  $^1\text{H}$  and  $^{13}\text{C}$  spectra peaks. Identification was also supported with high-resolution mass spectrometry, with an  $[\text{M} + \text{H}]^+$  peak at 417.1080 close to the calculated 417.1081 value.

### 2.3.4 - Synthesis of 4-bromo-9-(pyridin-4-yl)-quinolino[7,8-*h*]quinoline (Q14)

With a view to either improving the yield with an alternative route to 4,9-di(pyridin-4-yl)quinolino[7,8-*h*]quinoline (Q5), or providing an avenue for the synthesis of compounds with differing coordinating substituents at the 4/9 positions, another target was the bromination of 9-(pyridin-4-yl)-quinolino[7,8-*h*]quinolin-4(1*H*)-one (Q11).<sup>11</sup>

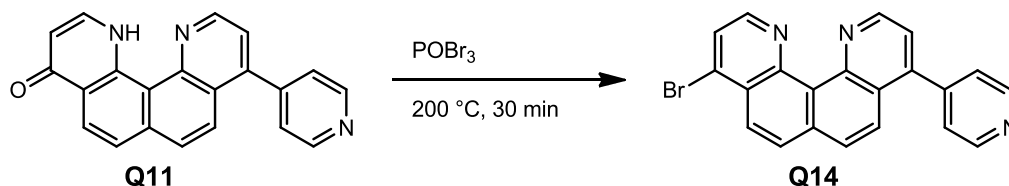
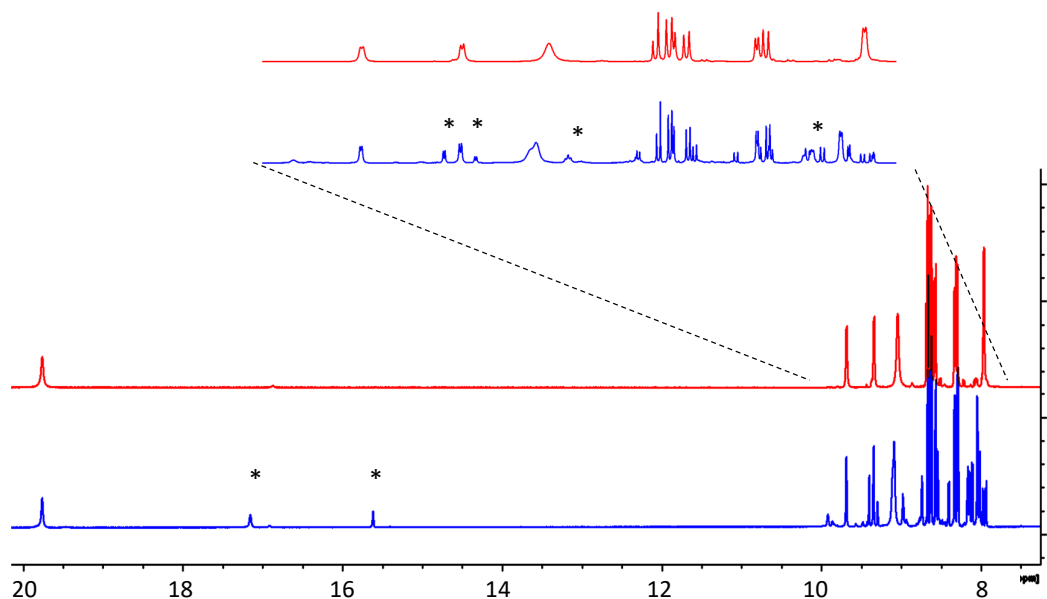


Figure 2-16: Synthesis of Q14 from Q11.

Using similar conditions to those employed in the synthesis of the di-heteroaryl bromide Q4, this reaction was successful, however purification was difficult. While most heteroaryl halide-containing QQs are reasonably stable at room temperature in a variety of solvents, Q14 appears to degrade in <24 hours in DMSO-*d*<sub>6</sub> (fig. 2-17) to multiple products (including the mono-pyridyl Q11), providing a challenge for obtaining high quality  $^{13}\text{C}$  NMR data, which requires longer data collection times.

The column difficulties encountered were those typical of many QQ derivatives – including limited solubility in a variety of solvents, and impurities having similar *R*<sub>f</sub> values to desired compounds. Eventually pure material was obtained without column chromatography by ensuring rigorous purity of starting materials and several cycles of washing in the workup. At a maximum yield ~ 54% (which was commonly lower), the yield of this step suggested this was not an efficient avenue for further non-symmetric QQ synthesis in the current form.



**Figure 2-17:**  $^1\text{H}$  NMR spectra of **Q14** taken after <1hr (top) ~30hrs (lower) in  $\text{DMSO-}d_6$ . Note the appearance of many new peaks (e.g. 17.2 and 15.6 ppm, highlighted by “\*” symbols), some of which correspond to degradation to **Q11**.

Sufficiently high-quality NMR data was obtained through the use of a more powerful 700 MHz spectrometer. This showed the spread of aromatic  $^1\text{H}$  and  $^{13}\text{C}$  peaks characteristic of a non-symmetric QQ derivative: In the  $^1\text{H}$  spectrum this includes 8x 1H aromatic signals corresponding to individual QQ core protons, and a further 2x 2H signals from the 4-pyridyl substituent, and in the  $^{13}\text{C}$  spectrum, **Q14** has 19  $^{13}\text{C}$  peaks. A strongly deshielded proton signal (19.78 ppm) was also observed, indicating single protonation of the central nitrogen atoms. As the product degraded quickly in  $\text{DMSO-}d_6$ , and solubility was limited, collecting appropriate  $^{13}\text{C}$  data was prioritised. This led to some product degradation taking place before the 2D spectra were collected, however their comparison to the non-degraded  $^1\text{H}$  and  $^{13}\text{C}$  spectra allowed them to still be useful in completing assignments. High-resolution mass spectrometry supported the identification of **Q14** – the observed peak of 386.0280 closely matched the calculated value (386.0287), with the expected M+2 peak from the bromine substituent in a ~1:1 ratio.

### 2.3.5 - Non-symmetrical QQ derivatives - Summary

Pathways exploring the formation and chemistry of non-symmetrical QQ derivatives were developed through the synthesis and characterisation of several new compounds, which included expansion of the known reactivity of low solubility derivatives (**Q1** and **Q2**). With the keto-enol tautomerism of QQ making competing hydrolysis reactions a common occurrence in QQ synthesis, taking advantage of the property for synthetic purposes is a clear avenue for future research.

### 2.4 - 9-methoxyquinolino[7,8-*h*]quinoline-4(1*H*)-one

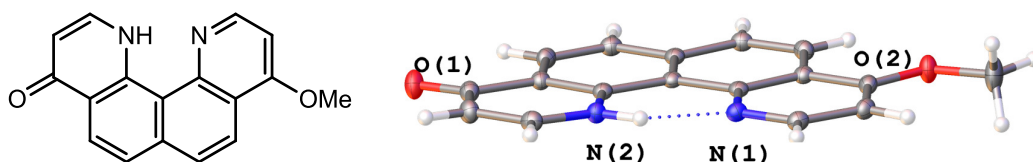


**Figure 2-18:** Schematic (left) and crystal (right) structures of 9-methoxyquinolino[7,8-*h*]quinoline-4(1*H*)-one showing two different viewpoints. Image generated in Olex2 with 50% ellipsoids.<sup>8</sup>

Attempts by the Buchner group to recrystallise possible Be-QQ derivative complexes often resulted in ligand decomposition (See Chapter 6 for more information). In the process of recrystallising a possible complex formed between Be(II) and 4,9-dimethoxyquinolino[7,8-*h*]quinoline (**Q20**),<sup>11, 15</sup> an X-ray structure was collected of the partially hydrolysed 9-methoxyquinolino[7,8-*h*]quinoline-4(1*H*)-one (fig. 2-19).

This structure was solved in the  $P2_1/n$  monoclinic space group with an  $R_1$  value of 3.98%. The expected keto-tautomer structure is observed, with the shared centrally-bound tautomeric proton and flat, almost planar ring structure, with an  $N\cdots N$  distance of 2.6388(13) Å and a torsional twist of 1.18°. The molecules packed in stacks of anti-parallel chains as shown in figure 2-19. X-ray summary data can be found in appendix B.



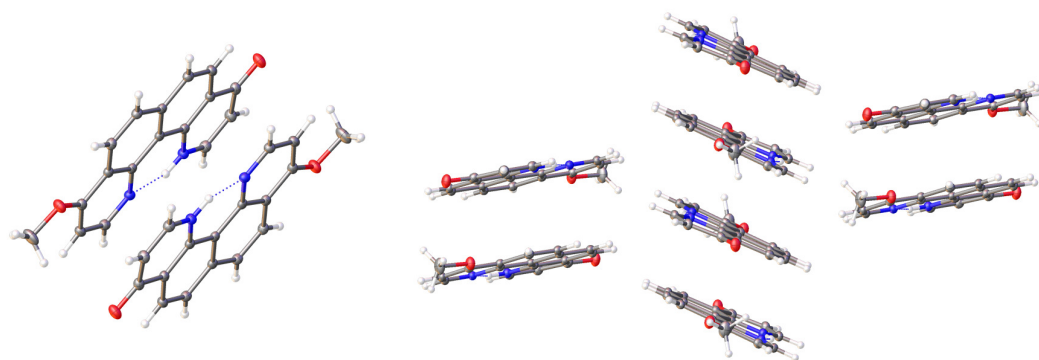


Figure 2-19: Crystal structure packing of 9-methoxyquinolino[7,8-*h*]quinoline-4(1*H*)-one. Images generated in Olex2 with 50% ellipsoids.<sup>8</sup>

## 2.5 - Selected Incomplete/unsuccessful QQ Transformations

Throughout the exploration and development of the chemistry of quinolino[7,8-*h*]quinoline derivative, many different types of transformations were attempted that were either unsuccessful or resulted in mixtures of products containing the desired compound that could not be effectively separated. This section discusses these attempts.

### 2.5.1 - Synthesis of 4,9-di(4-benzoic acid ethyl ester)quinolino[7,8-*h*]quinoline (Q8)

To increase the scope of functional groups involved in QQ synthesis, the benzoic ester target **Q8** was attempted. This was chosen above the benzoic acid equivalent to avoid potential complications of the carboxylic acid group and the QQ core, such as the possibility of speeding up hydrolysis of side groups. Using the benzoic ester also allowed for simple conversion of the boronic acid starting material to the pinacol ester analogue, based on prior successes with this moiety.

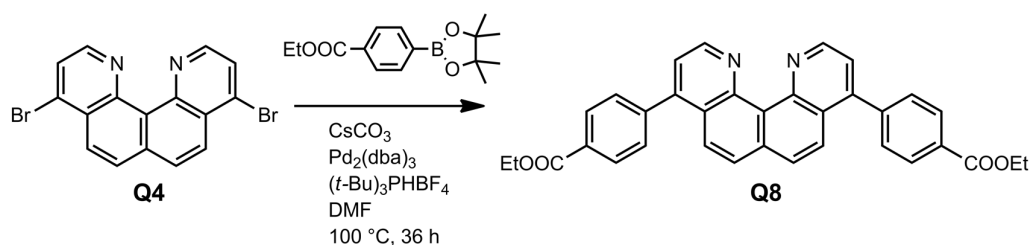


**Figure 2-20: Synthesis of Q8 from Q4.**

However, while **Q8** was synthesised, purification from side products proved difficult and clean compound isolation was not achieved. Attempts included a variety of column chromatography and recrystallisation conditions, involving a range of solvents (such as  $\text{CHCl}_3$ , DCM, DCE, MeOH and  $\text{Et}_3\text{N}$ ) in different ratios. Mass spectrometry indicated the presence of the desired product along with the monosubstituted derivative (fig. 2-21).

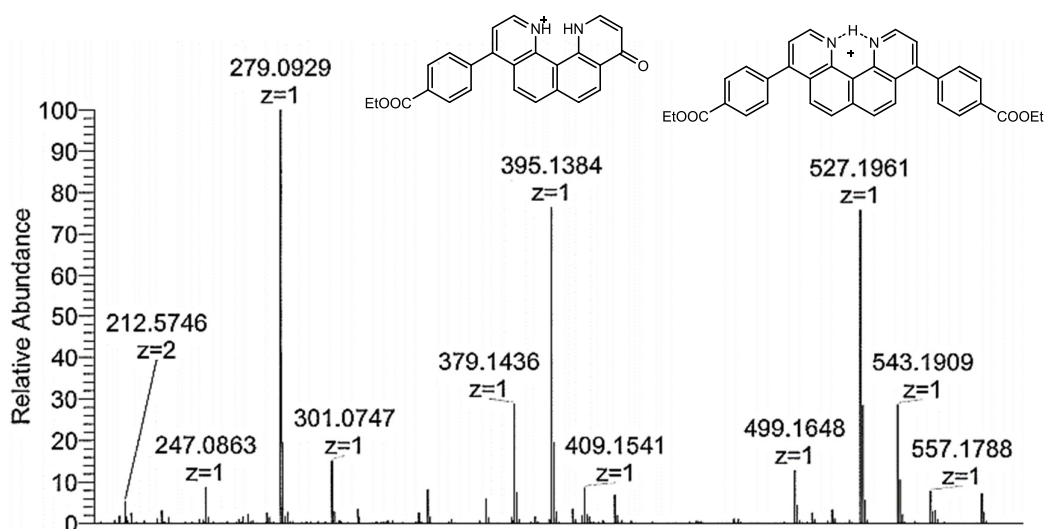


**Figure 2-21: High-resolution mass spectrum of Q8 synthesis.**

## 2.5.2 - Sonogashira Coupling

It was hypothesised that if extended coordination cages were to be formed from QQ derivatives, these would be less strained and more favourable with ligands where the coordinating side groups (e.g. pyridin-3-yl and -4-yl) were positioned further from the bulky QQ core, reducing potential steric hinderance to metal coordination. The Crowley group has achieved excellent results using ligands with ethynyl bridges (e.g. fig. 2-22) in forming coordination cages, so Sonogashira coupling was attempted with QQ.<sup>101</sup>

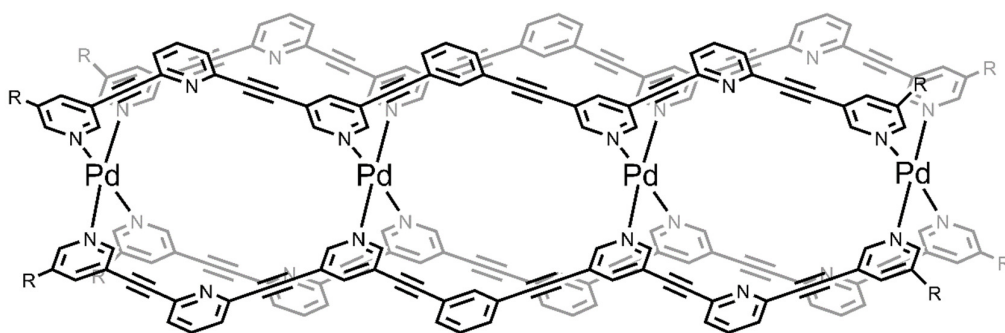


**Figure 2-22:** Triple-cavity Pd<sub>4</sub>L<sub>4</sub> cage constructed by Crowley and coworkers, where R=O(CH<sub>2</sub>)<sub>2</sub>O(CH<sub>2</sub>)<sub>2</sub>OCH<sub>3</sub>. Image adapted from Ref. [101]. For further permissions related to this image, contact the ACS. <https://pubs.acs.org/doi/10.1021/jacs.6b11982>. Copyright American Chemical Society (2017).<sup>101</sup>

Like the Suzuki-Miyaura coupling attempts, difficulties also arose during the Sonogashira coupling attempts, which focused on 3- and 4-ethynyl pyridine coupling partners – this included degradation, side-product formation, and problematic purification. Again the most common occurring reaction was that of the hydrolysis of the halides in the 4 and 9 positions, either resulting in the formation mono-substituted derivatives, or of **Q9**, both of which contained the keto tautomer group.

Variations in reaction conditions included changes in catalyst, reaction time, temperature, and reactant ratios – these variations altered the ratios of mono to disubstituted products, but they were difficult to separate and clean products were not obtained to allow for full characterisation.

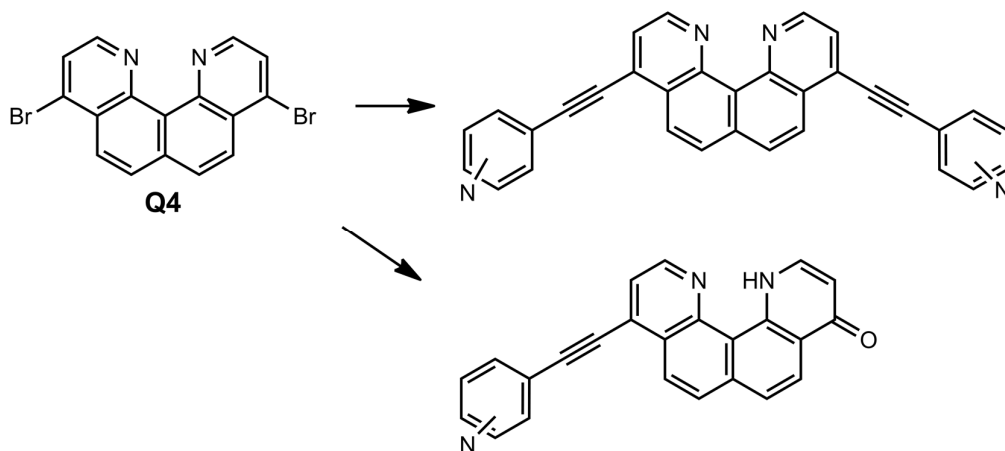


**Figure 2-23:** Synthesis of 4,9-di(X-ethynylpyridyl)quinolino[7,8-*h*]quinoline and 4-(X-ethynylpyridyl)-9-oxo-9,12-dihydroquinolino[7,8-*h*]quinoline from **Q4**, where X = 3 or 4.

Other impurities are also believed to contain alkyne homo-coupled products from the 4-ethynylpyridine starting material, a common competing side reaction in this type of transformation.<sup>102</sup> Purification challenges of these reaction products included a tendency to form oils rather than solid precipitates or crystalline material, and streaking under a large range of column conditions.

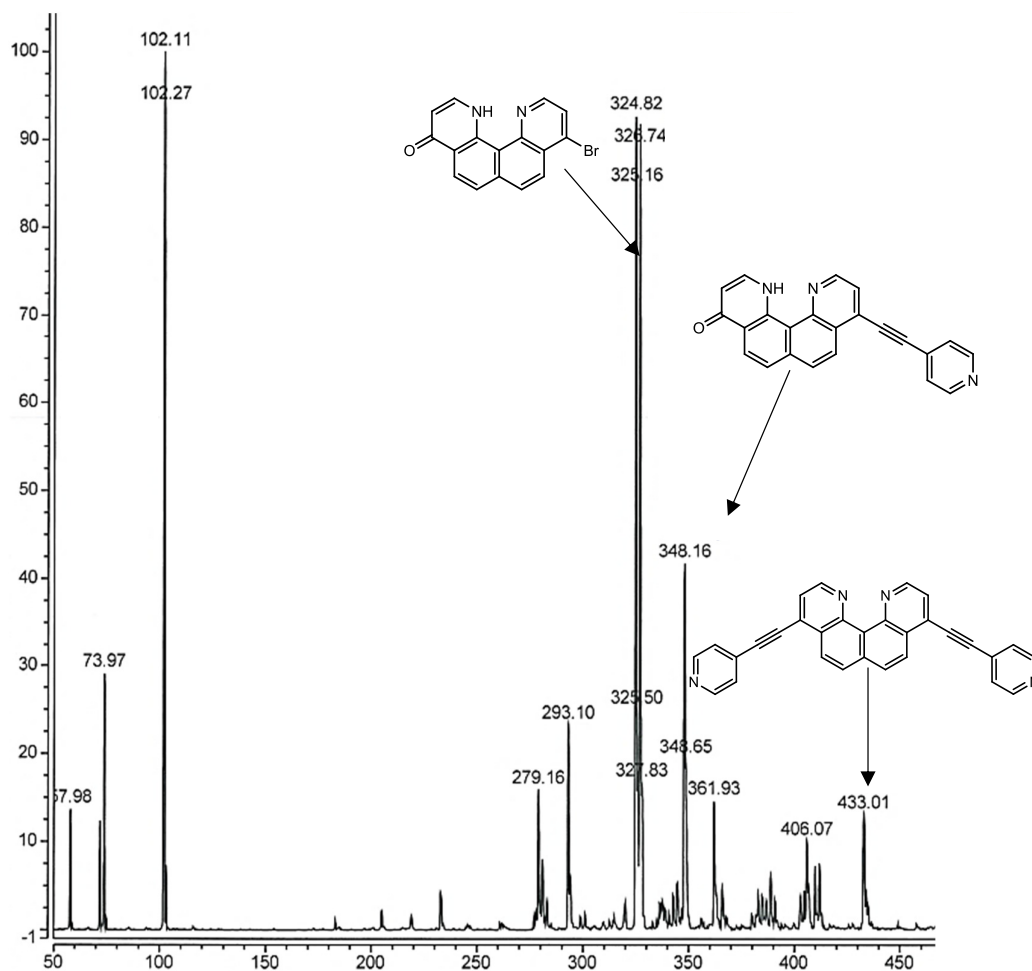


**Figure 2-24: Low-res mass spectrum of a Sonogashira coupling attempt showing three different products.**

### 2.5.3 - Transhalogenation

As previously discussed, many QQ derivative coupling reactions were made more difficult by the occurrence of partial halide hydrolysis, resulting in incomplete conversion. As 4,9-dibromoQQ showed improved conversion rates over 4,9-dichloroQQ,

attempts were made to synthesise the iodo analogue 4,9-diiodoquinolino[7,8-*h*]quinoline to explore test its coupling efficiency, with the chloride **Q3** as the reactant due to its relative ease/reduced cost of synthesis over **Q4**. Bissember and Banwell had reported successful quinoline transhalogenations using sodium iodide (NaI) and acetic anhydride in a microwave reaction (3 h, 80 °C), however attempts to apply this to QQ were unsuccessful, with only starting material observed in the products.<sup>103</sup>

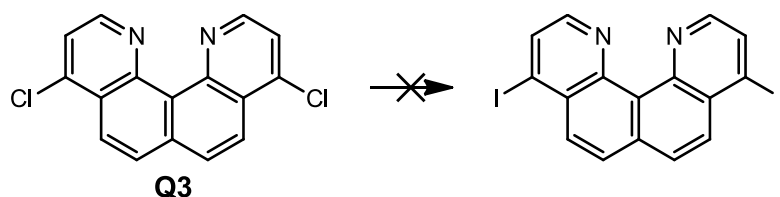


**Figure 2-25: Attempted transhalogenation of **Q3** to 4,9-diiodoquinolino[7,8-*h*]quinoline**

Another quinoline-based method for a chloro- to iodo- transformation was published by Cheruku et al.,<sup>104</sup> where 4,7-dichloroquinoline was converted into 7-chloro-4-iodoquinoline by heating the compound to 130 °C in hydriodic acid (HI) overnight.<sup>104</sup> A similar procedure was adapted and trialled for QQ, using 4,9-dichloroQQ heated in an excess of neat HI over 1-3 days, however this method was also unsuccessful, resulting in a mixture of multiple different products.

#### 2.5.4 - QQ boronic ester – Change of coupling partners

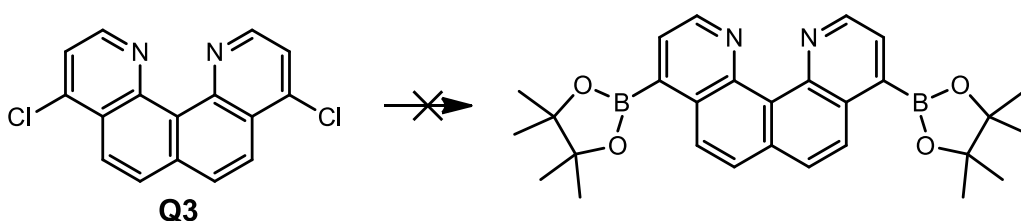


**Figure 2-26: Attempted formation of 4,9-bis(4,4,5,5-tetramethyl-1,3,2-dioxaborolan-2-yl)quinolino[7,8-*h*]quinoline**

Another approach to the goal of improving QQ couplings was the swap of coupling partners, converting 4,9-dichloroQQ into a boronic acid pinacol ester compound. A promising method was published by Qiu et al.,<sup>66</sup> which utilised 4,9-dichloroQQ directly

in conjunction with bispinacolato diboron and a PdCl<sub>2</sub>(dppf) catalyst. However successful replication to give sufficiently pure products was not achieved.

### 2.5.5 - 6,7-dinitroquinolino[7,8-*h*]quinoline-4,9(1*H*,12*H*)-dione

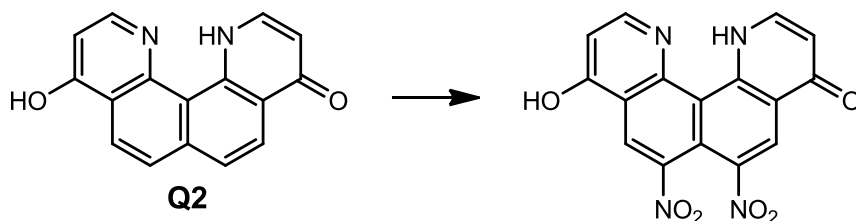


**Figure 2-27: Synthesis of 6,7-dinitroquinolino[7,8-*h*]quinoline-4,9(1*H*,12*H*)-dione**

Nitration of the QQ core has been previously successful for **Q3**, however has not yet been confirmed for the bromide analogue **Q4**. A possible path to 4,9-dibromo-6,7-dinitroquinolino[7,8-*h*]quinoline can be envisaged through the dioxo species **Q2**, or other nitro substituted QQ derivatives. However, the large number of aromatic hydrogen signals on the <sup>1</sup>H NMR spectrum indicated the formation of several different products, potentially involving different numbers of nitro groups. With limited solubility and the presence of more than one side product, the mixture proved too time consuming to isolate.

### 2.5.6 - 4-bromo-9-chloro-quinolino[7,8-*h*]quinoline

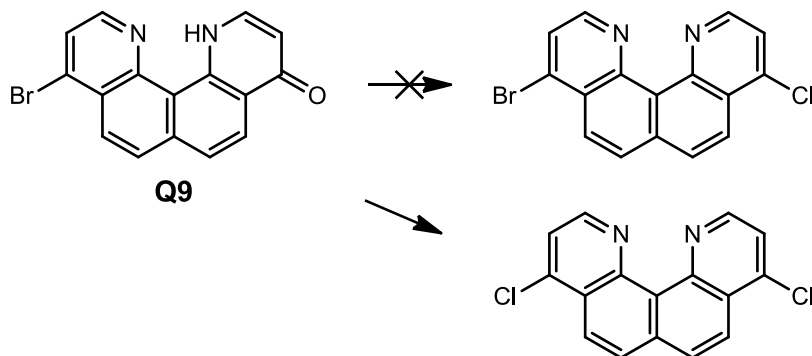


**Figure 2-28: Synthesis of 4-bromo-9-chloro-quinolino[7,8-*h*]quinoline**

An attempt was made to synthesise the new non-symmetric derivative, 4-bromo-9-chloro-quinolino[7,8-*h*]quinoline by chlorinating **Q9**, using the same method used on quinolino[7,8-*h*]quinoline-4,9-(1*H*,12*H*)-dione (**Q2**). A similar transformation in literature successfully halogenated 7-bromo-4(1*H*)-quinolone to produce 4-chloro-7-bromoquinoline,<sup>105</sup> however it appeared that with **Q9** as the starting material, double halide substitution to the dichloride species **Q3** occurred instead (fig. 2-29).

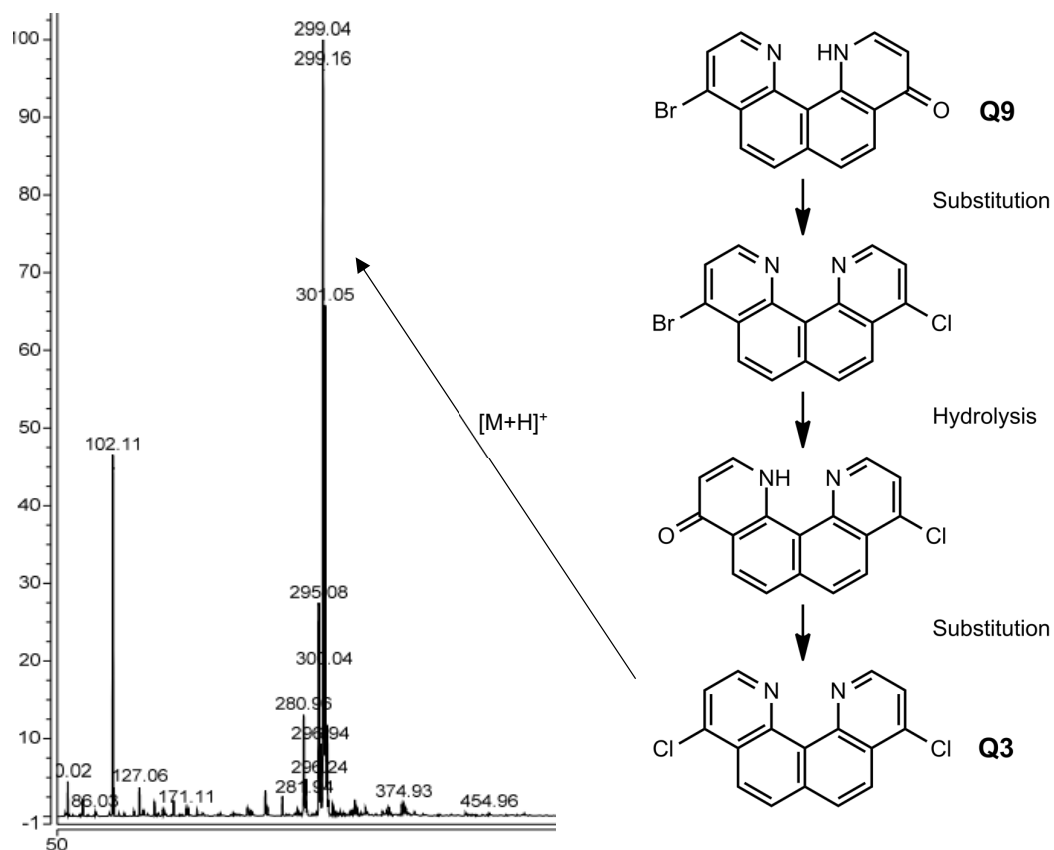


**Figure 2-29: Mass spectrum of attempted formation of 4-bromo-9-chloro-quinolino[7,8-*h*]quinoline (left) and proposed mechanism (right).**

As there is no further stabilisation to be achieved by adding a second oxygen to **Q9** (2.2.1.1), it is proposed that the reaction proceeds first by the substitution of a single chloride, then the more reactive bromide substituent is hydrolysed by the presence of adventitious water in the reaction to give the chloride analogue of **Q9**. Substitution of the second chloride atom then occurs with the excess phosphoryl chloride present to give **Q3** (fig. 2-29(right)).

## 2.6 - Non-QQ Synthesis

### 2.6.1 - Synthesis and characterisation of a boronic acid anhydride-based ligand

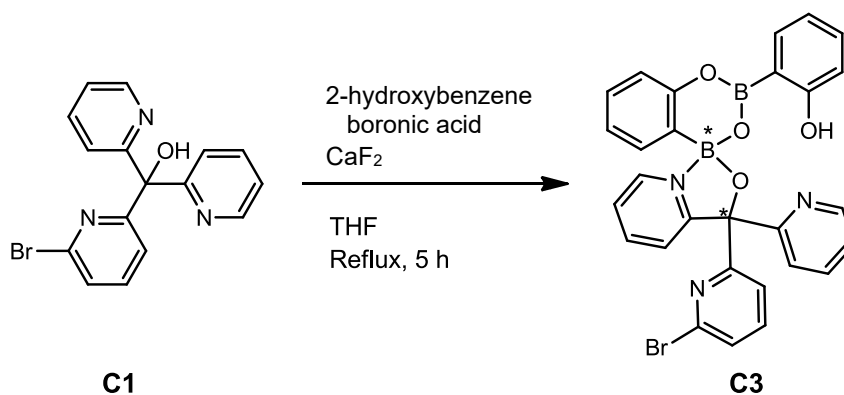


**Figure 2-30: Synthesis of C3 from C1**

The compound **C3** was synthesised from a failed Suzuki-Miyaura coupling attempt of **C1** to make a tetradentate ligand (by a former member of the Plieger Group).<sup>106</sup> It appears that instead of undergoing Suzuki-Miyaura coupling, the boronic acids had formed a 2:1 adduct with the starting material, shown in the crystal structure collected by collaborators (Buchner Group). At the time of the group member's thesis publication, time constraints prevented purification and full characterisation.

Clean synthesis of the boronic acid-anhydride was achieved by omitting the Pd(II) catalyst (thus preventing any coupling from taking place) and refluxing the other reaction components (**C1**, 2-hydroxybenzene boronic acid and calcium fluoride) in THF for five hours, followed by a simple workup to give an 88% isolated yield. NMR analysis showed two diastereoisomers were present at a ratio of ~1:1.2. The phenolic OH peaks (8.81 and 8.91 ppm) were identified by adding a small amount of D<sub>2</sub>O to the NMR tube and rerunning the spectrum, to observe which proton signals decreased due to the deuterium-hydrogen exchange. Attempts were made to separate the diastereoisomers by HPLC, crystallisation and column chromatography, but these were unsuccessful.

This characterisation research was published in *Eur. J. Inorg. Chem.*<sup>107</sup>



## 2.6.2 - Synthesis of 2-hydroxy-5-(3-pyridyl)-benzaldehyde oxime (L1)

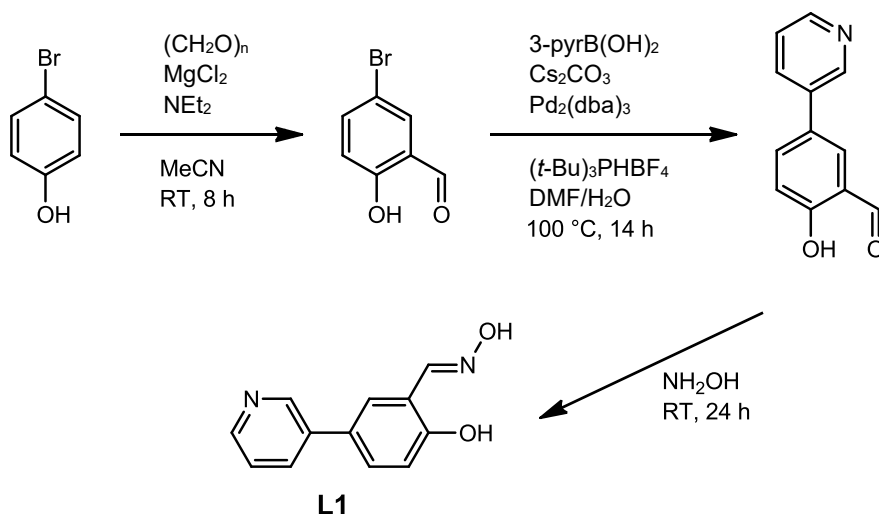


**Figure 2-31: Synthesis of 2-hydroxy-5-(3-pyridyl)-benzaldehyde oxime (L1) from 4-bromophenol.**

The previously discussed obstacles involved in the synthesis, purification, and solubility of many quinolino[7,8-*h*]quinoline derivatives reduced their viability as ligands for coordination cages within the timescale of this project, so a side research project began to explore other compounds. This led to the synthesis of **L1** starting with the formylation of 4-bromophenol, followed by Suzuki-Miyaura coupling, then oximation (3.3.2), to give a new ligand with high coordination potential, possibly as a tripodal ligand.<sup>108</sup>

The design of **L1** was based on the successful use of several of its components in coordination chemistry literature. Ligands featuring the imine-based salen substructure (*N,N'*-ethylenebis(salicylimine)) are common,<sup>109</sup> and the oxime analogue moiety of **L1**, salicyladoxime, is found in a range of metallo-organic structures, particularly in coordination clusters.<sup>110-112</sup> Pyridine substituents are ubiquitous in coordination chemistry, including in coordination cages,<sup>38</sup> and the angle of the coordinating nitrogen atom in 3-pyridyl groups is conducive to the formation of discrete structures, such as the cage shown in figure 2-22.<sup>37,101,113</sup> Additionally, success was achieved by MacLachlan and coworkers with an imine structure similar to **L1** in the formation of metallomacrocycles (fig. 2-32) which aggregated into columnar structures, however the oxime ligand **L1** was not published.<sup>114</sup>

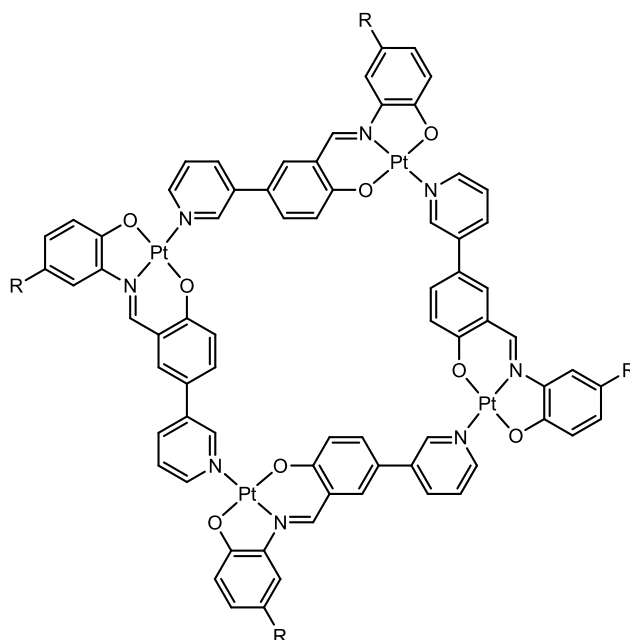


**Figure 2-32: Pt<sub>4</sub>L<sub>4</sub> metallomacrocyclic synthesised by MacLachlan and coworkers.<sup>114</sup>**

Some details of 2-hydroxy-5-(3-pyridyl)-benzaldehyde synthesis were provided in a patent,<sup>115</sup> however the full synthetic procedure up to that point, and the conversion to the oxime, was based on a combination of sources for efficiency and to make use of existing chemical stocks.<sup>115-118</sup> A number of synthesis and purification issues were encountered, including side product formation in the formylation of 4-bromophenol, however the 5-bromosalicylaldehyde product could be isolated by flash silica gel column chromatography run with 100% dichloromethane, with the desired aldehyde the first compound to be eluted. These intermediate products were identified by NMR comparison to literature.

NMR analysis was consistent with final **L1** oxime ligand – along with minor changes to the chemical shift positions of the aromatic proton signals, was the disappearance of the aldehyde proton of 2-hydroxy-5-(3-pyridyl)-benzaldehyde, and appearance of the strongly deshielded oxime signal at 11.45 ppm (fig. C-32). Identification was supported by high resolution mass spectrometry.

Crystallisation attempts involving **L1** were unsuccessful.

## 2.7 - Conclusion

A number of new and novel quinolino[7,8-*h*]quinoline derivatives have been successfully synthesised and characterised. These include a range of both symmetric and non-symmetric compounds, and the research presented here both contributes significantly to the library of existing QQ compounds, and the number of synthetic pathways open to exploration. Many challenges were encountered in the process, including purification and competing reactions, some of which led to redirections in focus, others to opportunities. Going forward, useful potential synthetic foci include: expanding the library of non-symmetric compounds with further substitution of the 4,9 positions; an aim towards more soluble derivatives to reduce characterisation difficulties and widen applications (like coordination) and; exploring the use of more stringent water free conditions for symmetrical synthesis.

## Chapter 3 - Experimental Synthesis Methods

### 3.1 - General QQ experimental and characterisation notes

Due to the superbasic nature of these compounds, protonation was a common occurrence throughout synthesis and general handling. In most cases this did not appear to interfere with the use of the product in further reactions. Once protonation of a central nitrogen had occurred, in some cases it could be very difficult to remove without causing degradation. These strongly deshielded protons were visible in high ppm ranges (up to 24 ppm). In most cases, a thorough wash of an organic solution of the QQ derivative with strong aqueous potassium hydroxide ( $\geq 6$  M) was sufficient. In the case of the diamine **Q7**, however ( $pK_a$  23.97, see chapter 4), the KOH wash began to cause degradation, and a saturated bicarbonate was insufficient to deprotonate a central nitrogen. In this case deprotonation could be achieved using the strong base DBU, however this was not ideal as it remained with the QQ product and required an extra step to remove.

Another regular observation in QQ  $^1\text{H}$  NMR spectra is peak position shifts. These were seen between different product batches and were attributed to concentration effects (H-bonding,  $\pi$ - $\pi$  stacking), and interactions with solvents and/or impurities. Sometimes these shifts were significant. The example given below (fig. 3-1) compares the  $^1\text{H}$  NMR spectra in the 6.5-9.5 ppm range of two different batches of **Q7** (also at different concentrations). The lower (blue) spectrum displays peak shifts of up to 0.3 ppm compared to the upper (red) spectrum, which has a product concentration  $\sim 3$ -4x higher.

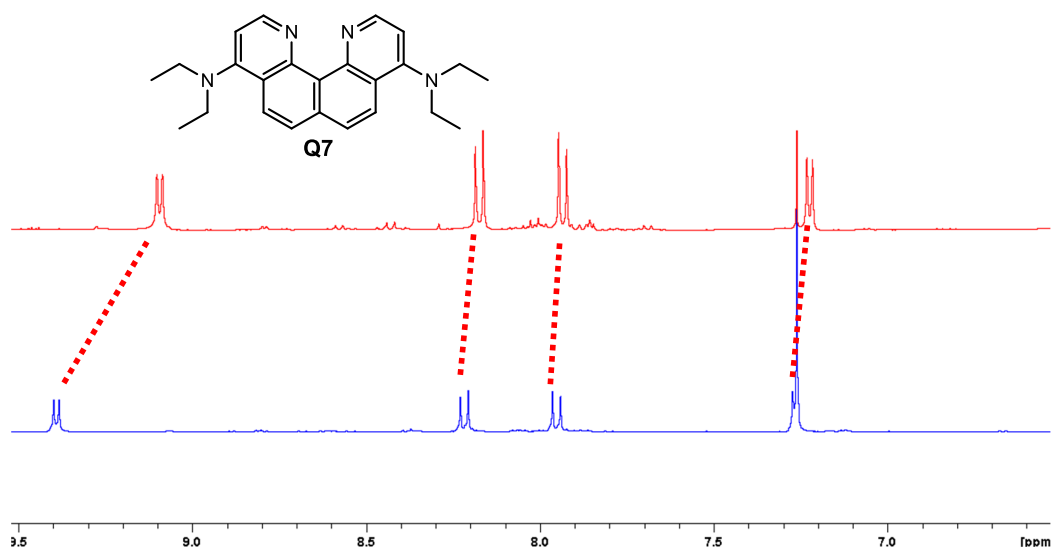


**Figure 3-1:  $^1\text{H}$  NMR spectra comparison of Q7 showing the aromatic region. Upper spectrum is  $\sim 3\text{-}4\text{x}$  more concentrated (exact concentrations were not recorded).**

It was also observed that longer range coupling to the proton sitting in the central nitrogen pocket sometimes causes additional peak splitting in the neighbouring proton signals.

Figure 3-2 shows the two aromatic proton peaks (A and B) that are most closely associated with the oxo-containing side of a non-symmetric mono-oxo QQ derivative. A peak pattern shift compared to that expected (where both proton signals should present as doublets) is believed to be caused by central proton effects. Initial observations set HA as a triplet, before a line refinement corrected to an overlapping dd (although the J coupling values are not quite equal).

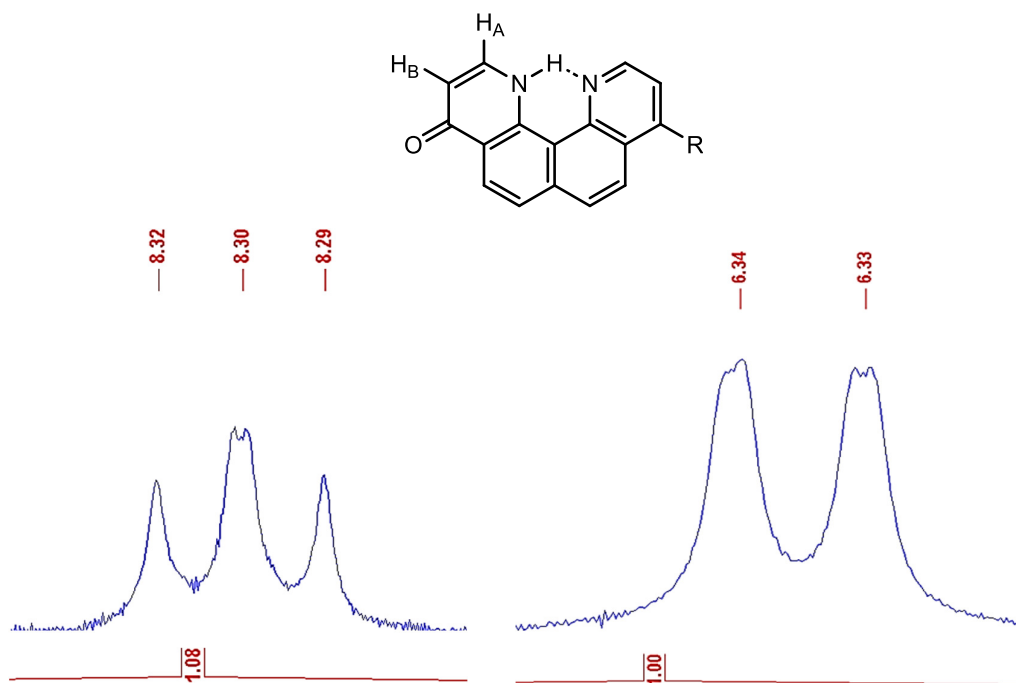


**Figure 3-2:** <sup>1</sup>H NMR signals corresponding to HA (left) and HB (right). Both proton signals should present as doublets, however this is not observed here.

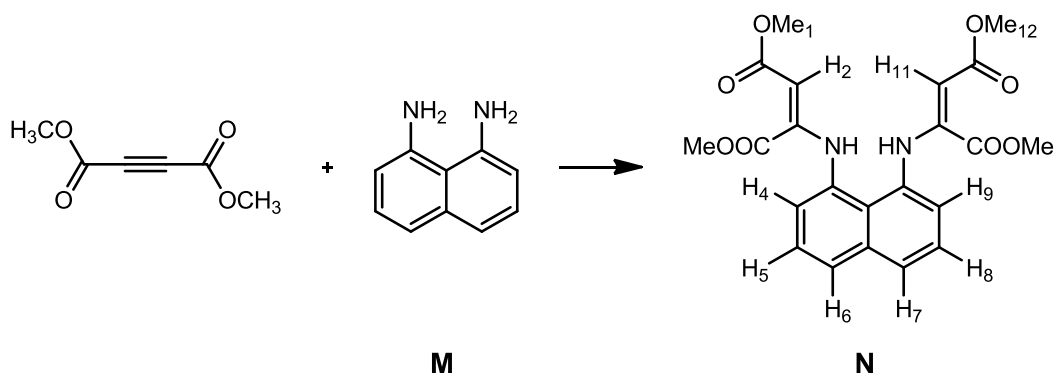
Unless otherwise stated, all reagents and solvents were purchased from commercial sources and used without purification. NMR spectra were collected on Bruker Avance 400, 500 and 700 MHz spectrometers. All chemical shifts are reported relative to residual solvent (<sup>1</sup>H, <sup>13</sup>C). Microanalyses were performed at the Campbell Microanalytical Laboratory at the University of Otago. High resolution mass spectra were recorded on a Thermo Scientific Q-Exactive Focus Hybrid Quadrupole-Orbitrap mass spectrometer. Electrospray mass spectra were recorded with a Thermo Scientific UltiMate 3000 spectrometer run in the positive ion mode. IR and UV-Vis spectra were recorded with a Nicolet 5700 FT-IR and a UV-1800 Shimadzu spectrophotometer respectively. Single crystal X-ray data were collected at a reduced temperature with a Rigaku Spider diffractometer equipped with a copper rotating anode X-ray source and a curved image plate detector. The crystals were mounted in an inert oil, transferred to the cold gas stream of the detector, and irradiated with graphite monochromated Cu- $K_{\alpha}$  ( $k = 1.54187 \text{ \AA}$ ) X-rays. The data were collected by the Crystal Clear program (v.1.4.0) and processed with FS-PROCESS to apply the Lorentz and polarisation corrections to the diffractions spots (integrated three-dimensionally). The structures were solved by direct

methods using SHELXS-97 and refined using the SHELXL-97 program.<sup>119</sup> Absorption correction was carried out empirically. Non-acidic hydrogen atoms have been placed in calculated positions.<sup>11</sup>

Note: Many of the experimental methods in this chapter are published in Rowlands et al.<sup>11</sup>

## 3.2 - Experimental methods

### 3.2.1 - Synthesis of tetramethyl-2,2'-(naphthalene-1,8-diylbis(azanediyl)) difumarate (**N**)

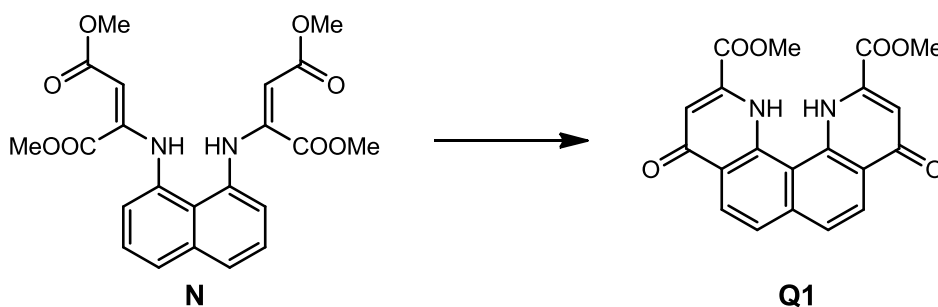


**N** was synthesised according to the reported procedures (modified).<sup>46</sup>

Recrystallised 1,8-diaminonaphthalene (40.8 mmol, 6.45 g, **M**) was dissolved in EtOH (500 ml). This dark red solution was added dropwise to DMAD (81.3 mmol, 10 ml), with stirring, over 1.5 h. The mixture was left to stir for another 1-2 hours, during which a yellow precipitate was formed, then placed in a refrigerator/freezer overnight. A brownish-yellow precipitate was collected by vacuum filtration and washed with 1:1 hexane : acetone (250 ml). A bright yellow precipitate was obtained in 47% yield (8.59 g). The <sup>1</sup>H NMR was consistent with the literature values.<sup>54</sup> <sup>1</sup>H NMR (DMSO-*d*<sub>6</sub>, 500 MHz)  $\delta$  = 10.12 (s, 2H, NH), 7.93 (d, *J* = 7.7 Hz, 2H, 4,9-*H*), 7.57 (t, *J* = 7.7 Hz, 2H, 5,8-*H*), 6.93 (d, *J* = 7.7 Hz, 2H, 6,7-*H*), 5.36 (s, 2H, 2,11-*H*), 3.59 (s, 6H, 1,12-*H*), 3.57 (s, 6H, 3,10-*H*) ppm.



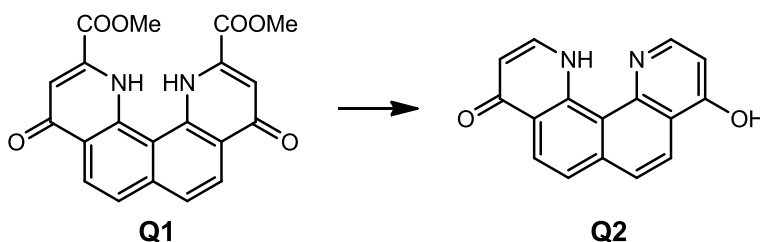
### 3.2.2 - Synthesis of 4,9-dioxo-1,4,9,12-tetrahydroquinolino[7,8-*h*]quinoline-2,11-dicarboxylate (Q1)



**Q1** was synthesised according to the reported procedure (modified).<sup>46</sup>

Diphenyl ether (60 ml) was preheated to 250 °C before **N** (5.65 mmol, 2.5 g) was added down the reflux condenser. The reaction mixture was stirred for 20 mins. The purple-brown solid formed was allowed to cool, then filtered and washed with acetone (200 ml) to give a tan clay-like product in 67% yield (1.8 g). The <sup>1</sup>H NMR was consistent with the literature values.<sup>55</sup> Note: The phenyl ether used in this reaction can be recovered by vacuum distillation. <sup>1</sup>H NMR (TFA-*d*, 500 MHz)  $\delta$  = 8.99 (d, *J* = 9.0 Hz, 2H, 5,8-*H*), 8.52 (d, *J* = 9.0 Hz, 2H, 6,7-*H*), 8.32 (s, 2H, 3,10-*H*), 4.53 (s, 6H, CH<sub>3</sub>) ppm.

### 3.2.3 - Synthesis of quinolino[7,8-*h*]quinoline-4,9-(1*H*,12*H*)-dione (**Q2**)

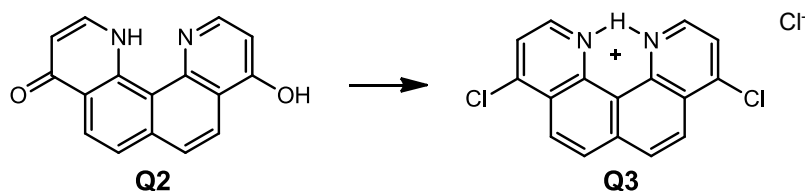


**Q2** was synthesised according to the reported procedure.<sup>41, 46, 54</sup>

Anhydrous sodium acetate (2.09 mmol, 0.172 g) and 4,9-dioxo-1,4,9,12-tetrahydroquinolino[7,8-*h*]quinoline-2,11-dicarboxylate **Q1** (2.11 mmol, 0.800 g) were stirred in water (80 ml) for a few minutes before being placed inside a 200 ml capacity Teflon lined stainless steel bomb. This was placed in an oven at 240 °C for 12 h (excluding heating/cooling time) and left stationary overnight. The bomb was removed and allowed to cool.

The opaque brown solution was centrifuged at 4000x rpm for 15-20 mins. The orange-brown aqueous layer was removed by decanting, and the process repeated with further water washes (2x 30 ml) and an EtOH wash (30 ml). The remaining precipitate was removed from the centrifuge tubes by firstly suspending in EtOH. The combined organic fractions were then dried first by rotary evaporation then further *in vacuo* overnight to give **Q1** in 78% yield (364 mg). <sup>1</sup>H NMR (TFA-*d*, 500 MHz)  $\delta$  = 9.12 (d, *J* = 6.3 Hz, 2H, 2,11-*H*), 8.95 (d, *J* = 9.0 Hz, 2H, 5,8-*H*), 8.48 (d, *J* = 9.0 Hz, 2H, 6,7-*H*), 7.69 (d, *J* = 6.3 Hz, 2H, 3,10-*H*) ppm.

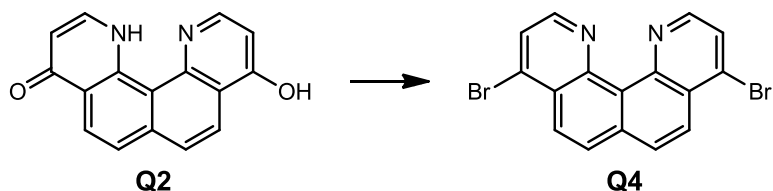
### 3.2.4 - Synthesis of 4,9-dichloroquinolino[7,8-*h*]quinoline (Q3)



**Q3** was synthesised according to the reported procedure.<sup>54</sup>

Phosphoryl chloride (26.4 mmol, 2.44 ml) was added to quinolino[7,8-*h*]quinoline-4,9-(1*H*,12*H*)-dione **Q2** (0.382 mmol, 100 mg). The flask and reflux condenser were degassed (under Ar) before adding to a 130 °C oil bath, and the reaction stirred for 8 mins. The reaction mixture was diluted with DCM (200 ml) and basified with 6M KOH<sub>(aq)</sub> (20 ml), followed by vigorous stirring for a few minutes. Water was added (200 ml), and the solution stirred for further 2 minutes before transferring to a separating funnel. The organic layer was separated, dried (MgSO<sub>4</sub>) and filtered. The solvent was removed by rotary evaporation and dried *in vacuo*. Yield 61% (70 mg). The <sup>1</sup>H NMR was consistent with the literature values.<sup>54</sup> <sup>1</sup>H NMR (CDCl<sub>3</sub>, 500 MHz)  $\delta$  = 9.29 (d, *J* = 5.0 Hz, 2H, 2,11-*H*), 8.60 (d, *J* = 8.9 Hz, 2H, 5,8-*H*), 8.48 (d, *J* = 8.9 Hz, 2H, 6,7-*H*), 8.22 (d, *J* = 3.8 Hz, 2H, 3,10-*H*) ppm.

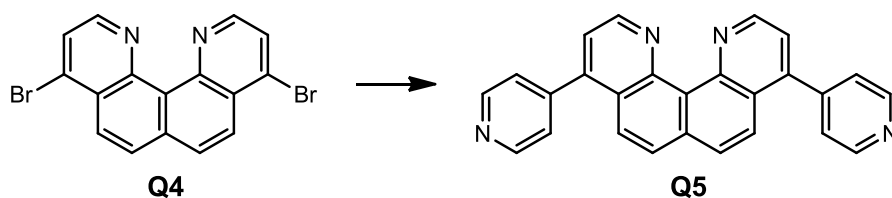
### 3.2.5 - Synthesis of 4,9-dibromoquinolino[7,8-*h*]quinoline (Q4)



**Q4** was synthesised according to the reported procedure.<sup>11, 54</sup>

Phosphorous oxybromide (2.08 mmol, 597 mg) was added to a degassed (under argon) sample of quinolino[7,8-*h*]quinoline-4,9-(1*H*,12*H*)-dione **Q2** (0.379 mmol, 100 mg). The flask, fitted with a reflux condenser, was added to a preheated 200 °C oil bath and left to stir for ~30 minutes. The black mixture was allowed to cool before being transferred quantitatively to a conical flask with a solution of 1:10 MeOH : DCM (44 ml), aided by sonication. 6M KOH<sub>(aq)</sub> (10 ml) was added, and the solution was stirred briefly before being transferred to a separating funnel. Distilled water was added (50 ml) and the orange organic layer was collected. The aqueous layer was washed with 1:10 MeOH : DCM solution to a total volume of ~ 80 ml. The organic solution was dried (MgSO<sub>4</sub>), filtered, and the solvent removed by rotary evaporation, yielding a yellow-brown solid in 89% yield (178 mg). No purification typically required. The <sup>1</sup>H NMR was consistent with the literature values.<sup>54</sup> <sup>1</sup>H NMR (CDCl<sub>3</sub>, 500 MHz) δ = 9.21 (d, *J* = 4.7 Hz, 2H, 2,11-*H*), 8.57 (d, *J* = 8.7 Hz, 2H, 5,8-*H*), 8.22 (d, *J* = 8.7 Hz, 2H, 6,7-*H*), 7.98 (d, *J* = 4.7 Hz, 2H, 3,10-*H*) ppm.

### 3.2.6 - Synthesis of 4,9-di(pyridin-4-yl)quinolino[7,8-*h*]quinoline (Q5)

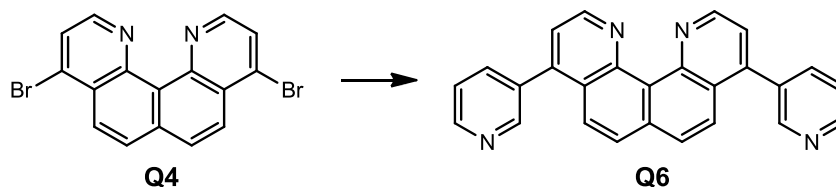


Dry DMF (20 mL) was added to a mixture of **Q4** (100 mg, 0.258 mmol), 4-pyridine pinacol ester (211 mg, 1.03 mmol), caesium carbonate (420 mg, 1.29 mmol) and the Pd(PPh<sub>3</sub>)<sub>4</sub> catalyst (30 mg, 0.026 mmol). The mixture was degassed and stirred at 80 °C for 21 h. Water (50 mL) was added and the residue extracted with CHCl<sub>3</sub>. The organic layer was washed with water (3 x 50 mL), dried with MgSO<sub>4</sub>, filtered and dried *in vacuo*.

Alternatively - dry DMF (20 mL) was added to a mixture of **Q4** (100 mg, 0.258 mmol), 4-pyridine pinacol ester (211 mg, 1.03 mmol), caesium carbonate (420 mg, 1.29 mmol) and the Pd(PPh<sub>3</sub>)<sub>4</sub> catalyst (30 mg, 0.026 mmol) in a glass microwave tube. The degassed reaction was performed in a microwave synthesiser at 80°C, 300 W for 2h. Water (50 mL) was added and the residue extracted with CHCl<sub>3</sub>. The organic layer was washed with water (3 x 50 mL), dried with MgSO<sub>4</sub>, filtered and dried *in vacuo*.

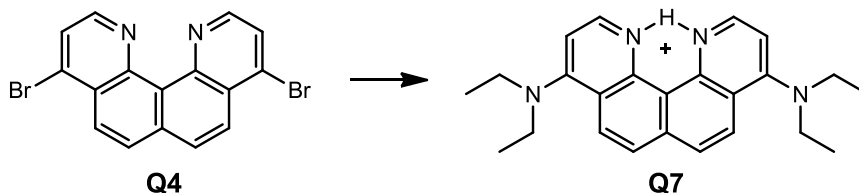
The product was purified by recrystallisation from hot CH<sub>2</sub>Cl<sub>2</sub> to give **Q5** (26 mg, 26%). Crystals suitable for X-ray crystallography were grown by slow evaporation of **Q5** in a 1:1:1 DCM : MeOH : CHCl<sub>3</sub> solvent mixture. <sup>1</sup>H NMR (700 MHz, CDCl<sub>3</sub>) δ = 9.46 (d, *J* = 4.2 Hz, 2H, 2,11-*H*), 8.84 (dd, *J* = 1.6, 4.3 Hz, 4H, 2-Py-*H*), 7.99 (d, *J* = 8.8 Hz, 2H, 5,8-*H*), 7.94 (d, *J* = 8.8 Hz, 2H, 6,7-*H*), 7.54 (d, *J* = 4.3 Hz, 2H, 3,10-*H*), 7.51 (dd, *J* = 1.6, 4.3 Hz, 4H, 3-Py-*H*) ppm. <sup>13</sup>C NMR (176 MHz, CDCl<sub>3</sub>): δ = 150.2 (C2-Py, C2'-Py), 149.8 (C2, C11), 147.9 (C12a, C12c), 146.5 (C4, C9), 145.6 (C4-Py, C4'-Py), 135.5 (C4a, C8a), 128.1 (C6, C7), 126.9 (C12b), 125.7 (C5, C8), 125.6 (C6a), 124.6 (C3-Py, C3'-Py), 121.0 (C3, C10) ppm. HRMS (ESI) *m/z*: [M + H]<sup>+</sup> Calcd for C<sub>26</sub>H<sub>17</sub>N<sub>4</sub> 385.1448; Found 385.1447. C<sub>26</sub>H<sub>16</sub>N<sub>4</sub>·0.8CH<sub>2</sub>Cl<sub>2</sub>: calculated C 71.35, H 3.93, N 12.43; Found C 71.35, H 3.79, N 12.76. UV-Vis (CHCl<sub>3</sub>) λ<sub>max</sub> (ε / L mol<sup>-1</sup> cm<sup>-1</sup>): 278 (58200), 359 (5820), 377 (6970) nm. IR (FT): ν̃ = 3033 (w), 1596 (s), 1580 (m), 1413 (s), 1067 (m), 871 (s), 830 (s), 775 (m), 704 (w) cm<sup>-1</sup>.

### 3.2.7 - Synthesis of 4,9-di(pyridin-3-yl)quinolino[7,8-*h*]quinoline (Q5)



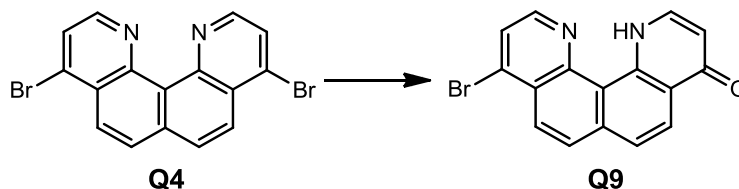
Dry DMF (25 mL) was added to a mixture of **Q4** (100 mg, 0.258 mmol), 3-pyridine boronic acid pinacol ester (211 mg, 1.03 mmol), caesium carbonate (420 mg, 1.29 mmol), (*t*-Bu)<sub>3</sub>PHBF<sub>4</sub> (8 mg, 0.026 mmol) and Pd<sub>2</sub>(dba)<sub>3</sub> (24 mg, 0.026 mmol). The suspension was stirred at 100 °C for 20 h under an atmosphere of Ar. Water (50 mL) was added and the reaction mixture was basified with 6M KOH (40 mL) and extracted with CHCl<sub>3</sub>. The organic layer was washed with water (3 x 50 mL), dried with MgSO<sub>4</sub>, filtered and dried *in vacuo*. The product was purified by recrystallisation from hot DCE to give **Q6** (30 mg, 30%). <sup>1</sup>H NMR (500 MHz, DMSO-*d*<sub>6</sub>): δ = 9.63 (d, *J* = 5.0 Hz, 2H, 2,11-*H*), 8.95 (br s, 2H, 2-Py-*H*), 8.90 (d, *J* = 4.0 Hz, 2H, 6-Py-*H*), 8.52 (d, *J* = 9.0 Hz, 2H, 5,8-*H*), 8.32 (d, *J* = 9.0 Hz, 2H, 6,7-*H*), 8.29 (d, *J* = 5.0 Hz, 2H, 3,10-*H*), 8.23 (d, *J* = 7.6 Hz, 2H, 4-Py-*H*), 7.77 (m, 2H, 5-Py-*H*) ppm. <sup>13</sup>C NMR (125 MHz, DMSO-*d*<sub>6</sub>): δ = 150.9 (C6-Py, C6'-Py), 150.2 (C2-Py, C2'-Py), 147.8 (C2, C11), 144.1 (C12a, C12c), 138.1 (C4-Py, C4'-Py), 136.5 (C3-Py, C3'-Py), 136.3 (C4, C9), 134.0 (C4a, C8a), 133.0 (C6a), 129.8 (C5, C8), 127.3 (C6, C7), 126.4 (C12b), 124.4 (C5-Py, C5'-Py), 124.0 (C3, C10) ppm. HRMS (ESI) *m/z*: [M + H]<sup>+</sup> Calcd for C<sub>26</sub>H<sub>17</sub>N<sub>4</sub> 385.1448; Found 385.1482.

### 3.2.8 - Synthesis of *N*<sup>4</sup>,*N*<sup>4</sup>,*N*<sup>9</sup>,*N*<sup>9</sup>-tetraethylquinolino[7,8-*h*]quinoline-4,9-diamine



Excess neat diethylamine (20 mL) was added to **Q4** (100 mg, 0.258 mmol) and heated under reflux for 48 – 72 h. Water (50 mL) was added and the residue was extracted with DCM (100 mL). The organic layer was washed with water (3 x 100 mL), dried with MgSO<sub>4</sub>, filtered and dried *in vacuo* to give **Q7** (86 mg, 90%). <sup>1</sup>H NMR (500 MHz, CDCl<sub>3</sub>): δ = 19.42 (s, 1H, NH), 9.22 (dd, *J* = 3.0, 6.2 Hz, 2H, 2,11-*H*), 8.23 (d, *J* = 9.1 Hz, 2H, 5,8-*H*), 7.98 (d, *J* = 9.1 Hz, 2H, 6,7-*H*), 7.30 (d, *J* = 6.2 Hz, 2H, 3,10-*H*), 3.68 (q, *J* = 7.1 Hz, 8H, CH<sub>2</sub>CH<sub>3</sub>), 1.38 (t, *J* = 7.1 Hz, 12H, CH<sub>2</sub>CH<sub>3</sub>) ppm. <sup>13</sup>C NMR (125 MHz, CDCl<sub>3</sub>): δ = 158.6 (C4, C9), 144.5 (C2, C11), 144.4 (C12a, C12b), 135.9 (C6a), 125.6 (C5, C8), 125.3 (C6, C7), 119.8 (C12b), 117.1 (C4a, C8a), 108.9 (C3, C12), 47.2 (CH<sub>2</sub>), 12.4 (CH<sub>3</sub>) ppm. HRMS (ESI/Orbitrap) *m/z*: [M + H]<sup>+</sup> Calcd for C<sub>24</sub>H<sub>29</sub>N<sub>4</sub> 373.2387; Found 373.2385.

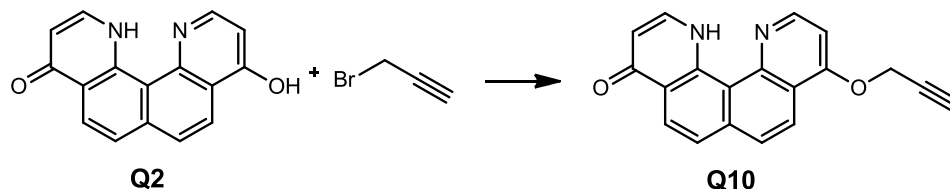
### 3.2.9 - Synthesis of 4-bromo-9-oxo-9,12-dihydroquinolino[7,8-*h*]quinoline (Q9)



A 2:3 MeOH : H<sub>2</sub>O (5 mL) was added to **Q4** (6 mg, 0.0155 mmol) and heated under reflux for ~14 h. The solvent was removed *in vacuo* then the precipitate dissolved in a solution of 24:1 CHCl<sub>3</sub> : MeOH (25 mL). The solution was washed with water (3 x 30 mL), dried with MgSO<sub>4</sub>, filtered, and dried *in vacuo* to give **Q9** (4 mg, 80%). <sup>1</sup>H NMR (500 MHz, CDCl<sub>3</sub>): δ = 15.49 (s, 1H, NH), 8.85 (d, *J* = 4.9 Hz, 1H, 5-*H*), 8.77 (d, *J* = 8.6 Hz, 1H, 2-*H*), 8.37 (d, *J* = 9.1 Hz, 1H, 7-*H*), 8.08 (d, *J* = 9.1 Hz 1H, 8-*H*), 7.99 (m, 2H, 6,11-*H*), 7.86 (d, *J* = 8.6 Hz, 1H, 3-*H*), 6.61 (d, *J* = 7.3 Hz, 1H, 10-*H*) ppm. <sup>13</sup>C NMR (125 MHz, CDCl<sub>3</sub>): δ = 178.4 (C9), 176.1 (C12a), 148.3 (C12c), 146.8 (C5), 146.5 (C4), 146.4 (C6a), 140.3 (C4a), 137.8 (C11), 137.1 (C8a), 130.4 (C8), 127.2 (C2), 126.5 (C7), 125.6 (C6), 123.5 (C3), 112.1 (C10), 108.1 (C12b) ppm. HRMS (ESI) *m/z*: = [M + H]<sup>+</sup> Calcd for C<sub>16</sub>H<sub>10</sub>BrN<sub>2</sub>O 326.9951; Found 326.9975.

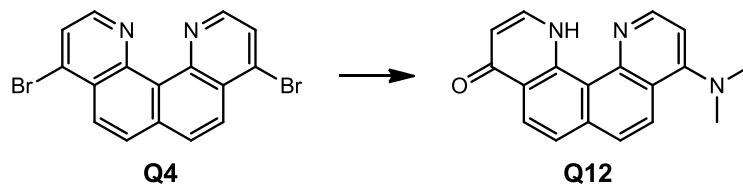


### 3.2.10 - Synthesis of 9-(2-propyn-1-yloxy)-quinolino[7,8-*h*]quinolin-4(1*H*)-one (Q10)



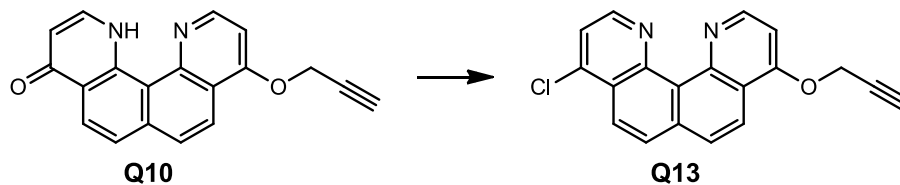
**Q2** (50 mg, 0.191 mmol) and K<sub>2</sub>CO<sub>3</sub> (80 mg, 0.579 mmol) were suspended in DMF (10 ml). Propargyl bromide (80% wt % toluene, 20  $\mu$ L, 0.181 mmol) was added and stirred at room temperature for 14-24 h. The reaction mix was cooled, filtered with cotton wool and filter paper, and dried *in vacuo* to give **Q10** (38 mg, 70%). <sup>1</sup>H NMR (500 MHz, DMSO-*d*<sub>6</sub>):  $\delta$  = 15.59 (s, 1H, NH), 9.08 (d, *J* = 5.5 Hz, 1H, 11-*H*), 8.43 (d, *J* = 8.7 Hz, 1H, 8-*H*), 8.33 (d, *J* = 8.9 Hz, 1H, 5-*H*), 8.29 (t, *J* = 6.7 Hz, 1H, 2-*H*), 8.14 (d, *J* = 9.1 Hz, 1H, 6-*H*), 7.95 (d, *J* = 8.7 Hz, 1H, 7-*H*), 7.49 (d, *J* = 5.5 Hz, 1H, 10-*H*), 6.32 (d, *J* = 7.2 Hz, 1H, 3-*H*), 5.27 (s, 2H, CH<sub>2</sub>), 3.80 (br s, 1H, CCH) ppm. <sup>13</sup>C NMR (125 MHz, DMSO-*d*<sub>6</sub>)  $\delta$  = 176.6 (C4), 160.4 (C9), 149.7 (C11), 147.6 (C12c), 139.9 (C2), 139.4 (C12a), 136.3 (C6a), 127.7 (C6), 125.2 (C8), 124.5 (C4a), 123.3 (C7), 121.4 (C5), 118.6 (C8a), 116.7 (C12b), 110.8 (C3), 104.1 (C10), 79.8 (CH<sub>2</sub>C), 78.0 (CCH), 56.9 (CH<sub>2</sub>) ppm. HRMS (ESI) *m/z*: [M + H]<sup>+</sup> Calcd for C<sub>19</sub>H<sub>13</sub>N<sub>2</sub>O 301.0972; Found 301.0970.

### 3.2.11 - Synthesis of 9-(dimethylamino)quinolino[7,8-*h*]quinoline-4(1*H*)-one (Q12)



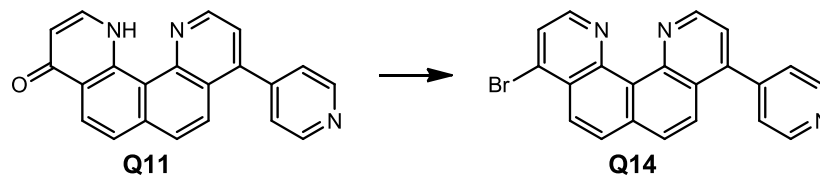
Dimethylamine solution (40% aq., 15 mL) was added to **Q4** (57 mg, 0.148 mmol) and heated under reflux for 24 - 48 h. Water (150 mL) was added and the residue was extracted with DCM (150 mL). The organic layer was washed with water (2 x 100 mL), dried with MgSO<sub>4</sub>, filtered, and dried *in vacuo* to give **Q12** (26 mg, 60%). <sup>1</sup>H NMR (500 MHz, CDCl<sub>3</sub>): δ = 16.15 (s, 1H, NH), 8.68 (d, *J* = 5.4 Hz, 1H, 11-*H*), 8.58 (d, *J* = 8.6 Hz, 1H, 8-*H*), 8.09 (d, *J* = 9.0 Hz, 1H, 6-*H*), 7.90 (t, *J* = 6.5 Hz, 1H, 2-*H*), 7.76 (d, *J* = 9.0 Hz, 1H, 5-*H*), 7.68 (d, *J* = 8.6 Hz, 1H, 7-*H*), 6.97 (d, *J* = 5.4 Hz, 1H, 10-*H*), 6.51 (d, *J* = 6.6 Hz, 1H, 3-*H*), 3.11 (s, 6H, CH<sub>3</sub>) ppm. <sup>13</sup>C NMR (125 MHz, CDCl<sub>3</sub>): δ = 178.3 (C4), 158.5 (C9), 148.9 (C12c), 147.2 (C11), 144.1 (C12a), 140.7 (C6a), 137.4 (C2), 136.2 (C4a), 125.8 (C5), 125.6 (C7), 124.6 (C6), 123.1 (C8), 120.5 (C8a), 117.6 (C12b), 111.5 (C10), 108.1 (C3), 44.1 (CH<sub>3</sub>) ppm. HRMS (ESI) *m/z*: [M + H]<sup>+</sup> Calcd for C<sub>18</sub>H<sub>16</sub>N<sub>3</sub>O 290.1288; Found 290.1278.

### 3.2.12 - Synthesis of 4-chloro-9-(2-propyn-1-yloxy)-quinolino[7,8-*h*]quinoline (Q14)



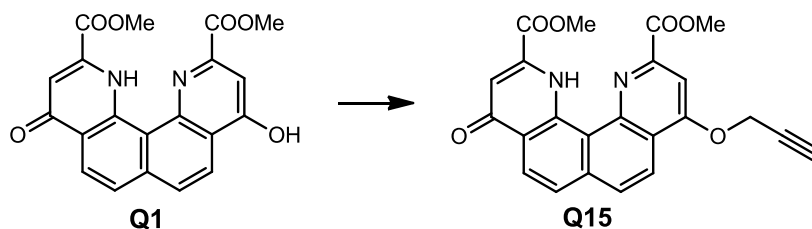
Phosphoryl chloride (10.7 mmol, 1.00 ml) was added to **Q10** (0.0466 mmol, 14 mg). The flask and reflux condenser were degassed (under Ar) before adding to a 130 °C oil bath, and the reaction stirred for 5-8 mins. The reaction mixture was diluted with CHCl<sub>3</sub> (50 ml) and washed twice with alternating H<sub>2</sub>O (60 ml) and brine (60 ml). The organic layer was dried with MgSO<sub>4</sub>, filtered, and dried *in vacuo* to give **Q13** (6 mg, 40%). <sup>1</sup>H NMR (500 MHz, DMSO-*d*<sub>6</sub>): δ = 18.35 (s, 1H, NH), 9.50 (br s, 1H, 11-*H*), 9.25 (br s, 1H, 2-*H*), 8.61 (m, 2H, 5,8-*H*), 8.52 (m, 2H, 6,7-*H*), 8.25 (br s, 1H, 3-*H*), 7.92 (d, *J* = 6.4 Hz, 1H, 10-*H*), 5.56 (s, 2H, CH<sub>2</sub>), 4.01 (s, 1H, CCH) ppm. <sup>13</sup>C NMR (125 MHz, DMSO-*d*<sub>6</sub>) δ = 166.6 (C9), 150.1 (C2), 147.3 (C11), 146.5 (C12c), 144.3 (C12a), 139.5 (C4), 137.5 (C6a), 130.2 (C6), 130.1 (C7), 126.6 (C5), 125.8 (C12b), 124.3 (C3), 123.1 (C8), 120.1 (C4a), 116.7 (C8a), 105.9 (C10), 81.6 (CCH), 77.2 (CCH), 59.6 (CH<sub>2</sub>) ppm. LRMS (ESI) *m/z*: [M + H]<sup>+</sup> Calcd for C<sub>19</sub>H<sub>11</sub>ClN<sub>2</sub>O 319.06; Found 319.23.

### 3.2.13 - Synthesis of 4-bromo-9-(pyridin-4-yl)quinolino[7,8-*h*]quinoline (Q14)



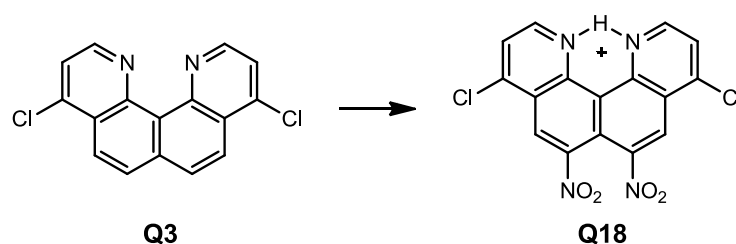
Phosphorous oxybromide (266 mg, 0.928 mmol) was added to **Q11** (100 mg, 0.309 mmol) and stirred at 200 °C for 30 min under an atmosphere of Ar. A MeOH : DCM solution (1:10, 33 mL) was added, the reaction mixture sonicated and then basified with 6M KOH (10 mL). Water (50 mL) was added to the reaction mixture and the organic layer collected. The aqueous layer was washed with MeOH : DCM (1:10, 66 mL) and the combined organic layers were dried with MgSO<sub>4</sub>, filtered, and dried *in vacuo* to give **Q14** (65 mg, 54%). <sup>1</sup>H NMR (700 MHz, DMSO-*d*<sub>6</sub>): δ = 19.78 (s, 1H, NH), 9.67 (d, *J* = 4.3 Hz, 1H, 11-*H*), 9.33 (d, *J* = 5.2 Hz, 1H, 2-*H*), 8.97 (s, 2H, 2-Py-*H*), 8.71 (m, 1H, 5-*H*), 8.66 (m, 1H, 8-*H*), 8.62 (d, *J* = 5.2 Hz, 1H, 10-*H*), 8.59 (dd, *J* = 1.2, 9.0 Hz, 1H, 6-*H*), 8.33 (d, *J* = 5.2 Hz, 1H, 3-*H*), 8.32 (m, 1H, 7-*H*), 7.83 (s, 2H, 3-Py-*H*) ppm. <sup>13</sup>C NMR (176 MHz, DMSO-*d*<sub>6</sub>) δ = 152.1 (C12c), 149.6 (C2-Py), 147.9 (C2), 146.1 (C11), 143.6 (C12a), 141.0 (C9), 139.0 (C4-Py), 137.0 (C6a), 130.7 (C8), 130.5 (C6), 129.2 (C5), 128.9 (C4), 127.8 (C10), 127.4 (C7), 127.3 (C12b), 126.0 (C3-Py), 124.7 (C3), 123.8 (C4a), 116.2 (C8a) ppm. HRMS (ESI) *m/z*: [M + H]<sup>+</sup> Calcd for C<sub>21</sub>H<sub>12</sub>BrN<sub>3</sub> 386.0287; Found 386.0280.

**3.2.14 - Synthesis of 9-(2-propyn-1-yloxy)-1,4,9,12-tetrahydro-4,9-dioxo-2,11-dimethylester-quinolo[7,8-h]quinoline-2,11-dicarboxylic acid (Q15)**



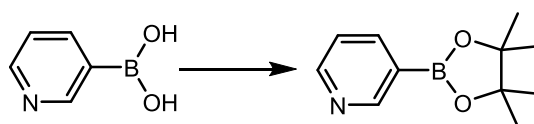
**Q1** (312 mg, 0.825 mmol) and K<sub>2</sub>CO<sub>3</sub> (342 mg, 2.47 mmol) were suspended in DMF (40 ml). Propargyl bromide (80% wt % toluene, 83  $\mu$ L, 0.742 mmol) was added and stirred at room temperature for 14-24 h. The reaction mix was cooled, filtered with cotton wool and filter paper, and the precipitate rinsed with 10 ml DMF. The solution dried *in vacuo* then resuspended in CHCl<sub>3</sub> (150 ml) and filtered into a separating funnel. The organic layer was washed twice with alternating H<sub>2</sub>O (70 ml) and brine (70 ml), then dried with MgSO<sub>4</sub>, filtered, and dried *in vacuo* to give **Q15** (33 mg, 11%). <sup>1</sup>H NMR (500 MHz, CDCl<sub>3</sub>):  $\delta$  = 15.29 (s, 1H, NH), 8.53 (d, *J* = 8.6 Hz, 1H, 5-*H*), 8.22 (d, *J* = 9.0 Hz, 1H, 8-*H*), 7.83 (t, *J* = 4.5 Hz, 2H, 7,10-*H*), 7.69 (d, *J* = 8.6 Hz, 1H, 6-*H*), 7.23 (s, 1H, 3-*H*), 5.10 (d, *J* = 2.1 Hz, 2H, CH<sub>2</sub>), 4.18 (s, 3H, COOCH<sub>3</sub>), 4.11 (s, 3H, COOCH<sub>3</sub>'), 2.72 (s, 1H, CCH) ppm. <sup>13</sup>C NMR (125 MHz, CDCl<sub>3</sub>)  $\delta$  = 178.2 (C4), 165.0 (COOMe'), 162.9 (COOMe), 161.3 (C9), 147.3 (C11), 147.1 (C12c), 139.6 (C12a), 137.6 (C6a), 137.6 (C2), 129.4 (C7), 126.1 (C5), 125.5 (C4a), 124.6 (C6), 121.9 (C8), 120.6 (C8a), 117.5 (C12b), 113.3 (C3), 103.3 (C10), 77.7 (CCH), 76.4 (CCH), 57.0 (CH<sub>2</sub>), 53.4 (CH<sub>3</sub>'), 53.3 (CH<sub>3</sub>) ppm. HRMS (ESI) *m/z*: [M + H]<sup>+</sup> Calcd for C<sub>23</sub>H<sub>17</sub>N<sub>2</sub>O<sub>6</sub> 417.1081; Found 417.1080.

### 3.2.15 - Synthesis of 4,9-dichloro-6,7-dinitroquinolino[7,8-*h*]quinoline (Q18)



An oil bath was preheated to 130 °C. Fuming nitric acid (1 ml) and conc. sulfuric acid (1 ml) were heated briefly to initiate NO<sub>2</sub><sup>+</sup> generation before 4,9-dichloroquinolino[7,8-*h*]quinoline (**Q3**) (50 mg) was added and the reaction stirred for 2 min at 130 °C. The reaction was poured onto ice and 6M KOH (20 ml) was added. The reaction mixture was diluted with a 1:10 MeOH : DCM solvent mixture (110 ml). The organic layer was separated, dried (MgSO<sub>4</sub>) and filtered, before the solvent was removed by rotary evaporation to give **Q18** (22mg, 35%). The <sup>1</sup>H NMR was consistent with the literature values.<sup>54</sup> <sup>1</sup>H NMR (500 MHz, DMSO-*d*<sub>6</sub>) δ = 15.59 (d, *J* = 5.2 Hz, 1H, NH), 9.31 (d, *J* = 5.0 Hz, 1H, 11-*H*), 9.15 (s, 1H, 5-*H*), 9.09 (s, 1H, 8-*H*), 8.37 (dd, *J* = 7.4 Hz, 5.2 Hz, 1H, 2-*H*), 8.34 (d, *J* = 5.0 Hz, 1H, 10-*H*), 6.52 (d, *J* = 7.4 Hz, 1H, 3-*H*) ppm.<sup>15</sup>

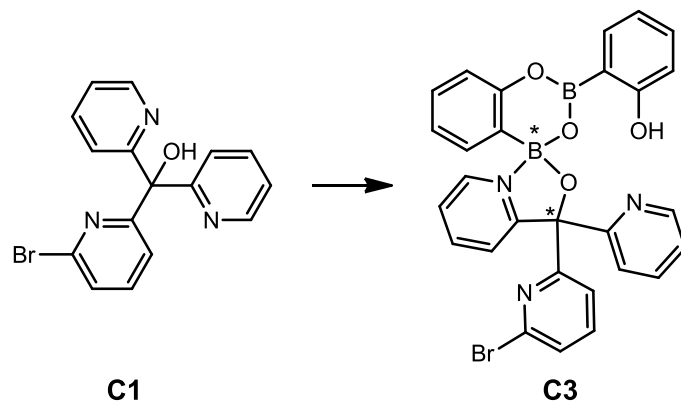
### 3.2.16 - Synthesis of 3-pyridine boronic acid pinacol ester



Method reproduced from Tan et al. (2015).<sup>93</sup> In brief: 3-pyridine boronic acid (100 mg, 0.81 mmol) was added to a solution of pinacol (116 mg, 0.97 mmol) in Et<sub>2</sub>O (10 ml). The solution was stirred at room temperature overnight. The product was dried *in vacuo* and used without further purification. Yield ~70 % (115 mg). The <sup>1</sup>H NMR was consistent with the literature values.<sup>120</sup> <sup>1</sup>H NMR (400 MHz, CDCl<sub>3</sub>) δ = 8.94 (s, 1H), 8.66 (dd, *J* = 1.6, 4.6 Hz, 1H), 8.05 (dd, *J* = 1.6, 8.2 Hz, 1H), 7.27 (dd, *J* = 4.6, 8.2 Hz, 1H), 1.35 (s, 12H) ppm.

### 3.3 - Other Experimental

#### 3.3.1 - Synthesis of a boronic acid anhydride-based ligand



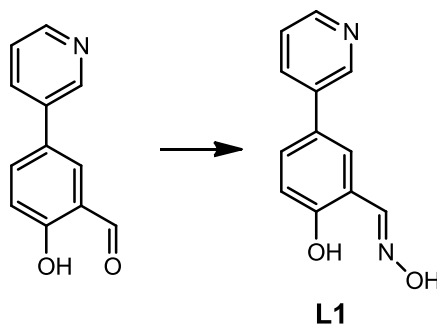
A mixture of **C1** (100 mg, 0.29 mmol), 2-hydroxybenzene boronic acid (100 mg, 0.73 mmol), and calcium fluoride (68.0 mg, 0.87 mmol) in THF (10 mL) was stirred under Ar at reflux for 5 h. The mixture was extracted with DCM (150 mL) and washed with water and brine alternatively (2 × 50 mL each). The organic layer was dried with anhydrous MgSO<sub>4</sub>, filtered, and the solvents evaporated in vacuo to afford an off-white solid (145 mg, 88 %).

<sup>1</sup>H NMR (700 MHz, CDCl<sub>3</sub>) major diastereoisomer: δ = 6.72–6.76 (m, 1H, *H*<sub>Ar</sub>), 6.86–6.96 (m, 2H, *H*<sub>Ar</sub>), 7.04 (dd, *J*<sub>HH</sub> = 7.3, 1.8 Hz, 1H, *H*<sub>Ar</sub>), 7.11–7.15 (m, 1H, *H*<sub>Ar</sub>), 7.22–7.34 (m, 3H, *H*<sub>Ar</sub>), 7.41–7.45 (m, 1H, *H*<sub>Ar</sub>), 7.52–7.60 (m, 2H, *H*<sub>Ar</sub>), 7.66–7.72 (m, 1H, *H*<sub>Ar</sub>), 7.80 (td, *J*<sub>HH</sub> = 7.8, 1.9 Hz, 1H, *H*<sub>Ar</sub>), 7.89–7.93 (m, 1H, *H*<sub>Ar</sub>), 7.99–8.04 (m, 1H, *H*<sub>Ar</sub>), 8.13–8.22 (m, 2H, *H*<sub>Ar</sub>), 8.58–8.60 (m, 1H, *H*<sub>Ar</sub>), 8.69 (d, *J*<sub>HH</sub> = 8.3 Hz, 1H, *H*<sub>Ar</sub>), 8.91 (s, 1H, OH); minor diastereoisomer: δ = 6.72–6.77 (m, 1H, *H*<sub>Ar</sub>), 6.87–6.96 (m, 2H, *H*<sub>Ar</sub>), 7.00 (dd, *J*<sub>HH</sub> = 7.1, 1.8 Hz, 1H, *H*<sub>Ar</sub>), 7.11–7.15 (m, 1H, *H*<sub>Ar</sub>), 7.22–7.34 (m, 3H, *H*<sub>Ar</sub>), 7.44–7.45 (m, 1H, *H*<sub>Ar</sub>), 7.52–7.60 (m, 2H, *H*<sub>Ar</sub>), 7.66–7.72 (m, 2H, *H*<sub>Ar</sub>), 7.89–7.93 (m, 1H, *H*<sub>Ar</sub>), 7.99–8.04 (m, 1H, *H*<sub>Ar</sub>), 8.13–8.22 (m, 2H, *H*<sub>Ar</sub>), 8.58–8.60 (m, 1H, *H*<sub>Ar</sub>), 8.71 (d, *J*<sub>HH</sub> = 8.4 Hz, 1H, *H*<sub>Ar</sub>), 8.81 (s, 1H, OH). <sup>11</sup>B NMR (160 MHz, CDCl<sub>3</sub>) δ = 8.2 (ω<sub>1/2</sub> = 282 Hz), 28.2 (ω<sub>1/2</sub> = 821 Hz). FT-IR (cm<sup>-1</sup>): 3308 (m; OH), 3064 (w), 3013 (w), 1619 (m), 1607 (w), 1575 (s), 1554 (w), 1475 (m), 1460 (m), 1444 (m), 1427 (m), 1397 (w), 1338 (m), 1316 (s, B-O), 1285 (m), 1226 (w), 1152 (w), 1134 (m), 1118 (m), 1082 (m), 1063 (m), 1033 (m), 1017 (m), 995

(w), 987 (w), 942 (w), 909 (w), 877 (w), 851 (w), 807 (w), 762 (s), 734 (m), 749 (m), 688 (w), 676 (m), 636 (w), 615 (w), 577 (w), 559 (w), 524 (w), 471 (w), 449 (w), 430 (w), 405 (w). HRMS (ESI)  $m/z$ :  $[M+H]^+$  Calcd for  $C_{28}H_{21}B_2BrN_3O_4$  564.0896; Found 564.0896.

Note: This synthetic procedure (3.3.1) is now published in in Eur. J. Inorg. Chem. (2019).<sup>107</sup>

### 3.3.2 - Synthesis of 2-hydroxy-5-(3-pyridyl)-benzaldehyde oxime (L1)



A solution of KOH (40 mg) in EtOH (5 ml) was added to a solution of Hydroxylamine hydrochloride (49 mg) in EtOH (5 ml), producing a white precipitate. The precipitate was filtered and washed with EtOH (5 ml) and the filtrate was added dropwise to a solution of 2-hydroxy-5-(3-pyridyl)-benzaldehyde (116 mg, 0.582 mmol) in EtOH (10 ml). The mixture was stirred at room temperature for 24 hours, then the solvent reduced and redissolved in  $CHCl_3$  (40 ml) and washed with  $H_2O$  (40 ml x 2). The organic layer was dried with anhydrous  $MgSO_4$ , filtered, and the solvents evaporated *in vacuo* to afford an off-white solid. The product was purified by recrystallisation from hot  $CHCl_3$  to give **L1** (106 mg, 85%).  $^1H$  NMR (500 MHz,  $DMSO-d_6$ ):  $\delta$  = 11.45 (br s, 1H, NOH), 10.34, br s, 1H, Ph-OH), 8.83 (d,  $J$  = 2.3 Hz, 1H, 11-H), 8.52 (dd,  $J$  = 1.3, 4.7 Hz, 1H, 9-H), 8.39 (s, 1H, 13-H), 8.00 (dt,  $J$  = 1.9, 8.0 Hz, 1H, 7-H), 7.84 (d,  $J$  = 2.3 Hz, 1H, 12-H), 7.62 (dd,  $J$  = 2.4, 8.5 Hz, 1H, 4-H), 7.45 (dd,  $J$  = 4.7, 8.0 Hz, 1H, 8-H), 7.02 (d,  $J$  = 8.5 Hz, 1H, 3-H) ppm.  $^{13}C$  NMR (125 MHz,  $DMSO-d_6$ ):  $\delta$  = 156.7 (C2), 148.3 (C9), 147.8 (C13), 147.6 (C11), 135.5 (C5), 133.9 (C7), 129.5 (C4), 128.7 (C6), 126.7 (C12), 124.3 (C8), 119.4 (C1), 117.3 (C3) ppm. HRMS (ESI)  $m/z$ :  $[M+H]^+$  Calcd for  $C_{12}H_{11}N_2O_2$  215.0815; Found 215.0814.



# Chapter 4 - Quinolino[7,8-*h*]quinoline $pK_{aH}$ Research

## 4.1 - Introduction

Chapter 1 introduced the proton-sponge potential of QQ derivatives due to their unique heterocyclic core structure. Like DMAN, the prototypal superbasic Proton Sponge™<sup>6</sup>, QQ is also a neutral organic compound with extraordinary base properties, with prominent structural differences that open up research avenues. These include the lack of hydrophobic shielding seen in DMAN, which could increase the rate of proton exchange and strength of basicity.<sup>42</sup>

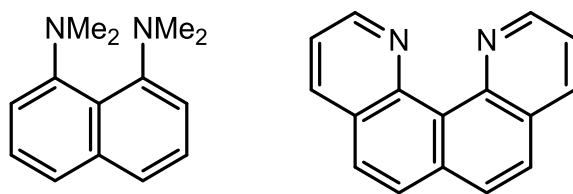


**Figure 4-1: Structure of the Proton Sponge™ DMAN (left) and quinolino[7,8-*h*]quinoline (right).**

There are multiple definitions of a ‘superbase’ present in literature. In 1993 P. Caubère remarked that an unambiguous definition did not at that point exist, and proposed that the term should be limited to “bases resulting from the mixing of two (or more) bases leading to new basic species possessing new properties”.<sup>121</sup> However, the work presented in this thesis operates on the alternative definition that has been used in a range of publications: – “bases with a  $pK_{aH}$  value of the conjugate acid greater than that of the proton sponge DMAN”, which is 18.63 in acetonitrile (12.2 in water).<sup>3, 11, 122</sup>

These neutral organic superbases play a variety of roles across different fields, ranging from gene therapy to catalysis.<sup>18</sup> Many research groups have focussed on expanding the range and increasing the strength of these structures since the original DMAN. Some focus on introducing buttressing type effects, altering the ‘skeleton’ framework by changing groups on the adjacent ring carbons (substituent X in fig. 4-2),<sup>18</sup> while others

affect the nitrogen centre by having  $sp^2$  rather than  $sp^3$  hybridised N donor atoms (e.g. in the commercially available DBU<sup>123</sup>) which lowers the steric hinderance (fig. 4-2).

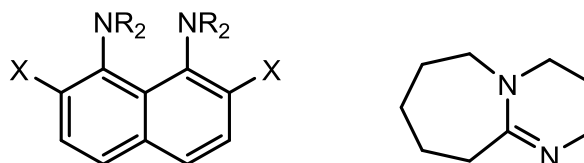


**Figure 4-2: Example of framework buttressing effects on organic bases (left) and hybridised N donor atoms in DBU (right).**

Like DMAN, proton sponges generally feature two (or more) nitrogen atoms that have either the proximity and/or flexibility to result in an intramolecular N-H...N hydrogen bond on chelation of a single proton.<sup>124</sup> Those with enhanced basicities – those strengthened above the levels observed in ‘ordinary’ organic bases such as amines or guanidines - share some common characteristics. These include (I) Electron lone pair repulsion causing base destabilisation, (II) reduction of steric strain by protonation and (III) intramolecular hydrogen bonding involving the incoming proton.<sup>18</sup> However, many proton sponges have slow rates of proton exchange caused by the steric factors that contribute to the basicity, reducing the usefulness in applications of ‘salt-free base-catalysed reactions’.<sup>124</sup>

As discussed in chapter 1, the destabilising overlap of the electron lone pairs on the nitrogen atoms in QQ derivatives causes a strain that manifests as a helical distortion. This strain disrupts the planarity of the structures (a factor required for aromaticity),<sup>125</sup> but can be relieved by the binding of a single proton, achieving a resonance stabilisation effect. As this strain is proportional to the electron density at those central positions, it is expected that altering this density could significantly affect the proton affinity: the strength of QQ basicity could be modified by the presence and position of electron withdrawing and/or donating substituents attached to the core structure. Electron withdrawing groups stabilise the neutral state (thereby decreasing basicity) by reducing the strength of electron repulsion. Hydrogen is designated as the arbitrary zero point, neither electron withdrawing nor donating (fig. 4-3).<sup>126</sup>

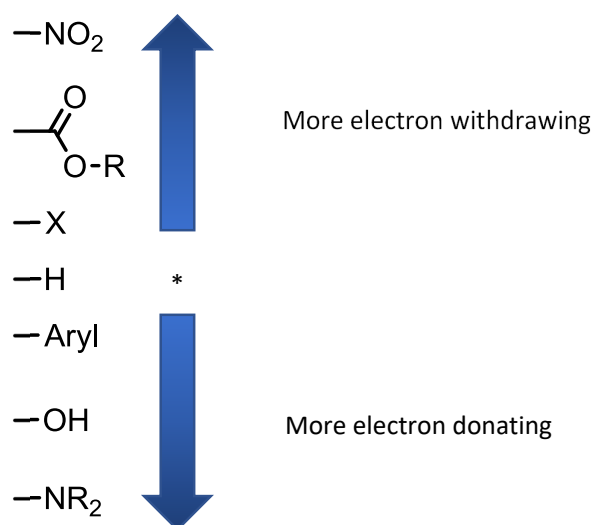


**Figure 4-3: Relative strength of selected electron withdrawing and donating substituents.**

The opportunity to explore this correlation began with the establishment of valued collaborations with international research groups. These groups, led by Prof. Ivo Leito (University of Tartu, Estonia) and Dr. Robert Vianello (Ruđer Bošković Institute, Croatia), determined the experimental and computational data presented in this chapter. This data was published in *The Journal of Organic Chemistry* in 2020. To indicate that the strength of basicity of each compound is measured as the  $pK_a$  of the conjugate acid, the term  $pK_{aH}$  is used.<sup>11</sup>

## 4.2 - Results and Discussion

Experimental  $pK_{aH}$  values were determined by the methods described in Rowlands et al.,<sup>11</sup> and were performed by the Leito Group. In brief: Titrant solutions in the range of  $1\text{-}5 \times 10^{-3} \text{ mol L}^{-1}$  were prepared using 99% triflic acid and *tert*-butylimino-tris(pyrrolidino)phosphorane. The QQ derivative under investigation and a reference base underwent titrations individually and as a mixture (in dry acetonitrile in the concentration range of  $1\text{-}14 \times 10^{-3} \text{ mol L}^{-1}$ ) while UV spectra were recorded. From this spectrophotometric data, the dissociation levels ( $\alpha$ ) of the conjugate acids could be determined, and the  $\Delta pK_{aH}$  between the QQ derivative and reference base calculated, according to the equations below. Two or more reference bases were used for each QQ derivative  $pK_{aH}$  determination to improve accuracy.

$$\alpha = \frac{[B]}{[B] + [BH^+]}$$

$$\Delta = \log \frac{\alpha_1(1 - \alpha_2)}{\alpha_2(1 - \alpha_1)}$$

Limited solubility of some of the QQ compounds caused difficulty. Two of the derivatives (**Q4** and **Q7**) were converted to triflate salts to further purify them prior to measurements being run. Data measured and calculated for QQ derivatives for which experimental data was attempted is shown in table 4-1, while table 4-3 presents calculated data for non-experimental compounds. R<sup>1</sup>-R<sup>3</sup> are used in this chapter to refer to QQ substituent positions for ease of discussion (fig. 4-4).

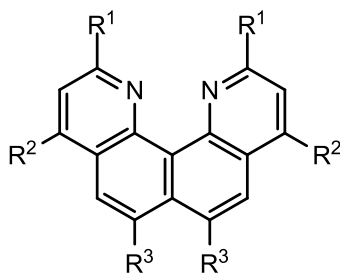


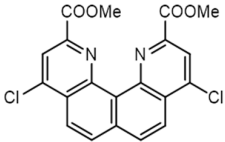
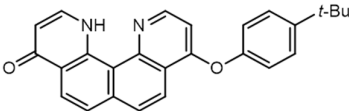
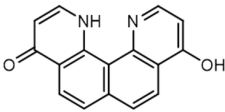
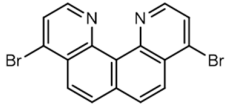
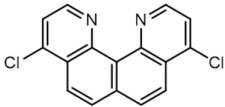
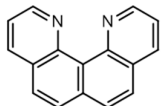
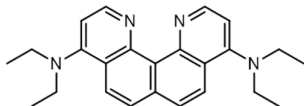
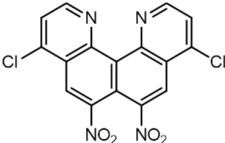
**Figure 4-4: Key to R<sup>1</sup>-R<sup>3</sup> QQ substituent position codes.**

Details of calculations producing computational proton affinities and basicities are described in Rowlands et al.,<sup>11</sup> and were completed by the Vianello Group. In brief: DFT calculations were performed at the level of B3LYP/6-311++G(3df,2p)//B3LYP/6-31+G(d,p), allowing for the calculation of the changes in free energy and enthalpy occurring on protonation. From these values, the gas phase basicity (GPB) and proton affinity (PA) quantities could be determined according to the equations discussed in chapter 5.<sup>11</sup> The effect of the acetonitrile solution was taken into account using the implicit isodensity polarizable continuum model (IPCM), allowing for the calculation of compound: pK<sub>aH</sub> values by the following equation.

$$pK_{aH}(\text{MeCN}) = 0.5751 \cdot PA(\text{MeCN}) - 144.1 \text{ units}$$

The methodology is validated by the close agreement between experimental and calculated data shown in Table 4-1.

**Table 4-1: Experimentally determined  $pK_{aH}$ , calculated proton affinities (PA), gas-phase basicities (GB) calculated  $pK_{aH}$  and helical torsional twists of quinolino[7,8-*h*]quinoline derivatives (in their neutral states).**

Structure	Experimental		Calculated		
	$pK_{aH}$ (in MeCN)	Proton Affinity (kcal mol <sup>-1</sup> )	Gas-phase basicity (kcal mol <sup>-1</sup> )	$pK_{aH}$ (in MeCN)	Torsional twist (°)
	9.24	248.8	240.8	9.9	28.4
	12.1	245.4	237.2	12.5	0
	12.21	242.9	235	12.4	0
	17.58	250.8	242.2	17.2	19
	17.64	251	243	17.3	21.1
	19.6	255.4	246.8	19.6	17.3
	23.97	269.5	260.8	23	29.1
	-	236.4	228.3	12.1	29.5

Interestingly, there appears to be little correlation between the magnitude of the helical torsional twist and the  $pK_{aH}$  of the QQ derivative (fig. 4-5), with substituent electronic contributions dominating the changes (fig. 4-6).<sup>11</sup> A range of electron withdrawing and donating substituents were tested, from nitro groups to secondary amines. As the theory indicates, increases in  $pK_{aH}$  values of the QQ derivatives correlated with increases in the electron donating strength of substituents. Although most of the compounds flattened to planar upon protonation, some retained slight twists, including: **Q18** - a 2.6° twist with the NO<sub>2</sub> group repulsions resulting in a slightly distorted structure, **Q16** – a 6.0° twist with the steric crowding of the ester substituents, and the diamine **Q7**.

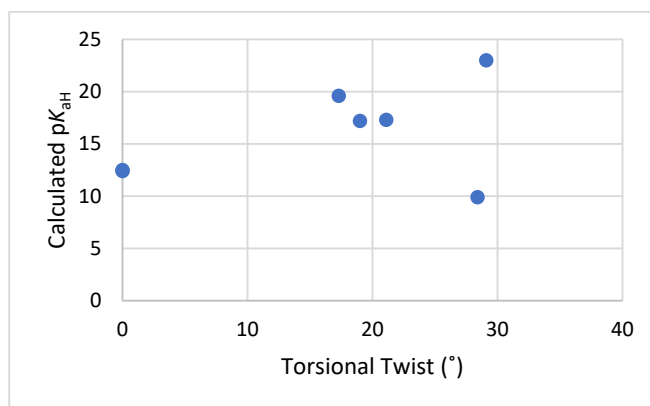


**Figure 4-5: Calculated  $pK_{aH}$  values compared to degree of torsional twists of synthesised QQ derivatives.**

With a lack of electron withdrawing substituents to reduce central electron density, pure unsubstituted QQ has an experimental  $pK_{aH}$  of 19.6, and, above DMAN's 18.63, can be categorised as the first QQ superbase of this series.

The addition of halide substituents to QQ weakened the basicity. Electron density was pulled away from the basic centre, reducing the repulsion between the lone pair electrons of the nitrogen atoms and easing the strain. This stabilised the neutral structures (and destabilised the corresponding conjugate acids), so the  $pK_{aH}$  values for **Q3** and **Q4** were dropped by more than two pH units to give 17.64 and 17.58 respectively.

An even more significant effect was observed with the inclusion of methyl ester groups at R<sup>1</sup>: the  $pK_{aH}$  of **Q16** was measured at 9.24, an entire 8.4 units less than that of

dichloride **Q3**. Having these groups situated close to the basic 'active' pocket increases the strength of the resonance effect, and shields the site, reducing the rate of proton exchange. This combines with the effects from the electron withdrawing nature of the esters to result in the reduced basicity. The importance of substituent position indicated by this derivative (**Q16**) is emphasised more clearly by the data in table 4-3.

A similarly strong resonance effect is observed with **Q18**, where the calculated  $pK_{aH}$  of 12.1 (>5 units lower than dichloride **Q3**) indicates a strong contribution of the electron withdrawing nitro substituents at R<sup>3</sup>. Unfortunately, the experimental  $pK_{aH}$  of **Q18** was unable to be measured as it appeared to degrade on transport to collaborators in Estonia.

For an example of substituents imparting an electron donating effect, the diamine containing QQ derivative **Q7** stands in significant contrast to the reduced basicities. The  $pK_{aH}$  of this derivative was measured at 23.97, 4.37 orders of magnitude stronger than unsubstituted QQ. Charge delocalisation, which stabilises the conjugate acid, is increased by the strongly electron donating diethylamino substituents at R<sup>2</sup>, making **Q7** a true superbases, the strongest of the QQ derivatives experimentally measured.

These effects, of varying the substituents on the  $pK_{aH}$  values of the compounds, have been quantified in table 4-2 and figure 4-6, based on the work by Remya and Suresh.<sup>127</sup> These researchers explored the quantification of substituent effects, defining >350 substituents as electron withdrawing/donating based on their having negative/positive values of  $\Delta V_c$ . This parameter is defined as the "difference between MESP [molecular electrostatic potential] at the nucleus of the para carbon of substituted benzene and a carbon atom in benzene", and has effects that are additive and able to be transferred across a variety of  $\pi$ -conjugated compounds.<sup>127</sup> Total  $\Delta V_c$  values, which indicate the strength of electronic effects, were calculated for each QQ derivative as listed in table 4-1, and are displayed in table 4-2 alongside the  $pK_{aH}$  for the corresponding compound.

**Table 4-2: Comparison of QQ basicity and sum of electron withdrawing effects using the quantity  $\Delta Vc$ . \*Experimental  $pK_{aH}$  values are listed for all except compound Q18, which is computationally derived.**

QQ Derivative	$\sim$ Total $\Delta Vc$ (kcal mol <sup>-1</sup> )	Experimental $pK_{aH}$
Q7	-23.8	23.97
Q19	-6.8	12.1
Q2	-4	12.21
Q17	0	19.6
Q3	14	17.64
Q4	15.2	17.58
Q16	31	9.24
Q18	56.4	12.1*

The  $\Delta Vc$  value for the 4-tert-butylphenoxy substituent of **Q19** was not listed in the publication of Remya and Suresh, therefore, the value for the closest match  $OCH_2CH=CH_2$  was substituted instead. Although less precise, the neutral electron donating substituents explored by Remya and Suresh cover a much smaller  $\Delta Vc$  range than the electron withdrawing, so the overall trend is valid.<sup>127</sup>

In figure 4-6, a clear negative trend can be observed between QQ basicity and  $\Delta Vc$ : As the total  $\Delta Vc$  value becomes more positive, meaning the sum of substituents becomes more strongly electron withdrawing, the QQ basicity weakens (fig. 4-6). Visually the outliers are clear in this graph. These include the tautomeric compounds **Q19** and **Q2** with  $pK_{aH}$  values of 12.1 and 12.21 respectively which exist mainly as the quinolinone tautomer in their neutral states. This motif means a proton already sits within the central QQ binding pocket and the repulsion of electron density between the nitrogen atoms is eased, stabilising the compounds and causing the energy difference between neutral and protonated states to reduce – this diminished the favourability of protonation, and hence the derivatives'  $pK_{aH}$  values.<sup>11</sup> The other compound with an anomalously low  $pK_{aH}$  is **Q16** – this has been attributed to the basic site shielding of the 2,11-substituted methyl esters described above.



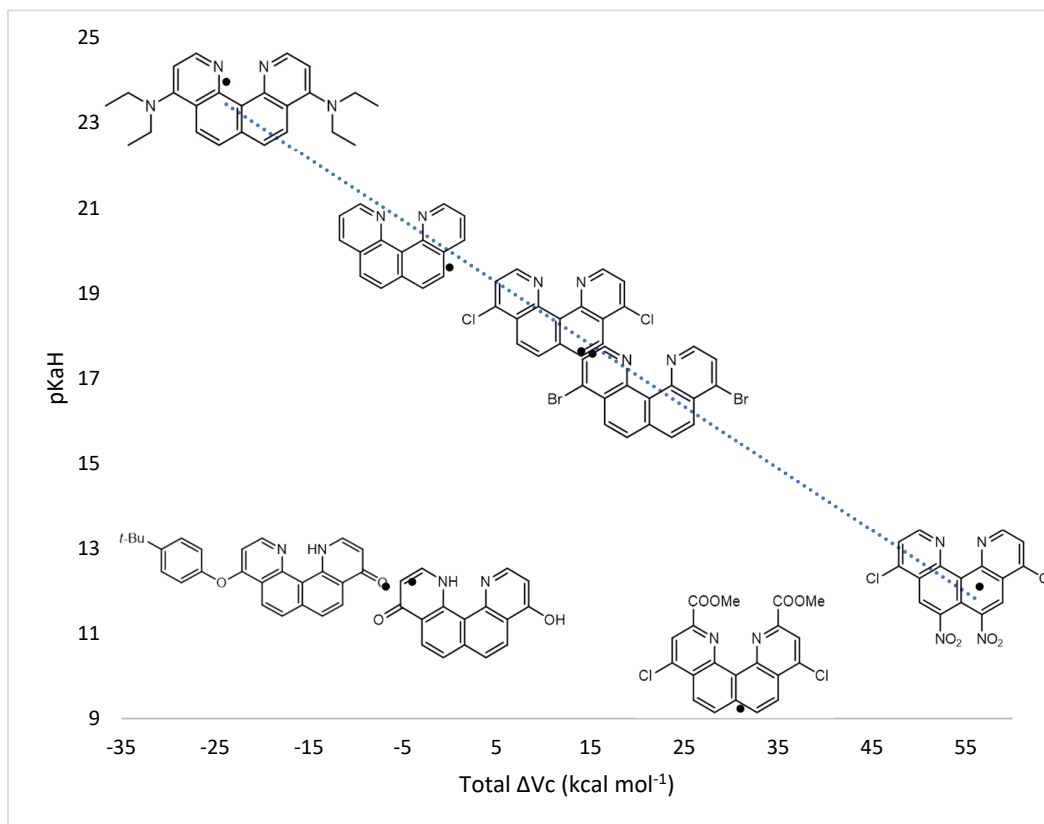
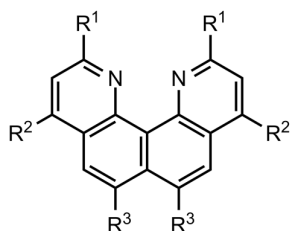


**Figure 4-6: Variation of QQ basicity correlated with substituent electronic effects.**

#### 4.2.1 - Theoretical QQ Derivatives

Computationally calculated basicities were calculated for the synthesised quinolino[7,8-*h*]quinoline derivatives. In addition, a theoretical series, functionalised with electron donating substituents, namely 1,1,3,3-tetramethylguanidino ( $\text{N}=\text{C}(\text{NMe}_2)_2$ ),  $\text{N},\text{N},\text{N}',\text{N}',\text{N}'',\text{N}''$ -hexamethylphosphorimidictriamido ( $\text{N}=\text{P}(\text{NMe}_2)_3$ ) or dimethylamino ( $\text{NMe}_2$ ) were also calculated, with an aim to increase the QQ basicity further.

**Table 4-3: Calculated data for theoretical QQ derivatives.**



Structure	Functionality	Proton Affinity (kcal mol <sup>-1</sup> )	Gas-phase basicity (kcal mol <sup>-1</sup> )	pK <sub>aH</sub> (in acetonitrile)
I	R <sup>1</sup> = NMe <sub>2</sub> , R <sup>2</sup> = R <sup>3</sup> = H	259.8	251.6	20.3
II	R <sup>1</sup> = N=C(NMe <sub>2</sub> ) <sub>2</sub> , R <sup>2</sup> = R <sup>3</sup> = H	281.4	272.6	29.9
III	R <sup>1</sup> = N=P(NMe <sub>2</sub> ) <sub>3</sub> , R <sup>2</sup> = R <sup>3</sup> = H	286.6	280.7	31.4
IV	R <sup>1</sup> = R <sup>3</sup> = H, R <sup>2</sup> = NMe <sub>2</sub>	269	261.4	23.6
V	R <sup>1</sup> = R <sup>3</sup> = H, R <sup>2</sup> = N=C(NMe <sub>2</sub> ) <sub>2</sub>	279.3	273.3	26
VI	R <sup>1</sup> = R <sup>3</sup> = H, R <sup>2</sup> = N=P(NMe <sub>2</sub> ) <sub>3</sub>	290.6	283.2	29.6
VII	R <sup>1</sup> = R <sup>2</sup> = H, R <sup>3</sup> = NMe <sub>2</sub>	262.8	254.9	20.8
VIII	R <sup>1</sup> = R <sup>2</sup> = H, R <sup>3</sup> = N=C(NMe <sub>2</sub> ) <sub>2</sub>	271.7	264.9	22.5
IX	R <sup>1</sup> = R <sup>2</sup> = H, R <sup>3</sup> = N=P(NMe <sub>2</sub> ) <sub>3</sub>	275.9	269.3	23
X	R <sup>1</sup> = R <sup>2</sup> = R <sup>3</sup> = NMe <sub>2</sub>	273.8	266.4	24.2
XI	R <sup>1</sup> = R <sup>2</sup> = R <sup>3</sup> = N=C(NMe <sub>2</sub> ) <sub>2</sub>	298.1	290.6	33.1
XII	R <sup>1</sup> = R <sup>2</sup> = R <sup>3</sup> = N=P(NMe <sub>2</sub> ) <sub>3</sub>	303.3	295.8	35.5

All theoretical derivatives presented in table 4-3 have a  $pK_{aH} > 18.63$  in acetonitrile, so would be classed as superbases. Of the substituents presented,  $-N=P(NMe_2)$  has the strongest electron donating effect, followed by  $-N=C(NMe_2)$  and  $-NMe_2$ . Unsurprisingly, the derivatives that contained electron donating substituents at more than one position (**X**, **XI**, **XII**) show stronger basicities than the lesser substituted (**I-IX**).

Tables 4-1 and 4-2 and figure 4-6 above demonstrated the influences of substituent type on basicity. While this is also shown in the data in table 4-3, more prevalent are the effects of substituent positioning. The closer the substituents  $-N=C(NMe_2)$  and  $-N=P(NMe_2)$  were located to the basic nitrogen atoms, the greater their magnitude of  $pK_{aH}$  upregulation (compared to unsubstituted QQ **Q17**): when these groups were positioned at  $R^1$ , the resulting base was stronger than first the analogous  $R^2$ , followed by  $R^3$  structures (fig. 4-7).

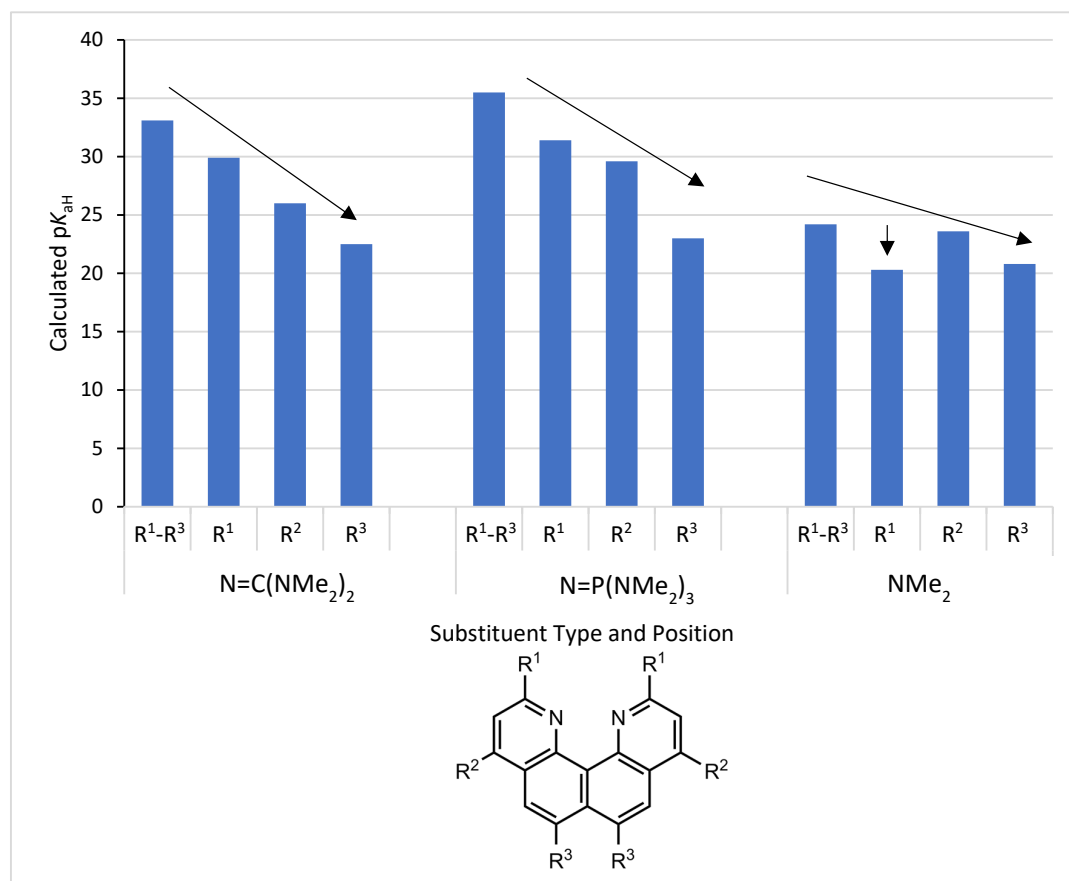
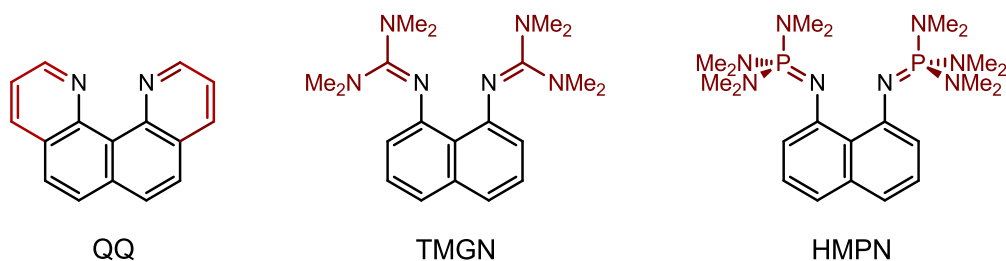


Figure 4-7: Effects of substituent position on resulting  $pK_{aH}$

A variation in this trend was observed with the substituent -NMe<sub>2</sub> – although the R<sup>2</sup> substituted **IV** still had a higher pK<sub>aH</sub> than the R<sup>3</sup> analogue **VII**, the R<sup>1</sup> derivative **I** anomalously had the smallest pK<sub>aH</sub>. This is likely this is due to hydrophobic shielding and steric hinderance effects of the close methyl groups (similar to that observed with **Q16**) reducing the rate of proton exchange.

### 4.3 - Comparison to existing Proton Sponges

Quinolino[7,8-*h*]quinoline derivatives show strong and tuneable pK<sub>aH</sub> properties, but the question remains on how these fit into the existing library of superbases. Although structurally different, similar obstacles are encountered with some QQ derivatives as by some of the Schwesinger bases (used as a reference in the QQ pK<sub>aH</sub> calculations),<sup>11</sup> including multistep syntheses and varying stabilities and solubilities.<sup>124</sup> Figure 4-8 compares QQ to two more structurally similar proton sponges: TMGN and HMPN.



**Figure 4-8: Structural comparison of quinolono[7,8-*h*]quinoline (left), TMGN (middle) and HMPN (right)**

As previously discussed, proton sponges can incorporate a variety of structural motifs. Like QQ, the neutral organic superbases in figure 4-8 build on the classic naphthalene proton sponge backbone, have *sp*<sup>2</sup> hybridised nitrogen atoms and can form strong intramolecular hydrogen bonds. QQ, TMGN and HMPN all use 1,8-diaminonaphthalene as a starting material in their synthesis.

Structurally, QQ has a slightly greater torsional angle (178.9° vs. 173.0°) and is less sterically crowded than 1,8-bis(tetramethylguanidino)naphthalene (TMGN), although the N⋯N distances are close (272.7 vs. 271.7 pm). The pK<sub>aH</sub> of this proton sponge is significantly higher than unsubstituted QQ at 25.1 in acetonitrile (compared to QQ's

19.6), but is close to the most basic of the experimental QQ derivatives, *N*<sup>4</sup>,*N*<sup>4</sup>,*N*<sup>9</sup>,*N*<sup>9</sup>-tetraethylquinolino[7,8-*h*]quinoline-4,9-diamine (**Q7**) with its *pK*<sub>aH</sub> of 23.97.<sup>124</sup>

Further research by the group that published TMGN produced HMPN, which combined aspects of both DMAN and Schwesinger's phozphazene base unit – the latter, a strongly electron donating moiety also featured in QQ compounds **VI**, **IX**, and **XII** in this chapter (table 4-3). HMPN has a greater neutral N···N distance than both QQ and TMGN at 282.3 pm. Its large inherent strain and strong resulting intramolecular H-bond leads to it holding a *pK*<sub>aH</sub> (in MeCN) of 29.9, which (at the time of publishing) was the most basic of the DMAN-based proton sponges, although it suffers from a low kinetic basicity (slow proton exchange).<sup>18</sup>

Both TMGN and HMPN are more stable to hydrolysis and decomposition than many other proton sponges, and HMPN forming a stable hydrate with excess D<sub>2</sub>O. However, both slowly decompose under basic conditions.<sup>18, 124</sup> QQ derivatives vary in their stability, with some (like unsubstituted QQ) highly stable to a variety of conditions, and others, particularly halide-containing structures, prone to hydrolysis in the presence of water.

The main obstacle that QQ derivatives have in relation to the proton sponges TMGN and HMPN, is their comparatively difficult syntheses. Although all three start from 1,8-diaminonaphthalene, the latter two have fewer steps with higher overall yields. TMGN has a relatively simple synthesis from 1,8-diaminonaphthalene and Vilsmeier salt, HMPN a few extra steps based on this.

The kinetic basicity of QQ derivatives has not been evaluated.

## 4.4 - Conclusion

The basicities for a series of synthesised quinolino[7,8-*h*]quinoline derivatives were evaluated, covering a range of more than 14  $pK_{aH}$  units. These effects appeared to be primarily electronic, caused by a variety of electron donating/withdrawing substituents. Two of these experimental compounds have a  $pK_{aH}$  higher than that of DMAN, so can be classed as neutral organic superbases, or proton sponges. The computationally calculated values for theoretical QQ derivatives were all in the superbasic range, and demonstrated the importance of the positioning of electron donating/withdrawing groups on the basicity. The high  $pK_{aH}$  values, derivative tunability and low steric hinderance of QQ derivatives gives them a place in the body of neutral organic superbases, but their synthetic obstacles mean further research is required for application purposes.

## Chapter 5 - Structural insights using Computational Chemistry

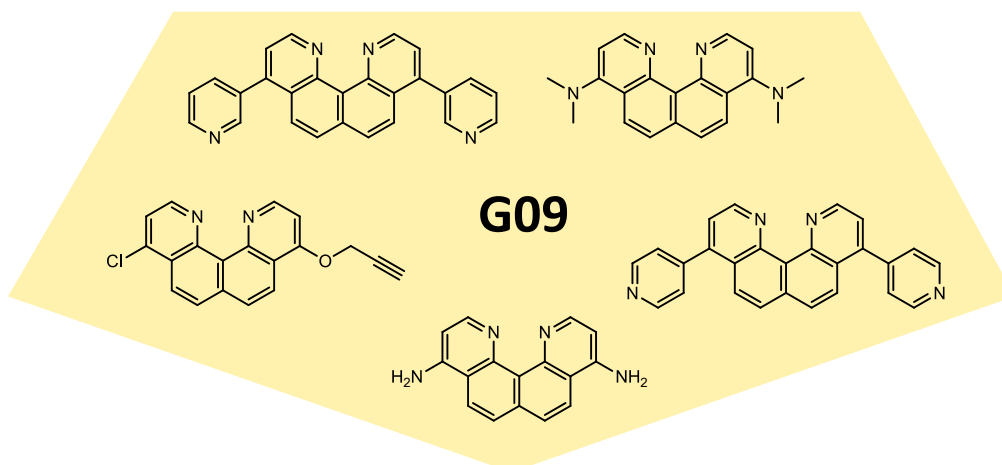


**Figure 5-1: Structures explored in this chapter using Gaussian09 (G09)**

Computational chemistry is a field that constantly evolves, with new techniques and progress in computational power. To experimental research chemists, electronic structure theory is a powerful tool to gain insight and understanding into the research undertaken in a laboratory. It can be used to predict spectral data and determine chemical and structural properties, such as  $pK_a$  values and optimised geometries. Many different methods of calculation have been established and these continue to be advanced, each with advantages for different systems and trade-offs between accuracy and computational cost. Some are based on quantum mechanical principles, others on classical mechanics – modelling large molecules often uses a hybrid approach. Depending on the chemical environment to be investigated, different approaches are made and revised, with prior literature precedence commonly providing starting points for the investigation.<sup>128</sup>

Current research on the structural properties of quinolono[7,8-*h*]quinoline derivatives is limited. Previous chapters have mentioned the difficulties encountered in attempts to produce crystals of many QQ derivatives that were of sufficient quality for single crystal X-ray analysis, so computational techniques were investigated. These calculations aimed

to gain further understanding of the physical structures of QQ derivatives, including the common structural changes observed between protonated and deprotonated states.

## 5.1 - Methods

The calculations were performed by Tyson Dais using Gaussian09 (G09, fig. 5-1).<sup>129</sup> For the simplicity of calculation, geometries were optimised in the gas phase. The functional and basis sets chosen were based on prior precedence in QQ and N-heterocyclic literature.<sup>11, 130</sup>

The calculations used DFT, with the  $\omega$ B97XD functional, and 6-311+G(2d,p) basis set:

- The  $\omega$ B97XD is a range-separated functional based on Becke's earlier 97 functional (B97) with some added dispersion correction (D). The basis set 6-311+G(2d,p) is a gaussian type (G, meaning gaussian type orbitals rather than the software) split-valence (6-311) basis set with two additional polarisation functions for non-hydrogen atoms (2d), one additional polarisation function for hydrogen atoms (p), and diffuse functions added to the heavy atoms (+).

Prior research has shown the energy barrier for the transfer of single hydrogen between each nitrogen atom in the central core to be low,<sup>11</sup> so to reduce computational time cost the hydrogen atom involved in protonation was attached to one nitrogen (N1, fig. 5-4).

Non-symmetric QQ derivatives with a tautomeric oxygen group at the 4 position (quinolino[7,8-*h*]quinoline-4(1*H*)-one derivatives) were excluded from these calculations as their neutral forms exist in the more stable quinolinone tautomer – this form is under low strain as a proton balances the central nitrogen atom repulsion, causing the planar structure to dominate. See Chapter 1 for further information.

The results contain the optimised geometry for  $N^4, N^4, N^9, N^9$ -tetramethylquinolino[7,8-*h*]quinoline-4,9-diamine instead of the synthesised ethyl derivative (**Q7**) due to computational time constraints. Although initially attempted, the flexibility of the ethyl groups was causing the calculations to take a long time, so the substitution was made.



Other  $pK_{aH}$  measurements (Chapter 3) showed the substituent  $NMe_2$  to have similar effects to  $NEt_2$  at the 4 and 9 positions.

Images were generated with Olex2<sup>8</sup> and Mercury.<sup>131</sup>

## 5.2 - Results and Discussion

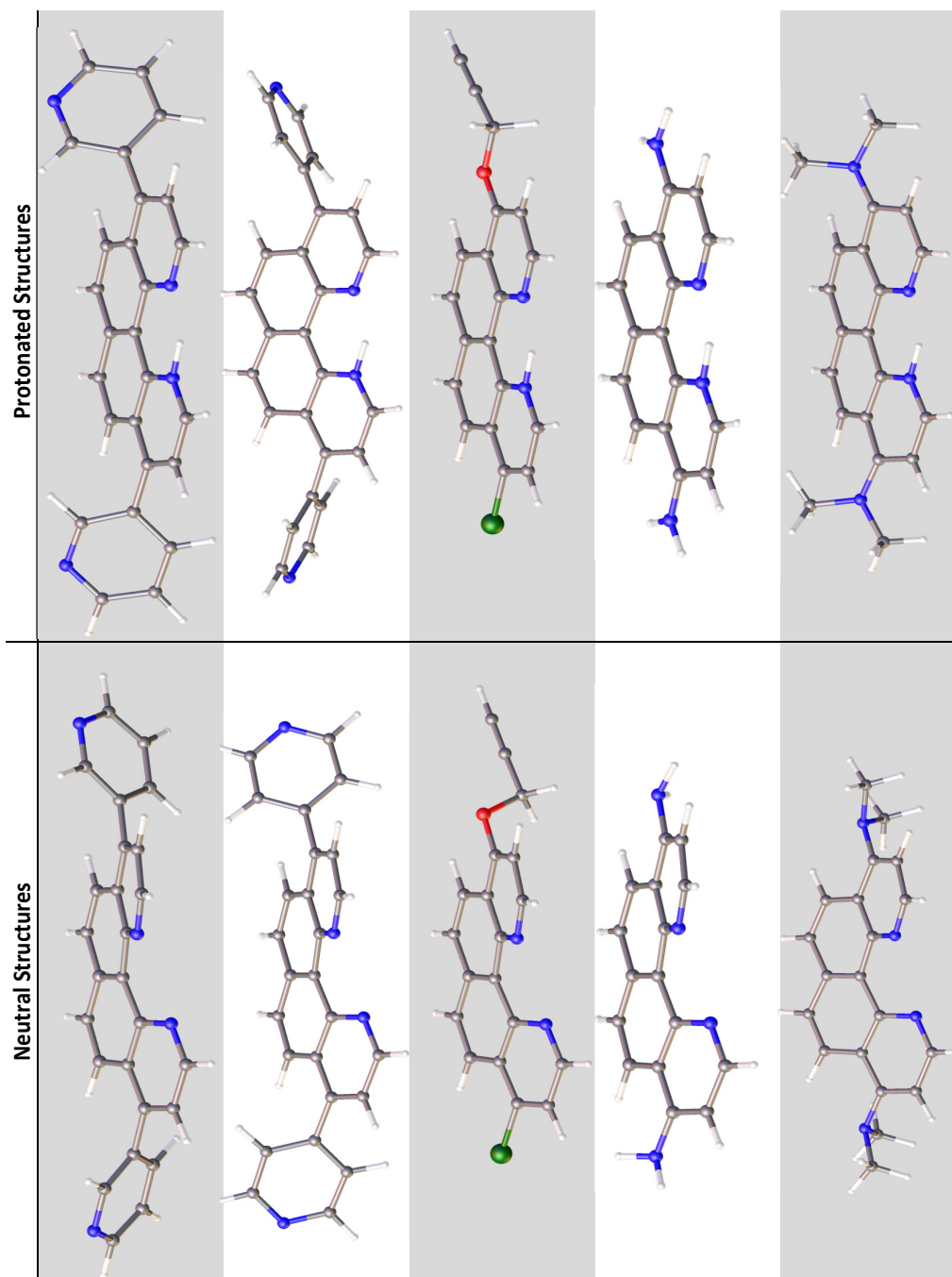


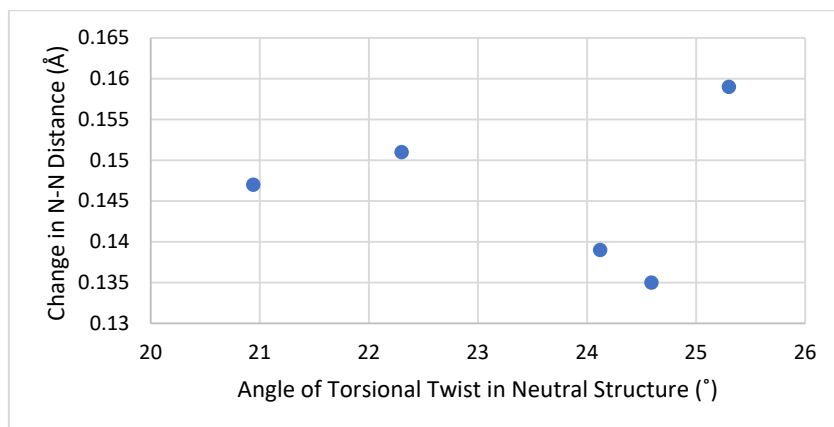
Figure 5-2: Optimised gas-phase neutral geometries of A: 4,9-di(3-pyridyl)quinolino[7,8-*h*]quinoline (Q6); B: 4,9-di(4-pyridyl)quinolino[7,8-*h*]quinoline (Q5); C: 4-chloro-9-(2-propyn-1-yloxy)-quinolino[7,8-*h*]quinoline (Q13); D: 4,9-diaminoquinolino[7,8-*h*]quinoline; E:  $N^4, N^4, N^9, N^9$ -tetramethylquinolino[7,8-*h*]quinoline-4,9-diamine (left) and protonated geometries (right).

Figure 5-2 shows ten structures: the gas-phase optimised geometries of five quinolino[7,8-*h*]quinoline derivatives in their neutral and protonated forms. As expected, the torsional twist of each compound in the neutral form flattened to a planar configuration upon protonation (as the electronic strain was reduced). Accompanying this was the reduction of N...N distances to below 2.6 Å, which allowed for very strong binding of that central hydrogen (table 5-1).

**Table 5-1: Selected structural properties of calculated QQ structures. Angles and distances calculated using Olex2.**

Structure	N...N Distance (Å)	N-H Bond Length (Å)	H...N Distance (Å)	Torsional Twist (°)
<b>A</b>	2.724	-	-	24.12
<b>AH+</b>	2.585	1.053	1.676	-0.03
<b>B</b>	2.723	-	-	24.59
<b>BH+</b>	2.588	1.052	1.680	-0.05
<b>C</b>	2.724	-	-	20.94
<b>CH+</b>	2.577	1.058	1.658	-0.01
<b>D</b>	2.727	-	-	25.30
<b>DH+</b>	2.568	1.052	1.659	-0.28
<b>E</b>	2.724	-	-	22.30
<b>EH+</b>	2.573	1.050	1.667	0.14

The reduction in N...N distances across the derivatives examined covered a range of 0.24 Å (between 0.159 and 0.135 Å), with the greatest change observed with the diamine derivative (**D**), at ~18% more than that observed for the smallest shift (4-pyridyl derivative **B**). There appears to be little correlation between magnitude of the torsional twist in the neutral state and the resulting N...N distance in the protonated form (fig. 4-5), or the magnitude of the N...N distance change (fig. 5-3), or the calculated strength of basicity (fig. 5-7) – so the twist in the neutral structure is not a useful feature for predicting protonated geometric properties, or derivative basicities.



**Figure 5-3: Comparison between angle of torsional twist in QQ derivative neutral structures and magnitude of N...N distance change upon protonation**

Previous QQ research indicated a variety of bond length and spatial changes upon QQ coordination that mediated the chelation of ions of various sizes (see Chapter 1),<sup>15</sup> so from the optimised geometries, bond lengths changes (upon protonation) were calculated. The magnitude of these changes, which were similar across the different derivatives, can be seen in figure 5-4. A table of QQ core bond lengths can be found in appendix D.

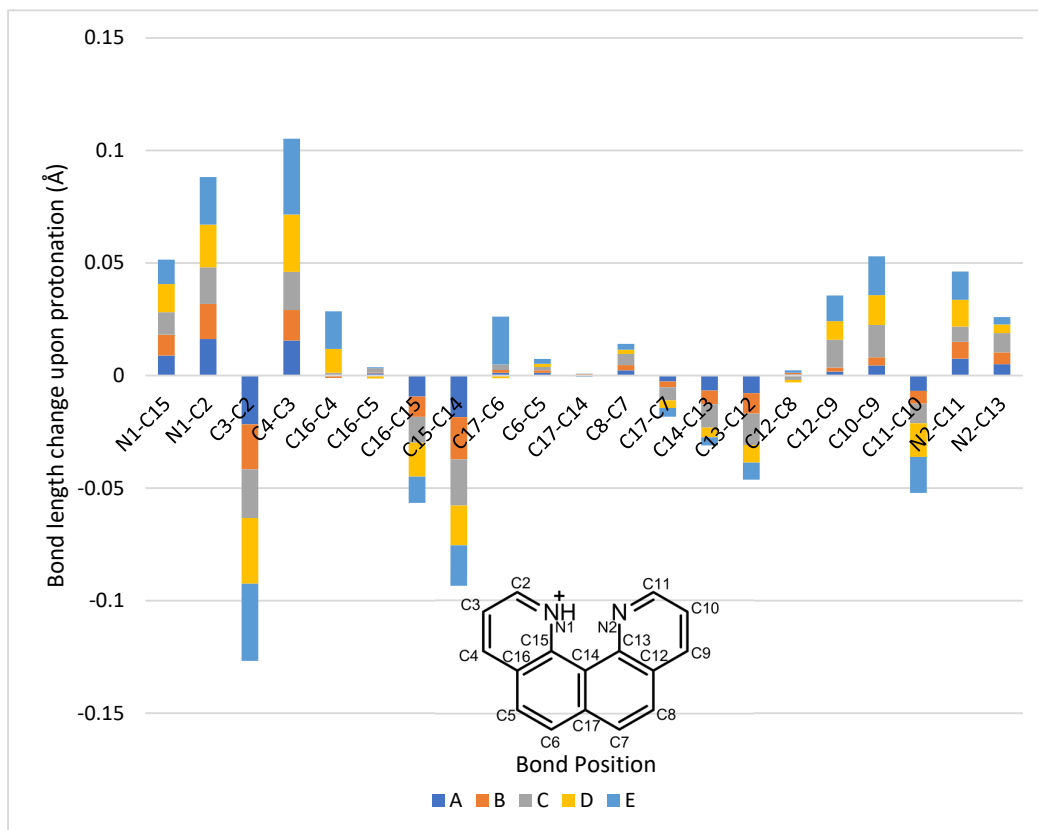


**Figure 5-4: Change in bond lengths in QQ core of derivatives A-E upon protonation. Bonds associated with the ‘protonated’ quinoline side (N1) to the left and the ‘non-protonated’ to the right.**

As described in 5.1, the proton was assigned to one nitrogen atom for reduced computational cost. It was observed that bond length changes (both increases and decreases) were of a greater magnitude for those associated with this (N1) donor quinoline (fig. 5-4, left) than the neutral (N2) acceptor quinoline half (fig. 5-4, right). This is consistent with the shorter N-H distance having a greater effect on the rings’ electron density.

The changes in bond lengths are further illustrated in figure 5-5. Significant increases in bond lengths were observed in several bonds of the heterocyclic rings (orange) upon protonation, while the upper bonds of the lower rings had corresponding decreases (blue), consistent with the reduction of repulsion in the core (as the nitrogen atoms are brought closer together) and concurrent flattening of the torsional twist. Small increases and decreases were also observed in the C17-C6 and C17-C7 bonds of the backbone respectively, mediating the twist. Bonds depicted in grey/black showed little change (on

average) – these ring locations, further away from the N···N electrostatic repulsion, show little of the twist in the neutral form so were expected to experience less changes upon protonation.

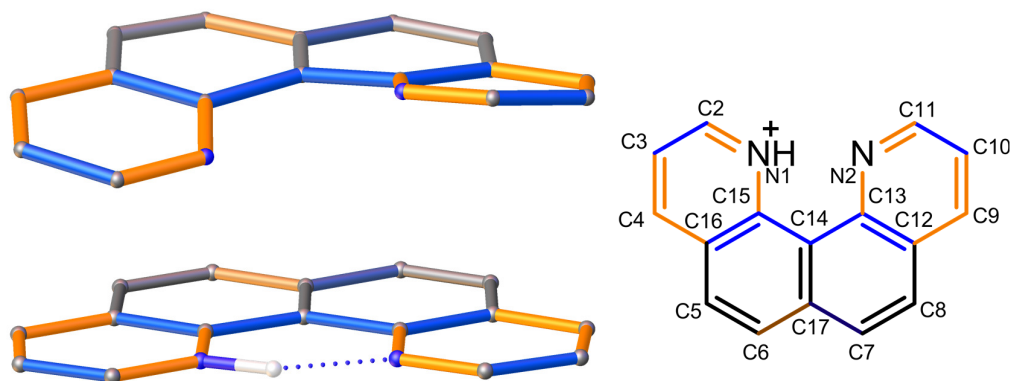


**Figure 5-5: QQ core structure with bonds that significantly change upon protonation. Orange bonds increase length, blue decrease, and grey/black show little change.**

Changes were also observed with some of the side groups upon protonation, the most noteworthy of which was with 4-chloro-9-(2-propyn-1-yloxy)-quinolono[7,8-*h*]quinoline (C, **Q13**). The 2-propyn-1-yloxy substituent was rotated from a ~perpendicular angle to one where the alkynyl group was almost in plane with the QQ core (fig. 5-2C). Additionally, slight bowing of the QQ core could be seen in the dimethyl amino derivative (E), likely due to steric repulsion of the methyl groups (fig. 5-6).

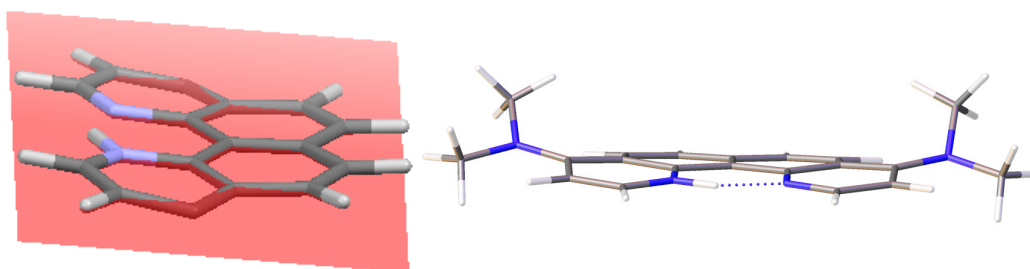


**Figure 5-6: Optimised structure images of protonated E with calculated plane (left) showing slight bowing. NMe<sub>2</sub> side groups omitted from the left image for clarity of the plane.**

### 5.2.1 - Gas Phase Basicity

From the frequency outputs of the optimised geometry calculations that produced the structures shown in figure 5-2, the gas phase basicities (GPB) and proton affinities (PA)

could be calculated. Gas phase basicity and proton affinities are defined by IUPAC as the ‘negative of the Gibbs energy change associated with the reaction in the gas phase’ and the ‘negative of the enthalpy change in the gas phase reaction (real or hypothetical) between a proton (more appropriately hydron) and the chemical species concerned’.<sup>132</sup> The properties were calculated using the frequency outputs from the equations below (similar to the method used by collaborators for the data presented in chapter 4, described in Rowlands et al.<sup>11</sup>).

$$\begin{aligned}
 & QQ_{(g)} + H_{(g)}^+ \rightarrow QQH_g^+ \\
 & \Delta G_{Total} = \Delta G_{QQH^+} - (\Delta G_{QQ} + \Delta G_{H^+}) \\
 & \text{Gas Phase Basicity (GPB)} = -\Delta G_{Total}
 \end{aligned}$$

Similarly:

$$\begin{aligned}
 & \Delta H_{Total} = \Delta H_{QQH^+} - (\Delta H_{QQ} + \Delta H_{H^+}) \\
 & \text{Proton Affinity (PA)} = -\Delta H_{Total}
 \end{aligned}$$

Where  $\Delta G_{QQH^+}$ ,  $\Delta G_{QQ}$ ,  $\Delta H_{QQH^+}$ ,  $\Delta H_{QQ}$  are the sums of the electronic and thermal free energies and enthalpies of the protonated and neutral QQ derivatives.  $\Delta G_{H^+}$  is the free energy of a proton at -0.01 a.u, and  $\Delta H_{H^+}$  the enthalpy at 0.00236 a.u, (1 a.u. = 627.510 kcal mol<sup>-1</sup> used for the conversion). The calculated basicities and affinities are presented in table 5-2. For details of the energies and enthalpies used for the calculations, see appendix D.

**Table 5-2: Calculated gas phase basicities (GPB) and proton affinities (PA) of calculated QQ derivatives, where QQ represents quinolino[7,8-*h*]quinoline. The substituents are attached at the 4 and 9 positions. Sorted in order of descending GPB.**

	Structure	GPB (kcal mol <sup>-1</sup> )	PA (kcal mol <sup>-1</sup> )
<b>D</b>		263.2	270.5
<b>E</b>		262.3	269.0
<b>C</b>		251.4	258.7
<b>A</b>		249.3	256.1
<b>B</b>		247.4	253.8

As expected, the strongest GPB and PA values were observed in the derivatives with the strongly electron donating amine substituents (**D** and **E**), reduced for **C** with the combination of the electron withdrawing Cl and donating OR groups, and weakest for the 3- and 4-pyridyl derivatives **A** and **B**. Additionally, as previously noted, there is no apparent correlation between the calculated basicities and the degree of torsional twist in the neutral structures (fig. 5-7).

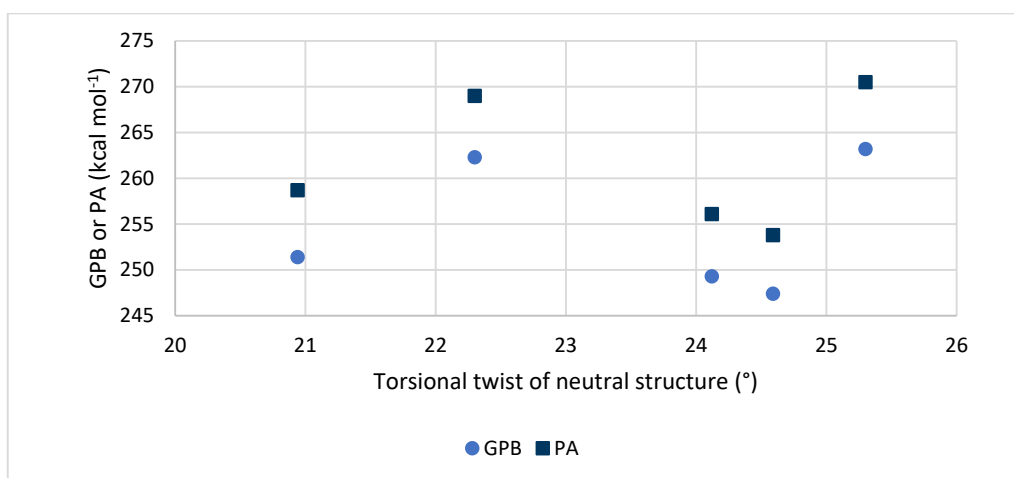


**Figure 5-7: Calculated basicity (Gas Phase Basicity (GPB, circle) or Proton Affinity (PA, square)) compared with degree of torsional twist in the neutral structures.**



### 5.3 - Conclusion

Computational techniques have been used to calculate the optimised geometries and frequencies of a range of quinolino[7,8-*h*]quinoline derivatives. The resulting optimised structures provided insight into the structural changes taking place upon protonation of the central di-nitrogen site. These included increases in the length of the C-N bonds and those opposite in the pyridyl rings of the QQ core, along with decreases in several others (fig. 5-5), changes which were in the same direction but of greater magnitude in the parent quinoline where the central proton was fixed (N1) (fig. 5-4). As the repulsion between the lone electron pairs of the nitrogen atoms is reduced by protonation, the bond length changes were accompanied by reductions of helical twists from  $>20^\circ$  to almost planar configurations.

This technique can now be used to explore more quinolino[7,8-*h*]quinoline structures, predict their relative basicities and seek new synthetic targets.

## Chapter 6 - Coordination

### 6.1 - Quino[7,8-*h*]quinoline Coordination - General

As discussed in chapter 1 (introduction), the coordination properties of many neutral organic superbases have yet to be explored. In many cases, this is due to steric constraints, where the structural aspects that enable the high basicities of many proton sponges also limit their coordination potential.

Chapter 4 discussed how the highly strained heterocyclic structure of QQ derivatives make them ideal candidates for proton sponges or superbases. In addition to protonation, this strain (caused by the electronic repulsion of nitrogen atom electron lone pairs) can also be relieved by coordination of a cationic species.

As discussed in chapter 1, research has shown quinolino[7,8-*h*]quinoline derivatives to be capable of a variety of bond length and spatial changes within the ring structure that mediates coordination.<sup>41</sup> With smaller ions, a reduced N...N distance was observed, with corresponding C-C bond distances in the other parts of the molecule adjusting around a central pivot point. Accordingly, when larger ions are complexed, the opposite occurs (fig. 6-1A). The small N...N 'bite' size also means that while these larger metal ions can be successfully coordinated, they are forced out of the central plane, and result in significant bowing of the core ring structure as seen in the X-ray structure of the Cu(II) QQ complex shown in figure 6-1C.<sup>58</sup>

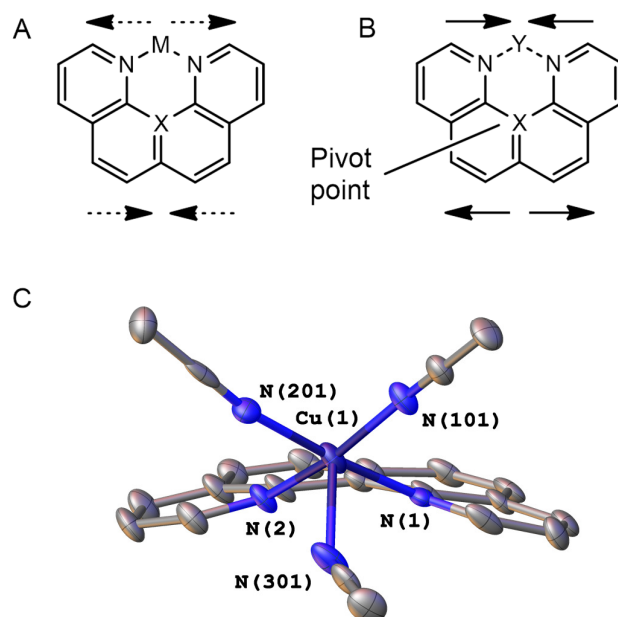


**Figure 6-1:** QQ spatial changes associated with (a) coordination to large metal ions such as Pt and Re and (b) protonation or coordination to smaller ions such as  $\text{BF}_2$ . (C): X-ray structure of a Cu-QQ complex, produced in Olex2 with 50% ellipsoids from CCDC file NIBSIC.<sup>8</sup> Anions and hydrogen removed for clarity. (a)/(b) reproduced from Shaffer et al., 2012.<sup>41</sup>

The first transition metal complex involving a QQ derivative was published in 2001. A substructure search of Scifinder and the CCDC (290720) shows that to date, there have been eight structurally characterised QQ complexes published since that time, using only 4,9-dichloroquinolino[7,8-*h*]quinoline (**Q3**) and quinolino[7,8-*h*]quinoline (**QQ**) as ligands (Table 6-1). Only six of these have structures deposited in the CCDC (Pt and Mn complexes are not present).<sup>41</sup>

**Table 6-1: Summary of all complexes published to date involving quinolino[7,8-*h*]quinoline derivatives (excluding those only published in patents).**<sup>79, 133-134</sup>

QQ derivative	Coordinated ions (central cavity)
4,9-Dichloroquinolino[7,8- <i>h</i> ]quinoline ( <b>Q3</b> )	$\text{Pd(II)}^{56}$ , $\text{Pt(II)}^{56}$ , $\text{Re(I)}^{56}$ , $\text{Mn(I)}^{56}$ , $\text{B(III)}^{41}$ , $\text{Cu(II)}^{58}$
Quinolino[7,8- <i>h</i> ]quinoline ( <b>QQ</b> )	$\text{B(III)}^{41}$ , $\text{Cu(II)}^{58}$

Several potential factors contribute to the low numbers of QQ complexes, not least of which is the initial barrier of the difficulties encountered in ligand synthesis and purification. The limited solubility of many QQ derivatives is another challenge affecting

complexation - it both restricts the solvents available to trial complexation reactions, and, in many cases, leads to the formation of precipitates instead of crystalline metal complexes suitable for single-crystal X-ray crystallography. Additional factors include the competition between protonation of the ligand versus complexation, a common result from complexation attempts was a crystallised protonated ligand. Degradation by hydrolysis was also an obstacle. These challenges were all encountered during complexation attempts in this project.

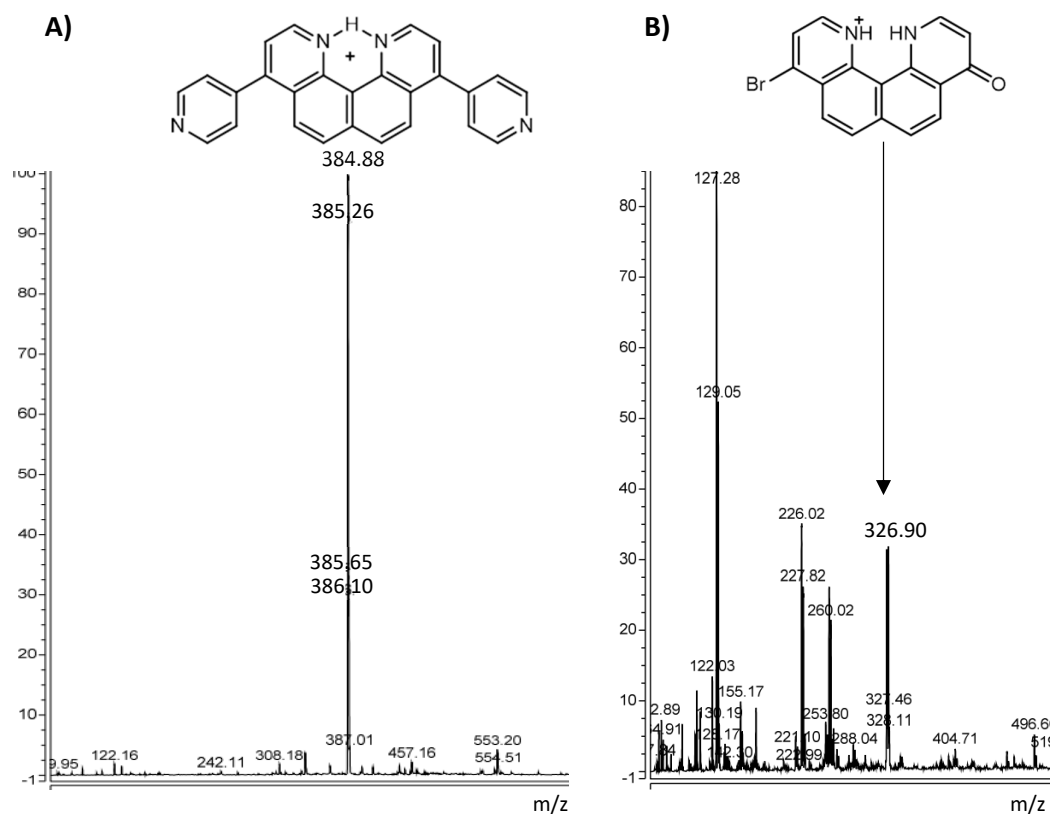
### 6.1.1 - Results

Table 6-2 shows selected complexation attempts during this project involving QQ derivatives, which were conducted concurrently with crystallisation either by slow evaporation or vapour diffusion. Crystallisation solvents in which the ligands were at least partially soluble included MeOH, CH<sub>3</sub>CN, DMF, DCM, CHCl<sub>3</sub> (and mixtures of these).

**Table 6-2: Selected QQ derivative complexation attempts**

Quino[7,8- <i>h</i> ]quinoline derivative	Ion
4,9-di(pyridin-3-yl)QQ ( <b>Q6</b> )	Cu(II)
	Pt(II)
	Pd(II)
4,9-di(pyridin-4-yl)QQ ( <b>Q5</b> )	B(III)
	Pd(II)
4,9-dibromoQQ ( <b>Q4</b> )	Cu(II)
<i>N</i> <sup>4</sup> , <i>N</i> <sup>4</sup> , <i>N</i> <sup>9</sup> , <i>N</i> <sup>9</sup> -tetraethylquinolino[7,8- <i>h</i> ]quinoline-4,9-diamine ( <b>Q7</b> )	Cu(II)

Possible complex formation was indicated in some by colour changes and/or small shifts in <sup>1</sup>H NMR spectra, but crystals of sufficient quality for single crystal X-ray crystallography were not obtained, and issues of solubility and ion ferromagnetism complicated the collection of NMR data. Mass spectra were collected on many of the samples, and protonated ligand peaks were often clear (e.g. fig. 6-2A). Some spectra indicated ligand decomposition had occurred (fig. 6-2B).



**Figure 6-2: Mass spectra of attempted complex formation. A: Attempted Q5-B(III) complexation showing only the Q5 ligand. B: Attempted Q4-Cu(II) complexation, showing decomposition of Q4 to the mono-halide Q9.**

Figure 6-3 shows the mass spectrum taken from a complexation attempt involving 4,9-di(pyridin-3-yl)QQ (**Q6**) and Pt(COD)Cl<sub>2</sub>. Peak patterning suggests a Pt coordination species was formed, however the formula of this is undetermined.

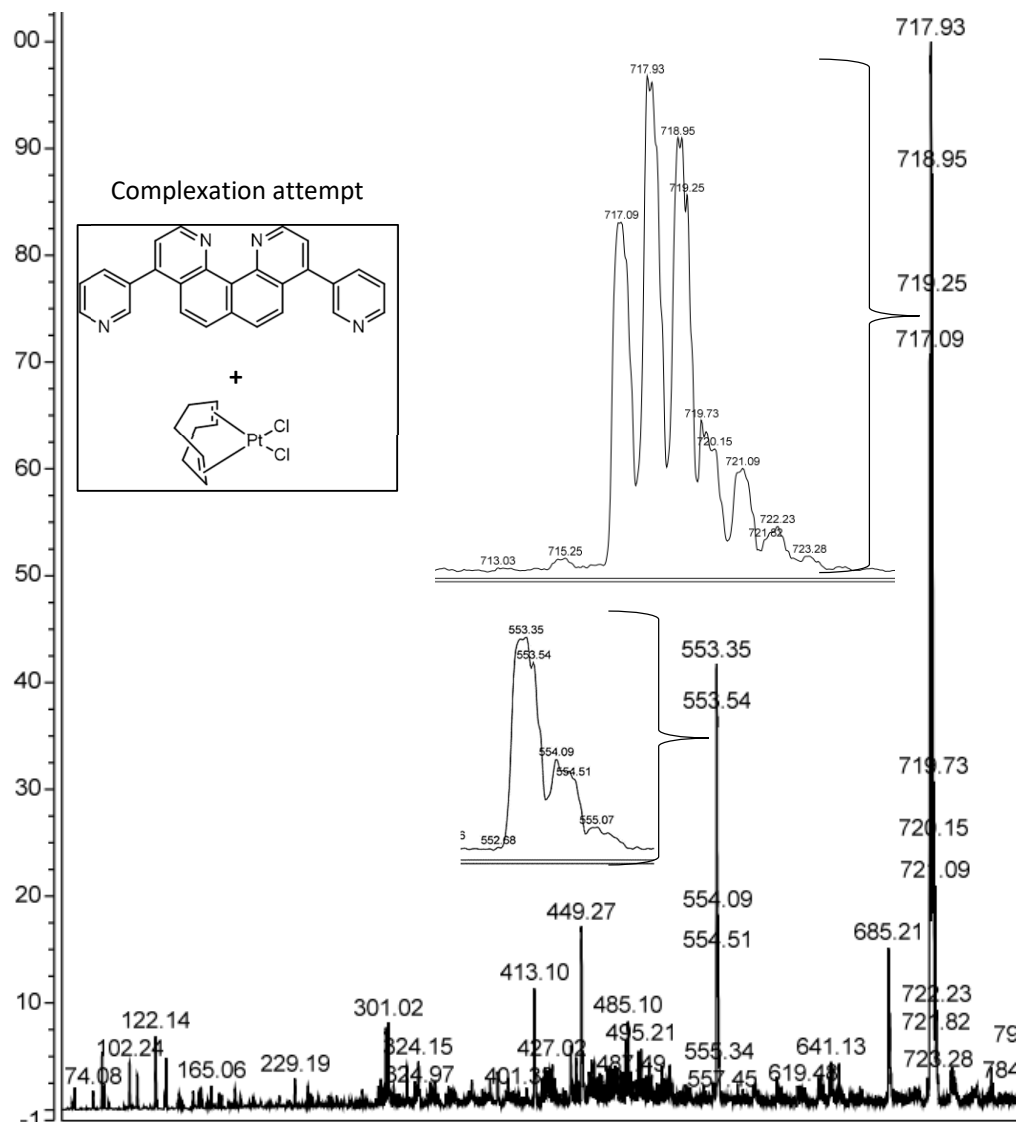


Figure 6-3: Mass spectrum of complexation attempt between Pt(II) and Q6.

It is possible that techniques available at other facilities, such as cold-spray mass spectrometry, could have provided evidence to support complexation of quinolino[7,8-*h*]quinoline derivatives, however exploration of the structural changes of QQ was the primary focus of these complexation attempts, so evidence other than X-ray crystallography was not ruthlessly pursued.

## 6.2 - Beryllium Coordination

Given the small size of the Be(II) ion, the proton sponge class of molecules (effective coordinators of small H<sup>+</sup> ions), were thought to offer an avenue for Be(II) chelation, so the QQ derivative family was pursued. Prior research had also established that QQ and 4,9-dichloroQQ can effectively bind the similarly sized B(III) ion, and is a good size match for the QQ core pocket, as seen by the close to planar structure in figure 6-4.<sup>41</sup>

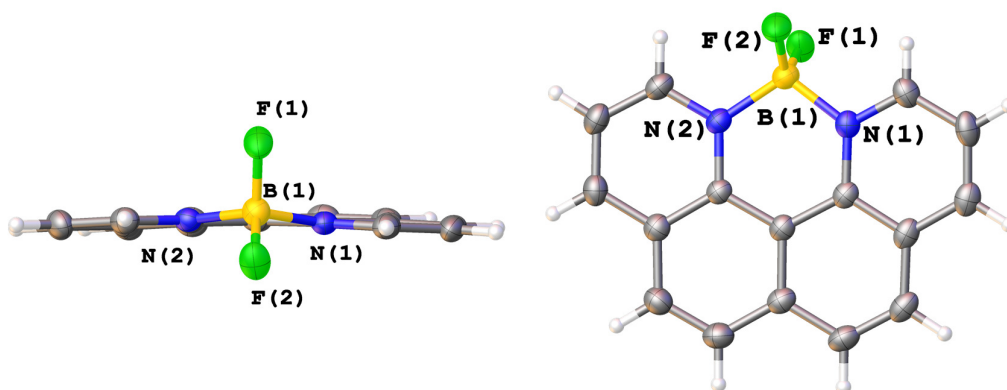


Figure 6-4: QQ-BF<sub>2</sub> complex with 50% ellipsoids.<sup>41</sup> Image generated in Olex2 from CCDC deposition number PANGAO.<sup>8</sup>

As the smallest and hardest metal ion it was theorised that, like B<sup>3+</sup>, Be<sup>2+</sup> may also be a good fit for the QQ core.

Due to the toxic nature of beryllium compounds, and the safety standards required to work with them the 'wet' beryllium chemistry of this project could not be carried out at Massey University.<sup>135</sup> A research collaboration had been established between prior members of the Plieger group and Dr. Magnus Büchner at the University of Tartu, Germany. The Büchner group, who are one of only a few worldwide that have the facilities to explore the Be coordination at a chemistry laboratory level, were interested in studying the use of QQs as coordinating compounds.

Samples of a variety of QQ derivatives were sent to the Büchner research group, covering a range of different substituents and core basicities (Table 6-3). Organometallic Be(II) complex synthesis first involves the formation of commonly used precursors, BeX<sub>2</sub>, where X= Br, Cl, or I. BeCl<sub>2</sub> is the only one with commercial availability. Significantly

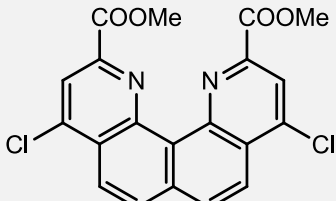
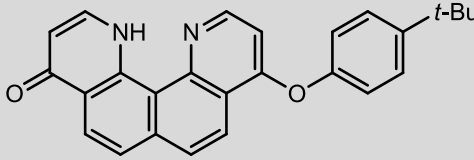
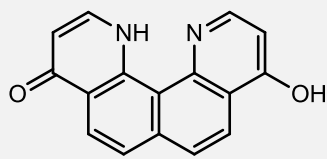
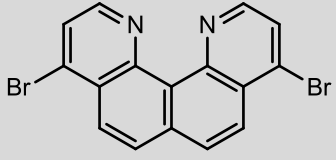
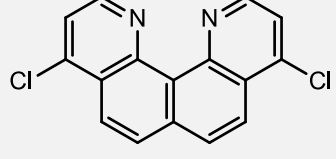
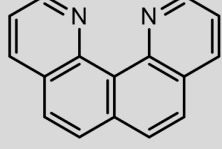
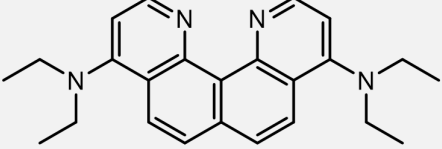
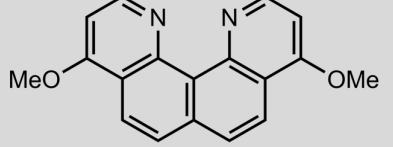
milder methods to produce these precursors were recently published by the Buchner Group. In brief: this included Be metal powder and condensed halide (liquid form) in separated sections of connected Schlenk apparatus. The halides were allowed to fill the apparatus under controlled pressures, and the metal powder heated, leading to deposition of BeBr<sub>2</sub> or BeCl<sub>2</sub> crystals later purified by sublimation.<sup>136</sup>

Many challenges were encountered in the QQ-Be(II) coordination process. The limited solubility of QQ compounds in solvents ideal for crystal growth (and in which BeBr<sub>2</sub> was also soluble) was one of the greatest obstacles and hampered collaborators' efforts to create and characterise any QQ complexes. Additionally, insoluble solids were frequently obtained instantly when BeBr<sub>2</sub> was mixed with the strongly chelating QQ-based ligands, which also made obtaining information by <sup>9</sup>Be NMR difficult. Decomposition (believed to be Be-mediated) often followed attempts to recrystallise these insoluble solids at higher temperatures. It was also found that Cl ion abstraction by BeBr<sub>2</sub> often occurred from Cl containing QQ ligands.

The <sup>9</sup>Be NMR spectra were complicated by the tendency of acetonitrile solvent molecules to readily exchange in solution with halides, so multiple species were often present in solution. Many different solvents were trialled, including MeCN, THF, CD<sub>2</sub>Cl<sub>2</sub>, CDCl<sub>3</sub>, C<sub>6</sub>D<sub>6</sub> and 1,2-difluorobenzene.



**Table 6-3: QQ derivatives sent to Germany for Beryllium coordination**

Name	Structure	$pK_{AH}$
Dimethyl-4,9-dichloroquinolino[7,8- <i>h</i> ]quinoline-2,11-dicarboxylate ( <b>Q16</b> )		9.24
9-(4-tert-Butylphenoxy)quinolino[7,8- <i>h</i> ]quinoline-4(1 <i>H</i> )-one ( <b>Q19</b> )		12.10
9-(Hydroxy)-quinolino[7,8- <i>h</i> ]quinoline-4(1 <i>H</i> )-one ( <b>Q2</b> )		12.21
4,9-Dibromoquinolino[7,8- <i>h</i> ]quinoline ( <b>Q4</b> )		17.58
4,9-Dichloroquinolino[7,8- <i>h</i> ]quinoline ( <b>Q3</b> )		17.64
Quino[7,8- <i>h</i> ]quinoline ( <b>Q17</b> )		19.6
<i>N</i> <sup>4</sup> , <i>N</i> <sup>4</sup> , <i>N</i> <sup>9</sup> , <i>N</i> <sup>9</sup> -tetraethylquinolino[7,8- <i>h</i> ]quinoline-4,9-diamine ( <b>Q7</b> )		23.97
4,9-Dimethoxyquinolino[7,8- <i>h</i> ]quinoline ( <b>Q20</b> )		-

Success was achieved with the ligand **Q2** and BeBr<sub>2</sub> to produce the first structurally characterised Be (II) QQ derivative complex (fig. 6-5). This is the 7<sup>th</sup> ion to be successfully

coordinated with a QQ derivative. Despite the low solubility of **Q2** (e.g. the NMR spectra are run in TFA-*d*), the complex was formed in acetonitrile from BeBr<sub>2</sub> and 9-(hydroxy)-quinolino[7,8-*h*]quinoline-4(1*H*)-one (**Q2**), and recrystallised at elevated temperatures to produce quality crystals, before the structure was collected and solved by Nils Spang of the Büchner group. X-ray structure determination data can be found in appendix E.

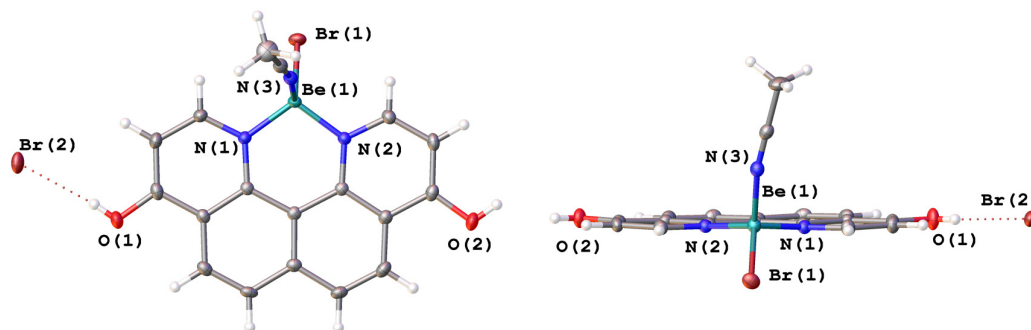


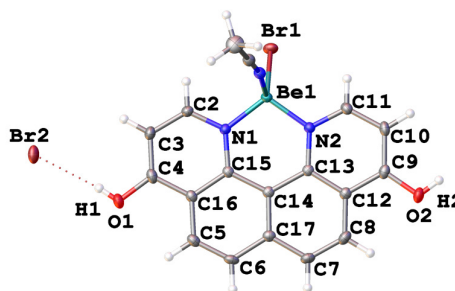
**Figure 6-5:** [BeBr(MeCN)(QQ(OH)<sub>2</sub>)]Br crystal structure (Be-QQ(OH)<sub>2</sub>) in two different views with 50% ellipsoids. Images generated in Olex2.<sup>8</sup>

The small, 4-coordinate Be(II) ion fits neatly within the coordination pocket of the QQ core to give a planar structure, with two sites occupied by the ligand N atoms, one by a bromide ion, and one by an acetonitrile solvent molecule. The second bromide ion from BeBr<sub>2</sub>, forms an intermolecular halogen bond between neighbouring ligands, with angles close to 180° (table 6-4).

Although the keto-enol tautomer of **Q2** is more energetically favourable (fig. 1.11), it appears that the complexation of Be(II) proceeds by the dienol- tautomer 4,9-dihydroxyquinolino[7,8-*h*]quinoline (**Q2**). As this less stable structure does not have a protonated central nitrogen atom, the binding pocket is more available for coordination and a greater stabilisation effect for the complexation process would occur.

**Table 6-4: Angles and distances associated with halogen bonding in Be-QQ(OH)<sub>2</sub> and complex naming key (right)**

Atoms	Angle (°)	Length Br-H Bond (Å)
O1-H1-Br2	173.62	2.37(3)
O2-H2-Br2	176.42	2.36(3)
H1-Br2-H2	117.08	-



This halogen bonding link forms chains of ligands packed together in alternate directions, with coordinated acetonitrile molecules which are angled almost perpendicular to the QQ-ligand plane (fig. 6-6).

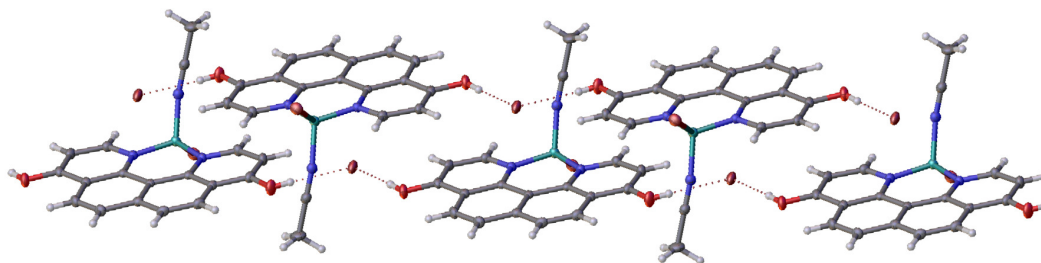


**Figure 6-6: Be-QQ(OH)<sub>2</sub> crystal structure showing a layer of packing (50% ellipsoids). Image generated in Olex2.<sup>8</sup>**

As X-ray structural data for 4,9-dihydroxyquinolino[7,8-*h*]quinoline ligand is unknown, 4,9-dichloroquinolino[7,8-*h*]quinoline (**Q3**) chelates are used for comparison of the structural parameters in table 6-5. This ligand is one of two QQ derivatives (currently in the CCDC database) that has been successfully coordinated to multiple ions.

**Table 6-5: Selected Distances (in Å) of QQ Complexes.** Blue represents distances shorter than (or equal to) the corresponding distance in neutral QQCl<sub>2</sub> (4,9-dichloroquinolino[7,8-*h*]quinoline, Q3) while orange represents greater length. The 'NCCCN plane' represents the plane formed by the 5 atoms of the central Q derivative binding pocket.

	QQCl <sub>2</sub>	[QQCl <sub>2</sub> ] H <sup>+</sup>	[QQ(OH) <sub>2</sub> ] Be(II)	[QQCl <sub>2</sub> ] B(III)	[QQCl <sub>2</sub> ] Cu(II)	[QQCl <sub>2</sub> ] Re(I)	[QQCl <sub>2</sub> ] Pt(II)
<b>CCDC Deposition Number</b>	834811	834812	-	835383	871819	164920	164921
<b>N···N</b>	2.768	2.591	2.703	2.551	2.748	2.804	2.810
<b>C15-C13</b>	2.585	2.539	2.561	2.511	2.560	2.585	2.484
<b>C6-C7</b>	2.444	2.467	2.449	2.467	2.467	2.390	2.408
<b>Ion - NCCCN plane</b>	-	0.001	0.091	0.098	0.868	1.133	0.999
<b>Torsional NCCN Twist (°)</b>	20.02	0.17	0.92	1.16	0.71	1.69	0.00

A)

B)

The Be-QQ(OH)<sub>2</sub> chelate is most similar to the structures containing small ions such as H<sup>+</sup> or B(III). In all three of these complexes, the central ion sits very neatly within the plane formed by the coordination pocket, as opposed to the significant deviation of the larger Cu(II), Re(I) and Pt(II) ion complexes. The distance C15-C13 is reduced in all complexes compared to the neutral twisted QQCl<sub>2</sub>, while the N···N is only decreased for the H<sup>+</sup>, Be(II), B(III) and Cu(II) ions, and is accompanied by increased C6-C7 distances. Of these changes, the clearest indicator of the pivot action is the increase in C6-C7 – this is consistent with the pincer movement **A** (table 6-5A). The reverse is observed with comparison to the coordination of the much larger ions Pt(II) and Re(I), which show increased N···N and decreased C6-C7 distances, according to movement **B** (table 6-5B). See appendix E for further details of the Be(II)-QQ(OH)<sub>2</sub> crystal structure.

Attempts by collaborators to coordinate and crystallise other Be(II) QQ derivative complexes are ongoing.

### 6.3 - Conclusion

Quinolino[7,8-*h*]quinoline derivatives have high potential for coordination to a range of ions. The exploration of this potential, however, has proved difficult. Challenges including the ligand synthesis, competition by protonation and degradation during complexation attempts, and solubility of the resulting complexes. However there is still scope for exploration and development. With very few QQ metal complexes existing in literature, the Be(II) complex presented in this chapter is a worthwhile achievement. Be-QQ(OH)<sub>2</sub> represents the first time this ion has been complexed with a QQ derivative, the only 4,9-dihydroxyquinolino[7,8-*h*]quinoline X-ray structure and complex known to date, and only the 7<sup>th</sup> ion to be complexed with a QQ compound.

## Chapter 7 - Future Work

There is plenty of scope for future research involving quinolino[7,8-*h*]quinoline derivatives, the main focus of which should include the synthesis of new derivatives (some of which was discussed briefly in 2.5).

Stringent water-free conditions may reduce side product formation and purification issues currently caused by hydrolysis, and well-established transformation methods that have proven successful under these conditions may have higher chances of success. Foci could include some of the computationally investigated derivatives of chapter 4 that showed extremely high  $pK_{aH}$  values (fig. 7-1).

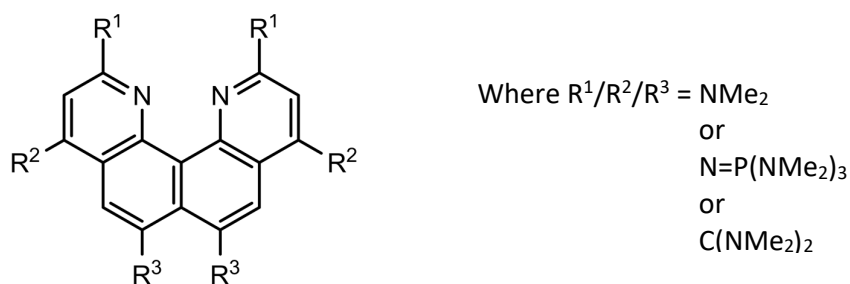


**Figure 7-1: Structure of computationally calculated QQ derivatives with high  $pK_{aH}$  values given in chapter 4.**

An example of this is the synthesis of 4,9-di(dimethylamine)quinolino[7,8-*h*]quinoline, an attempt described in 2.2.4. While the high water content of the reaction led to the synthesis of the mono-amine compound **Q12** (only the 40% aqueous dimethylamine solution was available), it is theorised that the di-substitution reaction may proceed if rigorously anhydrous conditions were utilised, possibly involving a THF or MeOH based dimethylamine solution.

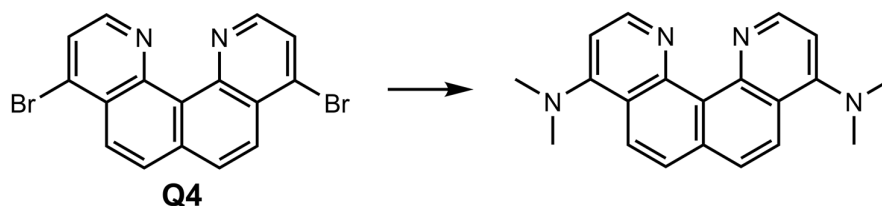


**Figure 7-2: Attempted synthesis of 4,9-di(dimethylamine)quinolino[7,8-*h*]quinoline**

Another avenue for future synthetic work is the extension of the new non-symmetric propynyloxy QQ derivative pathway, through the alteration of functional groups at the 4 position of **Q10** and **Q13** (substitution), and/or of the terminal alkyne group. Possible alkyne transformations could include click chemistry, catalytic hydrogenation, or hydration, depending on the stability of the C-O bond of the propynyloxy substituent under reaction conditions. These transformations may also be possible on the ester analogue **Q15**.<sup>125</sup>

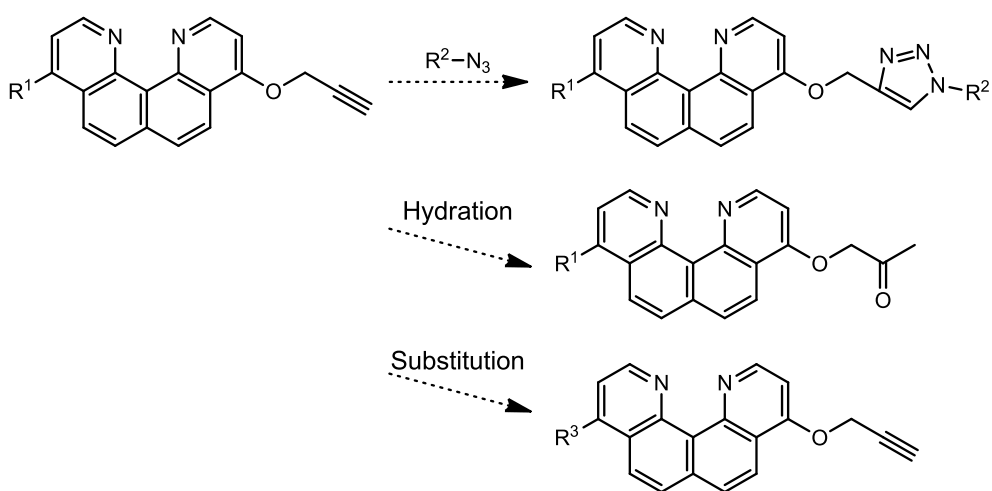


**Figure 7-3: Examples of possible transformations of Q10 and Q13 (R<sup>1</sup> = OH (tautomer) or Cl respectively). R<sup>2</sup>/R<sup>3</sup> = alkyl group.**

As the double substitution of diethylamine groups to **Q13** showed (2.3.2), it may also be possible to use **Q10**, **Q13** and/or **Q15** in synthesis that involves substitution of the propynyloxy group.

Non-symmetric QQ synthesis could be further developed through C-C coupling. Attempts to extend the non-symmetric Suzuki-Miyaura-coupled QQ pathway were met with difficulties of purity and compound degradation (**Q14**, 2.3.5) - however if the water sensitivity can be mitigated, for example through the exploration of singly 9-substituted alternatives to **Q10**, it is possible that new non-symmetric C-C coupled QQ derivatives could be created for coordination-based applications.

Coordination of QQ derivatives to new metals or with new derivatives has proved challenging to date. Synthetic foci to advance this should include aims for QQ derivatives with higher solubility to aid in crystallisation, and reduce issues encountered with the formation of insoluble precipitates, particularly with the Be(II) work (chapter 6). Research involving the more rigid quinolino[7,8-*h*]quinoline analogue, acequinolinoquinoline (fig. 7-4A), may have potential in this area: It was noted by authors to be ‘soluble in acetone, moderately in most other solvents, including alcohols and water,’<sup>59</sup> although it is possible that the reduced flexibility will reduce the range of potential coordination ion targets.

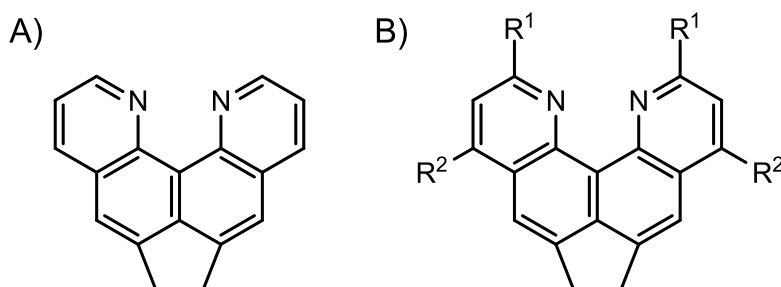


**Figure 7-4: A: Acequinolinoquinoline (aceQQ), also called dipyrdo[3,2-*e*:2',3'-*h*]acenaphthene.<sup>59</sup> B: AceQQ with possible functionalisation positions from synthesis by QQ methods.**

Future work could involve functionalising the pure aceQQ core (fig. 7-4A) directly, or attempting to use QQ methods to synthesise aceQQ in order to build in more opportunities for functionalisation control, through the ester or oxo groups inherent to the synthesis (R<sup>1</sup> and R<sup>2</sup> respectively fig. 7-4B).

If the current synthetic and solubility issues of quinolino[7,8-*h*]quinoline ligand building blocks can be overcome, viable ligands could be synthesised, with coordinating substituents extended out from the main structure to avoid steric hinderance (e.g. using Sonogashira coupling, see 2.5). As changing the group coordinated in the central di-nitrogen site changes angles of side groups, these structures would have applications in research developing tunable metallo-organic cages.



## Chapter 8 - Conclusion

Many challenges were present in the development of quinolino[7,8-*h*]quinoline chemistry, and these were either overcome or led to shifts in research focus.

New synthetic pathways were explored resulting in the synthesis of a range of new QQ derivatives, each featuring a variety of functional groups that contribute well to the current literature. The evaluation of experimental basicities for a series of QQ derivatives spanned more than 14  $pK_{aH}$  units, with effects appearing to be primarily electronic, caused by changes in the strength of electron donating/withdrawing substituents. By the definition of having a  $pK_{aH}$  higher than that of DMAN in acetonitrile (18.63), two of these could be classed as proton sponges, or neutral organic superbases, one being the pre-existing unsubstituted quinolino[7,8-*h*]quinoline (**Q17**) at 19.6 and the other *N*<sup>4</sup>,*N*<sup>4</sup>,*N*<sup>9</sup>,*N*<sup>9</sup>-tetraethylquinolino[7,8-*h*]quinoline-4,9-diamine (**Q7**) at a significantly higher 23.97. The halide derivatives **Q3** and **Q4**, with  $pK_{aH}$  values of 17.64 and 17.58, also approach the class. The effects resulting from the change in substituent positions was emphasised by the computational  $pK_{aH}$  calculations.

Structural analysis (chapter 5) showed the bond length and angle changes upon protonation of the central nitrogen binding site.

Development of the coordination potential of QQ derivatives, and analysis by X-ray crystallography, proved challenging, however success was achieved with a quality structure showing Be(II) bound to 4,9-dihydroxyquinolino[7,8-*h*]quinoline. This is the first time Be(II) has been chelated by a QQ derivative, and the structure represents only the 7<sup>th</sup> ion to be complexed with a QQ derivative to date since the first confirmed synthesis in 1987.

Quinolino[7,8-*h*]quinoline derivatives have many interesting and extremely useful properties, although further research is required to develop applications.



## References

1. Pozharskii, A. F.; Ozeryanskii, V. A.; Filatova, E. A., Heterocyclic superbases: retrospective and current trends. *Chem. Heterocycl. Compd.* **2012**, *48* (1), 200-219.
2. Ishikawa, T.; Harwood, L. M., Organic superbases: the concept at a glance. *Synlett* **2013**, *24* (19), 2507-2509.
3. Ishikawa, T., *Superbases for organic synthesis: guanidines, amidines, phosphazenes and related organocatalysts*. John Wiley & Sons: Chichester, U.K., 2009; p 336.
4. Gerson, F.; Haselbach, E.; Plattner, G., Radical anion of 1,8-bis(dimethylamino)naphthalene ("proton sponge"). *Chem. Phys. Lett.* **1971**, *12* (2), 316-319.
5. Brzezinski, B.; Grech, E.; Malarski, Z.; Sobczyk, L., Protonation of 1,8-bis(dimethylamino)naphthalene by various acids in acetonitrile. *J. Chem. Soc., Perkin Trans. 2* **1991**, (6), 857-859.
6. Alder, R. W.; Bowman, P. S.; Steele, W. R. S.; Winterman, D. R., The remarkable basicity of 1,8-bis(dimethylamino)naphthalene. *Chem. Commun.* **1968**, (13), 723-724.
7. Barner, B. A.; Faler, C. A.; Joullié, M. M., 1,8-Bis(dimethylamino)naphthalene. In *Encyclopedia of Reagents for Organic Synthesis*, Wiley Online Library: 2006.
8. Dolomanov, O. V.; Bourhis, L. J.; Gildea, R. J.; Howard, J. A. K.; Puschmann, H., OLEX2: a complete structure solution, refinement and analysis program. *J. Appl. Crystallogr.* **2009**, *42* (2), 339-341.
9. Mallinson, P. R.; Woźniak, K.; Wilson, C. C.; McCormack, K. L.; Yufit, D. S., Charge Density Distribution in the "Proton Sponge" Compound 1,8-Bis(dimethylamino)naphthalene. *J. Am. Chem. Soc.* **1999**, *121* (19), 4640-4646.
10. Stibrany, R. T.; Potenza, J. A., CEJGUU. *CSD Communication* **2006**.
11. Rowlands, G. J.; Severinsen, R. J.; Buchanan, J. K.; Shaffer, K. J.; Jameson, H. T.; Thennakoon, N.; Leito, I.; Lökov, M.; Kütt, A.; Vianello, R.; Despotović, I.; Radić, N.; Plieger, P. G., Synthesis and Basicity Studies of Quinolino[7,8-*h*]quinoline Derivatives. *J. Org. Chem.* **2020**, *85* (17), 11297-11308.
12. Kaljurand, I.; Saame, J.; Rodima, T.; Koppel, I.; Koppel, I. A.; Kogel, J. F.; Sundermeyer, J.; Kohn, U.; Coles, M. P.; Leito, I., Experimental Basicities of Phosphazene, Guanidinophosphazene, and Proton Sponge Superbases in the Gas Phase and Solution. *J. Phys. Chem. A* **2016**, *120* (16), 2591-2604.
13. Singh, A.; Ojha, A. K.; Jang, H. M., Strategic Design and Utilization of Molecular Flexibility for Straddling the Application of Organic Superbases using DFT Study. *ChemistrySelect* **2018**, *3* (2), 837-842.
14. Tandarić, T.; Vianello, R., Design of Exceptionally Strong Organic Superbases Based on Aromatic Pnictogen Oxides: Computational DFT Analysis of the Oxygen Basicity in the Gas Phase and Acetonitrile Solution. *J. Phys. Chem. A* **2018**, *122* (5), 1464-1471.
15. Shaffer, K. J.; Parr, D. C.; Wenzel, M.; Rowlands, G. J.; Plieger, P. G., The Proton Sponge Effect: Substitution of Quino[7,8-*h*]quinoline and the First Structurally Characterised Derivatives. *Eur. J. Org. Chem.* **2012**, (35), 6967-6975.
16. Valadbeigi, Y., Proton sponges and superbases with nitrogen, phosphorus, arsenic, oxygen, sulfur, and selenium as proton acceptor sites. *Chem. Phys. Lett.* **2020**, *754*, 137764.
17. Kovacevic, B.; Maksic, Z. B., The proton affinity of the superbase 1,8-bis(tetramethylguanidino)naphthalene (TMGN) and some related compounds: a theoretical study. *Chem. - Eur. J.* **2002**, *8* (7), 1694-1702.
18. Raab, V.; Gauchenova, E.; Merkoulov, A.; Harms, K.; Sundermeyer, J.; Kovacevic, B.; Maksic, Z. B., 1,8-Bis(hexamethyltriaminophosphazenylnaphthalene, HMPN: A

- Superbasic Bisphosphazene "Proton Sponge". *J. Am. Chem. Soc.* **2005**, *127* (45), 15738-15743.
19. McConnell, A. J.; Wood, C. S.; Neelakandan, P. P.; Nitschke, J. R., Stimuli-Responsive Metal-Ligand Assemblies. *Chem. Rev.* **2015**, *115* (15), 7729-7793.
  20. Mobian, P.; Kern, J.-M.; Sauvage, J.-P., Light-driven machine prototypes based on dissociative excited states: Photoinduced decoordination and thermal recoordination of a ring in a ruthenium(II)-containing [2]catenane. *Angew. Chem., Int. Ed.* **2004**, *43* (18), 2392-2395.
  21. Tan, C.; Chu, D.; Tang, X.; Liu, Y.; Xuan, W.; Cui, Y., Supramolecular Coordination Cages for Asymmetric Catalysis. *Chem. - Eur. J.* **2019**, *25* (3), 662-672.
  22. Zhao, L.; Jing, X.; Li, X.; Guo, X.; Zeng, L.; He, C.; Duan, C., Catalytic properties of chemical transformation within the confined pockets of Werner-type capsules. *Coord. Chem. Rev.* **2019**, *378*, 151-187.
  23. Zhu, Y.; Rebek Jr, J.; Yu, Y., Cyclizations catalyzed inside a hexameric resorcinarene capsule. *Chem. Commun.* **2019**, *55* (25), 3573-3577.
  24. Sinha, I.; Mukherjee, P. S., Chemical Transformations in Confined Space of Coordination Architectures. *Inorg. Chem.* **2018**, *57* (8), 4205-4221.
  25. Zhang, D.; Ronson, T. K.; Nitschke, J. R., Functional Capsules via Subcomponent Self-Assembly. *Acc. Chem. Res.* **2018**, *51* (10), 2423-2436.
  26. Gao, W.-X.; Zhang, H.-N.; Jin, G.-X., Supramolecular catalysis based on discrete heterometallic coordination-driven metallacycles and metallacages. *Coord. Chem. Rev.* **2019**, *386*, 69-84.
  27. Jongkind, L. J.; Caumes, X.; Hartendorp, A. P. T.; Reek, J. N. H., Ligand Template Strategies for Catalyst Encapsulation. *Acc. Chem. Res.* **2018**, *51* (9), 2115-2128.
  28. Jans, A. C. H.; Caumes, X.; Reek, J. N. H., Gold Catalysis in (Supra)Molecular Cages to Control Reactivity and Selectivity. *ChemCatChem* **2019**, *11* (1), 287-297.
  29. Fang, Y.; Powell, J. A.; Li, E.; Wang, Q.; Perry, Z.; Kirchon, A.; Yang, X.; Xiao, Z.; Zhu, C.; Zhang, L.; Huang, F.; Zhou, H.-C., Catalytic reactions within the cavity of coordination cages. *Chem. Soc. Rev.* **2019**, *48* (17), 4707-4730.
  30. Pluth, M. D.; Bergman, R. G.; Raymond, K. N., Proton-Mediated Chemistry and Catalysis in a Self-Assembled Supramolecular Host. *Acc. Chem. Res.* **2009**, *42* (10), 1650-1659.
  31. Brown, C. J.; Toste, F. D.; Bergman, R. G.; Raymond, K. N., Supramolecular Catalysis in Metal-Ligand Cluster Hosts. *Chem. Rev.* **2015**, *115* (9), 3012-3035.
  32. Breiner, B.; Clegg, J. K.; Nitschke, J. R., Reactivity modulation in container molecules. *Chem. Sci.* **2011**, *2* (1), 51-56.
  33. Brock, A. J.; Al-Fayaad, H.; Pfrunder, M. C.; Clegg, J. K., In *Functional supramolecular materials: from surfaces to MOFs*, Royal Society of Chemistry: Cambridge, U.K., 2017; Vol. 22, pp 325-387.
  34. Yoshizawa, M.; Kusukawa, T.; Fujita, M.; Yamaguchi, K., Ship-in-a-Bottle Synthesis of Otherwise Labile Cyclic Trimers of Siloxanes in a Self-Assembled Coordination Cage. *J. Am. Chem. Soc.* **2000**, *122* (26), 6311-6312.
  35. Yi, J. W.; Barry, N. P. E.; Furrer, M. A.; Zava, O.; Dyson, P. J.; Therrien, B.; Kim, B. H., Delivery of Floxuridine derivatives to cancer cells by water-soluble organometallic cages. *Bioconjugate Chem.* **2012**, *23* (3), 461-471.
  36. Jiao, J.; Li, Z.; Qiao, Z.; Li, X.; Liu, Y.; Dong, J.; Jiang, J.; Cui, Y., Design and self-assembly of hexahedral coordination cages for cascade reactions. *Nat. Commun.* **2018**, *9* (1), 1-8.
  37. Severinsen, R. J.; Rowlands, G. J.; Plieger, P. G., Coordination cages in catalysis. *J. Inclusion Phenom. Macrocyclic Chem.* **2020**, *96* (1-2), 29-42.

38. Yamasaki, T.; Ozaki, N.; Saika, Y.; Ohta, K.; Goboh, K.; Nakamura, F.; Hashimoto, M.; Okeya, S., First transition metal complex of 1,8-bis(dimethylamino)naphthalene (proton sponge). *Chem. Lett.* **2004**, *33* (7), 928-929.
39. Scifinder search performed April 2021. Refined by Research Topic: proton sponge (as entered). Duplicates removed. Filtered by Document Type (excl. Patent and Conference). Get Substances> Filtered by: Metal Containing, C atom containing. 1531 results. Possible proton sponge complexes selected. Get References>Filtered by 'proton sponge', Manual result sorting. <40 possible publications.
40. Koegel, J. F.; Xie, X.; Baal, E.; Gesevicius, D.; Oelkers, B.; Kovacevic, B.; Sundermeyer, J., Superbasic Alkyl-Substituted Bisphosphazene Proton Sponges: Synthesis, Structural Features, Thermodynamic and Kinetic Basicity, Nucleophilicity and Coordination Chemistry. *Chem. - Eur. J.* **2014**, *20* (25), 7670-7685.
41. Shaffer, K. J.; McLean, T. M.; Waterland, M. R.; Wenzel, M.; Plieger, P. G., Structural characterisation of difluoro-boron chelates of quino[7,8-*h*]quinoline. *Inorg. Chim. Acta.* **2012**, *380*, 278-283.
42. Zirnstein, M. A.; Staab, H. A., Quino[7,8-*h*]quinoline, a New Type of "Proton Sponge". *Angew. Chem. Int. Ed. Engl.* **1987**, *26* (5), 460-461.
43. Shaffer, K. J.; Davidson, R. J.; Burrell, A. K.; McCleskey, T. M.; Plieger, P. G., Encapsulation of the Be<sup>II</sup> Cation: Spectroscopic and Computational Study. *Inorg. Chem.* **2013**, *52* (7), 3969-3975.
44. Davalos, J. Z.; Lago, A. F.; Costa, J. C. S.; Santos, L. M. N. B. F.; Gonzalez, J., Thermochemical and structural properties of DMAN-"proton sponges". *J. Chem. Thermodyn.* **2012**, *54*, 346-351.
45. Krieger, C.; Newsom, I.; Zirnstein, M. A.; Staab, H. A., Structures of Quino[7,8-*h*]quinoline and Quino[8,7-*h*]quinoline. *Angew. Chem. Int. Ed. Engl.* **1989**, *28* (1), 84-86.
46. Honda, K.; Nakanishi, H.; Yabe, A., Reaction of 1,8-naphthalenediamine with dimethyl and diethyl acetylenedicarboxylates. *Bull. Chem. Soc. Jpn.* **1983**, *56* (8), 2338-2340.
47. Saupe, T.; Krieger, C.; Staab, H. A., 4,5-Bis(dimethylamino)phenanthrene and 4,5-Bis(dimethylamino)-9,10-dihydrophenanthrene: Syntheses and "Proton Sponge" Properties. *Angew. Chem. Int. Ed. Engl.* **1986**, *25* (5), 451-453.
48. Ginsburg, D., Syntheses of Heterocyclic Amines. In *Concerning Amines*, Ginsburg, D., Ed. Pergamon Press Ltd: Oxford, U.K., 1967; pp 170-174.
49. Iwai, I.; Hara, S., Polarization of aromatic heterocyclic compounds. LXXXIV. Nitration of benzo[*h*]quinoline. *Yakugaku Zasshi* **1950**, *70*, 394-400.
50. Nakayama, I., Polarization of Heterocyclic Compounds. XCIII Replacement Reactions of Carbon Radicals in the Gamma-Position of Quinoline Nucleus. *Yakugaku Zasshi* **1951**, *71* (12), 1391-1393.
51. Dufour, M.; Buu-Hoi, N. P.; Jacquignon, P., Carcinogenic nitrogen compounds. LVIII. Double Skraup reaction to diaza derivatives of some carcinogenic hydrocarbons. *J. Chem. Soc. C* **1967**, (15), 1415-1416.
52. Edel, A.; Marnot, P. A.; Sauvage, J. P., Unexpected synthesis of 2-methyl-1,3-diazapyrene from 1,8-diaminonaphthalene. *Tet. Lett.* **1985**, *26* (6), 727-728.
53. Baddar, F. G.; Warren, F. L., 80. Benzanthrones. Part I. The mechanism of Bally's reaction. *J. Chem. Soc.* **1938**, (0), 401-404.
54. Shaffer, K. Towards Selective Small Cation Chelation. PhD Dissertation, Massey University, 2010.
55. Zewge, D.; Chen, C.-y.; Deer, C.; Dormer, P. G.; Hughes, D. L., A Mild and Efficient Synthesis of 4-Quinolones and Quinolone Heterocycles. *J. Org. Chem.* **2007**, *72* (11), 4276-4279.

56. Wüstefeld, H.-U.; Kaska, W. C.; Schüth, F.; Stucky, G. D.; Bu, X.; Krebs, B., Transition Metal Complexes with the Proton Sponge 4,9-Dichloroquino[7,8-*h*]quinoline: Highly Twisted Aromatic Systems and an Extreme “Out-of-Plane” Position of the Coordinated Transition Metal Atom. *Angew. Chem. Int. Ed.* **2001**, *40* (17), 3182-3184.
57. Strauss, C. R.; Trainor, R. W., Reactions of ethyl indole-2-carboxylate in aqueous media at high temperature. *Aust. J. Chem.* **1998**, *51* (8), 703-705.
58. Shaffer, K. J.; Wenzel, M.; Plieger, P. G., The first structurally characterised copper(II) complexes of quino[7,8-*h*]quinoline ligands. *Polyhedron* **2013**, *52*, 1399-1402.
59. Pozharskii, A. F.; Ozeryanskii, V. A.; Mikshiev, V. Y.; Chernyshev, A. V.; Metelitsa, A. V.; Antonov, A. S., Proton-induced fluorescence in modified quino[7,8-*h*]quinolines: dual sensing for protons and  $\pi$ -donors. *Org. Biomol. Chem.* **2019**, *17* (35), 8221-8233.
60. Favre, H. A.; Powell, W. H., *Nomenclature of Organic Chemistry: IUPAC Recommendations and Preferred Names 2013*. Royal Society of Chemistry: Cambridge, U.K., 2013.
61. Rasmussen, S. C., The nomenclature of fused-ring arenes and heterocycles: a guide to an increasingly important dialect of organic chemistry. *ChemTexts* **2016**, *2* (4), 1-13.
62. Moss, G. P., Nomenclature of fused and bridged fused ring systems. *Pure Appl. Chem.* **1998**, *70* (1), 143-216.
63. Definitive Rules for Nomenclature of Organic Chemistry. *J. Am. Chem. Soc.* **1960**, *82* (21), 5545-5574.
64. Weyesa, A.; Mulugeta, E., Recent advances in the synthesis of biologically and pharmaceutically active quinoline and its analogues: a review. *RSC Adv.* **2020**, *10* (35), 20784-20793.
65. Jain, S.; Chandra, V.; Kumar Jain, P.; Pathak, K.; Pathak, D.; Vaidya, A., Comprehensive review on current developments of quinoline-based anticancer agents. *Arab. J. Chem.* **2019**, *12* (8), 4920-4946.
66. Qiu, Y.; Tang, J.; Li, Y.; Fan, H.; Duan, L.; Ren, X. Preparation of quinolino[7,8-*h*]quinoline compds. and their application as OLED. CN103664937A, 2014.
67. Panda, K.; Siddiqui, I.; Mahata, P. K.; Ila, H.; Junjappa, H., Heteroannulation of 3-bis(methylthio)acrolein with aromatic amines - a convenient highly regioselective synthesis of 2-(methylthio)quinolines and their benzo/hetero fused analogs - a modified skraup quinoline synthesis. *Synlett* **2004**, (3), 449-452.
68. Pawar, V. G.; Sos, M. L.; Rode, H. B.; Rabiller, M.; Heynck, S.; van Otterlo, W. A. L.; Thomas, R. K.; Rauh, D., Synthesis and biological evaluation of 4-anilinoquinolines as potent inhibitors of epidermal growth factor receptor. *J. Med. Chem.* **2010**, *53* (7), 2892-2901.
69. Scifinder search performed April 2021. Quinoline substructure searches performed with the 'any atom except H' variable at the 2, 3, 4, 5 and 6 carbon ring positions respectively. Refined by excluding metal-containing structures.
70. Boersma, C.; Bauschlicher, C. W., Jr.; Ricca, A.; Mattioda, A. L.; Peeters, E.; Tielens, A. G. G. M.; Allamandola, L. J., Polycyclic aromatic hydrocarbon far-infrared spectroscopy. *Astrophys. J.* **2011**, *729* (1, Pt. 1), 64.
71. Aihara, J., Kinetic instability of azafullerenes. *J. Mol. Struct.: THEOCHEM* **2000**, *532*, 95-102.
72. Peran, N.; Maksic, Z. B., Polycyclic croissant-like organic compounds are powerful superbases in the gas phase and acetonitrile - a DFT study. *Chem. Commun.* **2011**, *47* (4), 1327-1329.
73. Buu-Hoi, N. P.; Dufour, M.; Jacquignon, P., Carcinogenic nitrogen compounds. LXI. Skraup reactions with diamines derived from acenaphthene and anthracene. *J. Chem. Soc. C* **1968**, (16), 2070-2072.

74. Gamage, S. N.; Morris, R. H.; Rettig, S. J.; Thackray, D. C.; Thorburn, I. S.; James, B. R., Formation of a trimethyldihydroperimidinium cation from proton sponge [1,8-bis(dimethylamino)naphthalene] during base-promoted reactions of rhodium and ruthenium complexes. *J. Chem. Soc., Chem. Commun.* **1987**, (12), 894-895.
75. Wild, U.; Hubner, O.; Maronna, A.; Enders, M.; Kaifer, E.; Wadepohl, H.; Himmel, H.-J., The first metal complexes of the proton sponge 1,8-bis(*N,N,N',N'*-tetramethylguanidino)naphthalene: syntheses and properties. *Eur. J. Inorg. Chem.* **2008**, (28), 4440-4447.
76. Bucher, G., DFT Calculations on a New Class of C<sub>3</sub>-Symmetric Organic Bases: Highly Basic Proton Sponges and Ligands for Very Small Metal Cations. *Angew. Chem. Int. Ed.* **2003**, 42 (34), 4039-4042.
77. Bachrach, S. M.; Wilbanks, C. C., Using the Pyridine and Quinuclidine Scaffolds for Superbases: A DFT Study. *J. Org. Chem.* **2010**, 75 (8), 2651-2660.
78. Horbatenko, Y.; Vyboishchikov, S. F., Hydrogen Motion in Proton Sponge Cations: A Theoretical Study. *ChemPhysChem* **2011**, 12 (6), 1118-1129.
79. Shibata, K. Organic white electroluminescent devices. JP2010135689A, 2010.
80. Stoessel, P.; Mayer, H.; Kaska, W. C. Coordination compounds for organic electronic devices and devices using them. WO2011116857A1, 2011.
81. Kurata, T.; Ishidai, K. Electrolyte composition containing condensed aromatic amines for secondary battery and secondary battery using same. JP2012014973A, 2012.
82. Mueller, M.; Buchner, M. R., Beryllium Complexes with Bio-Relevant Functional Groups: Coordination Geometries and Binding Affinities. *Angew. Chem., Int. Ed.* **2018**, 57 (29), 9180-9184.
83. Janka, O.; Poettgen, R., The role of beryllium in alloys, Zintl phases and intermetallic compounds. *Z. Naturforsch., B: J. Chem. Sci.* **2020**, 75 (5), 421-439.
84. Kumberger, O.; Schmidbaur, H., Why is beryllium that toxic? Contributions of coordination chemistry to the clarification of molecular effects induced by the element. *Chem. Unserer Zeit* **1993**, 27 (6), 310-316.
85. Nixon, D. J.; Perera, L. C.; Dais, T. N.; Brothers, P. J.; Henderson, W.; Plieger, P. G., Tuning receptors for the encapsulation of beryllium<sup>2+</sup>. *Phys. Chem. Chem. Phys.* **2019**, 21 (35), 19660-19666.
86. Taylor, T. P.; Ding, M.; Ehler, D. S.; Foreman, T. M.; Kaszuba, J. P.; Sauer, N. N., Beryllium in the Environment: A Review. *J. Environ. Sci. Heal. A.* **2003**, 38 (2), 439-469.
87. Buchner, M. R., Beryllium-associated diseases from a chemist's point of view. *Z. Naturforsch., B: J. Chem. Sci.* **2020**, 75 (5), 405-412.
88. Emsley, J., *Nature's Building Blocks: An A-Z Guide to the Elements*. Oxford University Press Inc.: New York, USA, 2003; p 538.
89. Molnar, A., Efficient, Selective, and Recyclable Palladium Catalysts in Carbon-Carbon Coupling Reactions. *Chem. Rev.* **2011**, 111 (3), 2251-2320.
90. Miyaura, N.; Suzuki, A., Stereoselective synthesis of arylated (E)-alkenes by the reaction of alk-1-enylboranes with aryl halides in the presence of palladium catalyst. *J. Chem. Soc., Chem. Commun.* **1979**, (19), 866-867.
91. Kurti, L.; Czako, B., *Strategic Applications of Named Reactions in Organic Synthesis*. Elsevier Science: Cambridge, MA, USA, 2005; p 864.
92. Lennox, A. J. J.; Lloyd-Jones, G. C., Selection of boron reagents for Suzuki-Miyaura coupling. *Chem. Soc. Rev.* **2014**, 43 (1), 412-443.
93. Tan, P. W.; Haughey, M.; Dixon, D. J., Palladium(II)-catalysed ortho-arylation of N-benzylpiperidines. *Chem. Commun.* **2015**, 51 (21), 4406-4409.
94. Li, Y.-J.; Sasabe, H.; Su, S.-J.; Tanaka, D.; Takeda, T.; Pu, Y.-J.; Kido, J., Highly Efficient Green Phosphorescent OLED Based on Pyridine-containing Starburst Electron-transporting Materials. *Chem. Lett.* **2010**, 39 (2), 140-141.

95. Lima, C. F. R. A. C.; Rodrigues, A. S. M. C.; Silva, V. L. M.; Silva, A. M. S.; Santos, L. M. N. B. F., Role of the Base and Control of Selectivity in the Suzuki–Miyaura Cross-Coupling Reaction. *ChemCatChem* **2014**, *6* (5), 1291-1302.
96. Macrae, C. F.; Bruno, I. J.; Chisholm, J. A.; Edgington, P. R.; McCabe, P.; Pidcock, E.; Rodriguez-Monge, L.; Taylor, R.; van de Streek, J.; Wood, P. A., Mercury CSD 2.0 - new features for the visualization and investigation of crystal structures. *J. Appl. Crystallogr.* **2008**, *41* (2), 466-470.
97. Stille, J. K.; Lau, K. S. Y., Mechanisms of oxidative addition of organic halides to Group 8 transition-metal complexes. *Acc. Chem. Res.* **1977**, *10* (12), 434-442.
98. Zhang, W.; Li, Z.; Zhou, M.; Wu, F.; Hou, X.; Luo, H.; Liu, H.; Han, X.; Yan, G.; Ding, Z.; Li, R., Synthesis and biological evaluation of 4-(1,2,3-triazol-1-yl)coumarin derivatives as potential antitumor agents. *Bioorg. Med. Chem. Lett.* **2014**, *24* (3), 799-807.
99. Gschneidner, T. A.; Moth-Poulsen, K., A photolabile protection strategy for terminal alkynes. *Tet. Lett.* **2013**, *54* (40), 5426-5429.
100. Ohkubo, M.; Mochizuki, S.; Sano, T.; Kawaguchi, Y.; Okamoto, S., Selective Cleavage of Allyl and Propargyl Ethers to Alcohols Catalyzed by Ti(O-*i*-Pr)<sub>4</sub>/MX<sub>n</sub>/Mg. *Org. Lett.* **2007**, *9* (5), 773-776.
101. Preston, D.; Lewis, J. E. M.; Crowley, J. D., Multicavity [Pd<sub>n</sub>L<sub>4</sub>]<sup>2n+</sup> Cages with Controlled Segregated Binding of Different Guests. *J. Am. Chem. Soc.* **2017**, *139* (6), 2379-2386.
102. Domyati, D.; Latifi, R.; Tahsini, L., Sonogashira-type cross-coupling reactions catalyzed by copper complexes of pincer N-heterocyclic carbenes. *J. Organomet. Chem.* **2018**, *860*, 98-105.
103. Bissemer, A. C.; Banwell, M. G., Microwave-Assisted Trans-Halogenation Reactions of Various Chloro-, Bromo-, Trifluoromethanesulfonyloxy- and Nonfluorobutanesulfonyloxy-Substituted Quinolines, Isoquinolines, and Pyridines Leading to the Corresponding Iodinated Heterocycles. *J. Org. Chem.* **2009**, *74* (13), 4893-4895.
104. Cheruku, S. R.; Maiti, S.; Dorn, A.; Scorneaux, B.; Bhattacharjee, A. K.; Ellis, W. Y.; Vennerstrom, J. L., Carbon Isosteres of the 4-Aminopyridine Substructure of Chloroquine: Effects on pK<sub>a</sub>, Hematin Binding, Inhibition of Hemozoin Formation, and Parasite Growth. *J. Med. Chem.* **2003**, *46* (14), 3166-3169.
105. Su, T.; Zhu, J.; Sun, R.; Zhang, H.; Huang, Q.; Zhang, X.; Du, R.; Qiu, L.; Cao, R., Design, synthesis and biological evaluation of new quinoline derivatives as potential antitumor agents. *Eur. J. Med. Chem.* **2019**, *178*, 154-167.
106. Nixon, D. Catch <sup>94</sup>Be If You Can: Exploiting Second-Sphere Hydrogen Bonding Toward Chelation of Beryllium. Massey University, Manawatu, New Zealand, 2019.
107. Buchner, M. R.; Mueller, M.; Raymond, O.; Severinsen, R. J.; Nixon, D. J.; Henderson, W.; Brothers, P. J.; Rowlands, G. J.; Plieger, P. G., Synthesis of a Boronic Acid Anhydride Based Ligand and Its Application in Beryllium Coordination. *Eur. J. Inorg. Chem.* **2019**, *2019* (34), 3863-3868.
108. Li, K.; Zhang, L.-Y.; Yan, C.; Wei, S.-C.; Pan, M.; Zhang, L.; Su, C.-Y., Stepwise Assembly of Pd<sub>6</sub>(RuL<sub>3</sub>)<sub>6</sub> Nanoscale Rhombododecahedral Metal–Organic Cages via Metalloligand Strategy for Guest Trapping and Protection. *J. Am. Chem. Soc.* **2014**, *136* (12), 4456-4459.
109. Cozzi, P. G., Metal–Salen Schiff base complexes in catalysis: practical aspects. *Chem. Soc. Rev.* **2004**, *33* (7), 410-421.
110. Woodhouse, S. S.; Dais, T. N.; Payne, E. H.; Singh, M. K.; Brechin, E. K.; Plieger, P. G., The structural manipulation of a series of Ni<sub>4</sub> defective dicubanes: Synthesis, X-ray Structures, Magnetic and Computational analyses. *Dalton Trans.* **2021**, *50* (15), 5318-5326.



111. Milios, C. J.; Piligkos, S.; Brechin, E. K., Ground state spin-switching via targeted structural distortion: twisted single-molecule magnets from derivatised salicylaldoximes. *Dalton Trans.* **2008**, (14), 1809-1817.
112. Mason, K.; Chang, J.; Garlatti, E.; Prescimone, A.; Yoshii, S.; Nojiri, H.; Schnack, J.; Tasker, P. A.; Carretta, S.; Brechin, E. K., Linking [FeIII<sub>3</sub>] triangles with "double-headed" phenolic oximes. *Chem. Commun.* **2011**, 47 (21), 6018-6020.
113. McMorran, D. A.; Steel, P. J., New U-shaped Components for Metallosupramolecular Assemblies: Synthesis and Coordination Chemistry of 2,6-bis(4-(3-pyridyloxy)phenoxy)pyrazine. *Supramol. Chem.* **2002**, 14 (1), 79-85.
114. Frischmann, P. D.; Guieu, S.; Tabeshi, R.; MacLachlan, M. J., Columnar Organization of Head-to-Tail Self-Assembled Pt<sub>4</sub> Rings. *J. Am. Chem. Soc.* **2010**, 132 (22), 7668-7675.
115. Patterson, J. B.; Lonergan, D. G. Aromatic aldehyde derivatives as IRE-1 $\alpha$  inhibitors and their preparation and use in the treatment of diseases. WO2008154484A1, 2008.
116. Meier, P.; Broghammer, F.; Latendorf, K.; Rauhut, G.; Peters, R., Cooperative Al(salen)-pyridinium catalysts for the asymmetric synthesis of trans-configured  $\beta$ -lactones by [2+2]-cyclocondensation of acyl bromides and aldehydes: investigation of pyridinium substituent effects. *Molecules* **2012**, 17, 7121-7150.
117. Raju, B. C.; Tiwari, A. K.; Kumar, J. A.; Ali, A. Z.; Agawane, S. B.; Saidachary, G.; Madhusudana, K.,  $\alpha$ -Glucosidase inhibitory antihyperglycemic activity of substituted chromenone derivatives. *Bioorg. Med. Chem.* **2010**, 18 (1), 358-365.
118. Wang, Q.; Chen, Q.; Li, C.; Lai, Q.; Zou, F.; Liang, F.; Jiang, G.; Wang, J., Discrimination of Pd<sup>0</sup> and Pd<sup>2+</sup> in solution and in live cells by novel light-up fluorescent probe with AIE and ESIPT characteristics. *Microchem. J.* **2020**, 153, 104503.
119. Sheldrick, G., *SHELX-97, Programs for Crystal Structure Analysis*,. University of Göttingen, Germany, 1998.
120. Kishi, N.; Li, Z.; Yoza, K.; Akita, M.; Yoshizawa, M., An M<sub>2</sub>L<sub>4</sub> Molecular Capsule with an Anthracene Shell: Encapsulation of Large Guests up to 1 nm. *J. Am. Chem. Soc.* **2011**, 133 (30), 11438-11441.
121. Caubere, P., Unimetal super bases. *Chem. Rev.* **1993**, 93 (6), 2317-2334.
122. Tshepelevitsh, S.; Kütt, A.; Lökov, M.; Kaljurand, I.; Saame, J.; Heering, A.; Plieger, P. G.; Vianello, R.; Leito, I., On the Basicity of Organic Bases in Different Media. *Eur. J. Org. Chem.* **2019**, (40), 6735-6748.
123. Togasaki, K.; Arai, T.; Nishimura, Y., Effect of Moderate Hydrogen Bonding on Tautomer Formation via Excited-State Intermolecular Proton-Transfer Reactions in an Aromatic Urea Compound with a Steric Base. *J. Phys. Chem. A* **2020**, 124 (33), 6617-6628.
124. Raab, V.; Kipke, J.; Gschwind, R. M.; Sundermeyer, J., 1,8-bis(tetramethylguanidino)naphthalene (TMGN): a new, superbasic and kinetically active "proton sponge". *Chem. - Eur. J.* **2002**, 8 (7), 1682-1693.
125. Clayden, J.; Greeves, N.; Warren, S. G., *Organic Chemistry*. 2nd ed.; Oxford University Press: New York, 2012.
126. Carey, F. A.; Giuliano, R. M., *Organic Chemistry*. McGraw-Hill: New York, 2011.
127. Remya, G. S.; Suresh, C. H., Quantification and classification of substituent effects in organic chemistry: a theoretical molecular electrostatic potential study. *Phys. Chem. Chem. Phys.* **2016**, 18 (30), 20615-20626.
128. Foresman, J.; Frisch, A., *Exploring Chemistry With Electronic Structure Methods, 3rd edition*. Gaussian: Wallingford, CT, 2015.
129. M. J. Frisch, G. W. T., H. B. Schlegel, G. E. Scuseria, M. A. Robb, J. R. Cheeseman, G. Scalmani, V. Barone, G. A. Petersson, H. Nakatsuji, X. Li, M. Caricato, A. Marenich, J. Bloino, B. G. Janesko, R. Gomperts, B. Mennucci, H. P. Hratchian, J. V. Ortiz, A. F. Izmaylov, J. L. Sonnenberg, D. Williams-Young, F. Ding, F. Lipparini, F. Egidi, J. Goings, B. Peng, A. Petrone, T. Henderson, D. Ranasinghe, V. G. Zakrzewski, J. Gao, N. Rega, G.

- Zheng, W. Liang, M. Hada, M. Ehara, K. Toyota, R. Fukuda, J. Hasegawa, M. Ishida, T. Nakajima, Y. Honda, O. Kitao, H. Nakai, T. Vreven, K. Throssell, J. A. Montgomery, Jr., J. E. Peralta, F. Ogliaro, M. Bearpark, J. J. Heyd, E. Brothers, K. N. Kudin, V. N. Staroverov, T. Keith, R. Kobayashi, J. Normand, K. Raghavachari, A. Rendell, J. C. Burant, S. S. Iyengar, J. Tomasi, M. Cossi, J. M. Millam, M. Klene, C. Adamo, R. Cammi, J. W. Ochterski, R. L. Martin, K. Morokuma, O. Farkas, J. B. Foresman, D. J. Fox *Gaussian 09*, ES64L-G09RevD.01; Gaussian, Inc.: Wallingford CT, 2016.
- 130.** Horak, E.; Babić, D.; Vianello, R.; Perin, N.; Hranjec, M.; Steinberg, I. M., Photophysical properties and immobilisation of fluorescent pH responsive aminated benzimidazo[1,2-*a*]quinoline-6-carbonitriles. *Spectrochim. Acta A.* **2020**, *227*, 117588.
- 131.** Macrae, C. F.; Edgington, P. R.; McCabe, P.; Pidcock, E.; Shields, G. P.; Taylor, R.; Towler, M.; van de Streek, J., Mercury: visualization and analysis of crystal structures. *J. Appl. Crystallogr.* **2006**, *39* (3), 453-457.
- 132.** IUPAC. Compendium of Chemical Technology. Compiled by McNaught, A. D.; Wilkinson, A. Blackwell Scientific Publications: Oxford, UK, 1997. Online version (2019-) created by S. J. Chalk. ISBN 0-9678550-9-8.
- 133.** Stoessel, P.; Mayer, H.; Kaska, W. C. Coordination compounds for organic electronic devices and devices using them. WO2011116857A1, 2011.
- 134.** Wüstefeld, H.-U.; Kaska, W. C.; Stucky, G. D.; Schueth, F.; Krebs, B. Transition metal complexes with proton sponges as ligands. WO2002059134A1, 2002.
- 135.** Naglav, D.; Buchner, M. R.; Bendt, G.; Kraus, F.; Schulz, S., Off the Beaten Track—A Hitchhiker's Guide to Beryllium Chemistry. *Angew. Chem. Int. Ed.* **2016**, *55* (36), 10562-10576.
- 136.** Mueller, M.; Pielhofer, F.; Buchner, M. R., A facile synthesis for BeCl<sub>2</sub>, BeBr<sub>2</sub> and BeI<sub>2</sub>. *Dalton Trans.* **2018**, *47* (36), 12506-12510.



## Appendices

### Appendix A – X-ray summary data for 4,9-di(pyridin-4-yl)quinolino[7,8-*h*]quinoline (Q4)

Table A-1: Crystal data and structure refinement for 4,9-di(pyridin-4-yl)quinolino[7,8-*h*]quinoline.

IDENTIFICATION CODE	4,9-DI(PYRIDIN-4-YL)QUINOLINO[7,8-H]QUINOLINE
EMPIRICAL FORMULA	C <sub>26</sub> H <sub>16</sub> N <sub>4</sub>
FORMULA WEIGHT	384.43
TEMPERATURE/K	163
CRYSTAL SYSTEM	orthorhombic
SPACE GROUP	Pbnb
A/Å	7.7745(4)
B/Å	14.5862(7)
C/Å	16.6756(12)
A/°	90
B/°	90
γ/°	90
VOLUME/Å <sup>3</sup>	1891.02(19)
Z	4
P <sub>calc</sub> G/CM <sup>3</sup>	1.350
M/MM <sup>-1</sup>	0.643
F(000)	800.0
CRYSTAL SIZE/MM <sup>3</sup>	0.15 × 0.1 × 0.05
RADIATION	CuKα (λ = 1.54187)
2θ RANGE FOR DATA COLLECTION/°	13.25 to 130.104
INDEX RANGES	-7 ≤ h ≤ 9, -17 ≤ k ≤ 15, -19 ≤ l ≤ 19
REFLECTIONS COLLECTED	12559
INDEPENDENT REFLECTIONS	1604 [R <sub>int</sub> = 0.0850, R <sub>sigma</sub> = 0.0873]
DATA/RESTRAINTS/PARAMETERS	1604/0/137
GOODNESS-OF-FIT ON F <sup>2</sup>	0.971
FINAL R INDEXES [I ≥ 2σ (I)]	R <sub>1</sub> = 0.0625, wR <sub>2</sub> = 0.1343
FINAL R INDEXES [ALL DATA]	R <sub>1</sub> = 0.1226, wR <sub>2</sub> = 0.1764
LARGEST DIFF. PEAK/HOLE / E Å <sup>-3</sup>	0.23/-0.29
EXPERIMENTAL:	

Single crystals of 4,9-dipyridylquino[7,8-*h*]quinoline were grown by slow evaporation of 4,9-di(pyridin-4-yl)quinolino[7,8-*h*]quinoline in a 1:1:1 solvent mixture of DCM, MeOH and CHCl<sub>3</sub>. A suitable crystal was selected and mounted in formalin on a Rigaku RAXIS conversion diffractometer. The crystal was kept at 163 K during data collection. Using Olex2 [1], the structure was solved with the Superflip [2] structure solution program using Charge Flipping and refined with the ShelXL [3] refinement package using Least

Squares minimisation. Hydrogen atoms were placed in calculated positions are allowed to ride on their attached atom.

1. Dolomanov, O.V., Bourhis, L.J., Gildea, R.J, Howard, J.A.K. & Puschmann, H. (2009), *J. Appl. Cryst.* 42, 339-341.
2. Palatinus, L. & Chapuis, G. (2007). *J. Appl. Cryst.*, 40, 786-790; Palatinus, L. & van der Lee, A. (2008). *J. Appl. Cryst.* 41, 975-984; Palatinus, L., Prathapa, S. J. & van Smaalen, S. (2012). *J. Appl. Cryst.* 45, 575-580.
3. Sheldrick, G.M. (2008). *Acta Cryst.* A64, 112-122.

**Table A-2: Bond Lengths for 4,9-di(pyridin-4-yl)quinolino[7,8-h]quinoline**

ATOM	ATOM	LENGTH/Å	ATOM	ATOM	LENGTH/Å
N1	C2	1.324(4)	C6	C16	1.430(3)
N1	C17	1.366(4)	C15	C16	1.403(5)
N2	C43	1.335(4)	C15	C17 <sup>1</sup>	1.445(4)
N2	C45	1.337(3)	C15	C17	1.445(4)
C2	C3	1.389(4)	C16	C6 <sup>1</sup>	1.430(3)
C3	C4	1.376(4)	C17	C18	1.432(4)
C4	C18	1.424(4)	C41	C42	1.403(4)
C4	C41	1.493(4)	C41	C46	1.379(4)
C5	C6	1.352(4)	C42	C43	1.372(4)
C5	C18	1.419(4)	C45	C46	1.394(4)

<sup>1</sup>-1/2-X,+Y,1/2-Z

**Table A-3: Bond Angles for 4,9-di(pyridin-4-yl)quinolino[7,8-h]quinoline**

ATOM	ATOM	ATOM	ANGLE/°	ATOM	ATOM	ATOM	ANGLE/°
C2	N1	C17	118.4(3)	C15	C16	C6 <sup>1</sup>	120.7(2)
C43	N2	C45	116.7(3)	N1	C17	C15	119.8(3)
N1	C2	C3	124.8(3)	N1	C17	C18	120.8(3)
C4	C3	C2	118.6(3)	C18	C17	C15	119.2(3)
C3	C4	C18	119.0(3)	C4	C18	C17	118.0(3)
C3	C4	C41	120.3(3)	C5	C18	C4	122.0(3)
C18	C4	C41	120.7(3)	C5	C18	C17	119.9(3)
C6	C5	C18	120.2(3)	C42	C41	C4	120.3(3)
C5	C6	C16	121.1(3)	C46	C41	C4	122.8(3)
C16	C15	C17 <sup>1</sup>	117.8(2)	C46	C41	C42	116.9(3)
C16	C15	C17	117.8(2)	C43	C42	C41	119.2(3)
C17 <sup>1</sup>	C15	C17	124.3(4)	N2	C43	C42	124.3(3)
C6	C16	C6 <sup>1</sup>	118.6(4)	N2	C45	C46	122.9(3)
C15	C16	C6	120.7(2)	C41	C46	C45	120.0(3)

<sup>1</sup>-1/2-X,+Y,1/2-Z

## Appendix B: – X-ray summary data for 9-methoxyquinolino[7,8-*h*]quinoline-4(1*H*)-one

Table B-1: Crystal data and structure refinement for 9-methoxyquinolino[7,8-*h*]quinoline-4(1*H*)-one.

IDENTIFICATION CODE	QQ-OME
EMPIRICAL FORMULA	C <sub>17</sub> H <sub>12</sub> N <sub>2</sub> O <sub>2</sub>
FORMULA WEIGHT	276.29
TEMPERATURE/K	100(2)
CRYSTAL SYSTEM	monoclinic
SPACE GROUP	P2 <sub>1</sub> /n
A/Å	7.1342(2)
B/Å	13.9472(4)
C/Å	12.5849(3)
A/°	90
B/°	101.454(2)
γ/°	90
VOLUME/Å <sup>3</sup>	1227.29(6)
Z	4
P <sub>calc</sub> G/CM <sup>3</sup>	1.495
M/MM <sup>-1</sup>	0.812
F(000)	576.0
CRYSTAL SIZE/MM <sup>3</sup>	? × ? × ?
RADIATION	CuKα (λ = 1.54178)
2θ RANGE FOR DATA COLLECTION/°	13.258 to 150.852
INDEX RANGES	-8 ≤ h ≤ 4, -17 ≤ k ≤ 17, -14 ≤ l ≤ 15
REFLECTIONS COLLECTED	17150
INDEPENDENT REFLECTIONS	2500 [R <sub>int</sub> = 0.0276, R <sub>sigma</sub> = 0.0130]
DATA/RESTRAINTS/PARAMETERS	2500/0/195
GOODNESS-OF-FIT ON F <sup>2</sup>	1.030
FINAL R INDEXES [I ≥ 2σ (I)]	R <sub>1</sub> = 0.0398, wR <sub>2</sub> = 0.1118
FINAL R INDEXES [ALL DATA]	R <sub>1</sub> = 0.0445, wR <sub>2</sub> = 0.1169
LARGEST DIFF. PEAK/HOLE / e Å <sup>-3</sup>	0.27/-0.24
<b>EXPERIMENTAL</b>	

Single crystals of C<sub>17</sub>H<sub>12</sub>N<sub>2</sub>O<sub>2</sub> [QQ-OME] were grown by recrystallisation in an unknown solvent\* [1]. A suitable crystal was selected and mounted then measured on a STOE STADIVARI diffractometer. The crystal was kept at 100(2) K during data collection. Using Olex2 [1], the structure was solved with the SHELXT 2014/5 [2] structure solution program using Unknown\* and refined with the SHELXL-2018/3 [3] refinement package using Unknown\* minimisation.

1. Dolomanov, O.V., Bourhis, L.J., Gildea, R.J., Howard, J.A.K. & Puschmann, H. (2009), J. Appl. Cryst. 42, 339-341.
2. SHELXT 2014/5 G. M Sheldrick., Göttingen, Germany, 2014.
3. SHELXL-2018/3, G. M Sheldrick Göttingen, Germany, 2018.

### Refinement model description

Number of restraints - 0, number of constraints - unknown.

Details:

1.a Aromatic/amide H refined with riding coordinates:

C1(H1), C2(H2), C10(H10), C11(H11), C12(H12), C13(H13), C15(H15), C16(H16)

1.b Idealised Me refined as rotating group:

C17(H00B,H00C,H00F)

**Table B-2: Bond Lengths for 9-methoxyquinolino[7,8-*h*]quinoline-4(1*H*)-one**

ATOM	ATOM	LENGTH/Å	ATOM	ATOM	LENGTH/Å
O1	C3	1.2485(15)	C5	C6	1.4411(15)
C1	C2	1.3590(17)	C6	C7	1.4509(15)
C1	N2	1.3535(15)	C6	C14	1.4174(15)
N1	C7	1.3729(15)	C7	C8	1.4145(15)
N1	C11	1.3210(15)	C9	C8	1.4228(16)
C2	C3	1.4440(16)	C9	C10	1.3798(16)
N2	C5	1.3751(15)	C8	C16	1.4284(16)
O2	C9	1.3468(14)	C10	C11	1.3988(16)
O2	C17	1.4365(14)	C12	C13	1.3609(16)
C4	C3	1.4717(15)	C13	C14	1.4227(15)
C4	C5	1.4022(15)	C14	C15	1.4313(15)
C4	C12	1.4201(16)	C15	C16	1.3571(16)

**Table B-3: Bond Angles for 9-methoxyquinolino[7,8-*h*]quinoline-4(1*H*)-one**

ATOM	ATOM	ATOM	ANGLE/°	ATOM	ATOM	ATOM	ANGLE/°
N2	C1	C2	123.19(11)	N1	C7	C8	121.74(10)
C11	N1	C7	117.73(10)	C8	C7	C6	119.22(10)
C1	C2	C3	120.24(11)	O2	C9	C8	115.55(10)
C1	N2	C5	121.40(10)	O2	C9	C10	125.09(10)
C9	O2	C17	116.98(9)	C10	C9	C8	119.36(10)
C5	C4	C3	121.36(10)	C7	C8	C9	118.11(10)
C5	C4	C12	119.38(10)	C7	C8	C16	120.63(10)
C12	C4	C3	119.27(10)	C9	C8	C16	121.26(10)
O1	C3	C2	123.53(11)	C9	C10	C11	117.88(10)
O1	C3	C4	121.47(11)	N1	C11	C10	125.16(10)
C2	C3	C4	115.00(10)	C13	C12	C4	120.88(11)
N2	C5	C4	118.73(10)	C12	C13	C14	120.64(10)
N2	C5	C6	120.26(10)	C6	C14	C13	120.75(10)
C4	C5	C6	121.01(10)	C6	C14	C15	120.22(10)
C5	C6	C7	124.17(10)	C13	C14	C15	119.03(10)
C14	C6	C5	117.33(10)	C16	C15	C14	121.31(10)
C14	C6	C7	118.50(10)	C15	C16	C8	120.12(10)
N1	C7	C6	119.04(10)				

## Appendix C: Selected Experimental NMR Characterisation

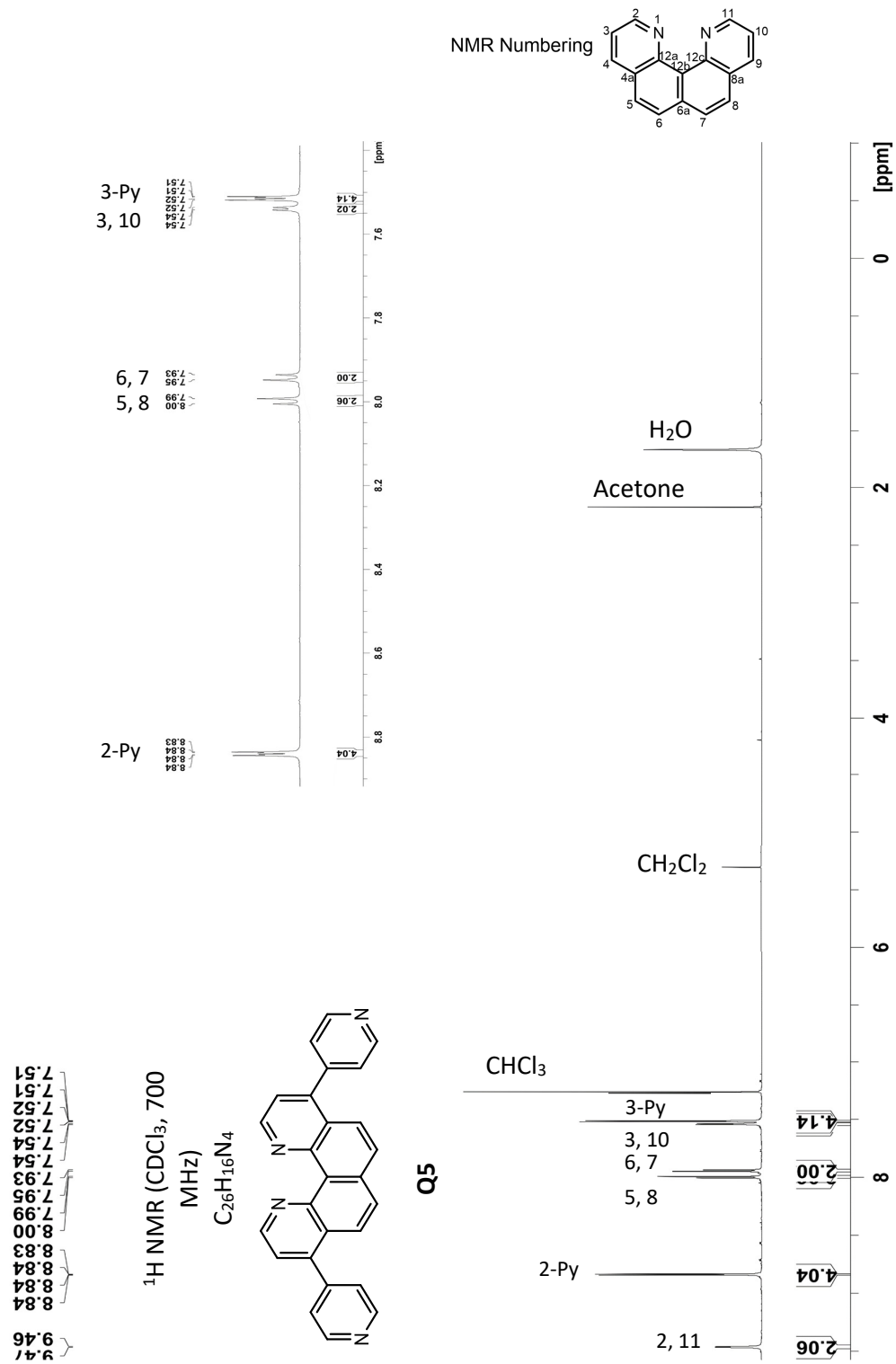


Figure C-1: <sup>1</sup>H NMR spectrum of 4,9-di(pyridin-4-yl)quinolino[7,8-*h*]quinoline (Q5)



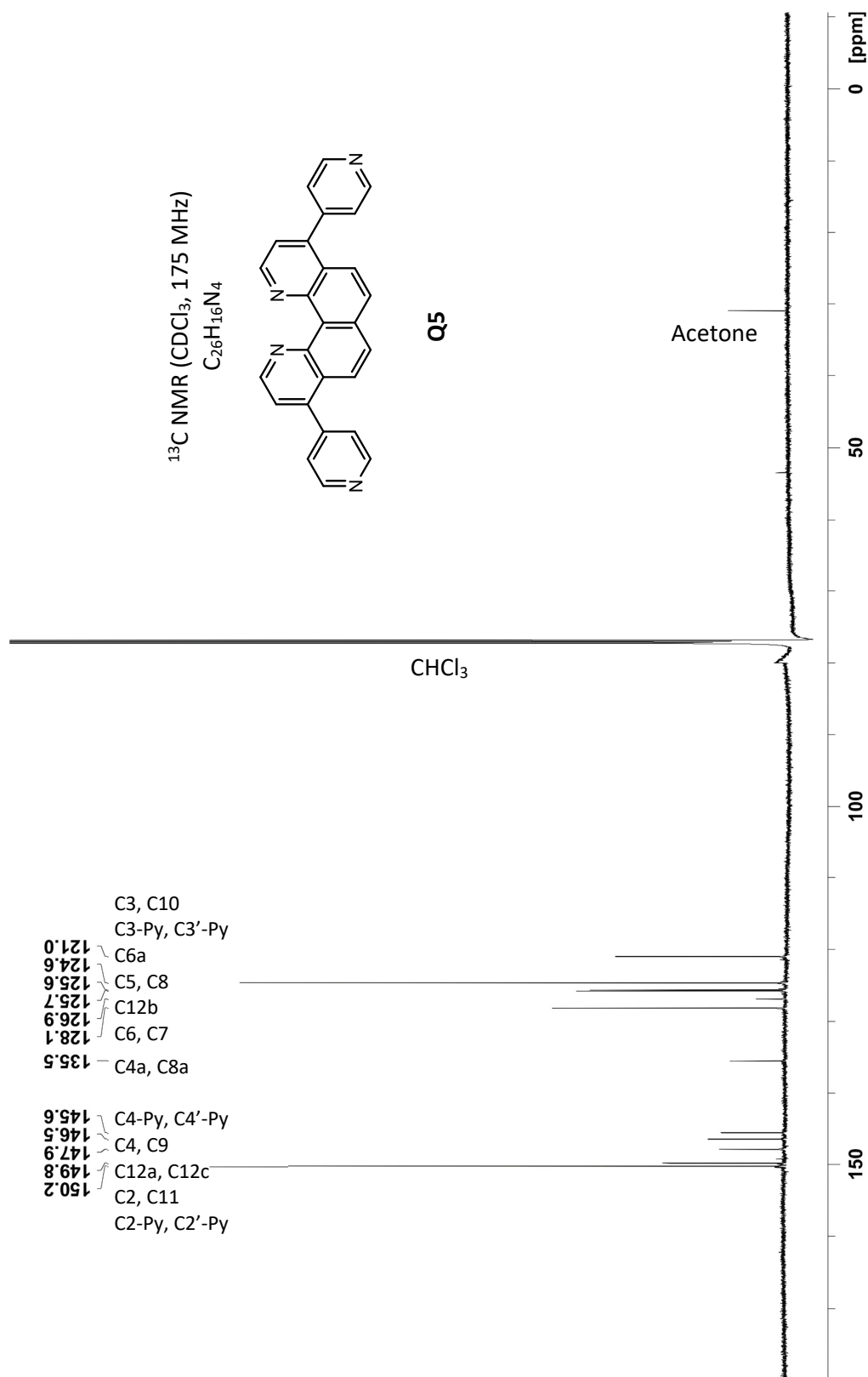


Figure C-2: <sup>13</sup>C NMR spectrum of 4,9-di(pyridin-4-yl)quinolino[7,8-h]quinoline (Q5)

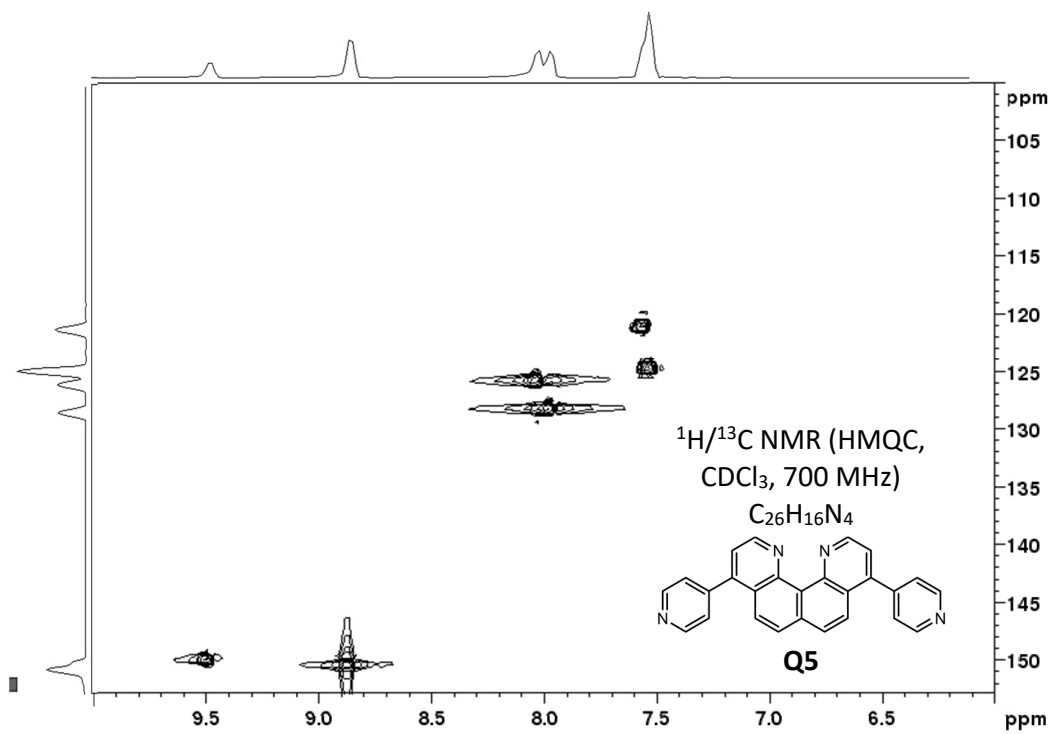
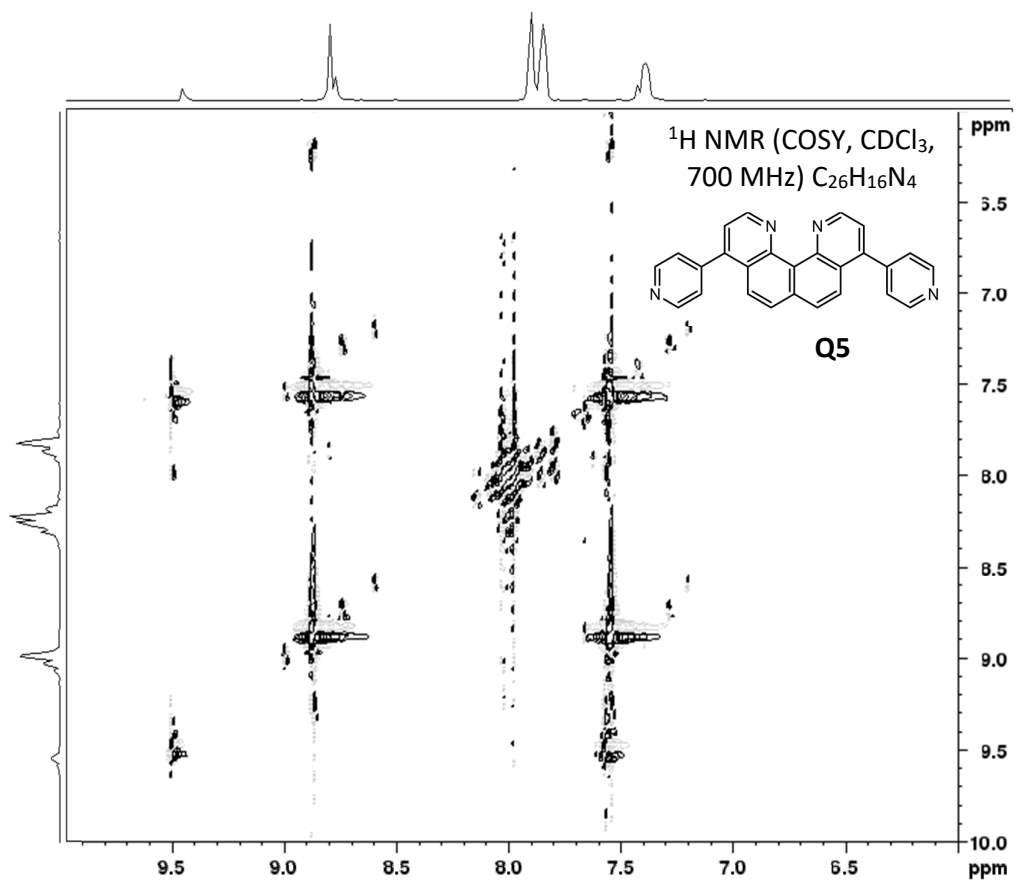


Figure C-3: COSY (top) and HMQC (lower) spectra of 4,9-di(pyridin-4-yl)quinolino[7,8-*h*]quinoline (Q5)

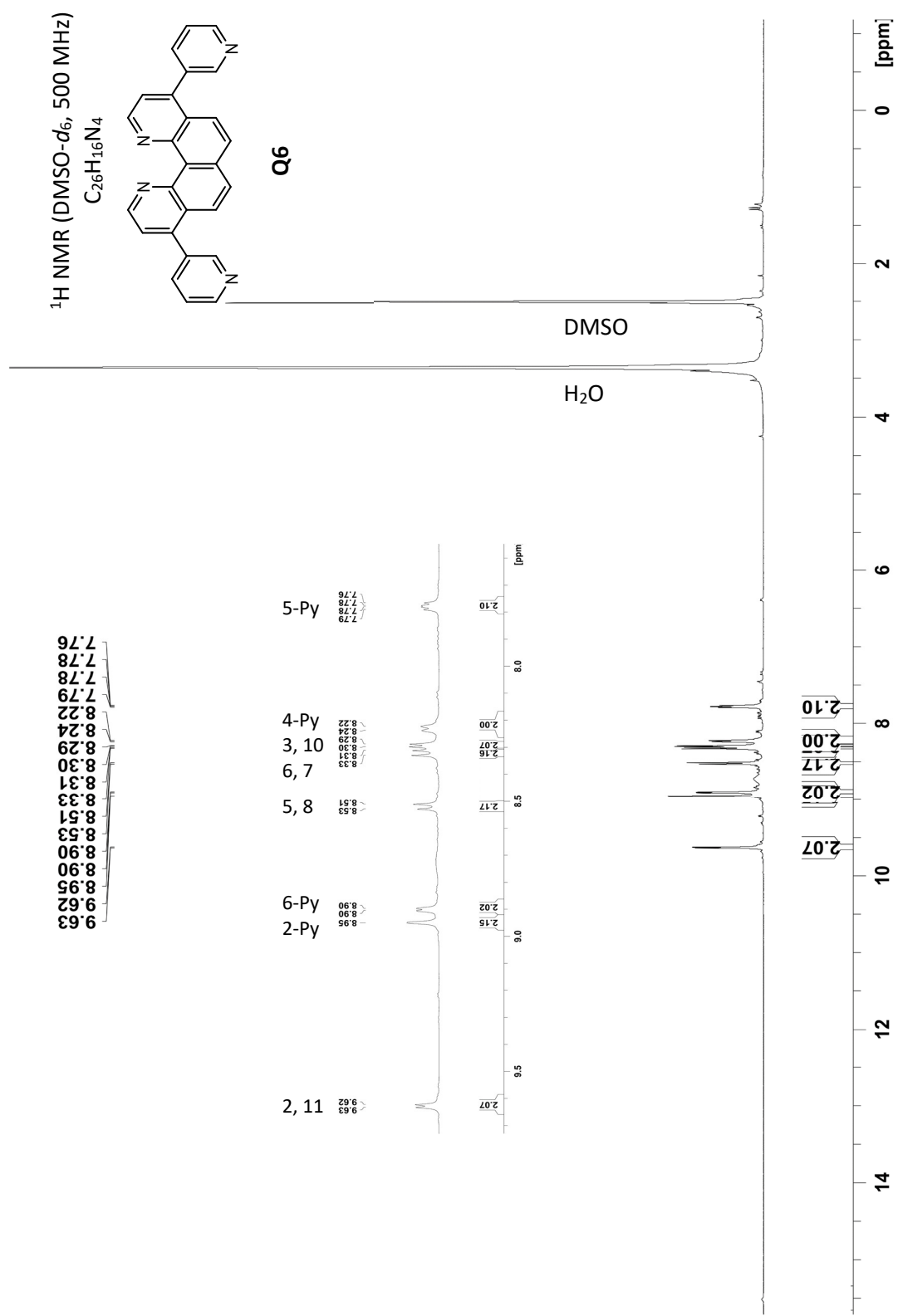


Figure C-4: <sup>1</sup>H NMR spectrum of 4,9-di(pyridin-3-yl)quinolino[7,8-h]quinoline (Q6)

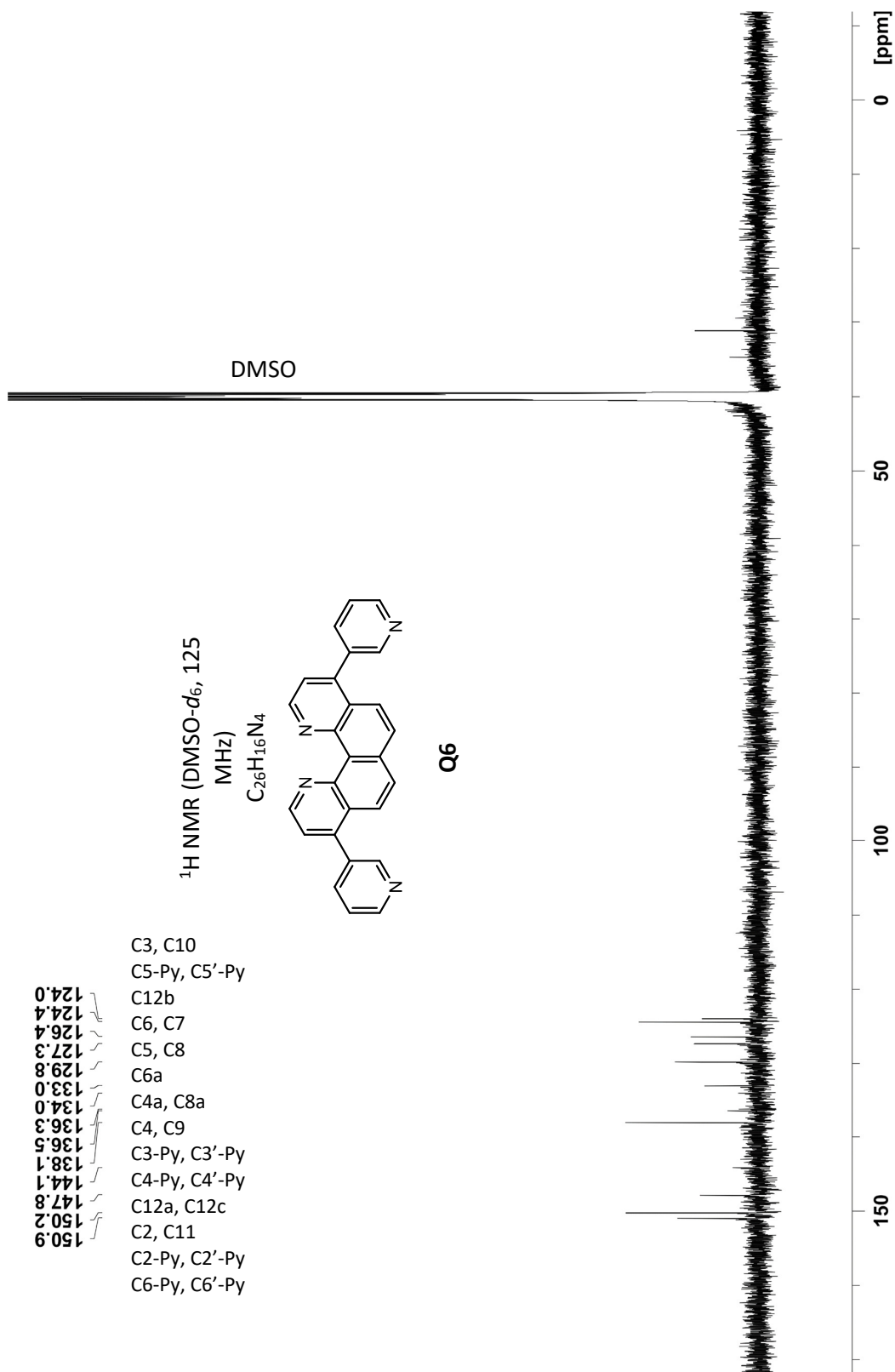


Figure C-5: <sup>13</sup>C NMR spectrum of 4,9-di(pyridin-3-yl)quinolino[7,8-*h*]quinoline (Q6)

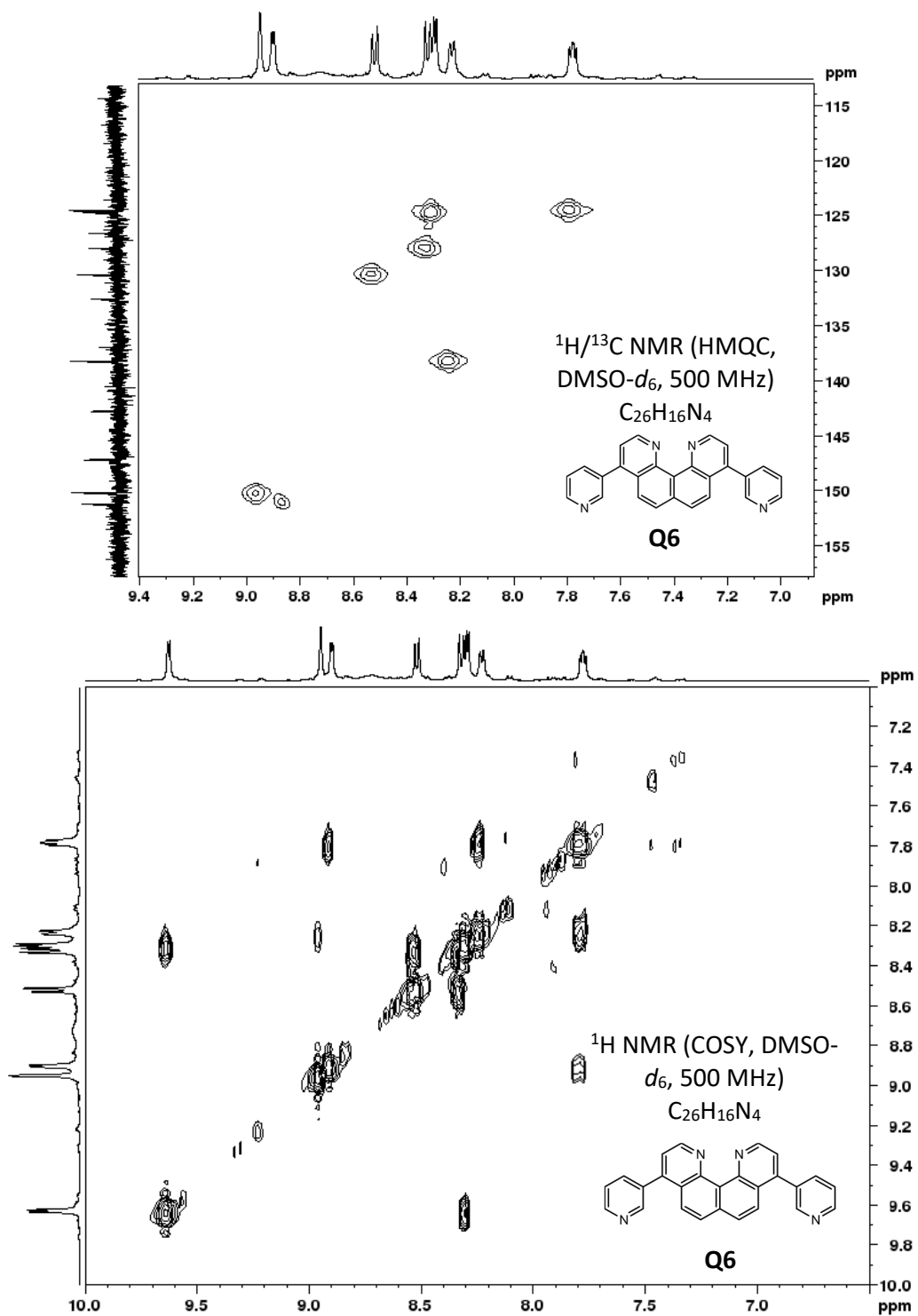


Figure C-6: HMQC (top) and COSY (lower) spectra of 4,9-di(pyridin-3-yl)quinolino[7,8-*h*]quinoline (Q6)



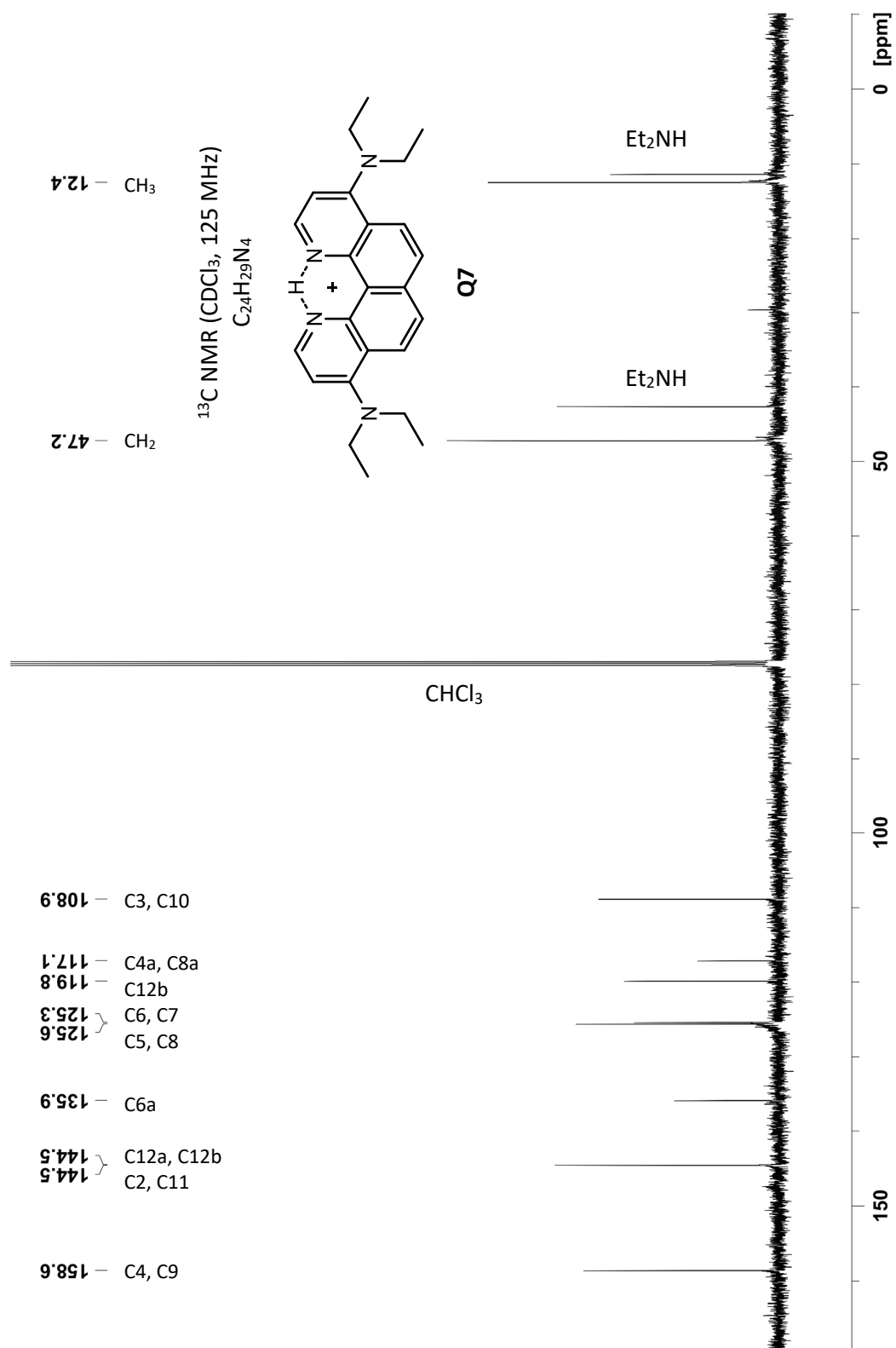


Figure C-8: <sup>13</sup>C NMR spectrum of *N*<sup>4</sup>,*N*<sup>4</sup>,*N*<sup>9</sup>,*N*<sup>9</sup>-tetraethylquinolino[7,8-*h*]quinoline-4,9-diamine (**Q7**)

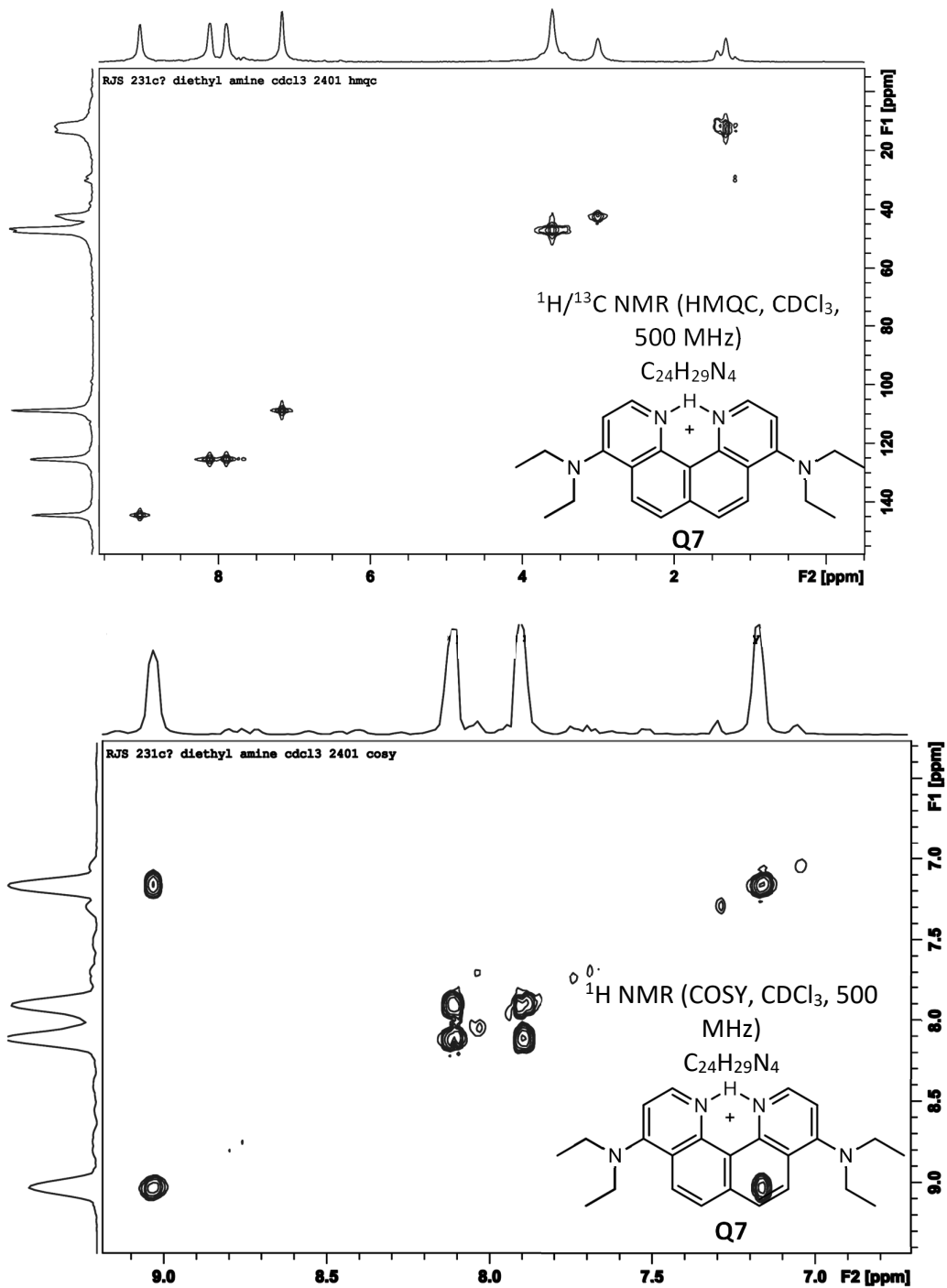


Figure C-9: HMQC (top) and COSY (lower) spectra of *N*<sup>4</sup>,*N*<sup>4</sup>,*N*<sup>9</sup>,*N*<sup>9</sup>-tetraethylquinolino[7,8-*h*]quinoline-4,9-diamine (Q7)





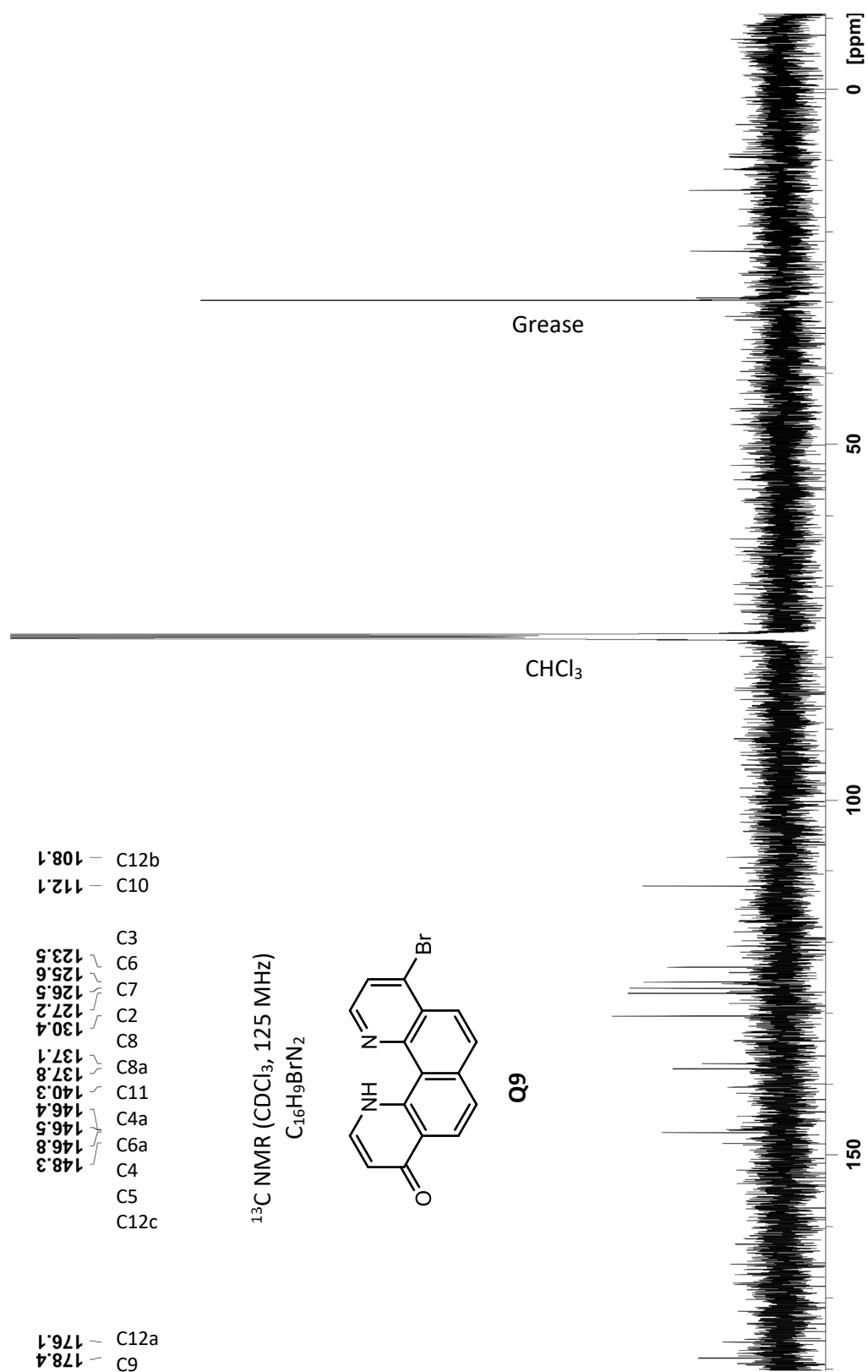


Figure C-11: <sup>13</sup>C NMR spectrum of 4-bromo-9-oxo-9,12-dihydroquinolino[7,8-*h*]quinoline (Q9)

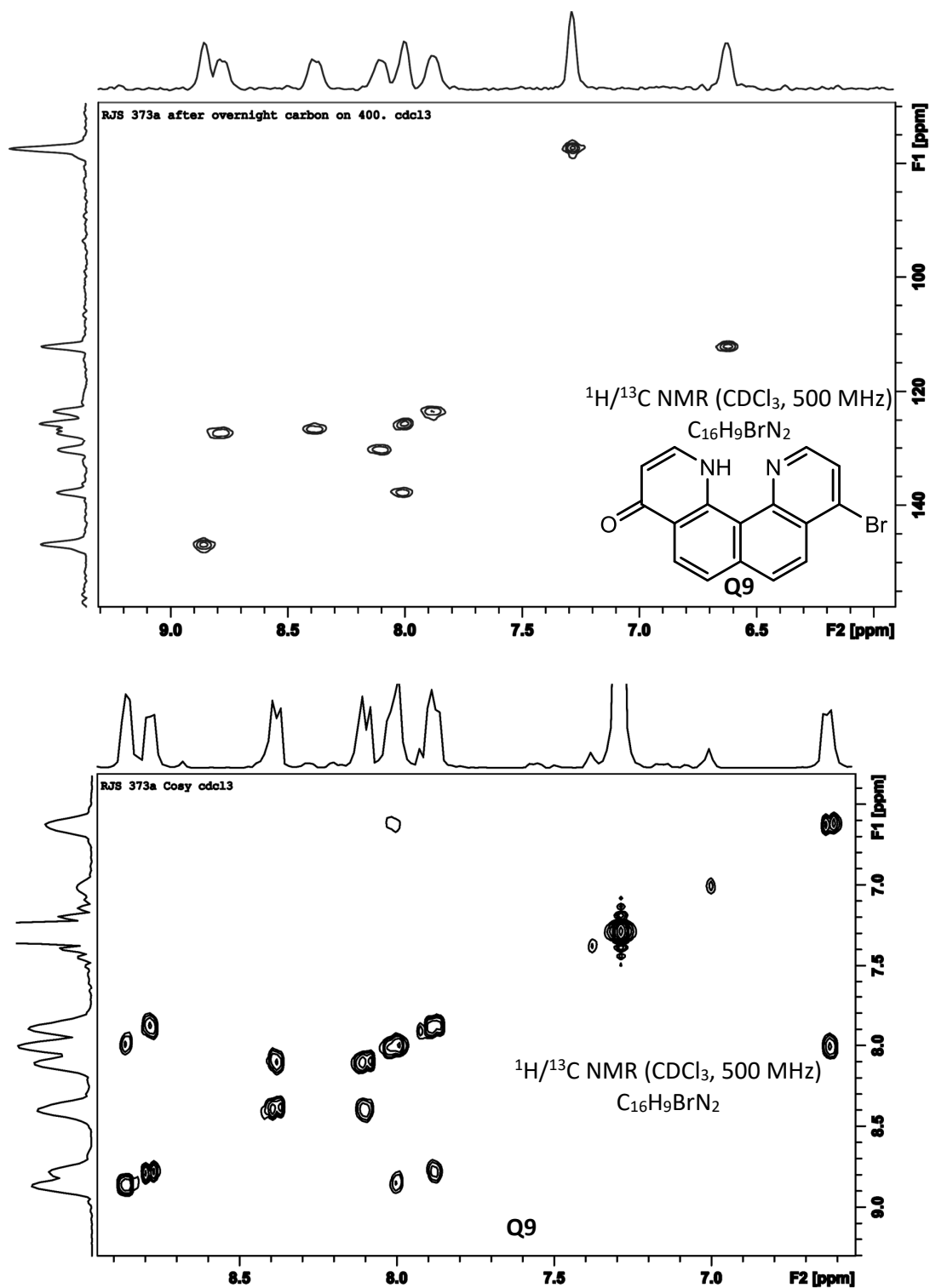


Figure C-12: HMQC (top) and COSY (lower) spectra of 4-bromo-9-oxo-9,12-dihydroquinolino[7,8-*h*]quinoline (Q9).

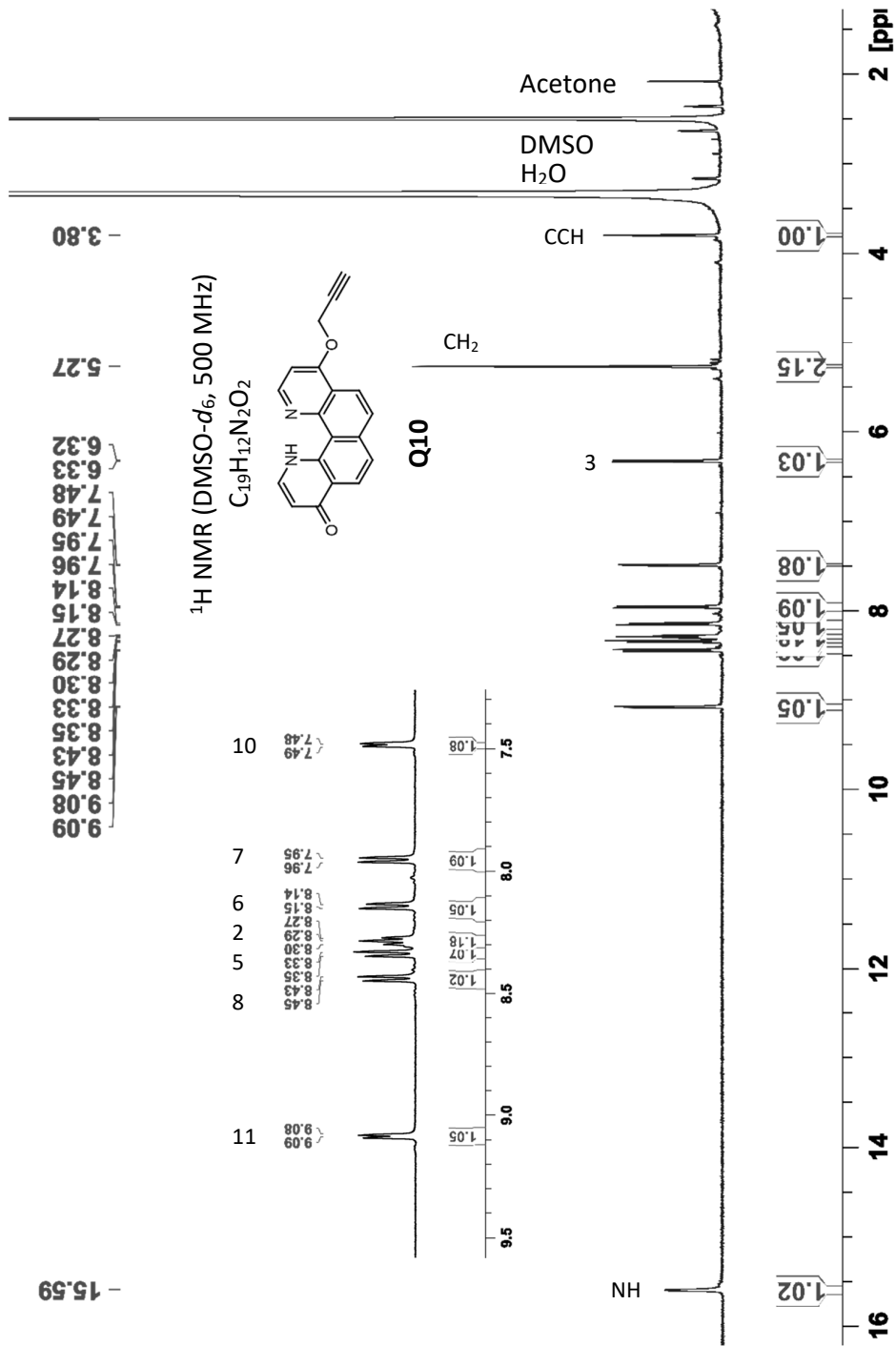


Figure C-13: <sup>1</sup>H NMR spectrum of 9-(2-propyn-1-yloxy)-quinolino[7,8-*h*]quinolin-4(1*H*)-one (Q10)

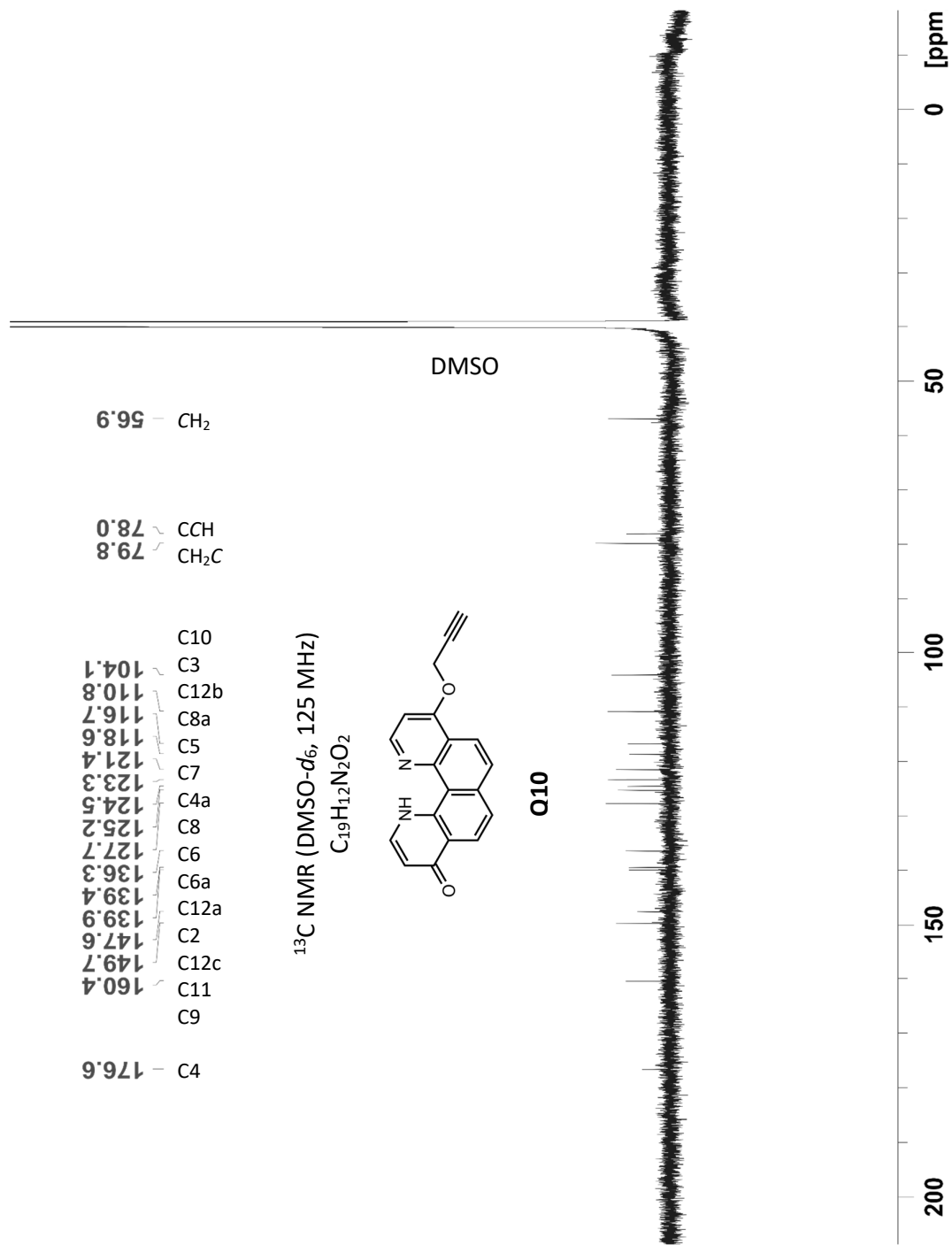


Figure C-14: <sup>13</sup>C NMR spectrum of 9-(2-propyn-1-yloxy)-quinolino[7,8-*h*]quinolin-4(1*H*)-one (Q10)

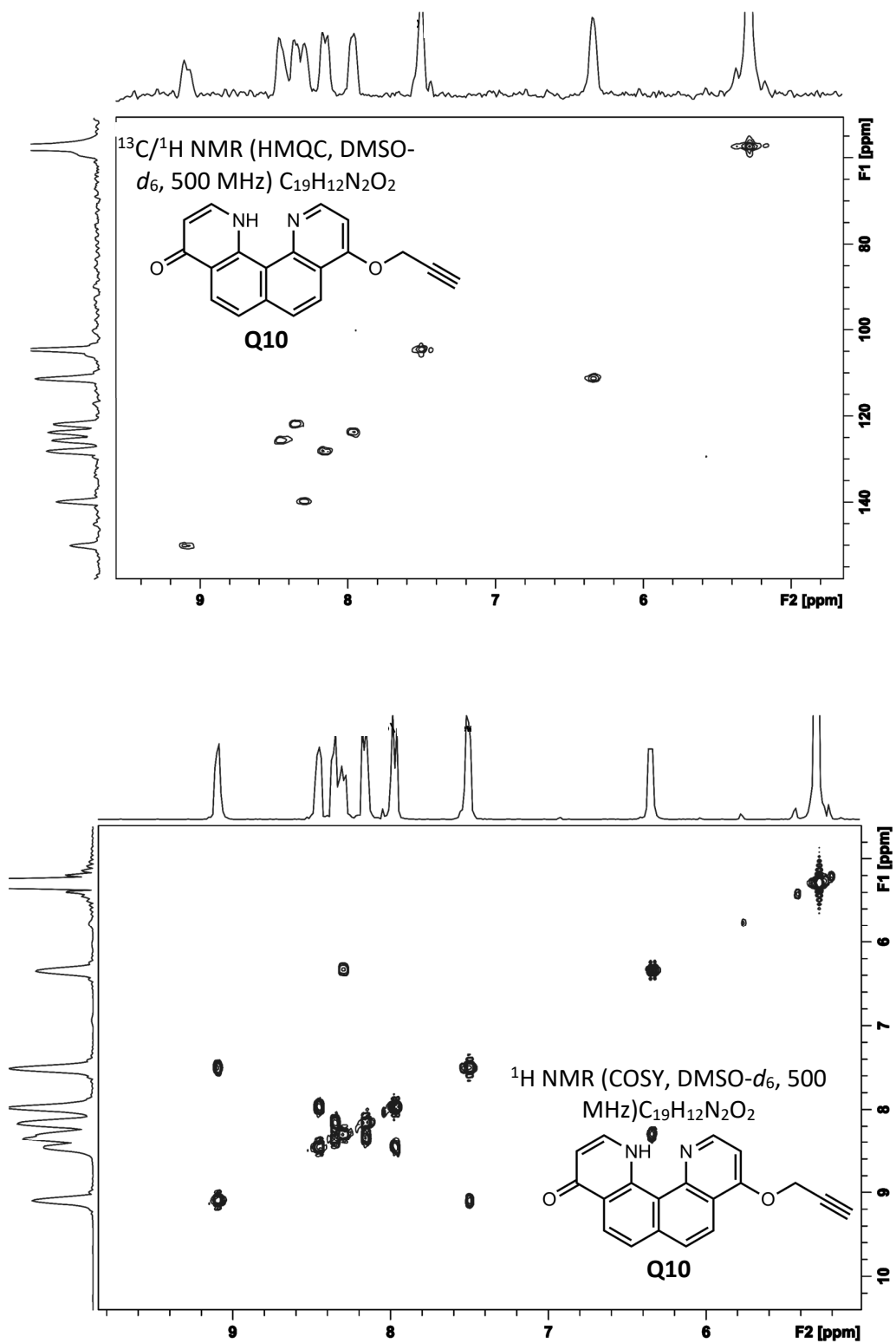


Figure C-15: HMQC (top) and COSY (lower) spectra of 9-(2-propyn-1-yloxy)-quinolino[7,8-*h*]quinolin-4(1*H*)-one (Q10)

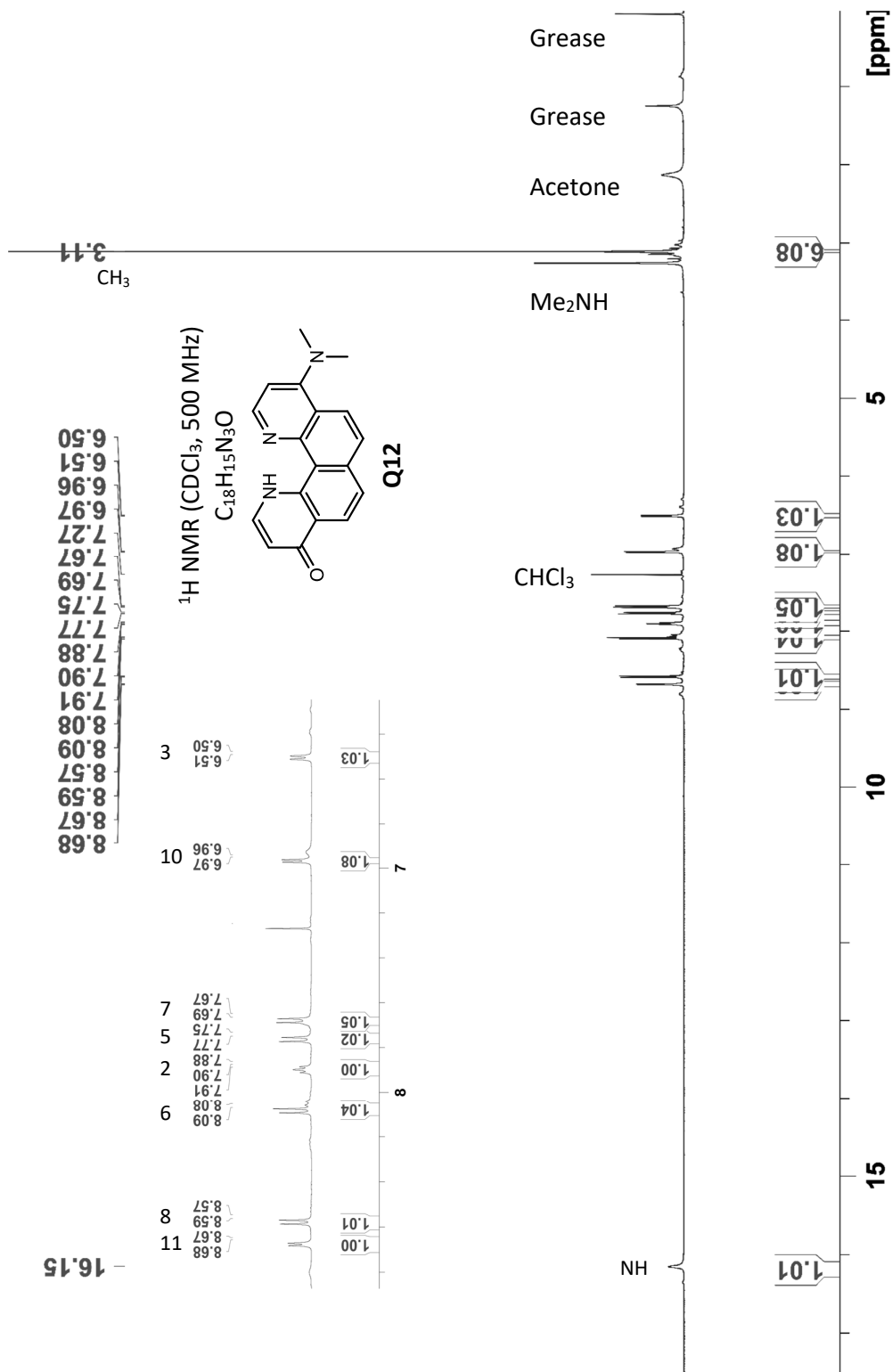


Figure C-16: <sup>1</sup>H NMR spectrum of 9-(dimethylamino)quinolino[7,8-*h*]quinoline-4(1*H*)-one (Q12)

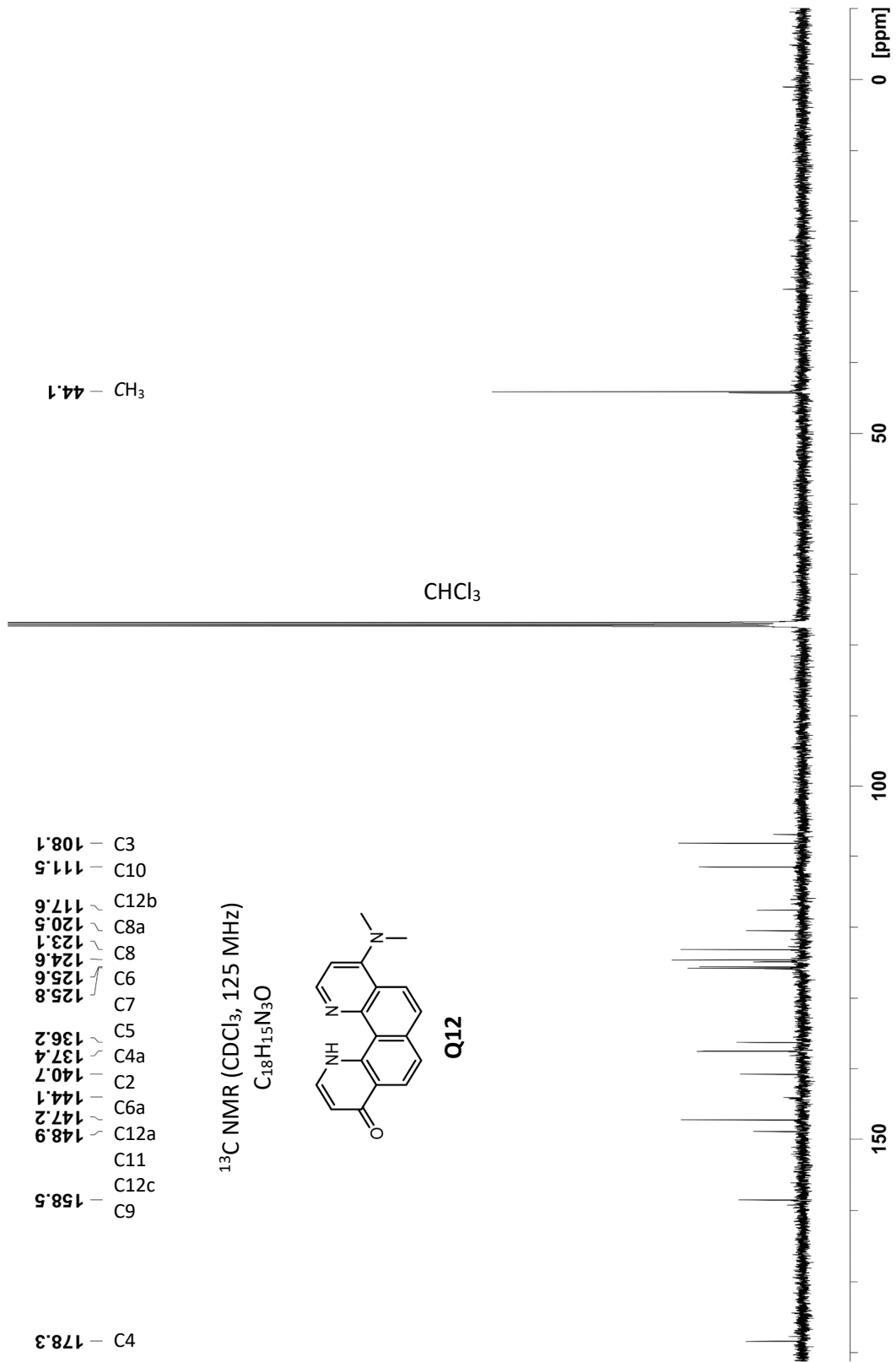


Figure C-17: <sup>13</sup>C NMR spectrum of 9-(dimethylamino)quinolino[7,8-*h*]quinoline-4(1*H*)-one (Q12)



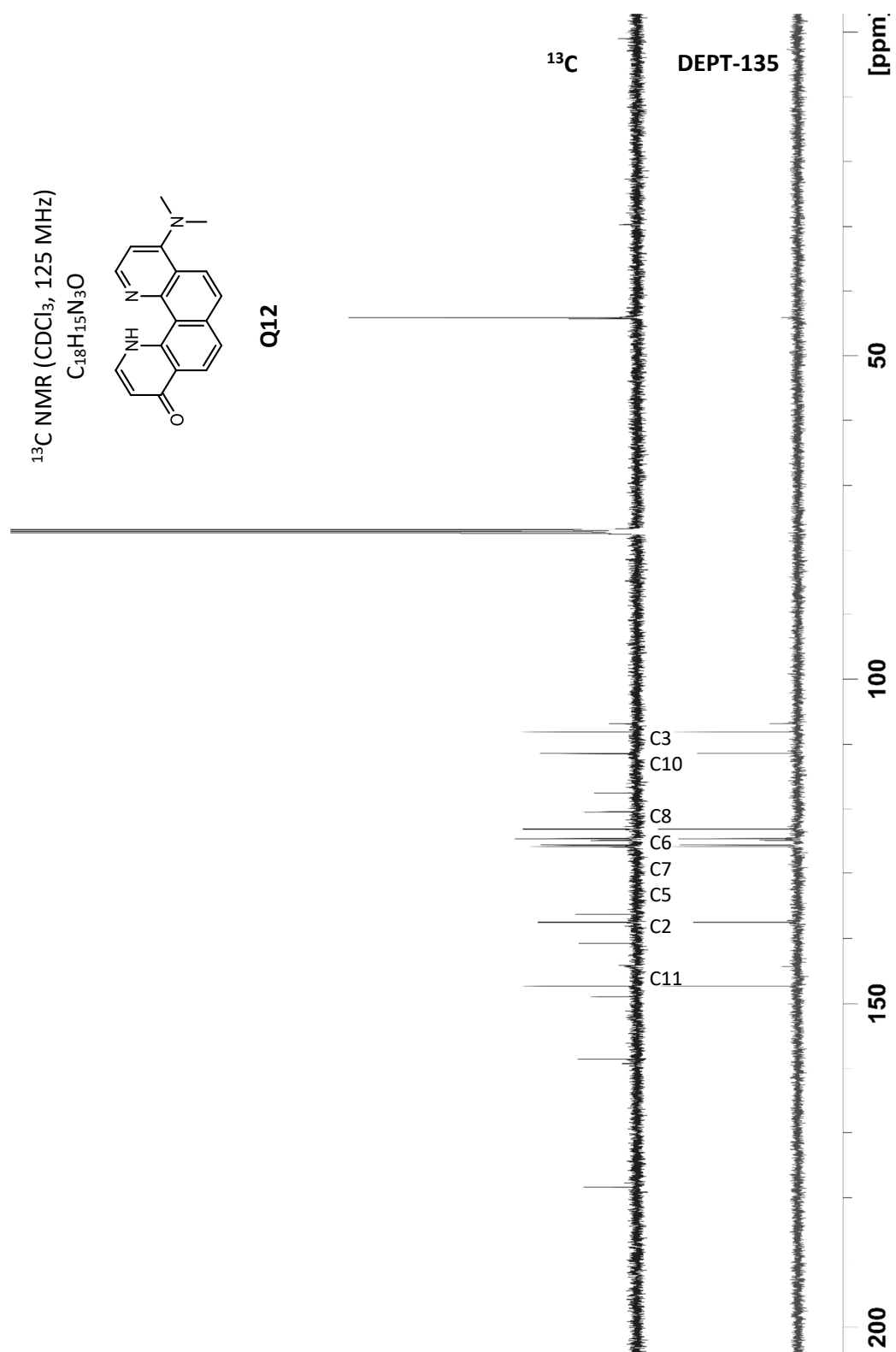


Figure C-18: Overlay of <sup>13</sup>C and DEPT-135 NMR spectra of 9-(dimethylamino)quinolino[7,8-*h*]quinoline-4(1*H*)-one (Q12)

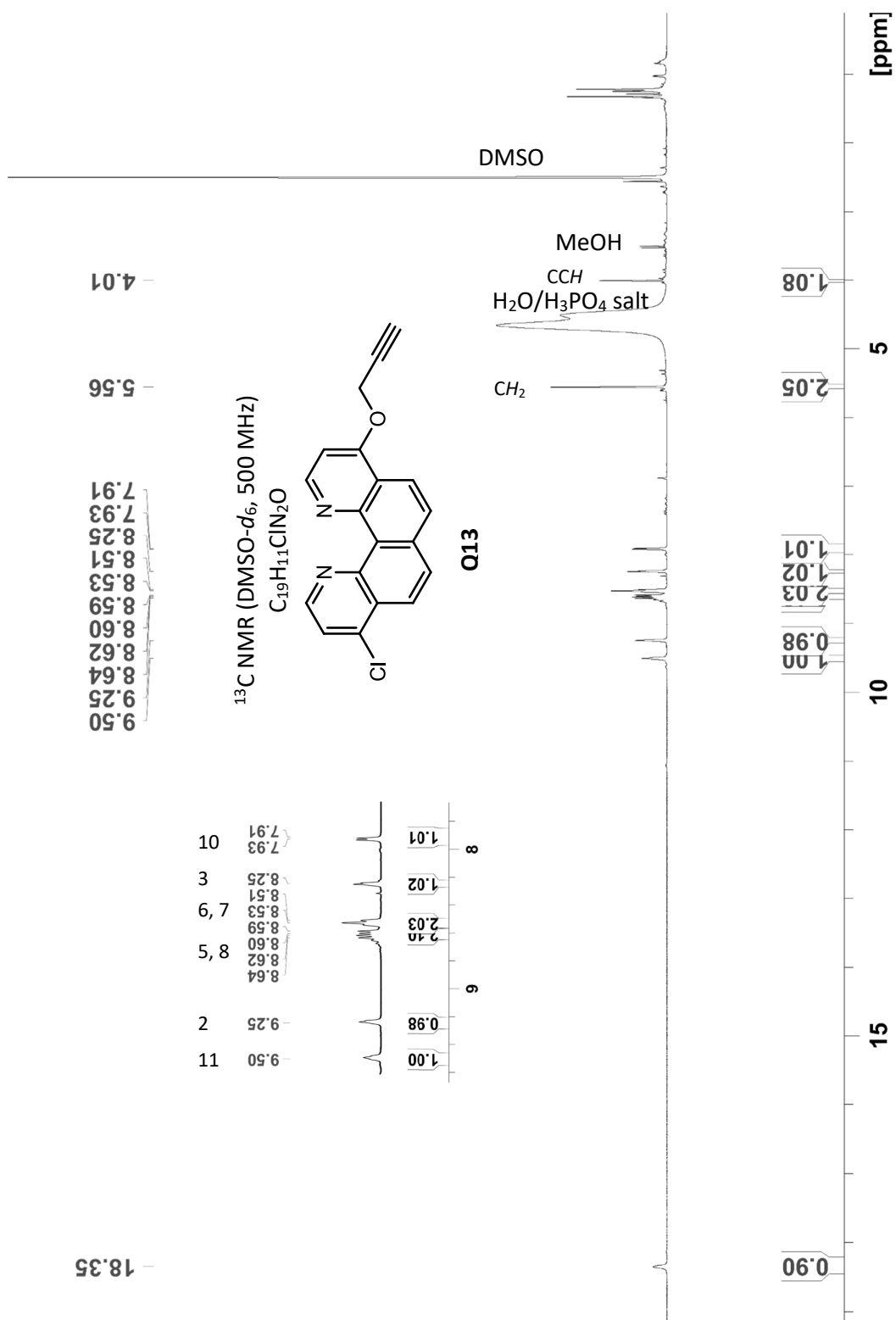


Figure C-19: <sup>1</sup>H NMR spectrum of 4-chloro-9-(2-propyn-1-yloxy)-quinolino[7,8-*h*]quinoline (Q13)

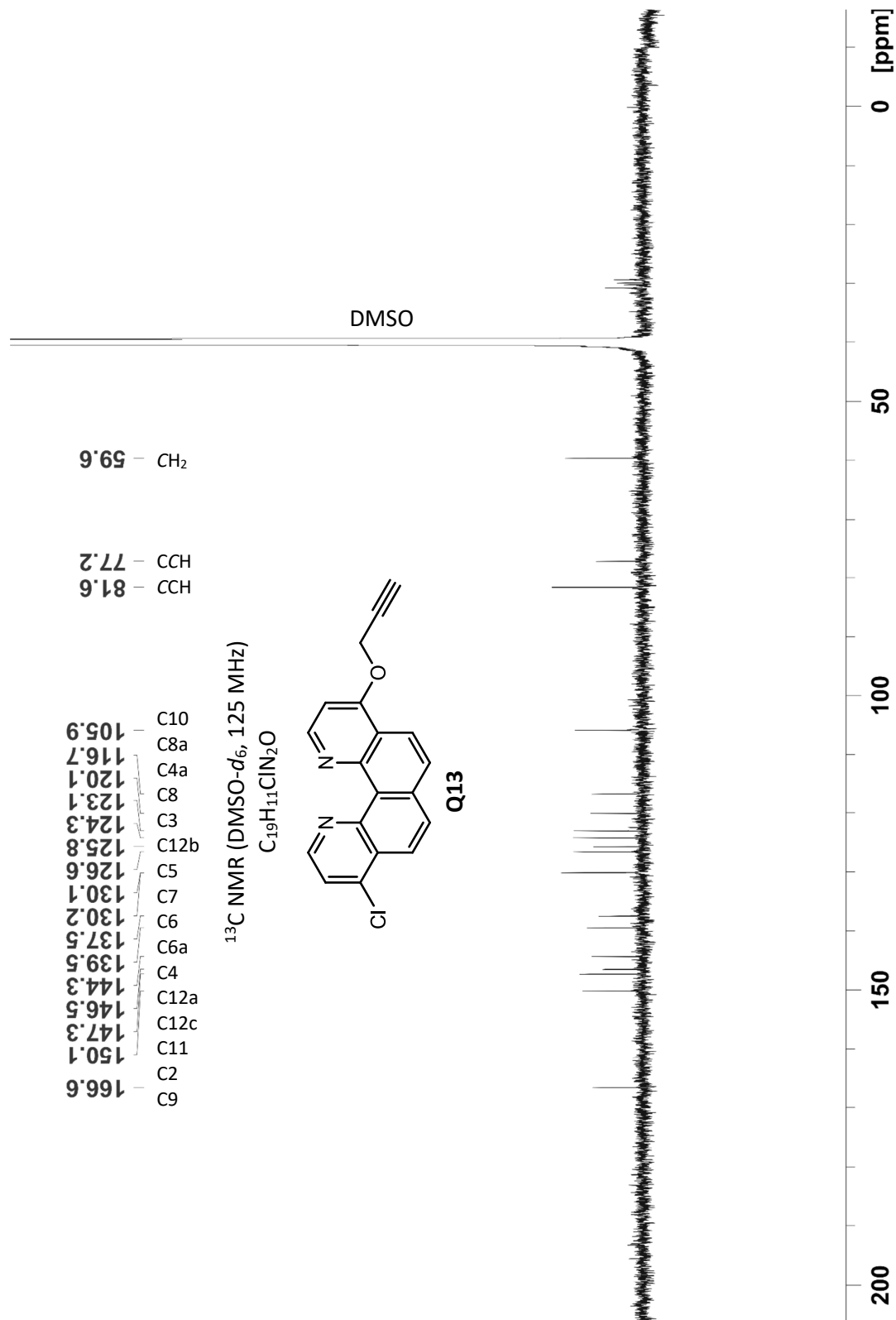


Figure C-20: <sup>13</sup>C NMR spectrum of 4-chloro-9-(2-propyn-1-yloxy)-quinolino[7,8-*h*]quinoline (Q13)

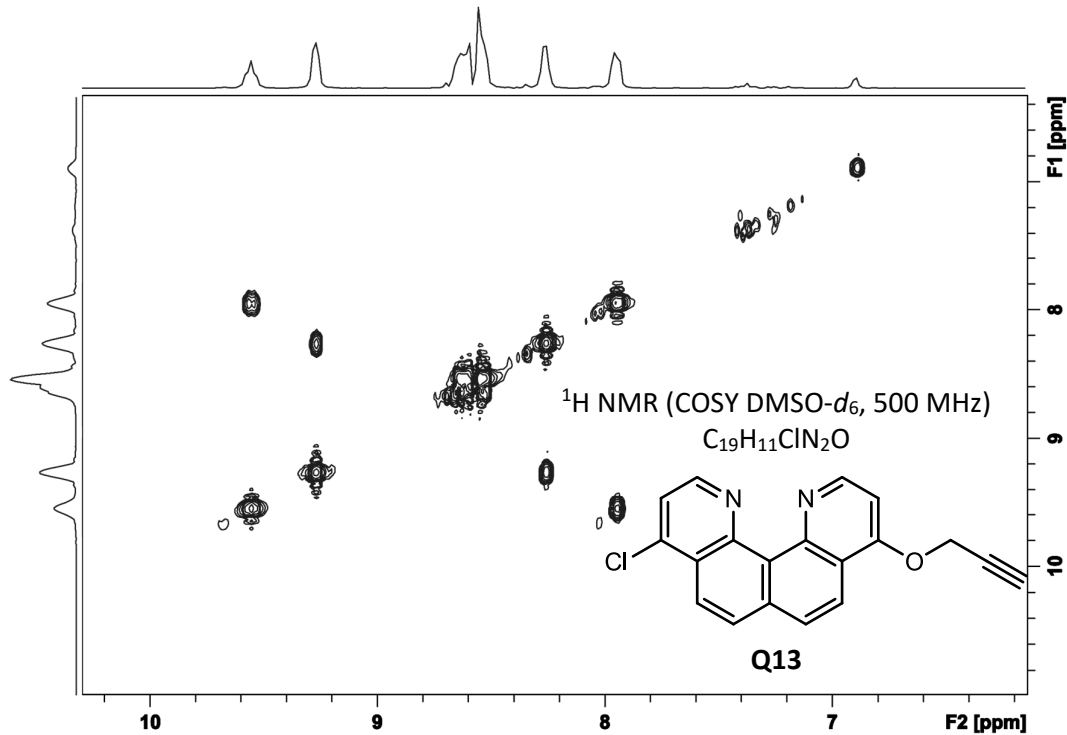
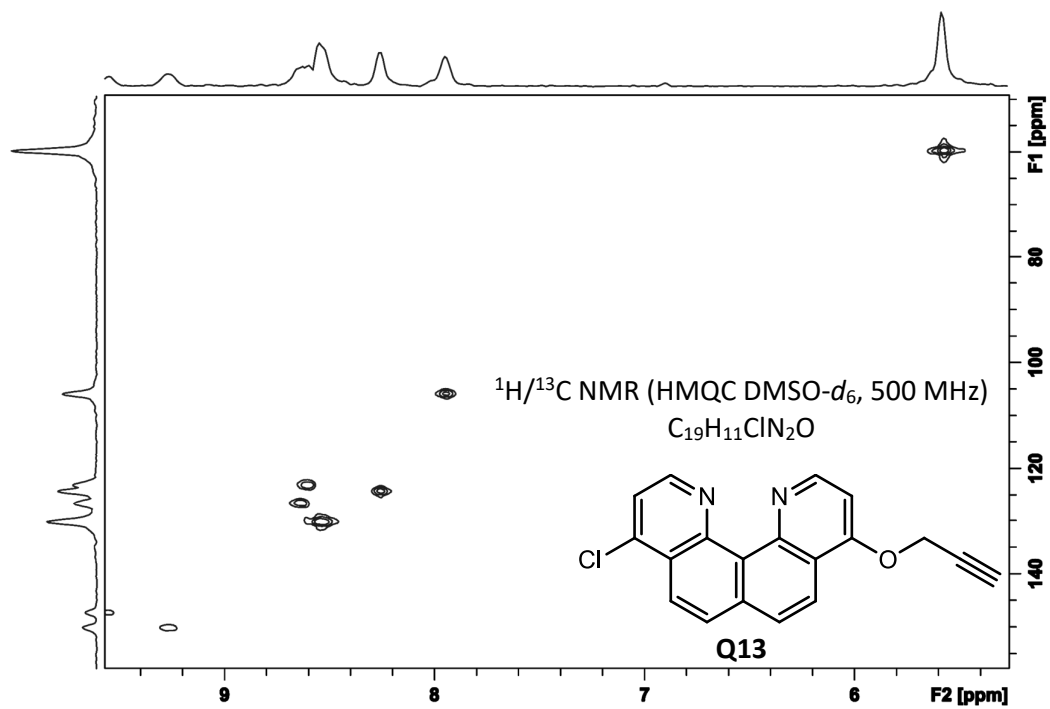


Figure C-21: HMQC (top) and COSY (lower) spectra of 4-chloro-9-(2-propyn-1-yloxy)-quinolino[7,8-*h*]quinolin-4(1*H*)-one (Q13)

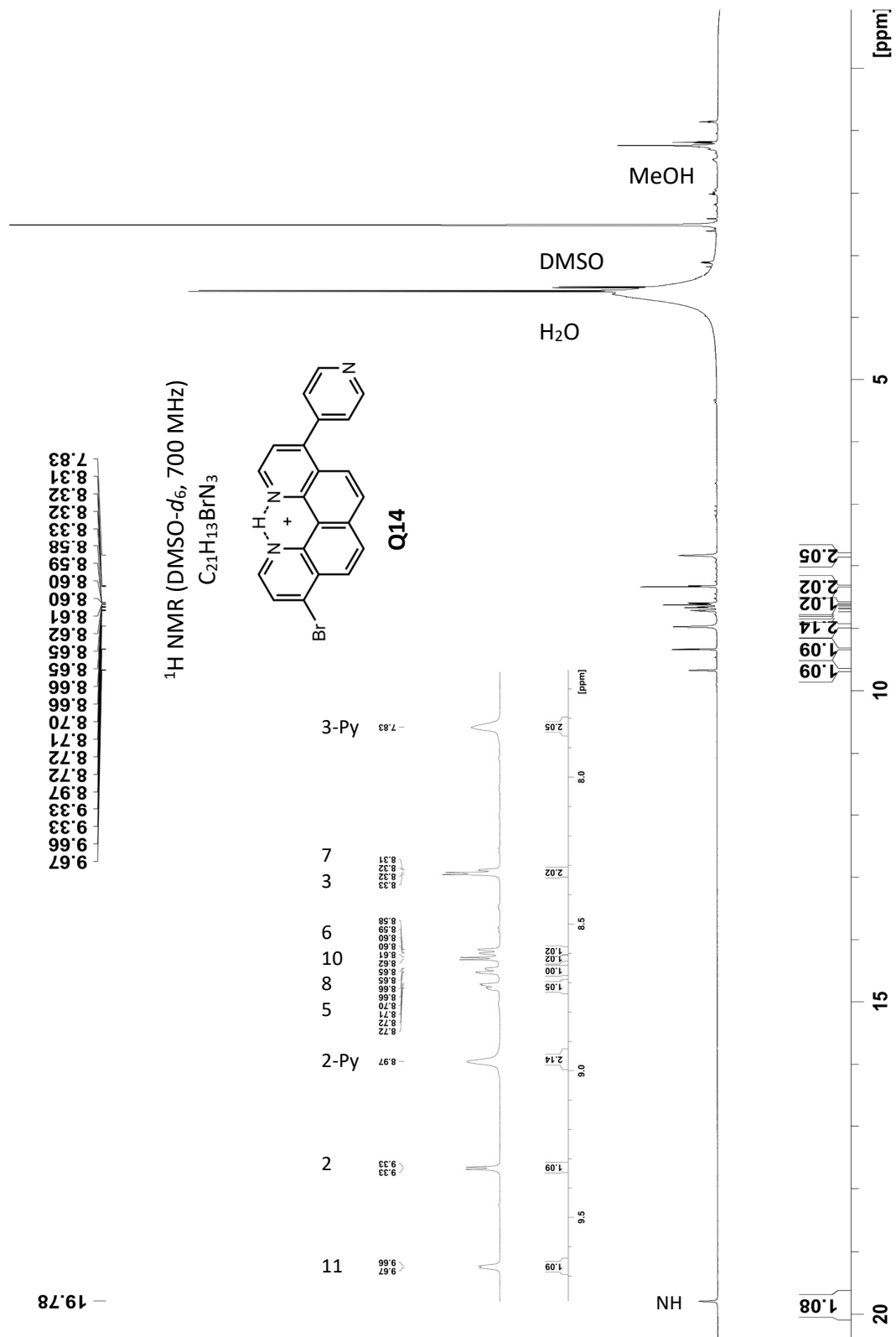


Figure C-22: <sup>1</sup>H NMR of 4-bromo-9-(pyridin-4-yl)quinolino[7,8-h]quinoline (Q14)

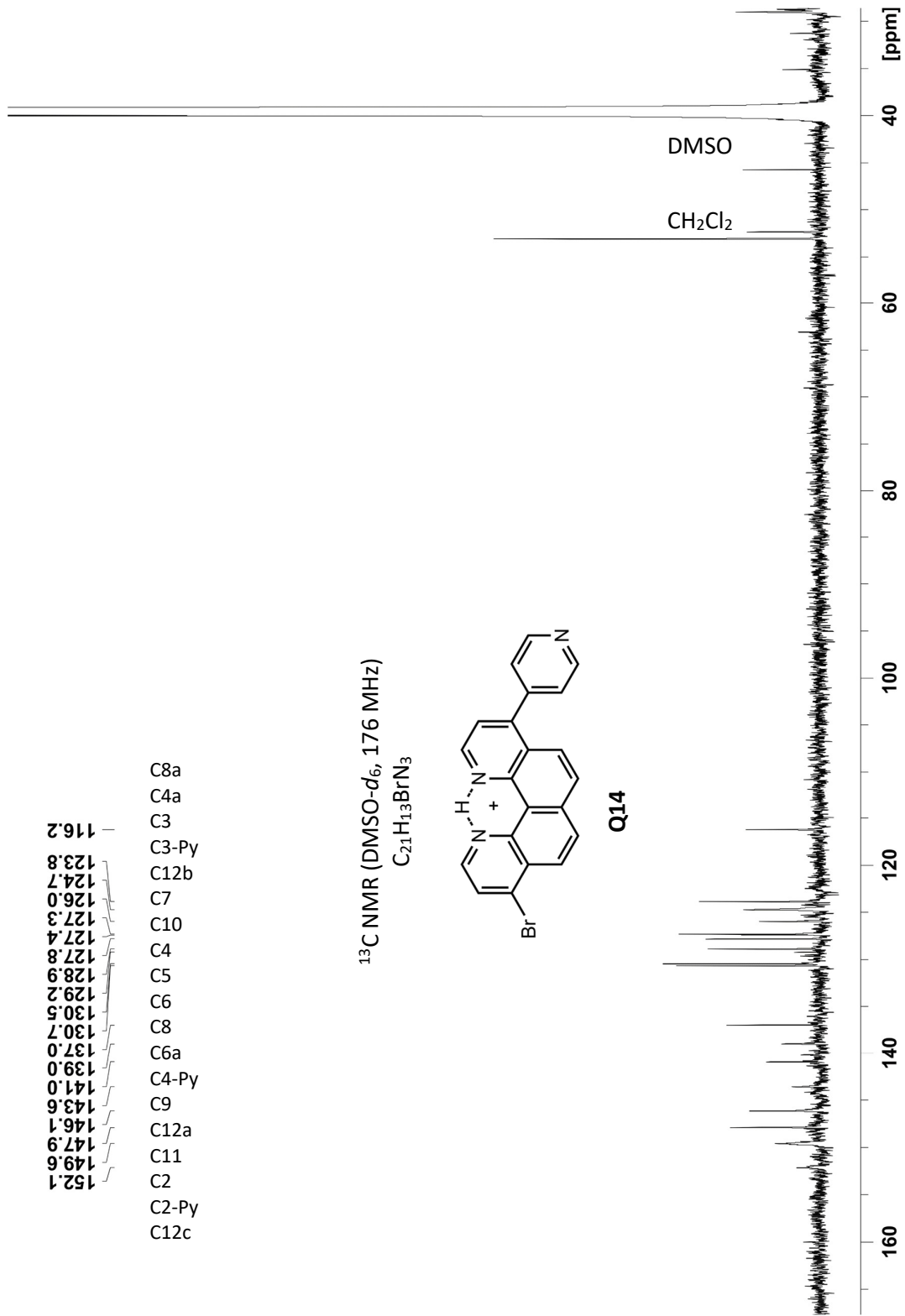


Figure C-23: <sup>13</sup>C NMR of 4-bromo-9-(pyridin-4-yl)quinolino[7,8-*h*]quinoline (Q14)

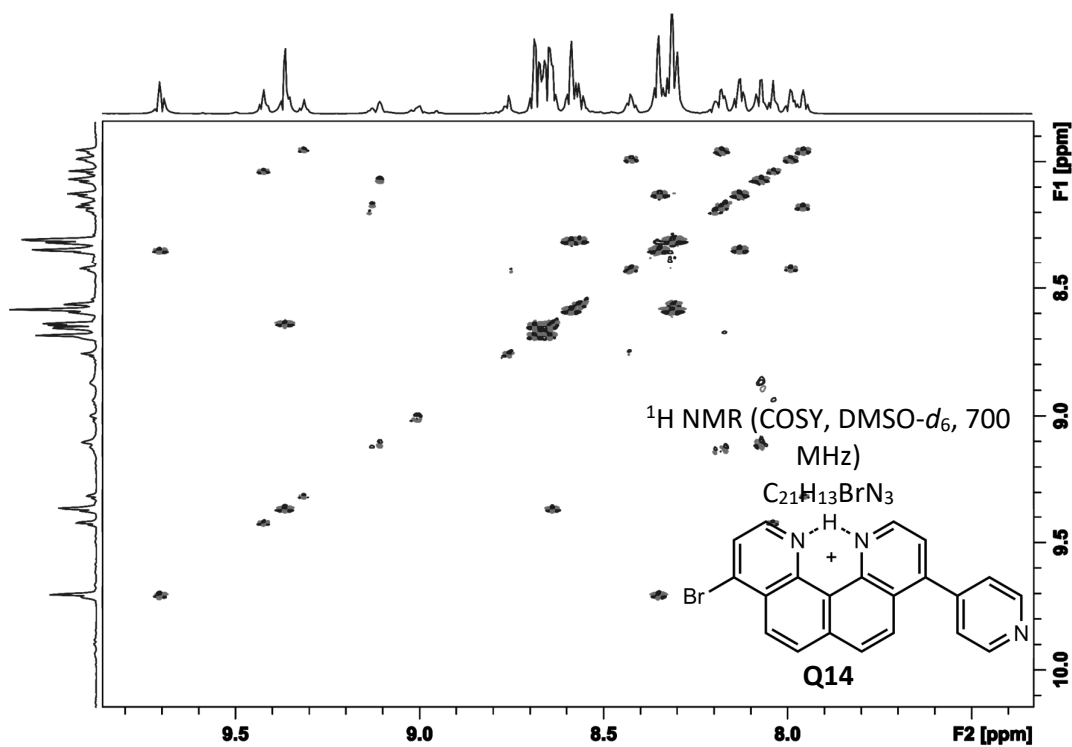
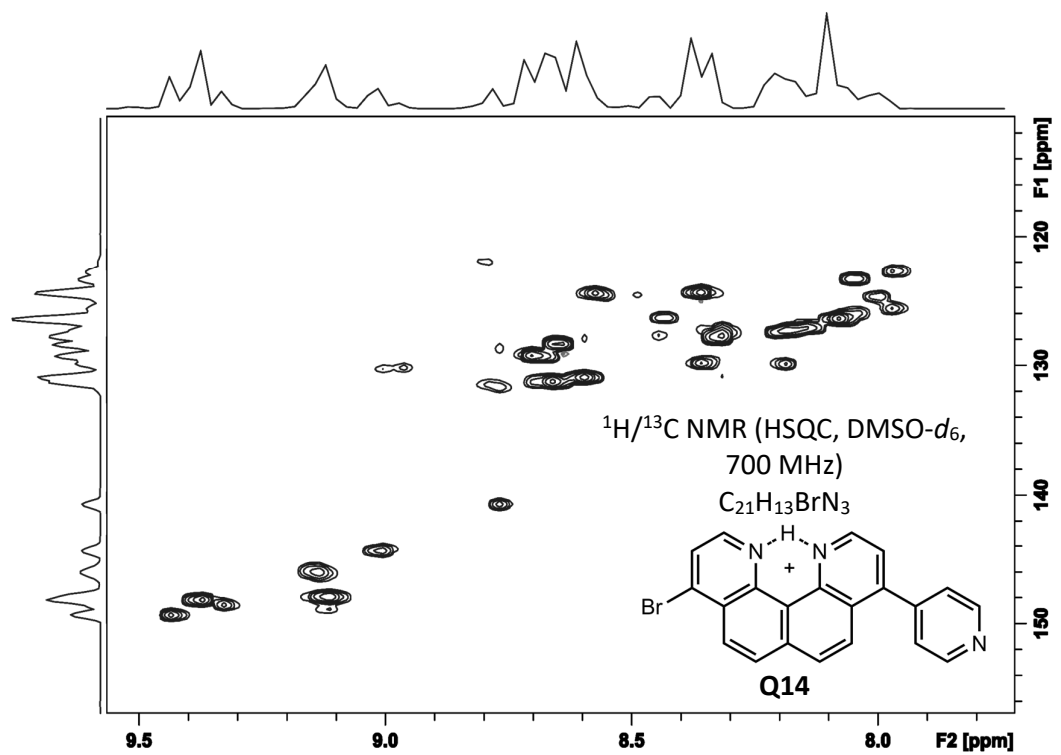


Figure C-24: HSQC (top) and COSY (lower) spectra of 4-bromo-9-(pyridin-4-yl)quinolino[7,8-*h*]quinoline (Q14)

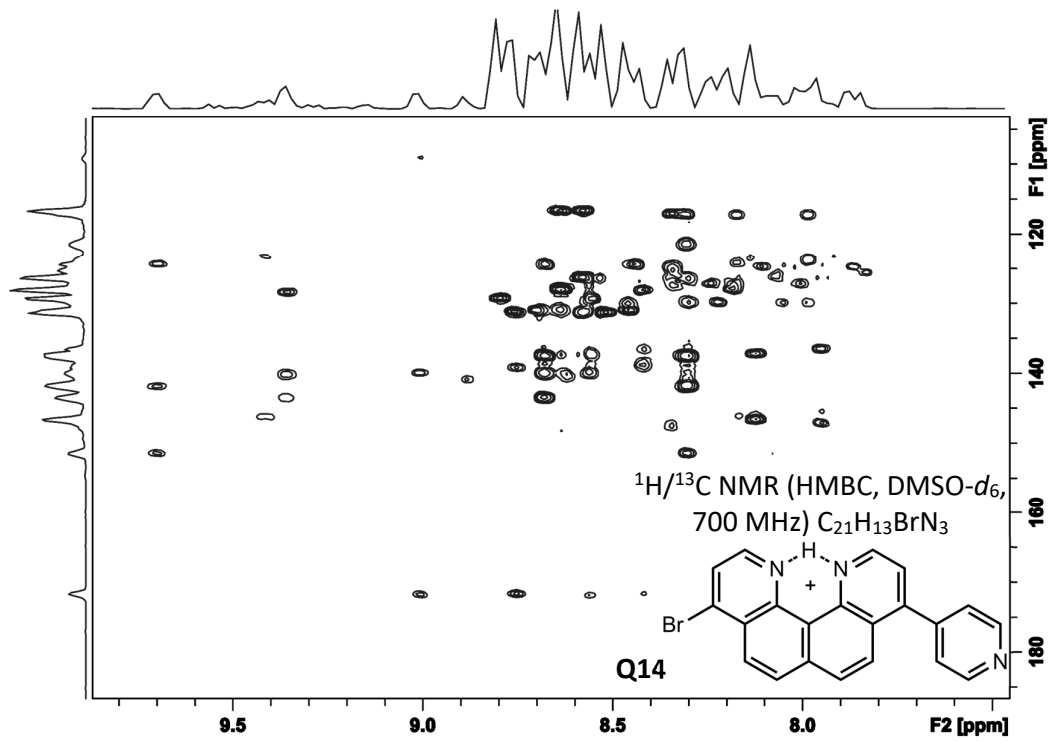


Figure C-25: HMBC spectrum of 4-bromo-9-(pyridin-4-yl)quinolino[7,8-*h*]quinoline (Q14)



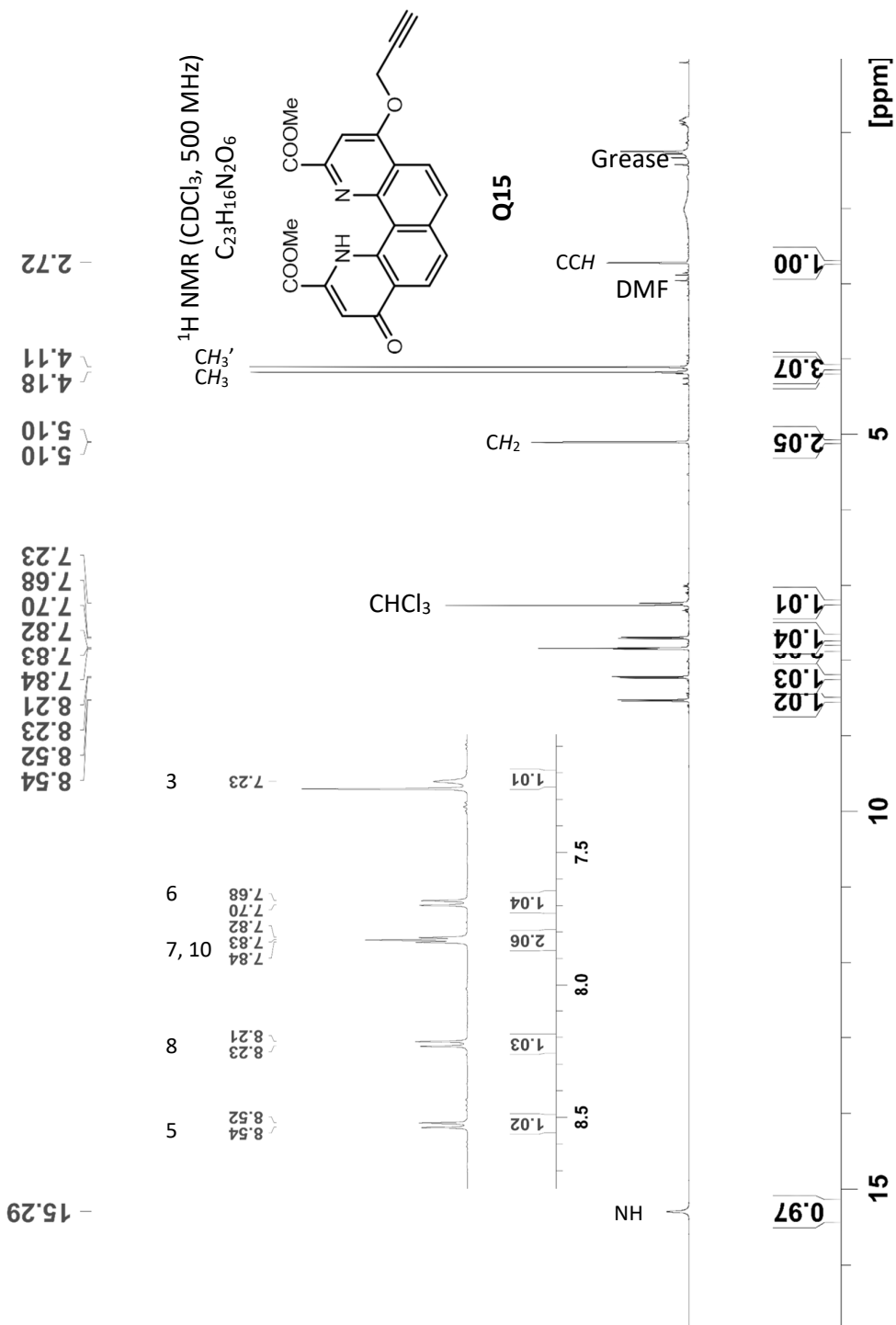


Figure C-26: <sup>1</sup>H NMR spectrum of 9-(2-propyn-1-yloxy)-1,4,9,12-tetrahydro-4,9-dioxo-2,11-dimethylester-quinolo[7,8-*h*]quinoline-2,11-dicarboxylic acid (Q15)

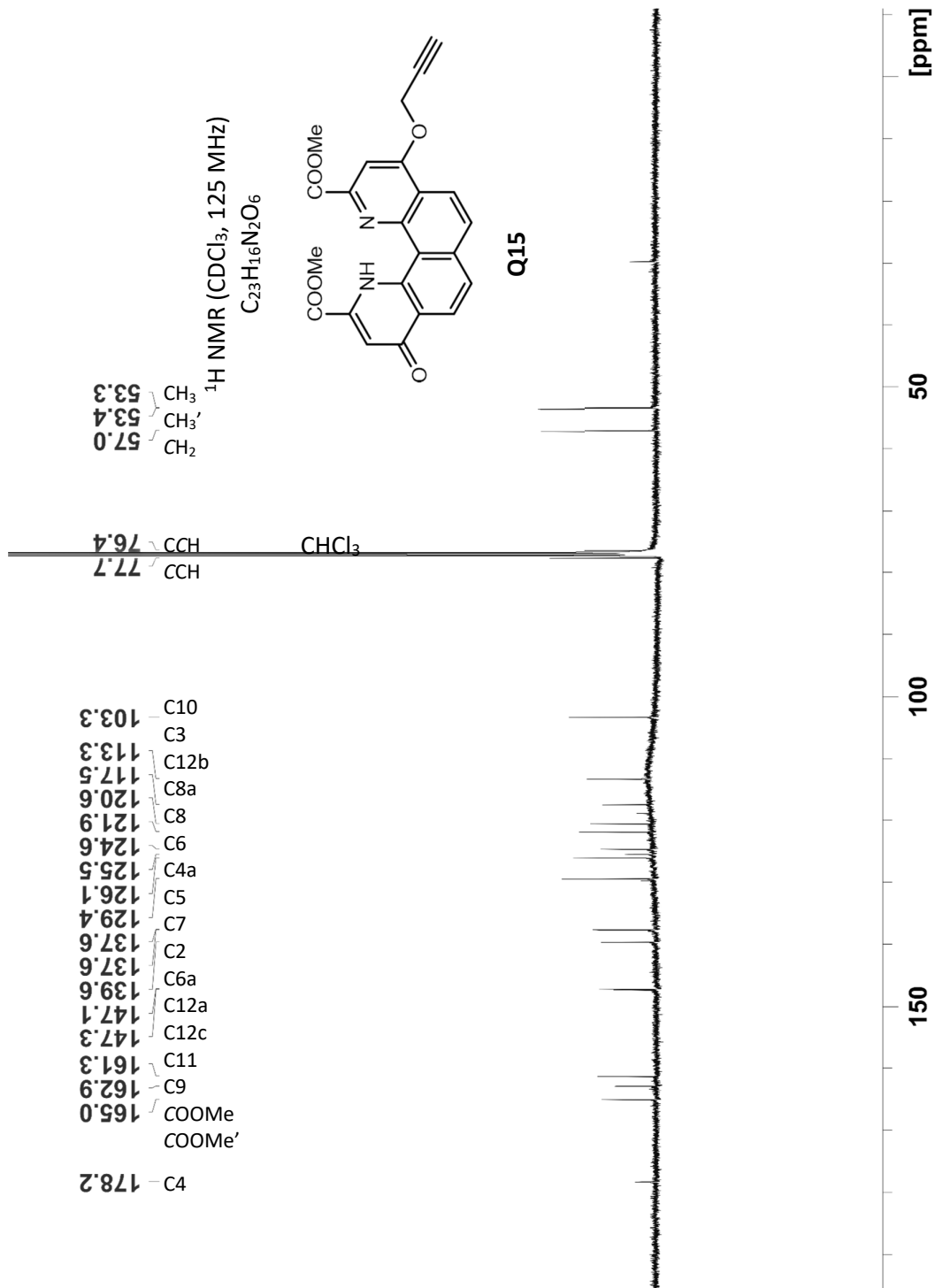


Figure C-27: <sup>13</sup>C NMR spectrum of 9-(2-propyn-1-yloxy)-1,4,9,12-tetrahydro-4,9-dioxo-2,11-dimethylester-quinolo[7,8-h]quinoline-2,11-dicarboxylic acid (Q15)

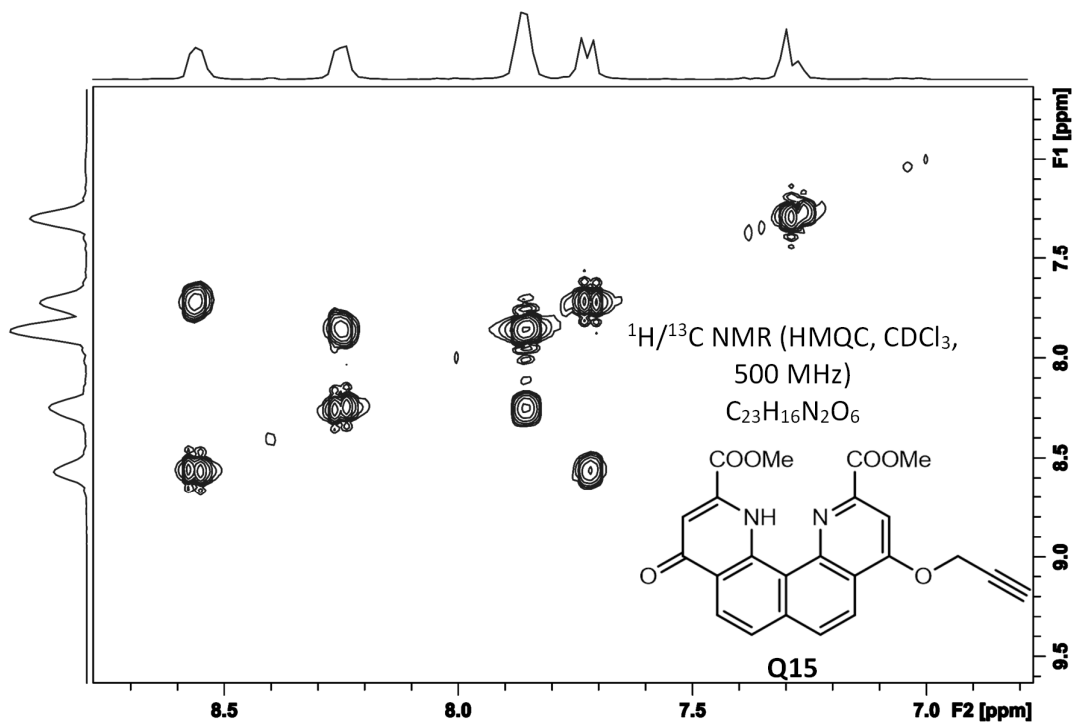
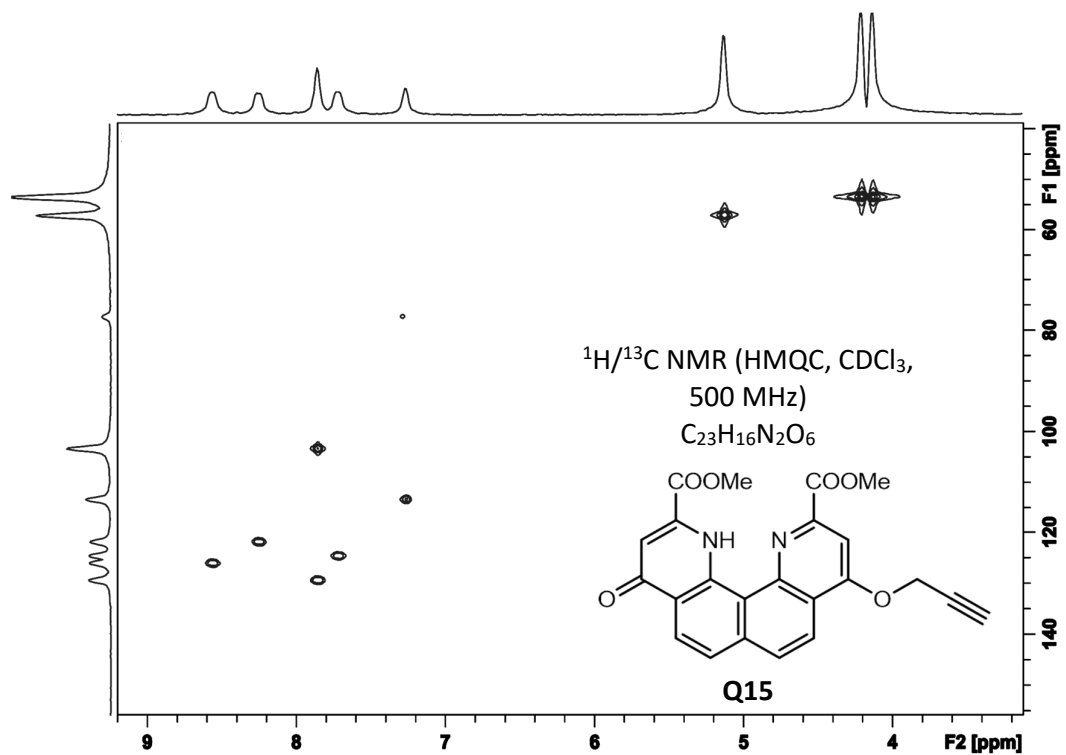


Figure C-28: HMQC (top) and COSY (lower) spectra of 9-(2-propyn-1-yloxy)-1,4,9,12-tetrahydro-4,9-dioxo-2,11-dimethylester-quino[7,8-*h*]quinoline-2,11-dicarboxylic acid (Q15)

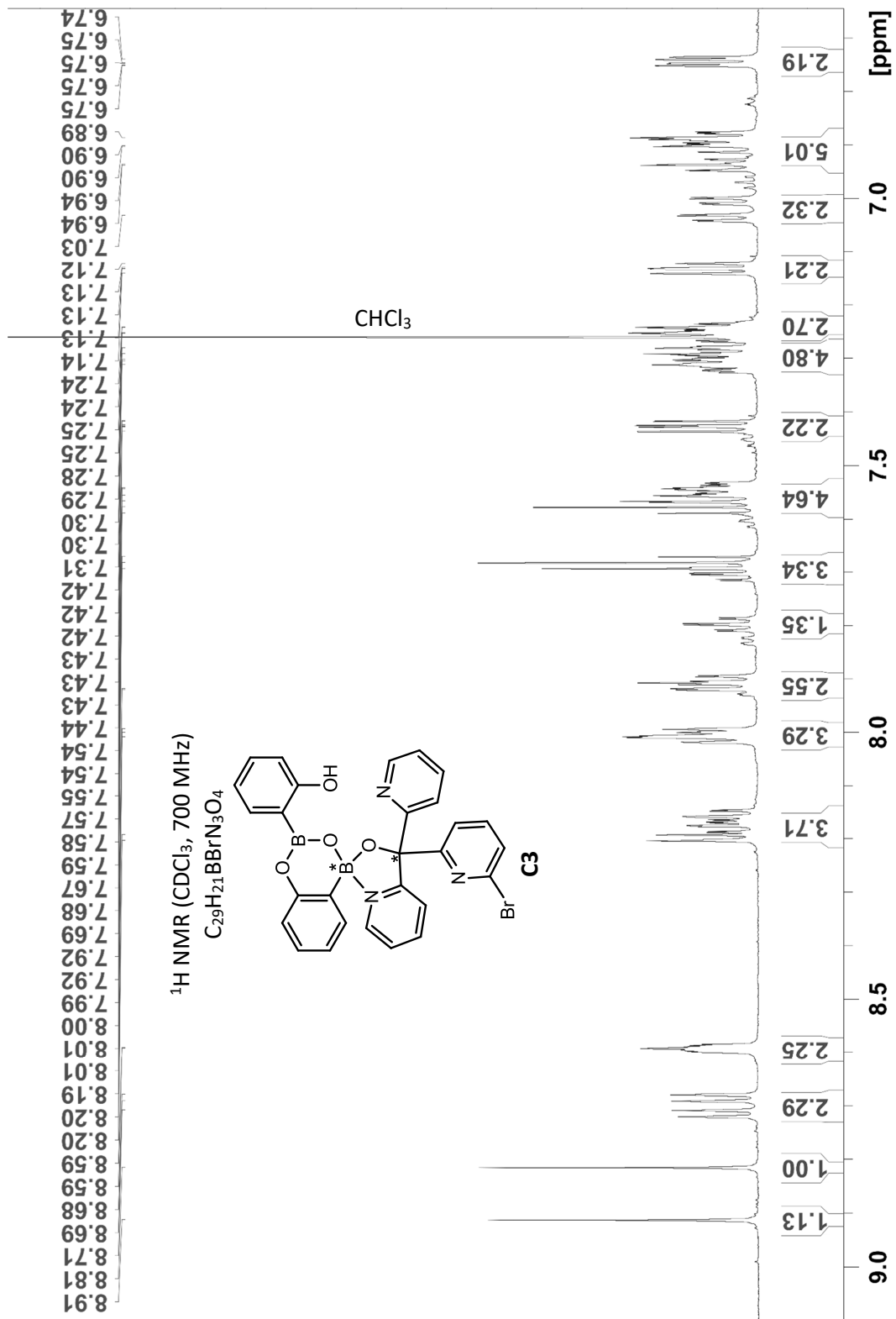


Figure C-29: <sup>1</sup>H NMR spectrum of a boronic anhydride-based ligand (compound 3)

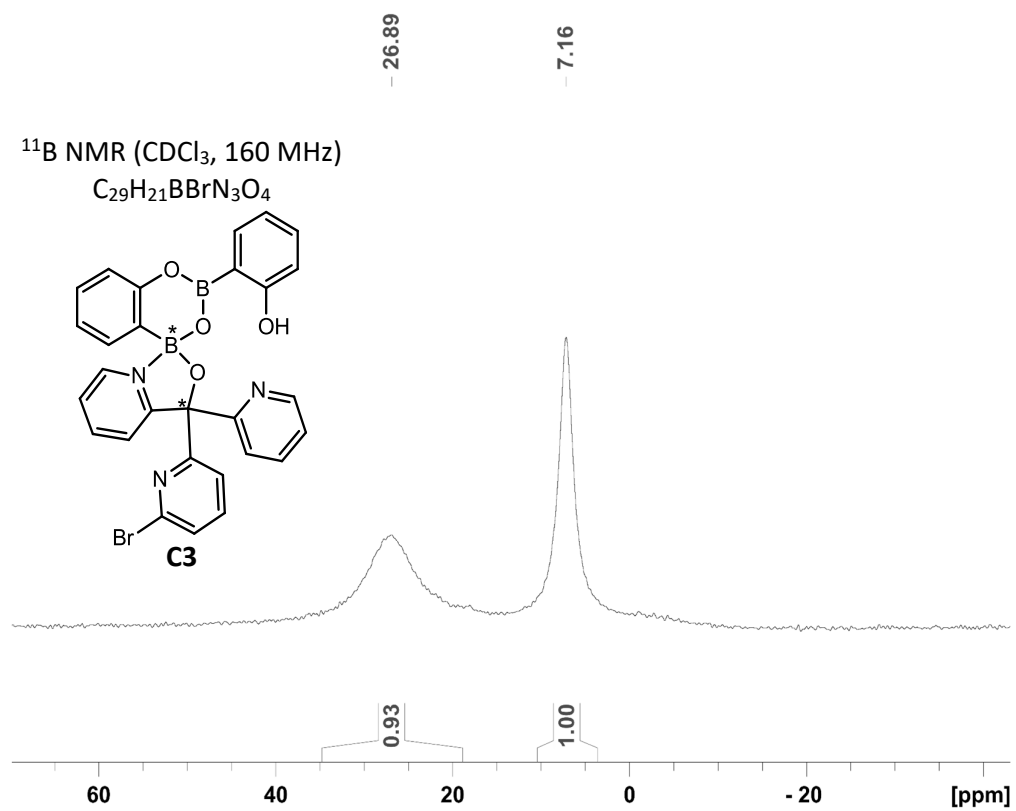


Figure C-30:  $^{11}\text{B}$  NMR spectrum of a boronic anhydride-based ligand (compound 3) in  $\text{CDCl}_3$ . External  $\text{BF}_3 \cdot \text{Et}_2\text{O}$  standard used.

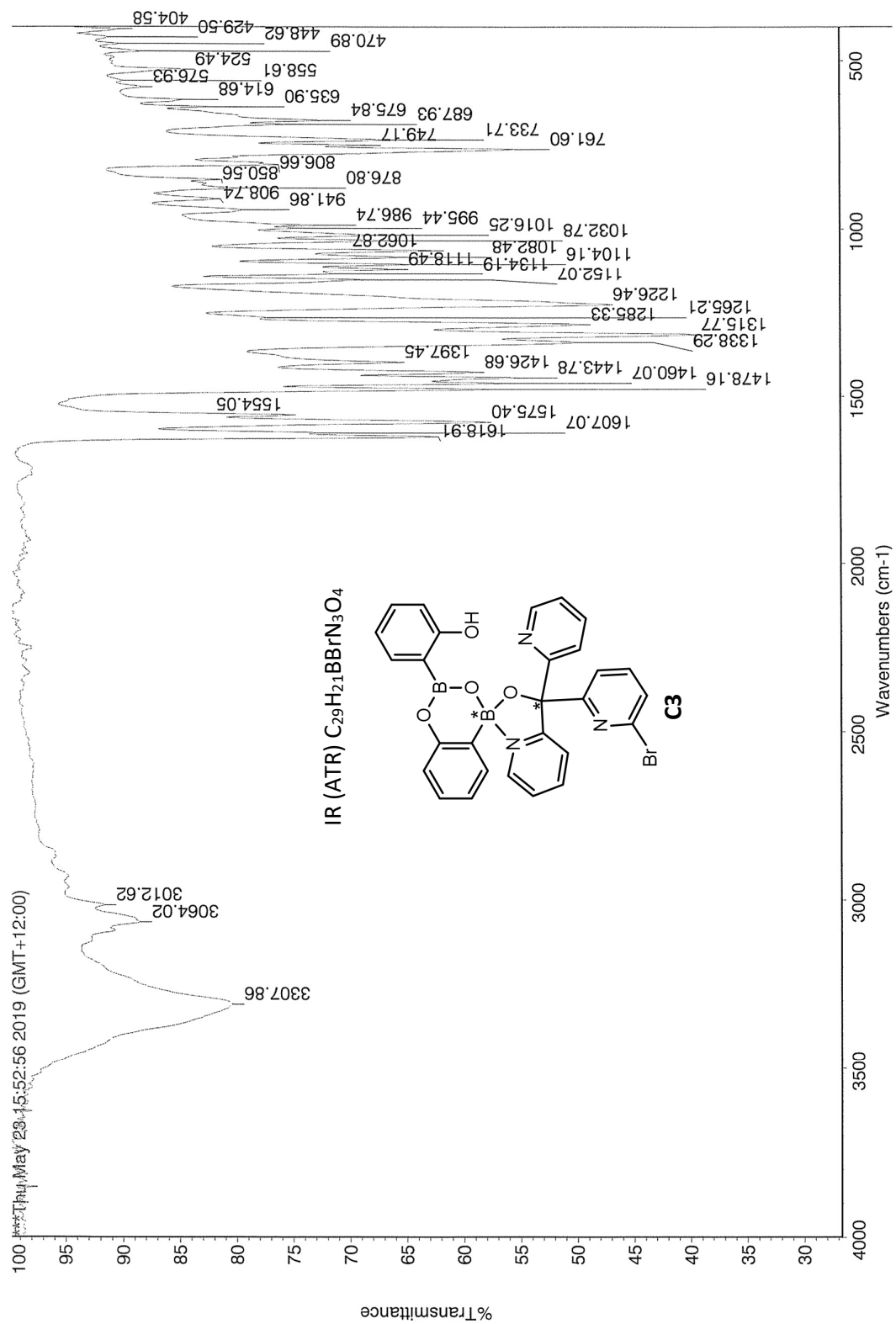


Figure C-31: IR spectrum (ATR) of a boronic anhydride-based ligand (compound 3)



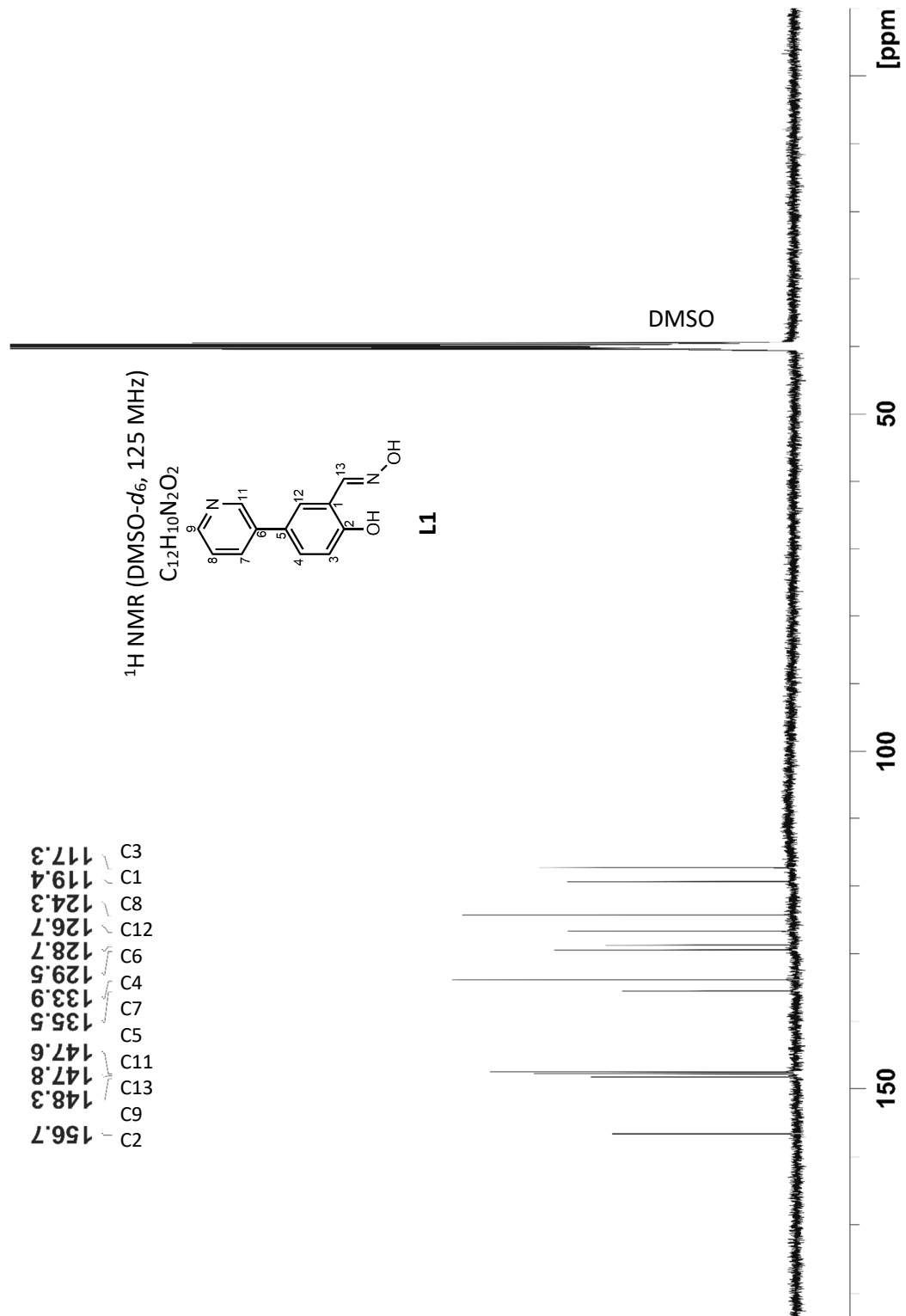


Figure C-33: <sup>13</sup>C spectrum of 2-hydroxy-5-(3-pyridyl)-benzaldehyde oxime (L1)



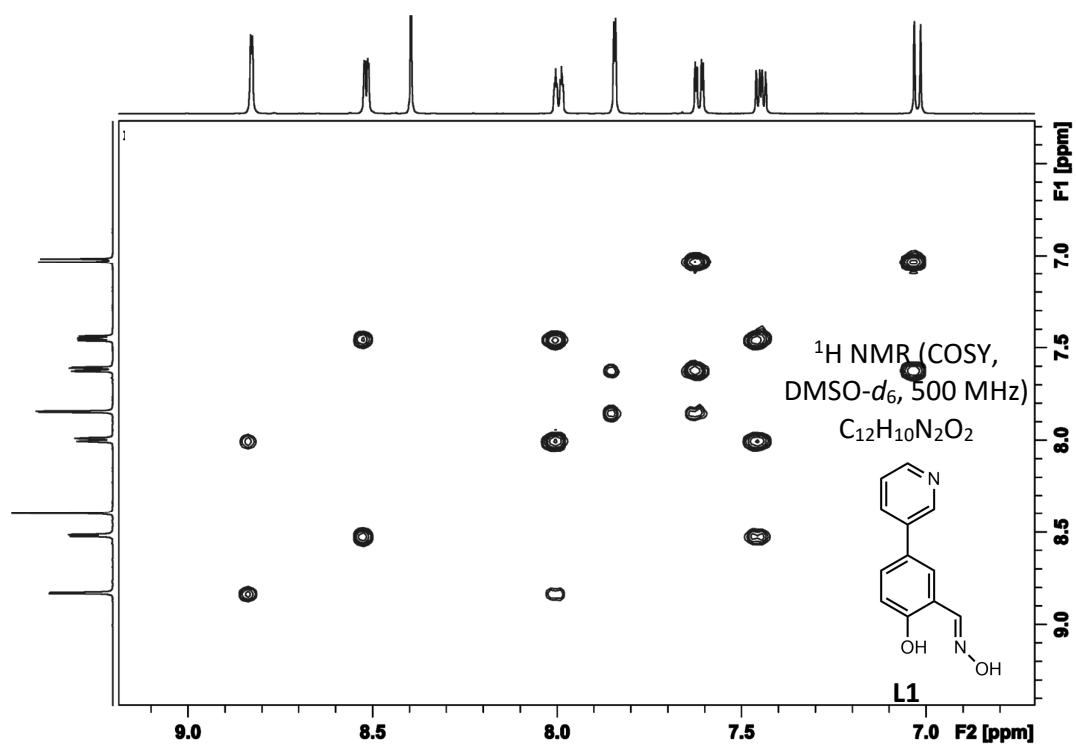
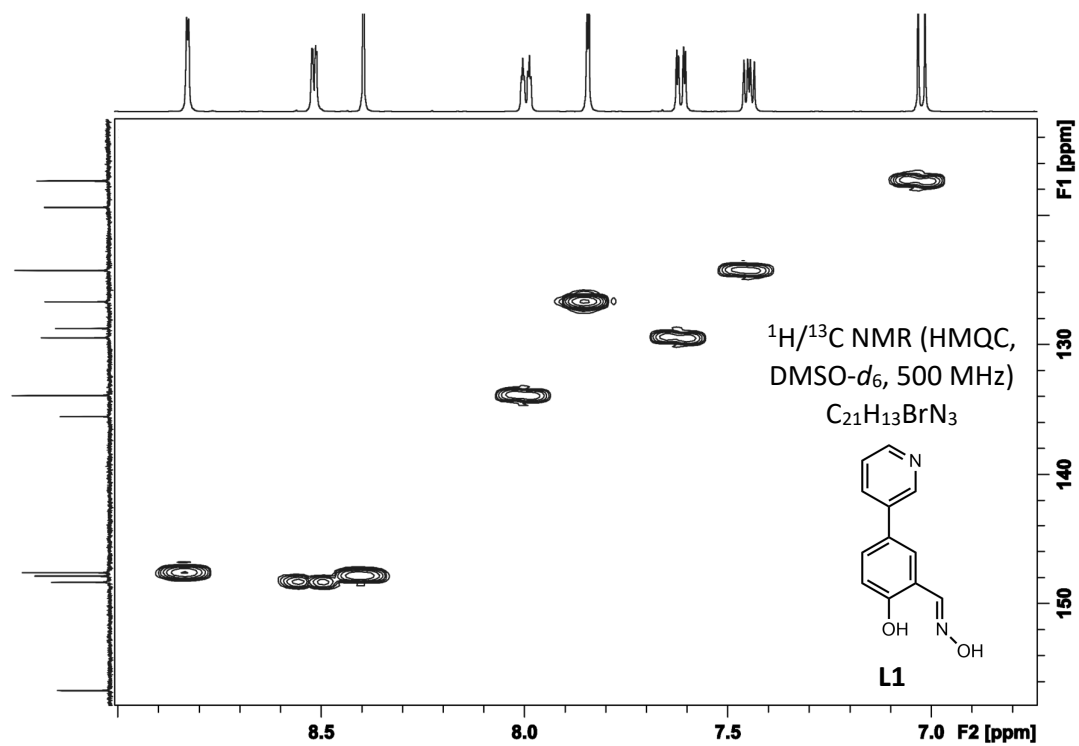


Figure C-34: HMQC (top) and COSY (lower) spectra of 2-hydroxy-5-(3-pyridyl)-benzaldehyde oxime (L1)

## Appendix D: QQ Computational

**Table D-1: Bond lengths and changes of neutral and protonated structures of Chapter 5. Lengths and length changes given in Å.**

BOND	A	AH+	CHANGE (AH+)-A	B	BH+	CHANGE (BH+)-B	C	CH+	CHANGE (CH+)-C	D	DH+	CHANGE (DH+)-D	E	EH+	CHANGE (EH+)-E
N1-C15	1.34964	1.35853	0.00889	1.34935	1.35860	0.00925	1.34841	1.35842	0.01001	1.34947	1.36195	0.01249	1.35154	1.36239	0.01086
N1-C2	1.30786	1.32407	0.01621	1.30818	1.32379	0.01561	1.30764	1.32390	0.01626	1.31022	1.32920	0.01898	1.30722	1.32833	0.02112
C3-C2	1.40064	1.37895	-0.02169	1.40029	1.38032	-0.01997	1.40150	1.37988	-0.02162	1.39563	1.36642	-0.02921	1.40070	1.36644	-0.03426
C4-C3	1.37196	1.38756	0.01560	1.37200	1.38550	0.01350	1.36422	1.38118	0.01696	1.37698	1.40246	0.02548	1.37578	1.40945	0.03367
C16-C4	1.41863	1.41892	0.00029	1.41798	1.41691	-0.00107	1.41012	1.41107	0.00096	1.42202	1.43262	0.01060	1.42599	1.44268	0.01669
C16-C5	1.42573	1.42673	0.00100	1.42635	1.42666	0.00032	1.42243	1.42438	0.00195	1.42304	1.42170	-0.00134	1.42377	1.42418	0.00041
C16-C15	1.41990	1.41055	-0.00935	1.41915	1.41015	-0.00900	1.42147	1.40994	-0.01153	1.41774	1.40269	-0.01504	1.41632	1.40467	-0.01166
C15-C14	1.45198	1.43352	-0.01846	1.45215	1.43335	-0.01880	1.45260	1.43208	-0.02052	1.45353	1.43589	-0.01764	1.45416	1.43597	-0.01818
C17-C6	1.42547	1.42673	0.00126	1.42595	1.42716	0.00121	1.42627	1.42874	0.00247	1.42476	1.42355	-0.00121	1.40058	1.42182	0.02125
C6-C5	1.34943	1.35065	0.00123	1.34947	1.35060	0.00113	1.34888	1.35035	0.00146	1.35020	1.35161	0.00141	1.34992	1.35210	0.00217
C17-C14	1.39880	1.39889	0.00009	1.39854	1.39900	0.00046	1.40038	1.40070	0.00032	1.40054	1.40039	-0.00015	1.40058	1.40020	-0.00037
C8-C7	1.34944	1.35177	0.00233	1.34950	1.35182	0.00232	1.34952	1.35447	0.00495	1.35019	1.35209	0.00189	1.34947	1.35204	0.00257
C17-C7	1.42568	1.42303	-0.00265	1.42575	1.42322	-0.00253	1.42678	1.42093	-0.00585	1.42476	1.42140	-0.00336	1.42508	1.42121	-0.00387
C14-C13	1.45263	1.44594	-0.00668	1.45155	1.44547	-0.00608	1.45324	1.44286	-0.01038	1.45354	1.44925	-0.00429	1.45332	1.44971	-0.00361
C13-C12	1.41919	1.41136	-0.00783	1.41983	1.41075	-0.00909	1.41675	1.40284	-0.01391	1.41774	1.40988	-0.00785	1.41710	1.40952	-0.00758
C12-C8	1.42624	1.42673	0.00049	1.42586	1.42664	0.00077	1.42259	1.42064	-0.00195	1.42305	1.42195	-0.00110	1.42315	1.42422	0.00107
C12-C9	1.41903	1.42079	0.00176	1.41761	1.41941	0.00180	1.41203	1.42438	0.01235	1.42201	1.43025	0.00824	1.42439	1.43580	0.01141
C10-C9	1.37240	1.37690	0.00450	1.37170	1.37533	0.00362	1.36572	1.38006	0.01434	1.37700	1.39024	0.01325	1.37415	1.39142	0.01727
C11-C10	1.40044	1.39360	-0.00684	1.40052	1.39485	-0.00567	1.40231	1.39359	-0.00872	1.39562	1.38068	-0.01493	1.40088	1.38492	-0.01597
N2-C11	1.30819	1.31570	0.00750	1.30791	1.31540	0.00749	1.30913	1.31590	0.00677	1.31024	1.32211	0.01188	1.30654	1.31909	0.01255
N2-C13	1.34938	1.35442	0.00504	1.34948	1.35472	0.00524	1.34996	1.35855	0.00858	1.34945	1.35330	0.00385	1.35176	1.35500	0.00324

**Table D-2: Free energies and enthalpies of computational structures (Chapter 5) used for gas phase basicity and proton affinity calculations.**

Structure	Neutral		Protonated					
	Free energy (a.u)	Free enthalpy (a.u)	Free energy (a.u)	Free enthalpy (a.u)	GPB (a.u)	GPB (kcal/mol)	PA (a.u)	PA (kcal/mol)
<b>A</b>	-1219.008445	-1218.934586	-1219.415741	-1219.342765	-0.397296	249.307058	-0.408179	256.1362451
<b>B</b>	-1219.008831	-1218.935074	-1219.413158	-1219.339529	-0.394327	247.443982	-0.404455	253.7993993
<b>C</b>	-1375.228242	-1375.16191	-1375.63885	-1375.574122	-0.400608	251.3853698	-0.412212	258.6669914
<b>D</b>	-835.689688	-835.632846	-836.119196	-836.061566	-0.419508	263.2453015	-0.431080314	270.50704
<b>E</b>	-992.786883	-992.718237	-993.214945	-993.146852	-0.418062	262.3379226	-0.428615	268.9600315

## Appendix E – Crystal data and refinement for [BeBr(MeCN)(QQ(OH)<sub>2</sub>)]Br

Table E-1: Crystal data and structure refinement for [BeBr(MeCN)(QQ(OH)<sub>2</sub>)]Br.

IDENTIFICATION CODE	[BEBR(MECN)(QQOH)]BR
EMPIRICAL FORMULA	C <sub>20</sub> BeN <sub>4</sub> Br <sub>2</sub> O <sub>2</sub> H <sub>15</sub>
FORMULA WEIGHT	512.19
TEMPERATURE/K	100(2)
CRYSTAL SYSTEM	monoclinic
SPACE GROUP	P2 <sub>1</sub> /n
A/Å	11.3825(3)
B/Å	9.6565(2)
C/Å	19.2412(5)
A/°	90
B/°	103.695(2)
γ/°	90
VOLUME/Å <sup>3</sup>	2054.77(9)
Z	4
P <sub>calc</sub> G/CM <sup>3</sup>	1.656
M/MM <sup>-1</sup>	5.202
F(000)	1012.0
CRYSTAL SIZE/MM <sup>3</sup>	? × ? × ?
RADIATION	CuKα (λ = 1.54178)
2θ RANGE FOR DATA COLLECTION/°	8.27 to 157.404
INDEX RANGES	-14 ≤ h ≤ 14, -12 ≤ k ≤ 11, -24 ≤ l ≤ 14
REFLECTIONS COLLECTED	24276
INDEPENDENT REFLECTIONS	4332 [R <sub>int</sub> = 0.0119, R <sub>sigma</sub> = 0.0069]
DATA/RESTRAINTS/PARAMETERS	4332/0/273
GOODNESS-OF-FIT ON F <sup>2</sup>	1.083
FINAL R INDEXES [I >= 2Σ (I)]	R <sub>1</sub> = 0.0195, wR <sub>2</sub> = 0.0505
FINAL R INDEXES [ALL DATA]	R <sub>1</sub> = 0.0209, wR <sub>2</sub> = 0.0538
LARGEST DIFF. PEAK/HOLE / E Å <sup>-3</sup>	0.43/-0.30
EXPERIMENTAL	

Single crystals of C<sub>20</sub>BeN<sub>4</sub>Br<sub>2</sub>O<sub>2</sub>H<sub>15</sub> [[BeBr(MeCN)(QQOH<sub>2</sub>)]Br] were grown by recrystallisation in CH<sub>3</sub>CN at elevated temperatures. A suitable crystal was selected and mounted then measured on a **STOE STADIVARI** diffractometer. The crystal was kept at 100(2) K during data collection. Using Olex2 [1], the structure was solved with the SHELXT-2018/2 [2] structure solution program using Dual Space and refined with the SHELXL-2018/3 [3] refinement package using the SHELXL software package and refined against F<sub>2</sub>.

1. Dolomanov, O.V., Bourhis, L.J., Gildea, R.J, Howard, J.A.K. & Puschmann, H. (2009), J. Appl. Cryst. 42, 339-341. Hübschle C. B., Sheldrick G. M., Dittrich B. J. Appl. Crystallogr. 2011, 44, 1281–1284.
2. SHELXT-2018/2, G. M Sheldrick., Göttingen, Germany, 2018.

3. SHELXL-2018/3, G. M Sheldrick Göttingen, Germany, 2018.

### Crystal structure determination of $[[\text{BeBr}(\text{MeCN})(\text{QOH})]\text{Br}]$

#### Refinement model description

Number of restraints - 0, number of constraints - unknown.

Details:

1.a Aromatic/amide H refined with riding coordinates:

C00D(H00D), C00G(H00G), C00H(H00H), C00I(H00I), C00L(H00L), C00M(H00M),  
C00N(H00N), C00O(H00O)

1.b Idealised Me refined as rotating group:

C00Q(H00A,H00B,H00C), C00S(H00E,H00F,H00J)

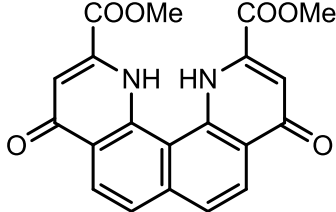
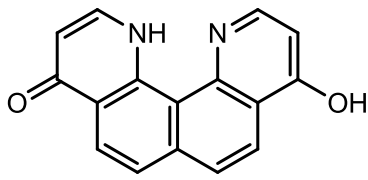
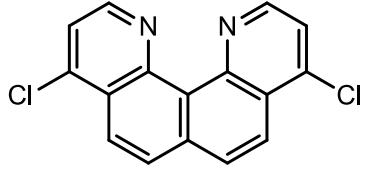
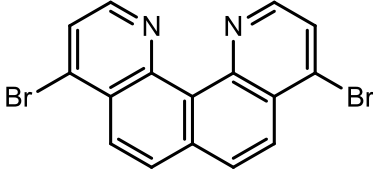
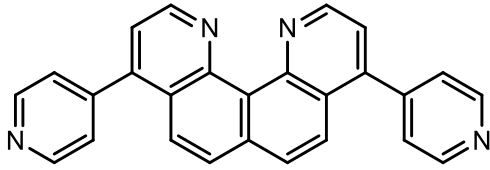
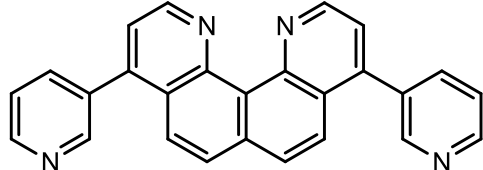
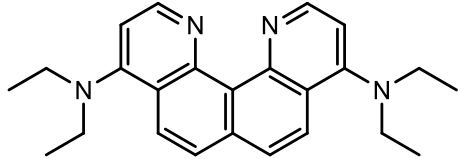
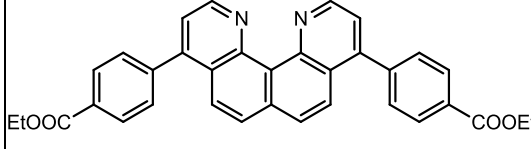
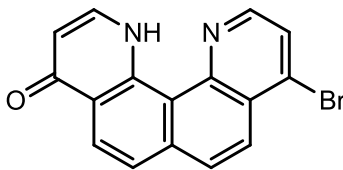
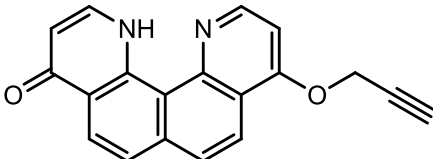
**Table E-2: Selected bond lengths of the Be-QQ(OH)<sub>2</sub> crystal structure**

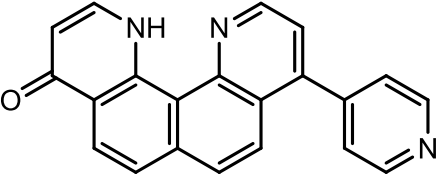
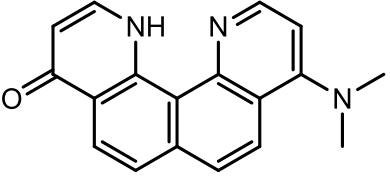
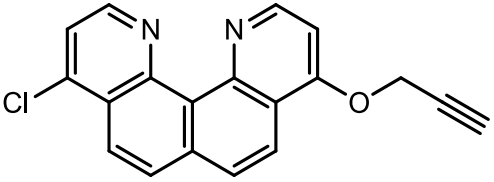
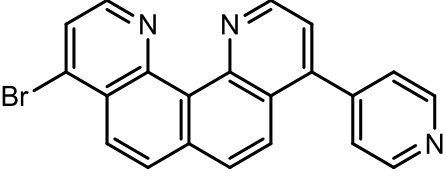
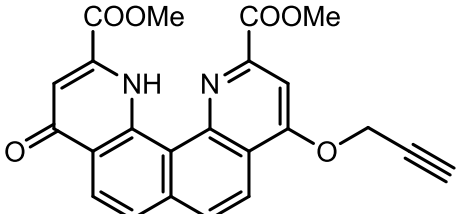
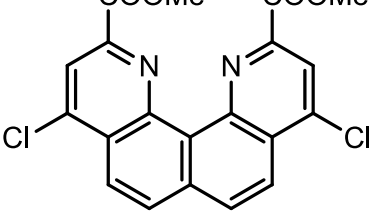
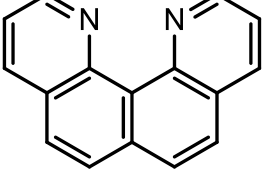
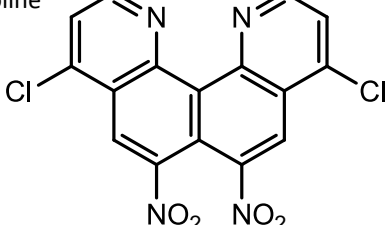
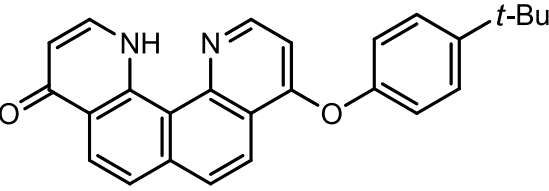
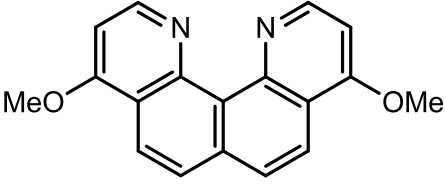
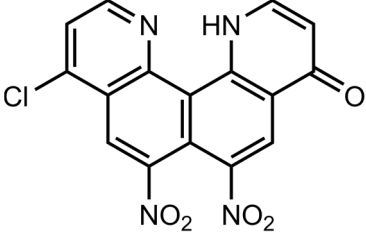
Bond	Length (Å)	Bond	Length (Å)	Bond	Length (Å)
N1 – C14	1.3705(19)	C16 – C15	1.412(2)	C9 – C12	1.426(2)
C15 – C14	1.447(2)	C16 – C4	1.423(2)	C12 – C13	1.417(2)
C14 – C13	1.446(2)	C4 – C3	1.374(2)	C12 – C8	1.416(2)
C14 – C17	1.406(2)	C3 – C2	1.385(2)	N1 – Be1	1.677(2)
C17 – C6	1.426(2)	C2 – N1	1.343(2)	N2 – Be1	1.679(2)
C17 – C7	1.433(2)	C13 – N2	1.368(2)	Be1 – Br1	2.149(2)
C7 – C8	1.352(2)	N2 – C11	1.339(2)	Br2 – H1	2.37(3)
C6 – C5	1.355(2)	C11 – C10	1.385(2)	Br2 – H2	2.36(3)
C5 – C16	1.417(2)	C10 – C9	1.374(2)		

**Table E-3: Selected angles of Be-QQ(OH)<sub>2</sub> structure**

Atoms				Angle (°)	Atoms				Angle (°)
C15	N1	Be1		123.03(12)	O2	C9	C10	124.08(15)	
C2	N1	C15		119.31(13)	O2	C9	C12	116.48(15)	
C2	N1	Be1		117.38(13)	O1	C4	C16	116.20(15)	
C13	N2	Be1		123.36(12)	O1	C4	C3	124.00(15)	
C11	N2	Be1		117.55(13)	N1	Be1	Br1	115.05(11)	
N2	C13	C14		120.58(13)	N1	Be1	N2	107.30(12)	
N1	C15	C14		120.78(13)	N2	Be1	Br1	113.32(11)	
C13	C14	C15		124.54(14)					

## Appendix F: QQ Derivative names and codes

<p><b>Q1</b> - 4,9-dioxo-1,4,9,12-tetrahydroquinolino[7,8-<i>h</i>]quinoline-2,11-dicarboxylate</p> 	<p><b>Q2</b> - Quinolono[7,8-<i>h</i>]quinoline-4,9-(1<i>H</i>,12<i>H</i>)-dione</p> 
<p><b>Q3</b> - 4,9-dichloroquinolino[7,8-<i>h</i>]quinoline</p> 	<p><b>Q4</b> - 4,9-dibromoquinolino[7,8-<i>h</i>]quinoline</p> 
<p><b>Q5</b> - 4,9-di(pyridin-4-yl)quinolino[7,8-<i>h</i>]quinoline</p> 	<p><b>Q6</b> - 4,9-di(pyridin-3-yl)quinolino[7,8-<i>h</i>]quinoline</p> 
<p><b>Q7</b> - <i>N</i><sup>4</sup>,<i>N</i><sup>4</sup>,<i>N</i><sup>9</sup>,<i>N</i><sup>9</sup>-tetraethylquinolino[7,8-<i>h</i>]quinoline-4,9-diamine</p> 	<p><b>Q8</b> - 4,9-di(4-benzoic acid ethyl ester)quinolino[7,8-<i>h</i>]quinoline</p> 
<p><b>Q9</b> - 4-bromo-9-oxo-9,12-dihydroquinolino[7,8-<i>h</i>]quinoline</p> 	<p><b>Q10</b> - 9-(2-propyn-1-yloxy)-quinolino[7,8-<i>h</i>]quinolin-4(1<i>H</i>)-one</p> 

<p><b>Q11</b> - 9-(pyridine-4-yl)quinolino[7,8-<i>h</i>]quinoline-4(1<i>H</i>)-one</p> 	<p><b>Q12</b> - 9-(dimethylamino)quinolino[7,8-<i>h</i>]quinoline-4(1<i>H</i>)-one</p> 
<p><b>Q13</b> - 4-chloro-9-(2-propyn-1-yloxy)-quinolino[7,8-<i>h</i>]quinoline</p> 	<p><b>Q14</b> - 4-bromo-9-(pyridin-4-yl)quinolino[7,8-<i>h</i>]quinoline</p> 
<p><b>Q15</b> - 9-(2-propyn-1-yloxy)-1,4,9,12-tetrahydro-4,9-dioxo-2,11-dimethylester-quinolo[7,8-<i>h</i>]quinoline-2,11-dicarboxylic acid</p> 	<p><b>Q16</b> - Dimethyl-4,9-dichloroquinolino[7,8-<i>h</i>]quinoline-2,11-dicarboxylate</p> 
<p><b>Q17</b> - Quino[7,8-<i>h</i>]quinoline</p> 	<p><b>Q18</b> - 4,9-dichloro-6,7-dinitroquinolino[7,8-<i>h</i>]quinoline</p> 
<p><b>Q19</b> - 9-(4-tert-Butylphenoxy)quinolino[7,8-<i>h</i>]quinoline-4(1<i>H</i>)-one</p> 	<p><b>Q20</b> - 4,9-dimethoxyquinolino[7,8-<i>h</i>]quinoline</p> 
<p><b>Q21</b> - 4-chloro-9-oxo-9,12-dihydro-6,7-dinitroquino[7,8-<i>h</i>]quinoline</p> 	

## Appendix G: Statements of Contribution

DRC 16



### STATEMENT OF CONTRIBUTION DOCTORATE WITH PUBLICATIONS/MANUSCRIPTS

We, the candidate and the candidate's Primary Supervisor, certify that all co-authors have consented to their work being included in the thesis and they have accepted the candidate's contribution as indicated below in the *Statement of Originality*.

Name of candidate:	Rebecca Jane Severinsen	
Name/title of Primary Supervisor:	Prof. Paul Plieger	
Name of Research Output and full reference:		
Rowlands, G. J., Severinsen, R. J., Buchanan, J. K., Shaffer, K. J., Jameson, H. T., Thomason, N., Leko, I., Lohm, M., Kitz, A., Vianello, R., Despotović, I., Radoš, N., Plieger, P. G., Synthesis and Basicity Studies of Quinodiol(7,8-epoxy)amine Derivatives. <i>J. Org. Chem.</i> 2020, 85 (17), 11297-11309.		
In which Chapter is the Manuscript /Published work:	Chapters 1-5	
Please indicate:		
<ul style="list-style-type: none"> <li>The percentage of the manuscript/Published Work that was contributed by the candidate:</li> </ul>	30%	
and		
<ul style="list-style-type: none"> <li>Describe the contribution that the candidate has made to the Manuscript/Published Work:</li> </ul>	Most of the experimental and characterisation work.	
For manuscripts intended for publication please indicate target journal:		
Candidate's Signature:	Rebecca Jane Severinsen	<small>Digitally signed by Rebecca Jane Severinsen DN: c=NZ, cn=Rebecca Jane Severinsen, e=r.j.severinsen@massey.ac.nz Reason: I am the author of this document. Location: your signing location here Date: 2021.06.03 14:56:03+1200 Foxit PDF Editor Version: 11.0.0</small>
Date:	03/06/21	
Primary Supervisor's Signature:	Paul Plieger	<small>Digitally signed by Paul Plieger DN: cn=Paul Plieger, c=NZ, o=Massey University, ou=School of Fundamental Sciences, email=p.g.plieger@massey.ac.nz Date: 2021.06.04 09:25:49 +1200</small>
Date:	04/06/2021	

(This form should appear at the end of each thesis chapter/section/appendix submitted as a manuscript/ publication or collected as an appendix at the end of the thesis)





MASSEY UNIVERSITY  
GRADUATE RESEARCH SCHOOL

## STATEMENT OF CONTRIBUTION DOCTORATE WITH PUBLICATIONS/MANUSCRIPTS

We, the candidate and the candidate's Primary Supervisor, certify that all co-authors have consented to their work being included in the thesis and they have accepted the candidate's contribution as indicated below in the *Statement of Originality*.

Name of candidate:	Rebecca Jane Severinsen
Name/title of Primary Supervisor:	Prof. Paul Plieger
Name of Research Output and full reference:	
Severinsen, R. J.; Rowlands, G. J.; Plieger, P. G., Coordination Cages in Catalysis. J. Inclusion Phenom. Macrocyclic Chem. 2020, 96 (1-2), 29-42.	
In which Chapter is the Manuscript /Published work:	Chapter 1
Please indicate:	
<ul style="list-style-type: none"> <li>The percentage of the manuscript/Published Work that was contributed by the candidate:</li> </ul>	90%
and	
<ul style="list-style-type: none"> <li>Describe the contribution that the candidate has made to the Manuscript/Published Work:</li> </ul>	
Review article researched and written by the candidate, edited by co-authors.	
For manuscripts intended for publication please indicate target journal:	
Candidate's Signature:	Rebecca Jane Severinsen <small>Digitally signed by Rebecca Jane Severinsen DN: c=NZ, CN=Rebecca Jane Severinsen, E=r.j.severinsen@massey.ac.nz Reason: I am the author of this document Location: your signing location here Date: 2021.06.03 14:46:03+12'00' Postal: PO Box 1100</small>
Date:	03/06/21
Primary Supervisor's Signature:	Paul Plieger <small>Digitally signed by Paul Plieger DN: cn=Paul Plieger, c=NZ, o=Massey University, ou=School of Fundamental Sciences, email=p.g.plieger@massey.ac.nz Date: 2021.06.04 09:23:55 +12'00'</small>
Date:	04/06/2021

(This form should appear at the end of each thesis chapter/section/appendix submitted as a manuscript/ publication or collected as an appendix at the end of the thesis)



MASSEY UNIVERSITY  
GRADUATE RESEARCH SCHOOL

## STATEMENT OF CONTRIBUTION DOCTORATE WITH PUBLICATIONS/MANUSCRIPTS

We, the candidate and the candidate's Primary Supervisor, certify that all co-authors have consented to their work being included in the thesis and they have accepted the candidate's contribution as indicated below in the *Statement of Originality*.

Name of candidate:	Rebecca Jane Severinsen	
Name/title of Primary Supervisor:	Prof. Paul Plieger	
Name of Research Output and full reference:		
<small>* Buchner, M. R.; Mueller, M.; Raymond, O.; Severinsen, R. J.; Nixon, D. J.; Henderson, W.; Brothers, P. J.; Rowlands, G. J.; Plieger, P. G. Synthesis of a Boronic Acid Anhydride Based Ligand and Its Application in Beryllium Coordination. Eur. J. Inorg. Chem. 2010, 2010 (34), 3863-3868.</small>		
In which Chapter is the Manuscript /Published work:	Chapter 2, Chapter 3	
Please indicate:		
<ul style="list-style-type: none"> <li>The percentage of the manuscript/Published Work that was contributed by the candidate:</li> </ul>	15%	
and		
<ul style="list-style-type: none"> <li>Describe the contribution that the candidate has made to the Manuscript/Published Work:</li> </ul>		
Experimental synthesis and characterisation of Compound 3.		
For manuscripts intended for publication please indicate target journal:		
Candidate's Signature:	Rebecca Jane Severinsen	<small>Digitally signed by Rebecca Jane Severinsen DN: c=NZ, CN=Rebecca Jane Severinsen, E=rj.severinsen@massey.ac.nz Reason: I am the author of this document Location: your signing location here Date: 2021.06.03 14:46:03+12'00' Foxit PDF Editor Version: 11.0.0</small>
Date:	03/06/21	
Primary Supervisor's Signature:	Paul Plieger	<small>Digitally signed by Paul Plieger DN: cn=Paul Plieger, c=NZ, o=Massey University, ou=School of Fundamental Sciences, email=p.g.plieger@massey.ac.nz Date: 2021.06.04 09:25:02 +12'00'</small>
Date:	04/06/2021	

(This form should appear at the end of each thesis chapter/section/appendix submitted as a manuscript/ publication or collected as an appendix at the end of the thesis)